Université catholique de Louvain
Institute of Condensed Matter and Nanosciences (IMCN)
Institute of Mechanics, Materials and Civil Engineering (iMMC)

Experimental and numerical study of ammonia combustion

Catherine Duynslaegher
September 2011

Jury members
Pr. E. Gaigneaux (president)
Pr. J. Vandooren (supervisor)
Pr. H. Jeanmart (supervisor)
Pr. O. Gicquel
Pr. J. Martin
Pr. D. Peeters
Pr. D. Puechberty

Thesis submitted in fulfillment of the requirements for the degree of Doctor in Sciences

©2011
Catherine Duynslaegher
All Rights Reserved

Knowing is a barrier which prevents learning.
Frank Herbert (1920-1986)

Research is to see what everybody else has seen, and to think what nobody else has thought.
Albert Szent-Gyorgi (1893-1986)

Acknowledgments

First of all I would like to thank my supervisors, Pr. Jacques Vandooren and Pr. Hervé Jeanmart. Pr. Vandooren has introduced me to the world of chemical kinetics. He has never hesitated to help me in the several experimental works I have performed, and I really thank him for that. Many thanks to Pr. Jeanmart for welcoming me into the TFL team and allowing me to perform experiments on a spark ignition engine. He was patient enough to share his knowledge with me on engines and thermodynamics, and his critical readings of this thesis has undoubtedly brought a special dimension to it.

I am very grateful to Pr. Joseph Martin, Pr. Daniel Peeters, Pr. Olivier Gicquel, Pr. Daniel Puechberty, and Pr. Eric Gaigneaux for having carefully read this thesis and for their very constructive comments.

This thesis has been financially supported with a Research Fellowship from the F.R.S.-FNRS.

I owe my deepest gratitude to Dr. Véronique Dias for her daily help and encouragements in all events encountered during these five years of research.

I would like to thank all the members of the combustion laboratory: Christiane, Nicolas, Valéry, Xavier, Hubert, Axel, and Pr. P.J. Van Tiggelen. Their help, advice, expertise and good spirits helped me greatly.

I am indebted to many of my colleagues from TFL who have supported me this last year. Among them, I would like to name Francesco and Nicolas for having helped me to decode this strange world of engineers and their strange language, Matthieu who helped me so many times with LaTeX that I have stopped counting, and all others who have generously contributed with much appreciated input: Amel, Antoinette, Benjamin, François H., François V., Frank, Isabelle, Ivan, Jean-Marie, Julien B., Julien V., Laurent, Lili, Michel, Nicolas, Philippe, Yann, and Yves.

I would like to show my gratitude to my family and friends who have made available their support in a number of ways during this PhD.

Finally, I am deeply grateful to my husband, Laurent, for his unconditional support throughout my thesis, and for being so patient and understanding when I was stressed. But most importantly, I am thankful for the everyday happiness that comes from being with him, my daughter Emilie, and my new son to come.

Extended Summary

Ammonia (NH_3) is an interesting vector of energy to use in spark ignition engines. The combustion of this fuel is less pollutant than oil, because there are no formation of carbon dioxide, carbon monoxide or of soot. Only NO_x production must be controlled. To know which reactions take place in engines, and so to regulate the NO_x formation, the combustion mechanism of ammonia has to be studied in several conditions of pressure and temperature. This was the main objective of this thesis.

First of all, ammonia combustion at low pressure has been experimentally and numerically investigated in order to deepen the comprehension of ammonia-air combustion kinetics. Eight $NH_3/H_2/O_2/Ar$ flames close to the stoichiometry with different initial composition or operating conditions have thus been analyzed using a molecular beam mass spectrometer. The effects of the variation of the initial hydrogen percentage, of the equivalence ratio and of the operation pressure have been investigated. Mole fraction profiles have been obtained for the following species : NH_3, NH_2, NO, N_2O, N_2, H_2, H_2O, OH, O_2 and Ar. Numerical simulations of these experimentally analyzed flames have been done with five ammonia combustion kinetic mechanisms available in the literature. Since none of those ones allowed to reproduce satisfactorily the experimental results, an improved mechanism has been established on the basis of the Konnov work [1]. Indeed, for this model, most of the calculated mole fraction profiles agreed with the experimental ones but a significant divergence was observed for N_2O and NH_2. Kinetic parameters of the formation and degradation reactions of these species have been modified to obtain an improved mechanism leading to a better agreement with all the detected species. This

improved mechanism has then been reduced in order to fit the requirements of a potential integration in a CFD simulation. The *reduced* ammonia combustion mechanism contains 80 elementary reactions and 19 chemical species. This *reduced* ammonia combustion mechanism has been used to simulate the eight analyzed ammonia flames leading to a good agreement between the experimental and the numerical results. This led also to a discussion on the impact of the several parameters (initial hydrogen content, equivalence ratio, pressure) on the species concentrations and on the kinetic reaction pathways. Excluding a slight effect on the NO formation, the initial hydrogen content did not have a significant impact on the composition of the burned gases but an increase of its initial percentage increased the adiabatic burning velocity and therefore moved the position of the flame front closer to the burner surface. Around stoichiometric conditions, a decrease of the equivalence ratio strongly increased the NO formation. Furthermore, at high temperature, the NO formation was favored as it has been noticed in flames where, due to different heat losses, the maximum temperature increased with a decrease of pressure. This implies that the temperature and the equivalence ratio must be well controlled in practical devices such as spark ignition engines.

Then, ammonia laminar flame speed has been numerically and experimentally investigated using the tube method. Indeed, ammonia-air laminar burning velocities had not been widely investigated in the past. The influence of the equivalence ratio and the dilution on ammonia laminar flame speed have thus been investigated. The experimental results have been compared to numerical simulation results obtained with the *reduced* ammonia combustion mechanism. An increased dilution led to a global linear decrease of the laminar flame speed. For an equivalence ratio equal to one, the measured ammonia laminar flame speed at the air-dilution was equal to 13.3 $cm.s^{-1}$. This value is significantly lower than the one for traditional fuels for which it is around 40 $cm.s^{-1}$. The effect of an equivalence ratio variation for a constant dilution showed a peak value under stoichiometric conditions and a decrease of the laminar flame speed around this maximum. The numerical results were in agreement with the observed effect and allowed to validate the *reduced* mechanism at atmospheric pressure. Finally, using this mechanism, numerical simulations of ammonia combustion at elevated pressure and temperature conditions such as those encountered in spark ignition engine combustion have been performed. Only the

kinetic aspect of the combustion has thus been taken into account. These simulations have shown that the maximum laminar burning velocity is reached in the rich side at an equivalence ratio of 1.1. In the vicinity of stoichiometric mixtures, the variation of the compression ratio has a significant effect on increasing the laminar burning velocity. An increase in compression ratio from 12:1 to 20:1 led to a 130% increase in laminar burning velocity. The adiabatic flame temperature shows a peak at an equivalence ratio around 1.00. It was found that adiabatic flame temperature increases slightly with the compression ratio. The nitrogen monoxide mole fraction reaches a maximum at $\phi = 0.95$. Increasing the compression ratio does not have a significant impact on the NO formation for the range of compression ratios investigated in this work because it leads only to a slight increase of the adiabatic temperature and as a consequence to a slight increase of the thermal NO formation. However, a huge decrease of the highest NO concentration is observed for rich mixtures ($\phi = 1.2$), with a NO maximum mole fraction of 50% less than the amount of NO found for an equivalence ratio of 0.95.

Finally, ammonia combustion in spark ignition engine conditions has been experimentally investigated. Ammonia combustion in spark ignition engines had been well investigated these last years but always with an additive to promote the reaction. The use of ammonia as envisioned in this work (ammonia-air combustion) had thus never been investigated to the best of our knowledge. The effects of the compression ratio, the spark timing and the equivalence ratio on the exhaust gases composition and the engine performances have been analyzed. When using ammonia as a fuel, one can imagine that the combustion will lead to important nitrogen oxides quantities in the burned gases. However, the nitrogen monoxide concentration was very low due to relatively low combustion temperatures and there was nearly no formation of nitrogen dioxide or nitrous oxide. However, the fraction of ammonia remaining in the exhaust gases in comparison to the quantity admitted in the fresh gases, around 8 to 10%, was particularly high and could not be explained only by the quenching effects (wall quenching and unburned fresh gases in the cylinder crevices). For conventional fuels, this quantity is indeed around 3%. A hypothesis of bulk quenching has been made to explain this important unburned fraction. The important quantity of hydrogen in the exhaust gases suggested that the residual ammonia was decomposed partially in hydrogen. Indeed, the evolution of

the 2 $NH_3 \rightarrow 3\ H_2 + N_2$ equilibrium constant for a wide range of pressures and temperatures indicated that the ammonia decomposition was not surprising for the conditions encountered during combustion. Based on these results, the optimum spark ignition engine running conditions has been obtained for a compression ratio of 15, a spark timing around 20°- 22 °before top dead center and an equivalence ratio between 0.95 and 1. These conditions are the best trade-off to reduce the ammonia ($\approx$ 8% of the quantity admitted in the fresh gases), the nitrogen monoxide ($\approx$ 800 ppm) and the hydrogen ($\approx$ 4000 ppm) contained in the exhaust gases while reaching the best engine performances by reducing the friction losses and increasing the effective efficiency (bmep $\approx$ 850 kPa, $P_e \approx 9$ kW, $\eta_e \approx 0.39$). This experimental study has shown that ammonia is a very interesting fuel to investigate because of its combustion properties very different from those of other conventional fuels. The study of such a fuel can help to understand low flame speed combustion phenomena as those encountered for lean flames.

Contents

I Flame Structure Study **11**

1 Literature review on ammonia combustion in flames **15**
1.1 Ammonia combustion 15
1.2 Nitrogen oxides 23

2 Experimental methods **27**
2.1 Presentation of the analyzed flames 27
2.2 Molecular beam–mass spectrometer sampling system 29
2.3 Determination of species concentrations 31
2.4 Measure of temperature profiles 36

3 Numerical simulations **41**
3.1 Presentation of Cosilab® 41
3.1.1 The appropriate model for the simulations 42
3.1.2 The reaction mechanism input file 45
3.1.3 Databases of thermodynamic and molecular data 48
3.1.4 The control document and initial profiles 50
3.2 Contribution calculation 51
3.3 Chemical kinetics of ammonia combustion 52
3.3.1 Mechanisms from the literature 53
3.3.2 Improvement of the Konnov mechanism 60
3.3.3 The *reduced* kinetic mechanism 71

4 Ammonia flames structure at low pressure **81**
4.1 Flame structure study at low pressure 81
4.1.1 Effect of the initial hydrogen content 82

4.1.2 Effect of the equivalence ratio 92
4.1.3 Effect of the pressure 100
4.2 Discussion on pressure variation 106
4.3 Ammonia-air combustion at low pressure 109

II Burning Velocity 119

5 Literature review on ammonia burning velocity 123
5.1 Burning velocity measurements 123
5.1.1 Methods with stationary flames 124
5.1.2 Methods with non stationary flames 125
5.2 Laminar burning velocity of ammonia 128

6 Experimental and numerical methods 133
6.1 Experimental conditions and validation of the setup 137
6.2 Flame surface area computation 140
6.3 Numerical determination of the burning velocity 141

7 Ammonia burning velocities 145
7.1 Validation of the experimental method 145
7.2 Laminar burning velocities at atmospheric pressure 147
7.3 Laminar burning velocities at sub-atmospheric pressure 152
7.4 Laminar burning velocities under elevated pressure conditions . 158
7.4.1 Standard temperature and pressure conditions 162
7.4.2 Effects of the compression ratio 165
7.4.3 Separated influences of temperature and pressure 168

III Combustion of ammonia in a SI engine 175

8 Literature review on the use of ammonia in SI engines 183

9 Experimental methods 191
9.1 The VARIMAX engine 192
9.1.1 Valve adjustment 192
9.1.2 Experimental determination of the compression ratio . . 192
9.2 Ammonia injection 197
9.3 Air intake 198

9.4 Exhaust gases analysis 198
9.4.1 Gas chromatography, for H_2 and N_2O. 199
9.4.2 UV Spectroscopy, for NH_3, NO and NO_2. 200
9.4.3 Combustion balance, for N_2, H_2O and O_2. 201
9.5 Engine performances monitoring 201
9.5.1 Basic quantities 201
9.5.2 Evaluation of basic quantities for ammonia 204

10 Ammonia combustion in SI engine conditions 207
10.1 Actual compression ratios 207
10.2 Exhaust gases analysis without combustion 208
10.3 Effect of the compression ratio 210
10.4 Effect of the spark timing 214
10.5 Effect of the equivalence ratio 217

List of Symbols and Acronyms

Part I : Flame Structure Study

SI : Spark Ignition
Cp : Heat capacity at constant pressure [kJ.mol^{-1}.K^{-1}]
Cv : Heat capacity at constant volume [kJ.mol^{-1}.K^{-1}]
ΔH^0_{298} : Standard enthalpy of reaction at 298 K [kJ]
OSHA : Occupational Safety and Health Administration
CFD : Computational Fluid Dynamics
ϕ : Equivalence ratio
$RAPRENO_x$: Rapid Reduction of NO_x
$\beta = f$: Branching ratio
k : Rate constant (units depend on reaction)
GRI-mech : Gas Research Institute mechanism
BAC-MP4 : Bond Additivity Corrections with fourth order Moller-Plesset perturbation theory
RRKM : Rice-Ramsperger-Kassel-Marcus
X_i : Mole fraction of species i
V_0 : Inlet flow [cm.s^{-1}]
p : Pressure [mbar, bar, atm, Pa, kPa]
MBMS : Molecular Beam Mass Spectrometry
IP : Ionization Potential [eV]
WP : Working Potential [eV]
I_i : Intensity of the signal of species i [mV]
S_i : Sensitivity factor of species i [mV]
Q_i : Effective ionization section of species i

T : Temperature [K]
T_g : Gas temperature [K]
T_c : Thermocouple temperature [K]
α : Heat exchange coefficient or Polarizability [W.m^{-2}.K^{-1}]
d : Wire diameter [m]
ε : Emissivity coefficient of the thermocouple
σ : Stefan-Boltzman constant [5.6998?10^{-8} W.m^{-2}.K^{-4}] or Lennard-Jones collision diameter [$\dot{A}$]
T_0 : Gas temperature [K]
R : Thermocouple resistance per unit of length [K.m^{-1}.W^{-1}]
I : Intensity of the alternative current [mV]
T_z : Temperature at a distance z [K]
T_{max} : Temperature in the burned gases [K]
Y_i : Mass fraction of species i
W_i : Molecular weight of species i [kg.mol^{-1}]
W : Mixture molecular weight [kg.mol^{-1}]
C_i : Molar concentration of species i [mol.m^{-3}]
C : Molar concentration of the mixture [mol.m^{-3}]
ρ_i : Partial mass density of species i [kg.m^{-3}]
ρ : Mass density of the mixture [kg.m^{-3}]
p_i : Partial pressure of species i [Pa]
D_m : Mass flux [kg.s^{-1}]
v : Gas flow velocity [m.s^{-1}]
A : Cross section [m^2] or Burner surface area [m^2]
x : Spatial coordinate
V_i : Diffusion velocity of species i [m.s^{-1}]
$\dot{\omega}_i$: Net molar reaction rate of species i per unit of volume [mol.m^{-3}s^{-1}]
λ : Thermal conductivity [W.K^{-1}.m^{-1}]
h_i : Specific enthalpy of species i [J.kg^{-1}]
V_i^D : Ordinary-diffusion velocity of species i [m.s^{-1}]
V_i^T : Thermal diffusion velocity of species i [m.s^{-1}]
V_c : Global flow velocity [m.s^{-1}]
D_i : Mixture-averaged diffusion coefficient [m^2.s^{-1}]
D_i^T : Thermal-diffusion coefficient of species i [m^2.s^{-1}]
$\nu_{ik}^{'}$: Stoichiometric coefficients of species i on the reactants side in reaction k
$\nu_{jk}^{''}$: Stoichiometric coefficients of species j on the products side in reaction k

M_i : Chemical symbol of reactant species i
M_j : Chemical symbol of product species j
ω_i : Net mass reaction rate of species i [kg.cm^{-3}.s^{-1}]
r_{fk} : Forward reaction rate of reaction k [mol.cm^{-3}.s^{-1}]
r_{bk} : Backward reaction rate of reaction k [mol.cm^{-3}.s^{-1}]
ν_{ik} : Net stoichiometric coefficient of species i in reaction k
r_k : Net reaction rate of reaction k [mol.cm^{-3}.s^{-1}]
k_{fk} : Rate coefficient of the forward reaction k (units depend on reaction)
k_{bk} : Rate coefficient of the backward reaction k (units depend on reaction)
K_{Ck} : Equilibrium constant (units depend on reaction)
$A_{fk} = A$: Pre-exponential factor in the Arrhenius equation
$\beta_{fk} = n$: Pre-exponential temperature exponent in the Arrhenius equation
$E_{fk} = E_a$: Activation energy [J.mol^{-1}] or [cal.mol^{-1}]
K_{Pk} : Equilibrium constant in terms of partial pressures
p^0 : Atmospheric pressure [1000 mbar, 1 bar, 1 atm, 101325 Pa, 101.325 kPa]
ΔS_k^0 : Standard entropy of reaction k [kJ.K^{-1}]
R : Ideal gas constant [8.31446 J?.K^{-1}.mol^{-1}]
ΔH_k^0 : Standard enthalpy of reaction k [kJ]
z_{ik} : Third-body efficiency of species i in reaction k
M : Non reacting partner (third-body)
s_i : Specific entropy of species i [J.kg^{-1}.K^{-1}]
h : Specific enthalpy of the gas mixture [J.kg^{-1}]
s : Specific entropy of the gas mixture [J.kg^{-1}.K^{-1}] or standard deviation
ϵ_k : Lennard-Jones potential [J]
μ_k : Dipole moment [D]
Z_{rot} : Collision frequency [s^{-1}]
H_i : Molar enthalpy [kJ.mol^{-1}]
S_i : Molar entropy [kJ.mol^{-1}.K^{-1}]
Dv_i : Volume flow rate of species i [m^3.s^{-1}]
S_k : Surface beyond curve of net reaction rate k
C_k : Contribution of reaction k [%]
Cf_k : Contribution of reaction k to the formation of species i [%]
Cc_k : Contribution of reaction k to the consumption of species i [%]
t : Student's coefficient
T_{exp} : Experimental flame temperature [K]
T_{ad} : Adiabatic flame temperature [K]

Part II : Burning Velocity

$S_u = S_L$: Laminar flame speed or burning velocity [m.s^{-1}]
S_p : Propagation speed [m.s^{-1}]
S_s : Spatial, displacement speed [m.s^{-1}]
S_u^0 : Laminar flame speed in standard pressure and temperature conditions [m.s^{-1}]
F : gas flow [m^3.s^{-1}]
$A = A_f$: flame surface area [m^2]
ρ_b : Mass density of the burned gases [kg.m^{-3}]
ρ_u : Mass density of the unburned gases [kg.m^{-3}]
E : Expansion factor
T_u : Temperature of the unburned gases [K]
T_b : Temperature of the burned gases [K]
V_u : Unburned gases velocity [m.s^{-1}]
a : Area of the tube section [m^2]
STP : Standard Temperature and Pressure conditions
D : Reduced tube diameter [m]
RU : Relative Uncertainty
LFL : Lower Flammable Limit
UFL : Upper Flammable Limit
C_{up} : Projection of the upper flame surface
C_{fi} : Front intersection between the flame surface and the tube
C_{bi} : Back intersection between the flame surface and the tube
$\dot{m}$: Mass flux [kg.m^{-2}s^{-1}]
S_v^α : Relative velocity sensitivity coefficient
$S_{S_u}^\alpha$: Relative sensitivity coefficient of the burning velocity
V : Volume [m^3]
CR : Compression Ratio
γ : Ratio of specific heats

Part III : Combustion of ammonia in a SI engine

CNG : Compressed Natural Gas
LPG : Liquified Petroleum Gas
LHV : Lower Heating Value [MJ.kg^{-1}]
VAT : Value Added Tax
CFR : Cooperative Fuel Research
MBT : Maximum Brake Torque
SCR : Selective Catalytic Reduction
$BTDC$: Before Top Dead Center
EO : Opening of the exhaust valve
EC : Closure of the exhaust valve
IO : Opening of the intake valve
IC : Closure of the intake valve
TDC : Top Dead Center
BDC : Bottom Dead Center
S : Entropy [J.K^{-1}]
U : Internal energy [J]
θ : Crank angle
$EPDM$: Ethylene Propylene Diene Monomer
$PTFE$: PolyTetraFluoroEthylene
TCD : Thermal Conductivity Detector
Abs : Absorbance
I_{in} : Intensity of the incident light [cd]
I_{out} : Intensity of the transmitted light [cd]
P_e : Effective power [W]
C_e : Effective torque [N.m]
rpm : Speed of rotation [s^{-1}]
η_e : Effective efficiency
$\dot{m}_c$: Fuel mass flow rate [kg.s^{-1}]
W_e : Effective work [J]
$bmep$: Brake mean effective pressure [Pa]
V_c : Engine displacement [m^3]
W_i : Indicated work [J]
$imep$: Indicated mean effective pressure [Pa]
$fmep$: Friction mean effective pressure [Pa]

η_{mec} : Mechanical efficiency
η_i : Indicated efficiency
m_c : Fuel mass admitted during the cycle [kg]
r_{air} : Air volumetric efficiency
m_{air} : Air mass admitted during the cycle [kg]
η_c : Combustion efficiency
Q_i : Real energy liberated by the combustion in the cylinder per cycle [J]
D : Engine bore [m]
u : Piston average linear speed [m.s^{-1}]
s : Number of strokes per cycle
$\frac{A}{F}$: Air fuel ratio
r : Global mixture volumetric efficiency
$\eta_{ti} = \eta$: Thermodynamic efficiency
K_x : Equilibrium constant in terms of mole fractions (units depend on reaction)
K_p : Equilibrium constant in terms of partial pressures (units depend on reaction)
$\Delta_r G^{\circ}{}_{(T)}$: Standard Gibbs free energy of reaction r at a temperature T [J]

Foreword

The problems of oil resources and CO_2 pollutant emissions becoming increasingly alarming, the search for alternatives to liquid fossil fuels is an important concern of our society. Many studies are devoted to the evaluation of the energy efficiency and the environmental impact of alternative fuels. Among these, liquefied petroleum gas, natural compressed gas, oxygenated fuels, biodiesel and hydrogen have been put forward. Even though hydrogen has been recognized as a promising fuel, implementing a global hydrogen-based economy is at present a non-feasible approach unless a suitable storage medium could be found [2]. The hydrogen low energy density is perhaps one of the greatest barriers to the implementation of hydrogen fueled vehicles. Furthermore, large investments are required to develop a hydrogen distribution infrastructure due to safety issues. Hydrogen is volatile and has a low flash point; therefore it presents a danger of explosion when associated with air. To bypass such difficulties, the use of ammonia in a modified spark ignition (SI) engine has been suggested. Since hydrogen must still be produced to obtain ammonia in large amount, it can be seen as a hydrogen vector. Similar to hydrogen, ammonia can be used as a clean energy carrier and storage medium because it can potentially be burned in an environmentally benign way, exhausting only water, nitrogen and a few quantity of nitrogen oxides.

Ammonia (NH_3) is a colorless gas, alkaline at standard conditions of pressure and temperature, with a characteristic pungent odor [3, 4]. Basic physical properties of this molecule are presented in the table below [5, 6].

Liquid Phase		
Vapor pressure (294 K)	8.88	bar
Liquid density (1 atm @ boiling point)	682	kg/m^3
Boiling point @ 1 atm	239.5	K
Liquid/gas equivalent (1 atm @ 288 K)	947	vol/vol
Latent heat of vaporization (1 atm @ boiling point)	1371.2	kJ/kg
Critical temperature	405.4	K
Critical pressure	112.8	bar
Gas Phase		
Gas density (1 atm @ boiling point)	0.86	kg/m^3
Gas density (1 atm @ 288 K)	0.73	kg/m^3
Compressibility (Z) (1 atm @ 288 K)	0.9929	
Specific gravity (air=1) (1 atm @ 293 K)	0.597	
Specific volume (1 atm @ 293 K)	1.411	m^3/kg
Viscosity (1 atm @ 273 K)	0.000098	poise
Heat capacity at cst pressure (C_p) (1 atm @ 288 K)	0.037	kJ/(mol.K)
Heat capacity at cst volume (C_v) (1 atm @ 288 K)	0.028	kJ/(mol.K)
Thermal conductivity (1 atm @ 273 K)	22.19	mW/(mK)
Miscellaneous		
Molecular weight	17.03	g/mol
Water solubility (1 atm @ 273 K)	862	vol/vol
Autoignition temperature	903	K
Lower flammable limit in air	15%	by volume
Upper flammable limit in air	28%	by volume
Octane rating	110	
Lower heating value	18.65	MJ/kg

Ammonia is derived, in its natural state, from the biological degradation of the nitrogenous matter contained in the organic waste or the soil [3, 7] and plays an important role in the nature nitrogen cycle [8]. The natural formation of ammonia represents only a small part of the global quantity of ammonia produced in the world. In the industry, ammonia is obtained by the catalytic reaction of nitrogen and hydrogen. Although process technology has been improved over the years, the basic chemistry is identical to the process developed by Haber and Bosch in the early 20^{th} century:

$$N_2\ (g) + 3\ H_2\ (g) \rightarrow 2\ NH_3\ (g)\ (\Delta H^0_{298} = \text{-}92{,}2\ \text{kJ/mole}).$$

The reaction is typically carried out over iron catalysts at temperatures around 400-600°C and pressures ranging around 200 atmospheres. Ammonia is obtained anhydrous, at -33°C, and stored at this temperature under atmospheric pressure. In practice, ammonia synthesis is usually coupled with hydrogen production to increase efficiency. The hydrogen is typically produced from natural gas or other hydrocarbons by steam reforming, but it can also be produced from water electrolysis ($\approx 4\%$ of the total H_2 production). The steam reforming process for methane is:

$$CH_4 + H_2O \rightarrow CO + 3\ H_2\ (\Delta H^0_{298K} = +\ 206\ \text{kJ})$$

favored at elevated temperature, low pressure and with a rhodium catalyst, followed by

$$CO + H_2O \rightarrow CO_2 + H_2\ (\Delta H^0_{298K} = \text{-}\ 41\ \text{kJ})$$

favored at low temperature and with a platinum catalyst.
The global reaction $CH_4 + 2\ H_2O \rightarrow CO_2 + 4\ H_2$ ($\Delta H^0_{298K} = +\ 165$ kJ) is thus endothermic. World production of ammonia in 2008 was around 136 million tons [9]. Main producers are China (44.6Mt), Europe (15Mt), India (11Mt), Russia (11Mt) and the United States of America (8.2 Mt).

Fertilizer production represents almost 90% of the use of ammonia. This latter is also used to produce plastics, nitric acid, explosives, and for refrigerant purposes [10, 11]. From its fertilizer use in United States, approximately 1 million of farms have access to anhydrous ammonia. Distribution infrastructures already exist to provide 4 millions tons of ammonia to those farms as a nitrogen supplement for soil [12].

There are significant barriers associated with the use of ammonia as a fuel. First and foremost is the safety hazard associated with ammonia. Ammonia is a poisonous gas with an OSHA (Occupational Safety and Health Administration) exposure limit of 50 ppm [5]. Its health effects are summarized in the table below. Nevertheless, ammonia is a commonly used industrial and agricultural chemical and can be handled safely.

Effect	**NH_3 concentration in air (by volume)**
Least perceptible odor	5 ppm
Readily detectable odor	20-50 ppm
No discomfort or impairment of health for prolonged exposure	50-100 ppm
General discomfort and eye tearing, no lasting effect on short exposure	150-200 ppm
Severe irritation of eyes, ears, nose and throat, no lasting effect on short exposure	400-700 ppm
Coughing, bronchial spasms	1700 ppm
Dangerous, less than 1/2 hour exposure may be fatal	2000-3000 ppm
Serious edema, strangulation, asphyxia, rapidly fatal	5000-10000 ppm
Immediately fatal	10000 ppm (1%)

Furthermore, ammonia is corrosive for several metals as brass or copper. Its handling requires the use of appropriate metals like aluminum, ferritic or stainless steels. Plastics or elastomers have also to be correctly selected [6].

The use of ammonia as an alternative to fossil fuels raises the question of the energy balance of the conversion of natural gas into ammonia by opposition to the direct use of natural gas in engines. This comparison is presented below together with the same energy balance for the use of hydrogen or methanol produced in both cases from natural gas.

In general, an energy balance must take into account the several aspects linked to the production and the use of a fuel [13]. It must therefore consider the

following parts:

- The **production**, taking into account the energy cost of the production or extraction of the feedstock.

- The **transport**, which considers the energy needed to transport feedstocks to the transformation site and to transport the transformed material to the distribution site.

- The **transformation** process considering the global energy requirement of the feedstock conversion into an adapted vector for the envisaged use (in the case of this study, a use in an on-board engine).

- The **distribution**, in which the energy needed for the distribution of the final product to the consumers is considered.

- The **use** of the energy vector which considers the potential energy that can be recuperated when using the energy vector (in this case, the lower heating value, LHV, of the fuel).

Carrying out such an energy balance is not obvious. Assumptions that are made in conversion, storage, transport and distribution processes in each cases must be well-defined. The aim of this short energy balance overview is to compare the several envisaged possibilities. Several simplifications have thus been made. The first one is to neglect the energetic cost of the feedstock production. Indeed, since currently hydrogen as well as ammonia or methanol are formed from natural gas, the production part of the feedstock is identical for the four proposed energetic vectors. The second assumption is to remove the transport energetic costs from the balance. Those ones are considered to be similar for the several energy vectors and negligible compared to the feedstock transformation costs. The same is assumed for the distribution costs. This is even more justified by the assumptions made in the transformation energetic costs and presented below.

- For direct use of natural gas, the energetic cost of gas compression until 350 bars is considered to represent 2 to 4% of the LHV energetic content of the gas.

- For ammonia, the fabrication process is depicted in the diagram below [14]. The ammonia is obtained liquid at room temperature under 10 bars. The total energy requirement of the process is 28.8-31.5 GJ per ton of NH_3 for a stand-alone plant with no energy export and no other import than feedstock and energy [14].

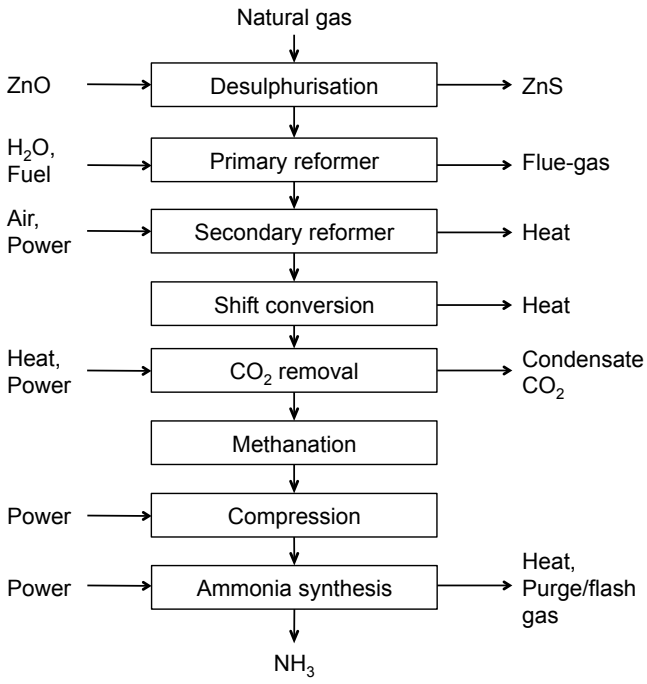

- For hydrogen, the energetic cost of the compression or liquefaction process is added to the energetic cost of the steam reforming process presented in the diagram below [15]. The hydrogen production process energetic efficiency is around 69 to 83% [15–17]. The compression process at 350 bars requires 8 to 15% of energy in terms of hydrogen LHV [17]. The liquefaction process is quite more energy expensive and requires 25 to 40% of the energy content in terms of hydrogen LHV [17].

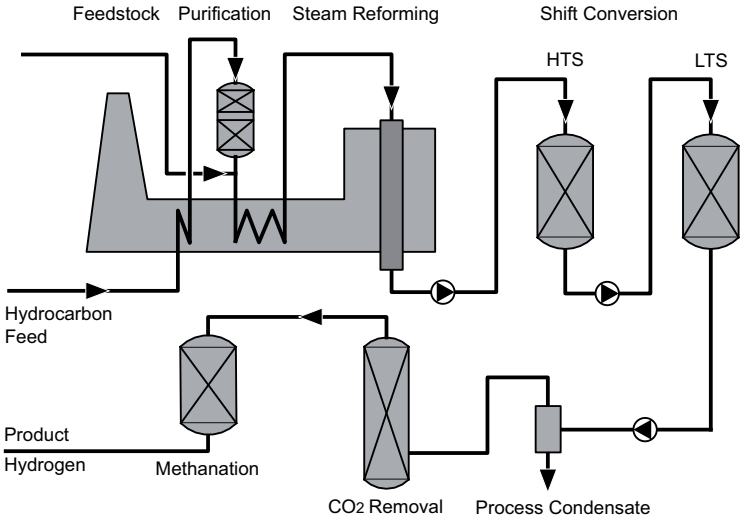

- Finally, for methanol, the production process is presented in the diagram below [18]. The total energy requirement of the process is 30-35 GJ per ton of CH_3OH for a stand-alone plant with no energy export and no other import than feedstock and energy [18, 19].

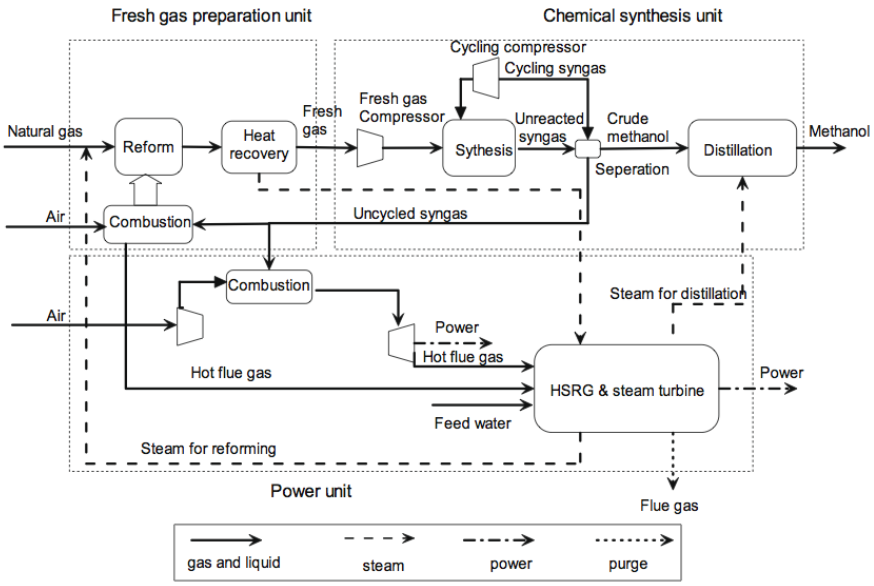

This allows thus to obtain for each energy vector the yield of the processes required to obtain a fuel that can be stored in a vehicle tank. Those ones are presented in the table below.

Energetic vector	**Energetic yield in term of LHV**
Compressed natural gas	96 - 98%
Compressed ammonia	59 - 65%
Compressed hydrogen	60 - 75%
Liquid hydrogen	41 - 62%
Methanol	57 - 65%

Excepted for liquified hydrogen, the very close values of the ammonia, compressed hydrogen and methanol energetic yields suggest on the one hand that the use of ammonia as an alternative to fossil fuels can be envisaged and on the other hand that a more global and detailed study considering the energetic costs of transport and distribution of the several suggested alternatives is needed. Such a study must also take into account the environmental aspects and consider the non-polluting ways of hydrogen, ammonia and methanol production by producing hydrogen from electrolysis and methanol from biomass or CO_2 for example. It is obvious that only those environmental considerations can tip the balance toward the use of an alternative fuel in place of the direct use of natural gas in an engine.

The successful application of ammonia as an alternative transportation fuel should be based on a detailed understanding of its combustion characteristics. The main objective of this thesis is thus the study of the ammonia combustion reaction in several conditions of pressure and temperature :

$$2\ NH_3 + \tfrac{3}{2}\ (O_2 + 3.76\ N_2) \rightarrow \dots$$

The first part of this thesis, devoted to a low pressure ($\pm$ 50 mbar) ammonia flames structure study, allows a more fundamental investigation of the ammonia consumption and products formation pathways. The kinetic of ammonia at low pressure has naturally already been studied in the past but some dark points remain concerning the formation and consumption pathways of some intermediates such as NH_2 and N_2O. An experimental investigation will be the opportunity of a discussion on the individual impact of several initial parameters (initial hydrogen content, equivalence ratio, pressure) on species

concentrations and on kinetic reaction pathways. Then, the elaboration of a kinetic mechanism able to reproduce the experimentally observed phenomena will be the main objective of this first part.

In **the second part** of this thesis, an ammonia laminar burning velocity study allows to investigate the kinetic of ammonia under atmospheric pressure. Even if ammonia flame speed has been studied in the past by several experimental methods, the investigated flames were in most cases pure ammonia-oxygen flames or with only small dilutions. Because of its low value, the laminar flame speed of ammonia in air is to date still unknown and in that way this part makes a significant contribution in the field of ammonia combustion research. The influence of the equivalence ratio and dilution on ammonia laminar flame speed will be experimentally and numerically investigated. The kinetic mechanism established at low pressure in the first part will be validated at atmospheric pressure thanks to those laminar flame speeds. Finally, using this kinetic model, other numerical simulations will be performed in order to analyze the influence of a lower and a higher pressure on the laminar flame speed. The variation of the laminar burning velocity with the equivalence ratio, the initial hydrogen percentage and the dilution for several sub-atmospheric pressures will be studied and the kinetic of ammonia combustion under pressure and temperature conditions encountered in spark ignition engines will be analyzed.

This leads to **the third part** of this thesis which investigates experimentally the combustion of ammonia in a spark ignition engine. Ammonia combustion in spark ignition engines has been well investigated these last years but always with an additive to promote the reaction. The use of ammonia as envisioned in this work has thus never been investigated to the best of our knowledge. The effects of the compression ratio, the spark timing and the equivalence ratio on the exhaust gases composition and the engine performances are analyzed. This study presents a double interest, on the one hand because it concerns the study of a low flame speed fuel behavior in a spark ignition engine and on the other hand because the use of such a fuel allows high compression ratios while spark ignition is used achieving thus higher yields than expected and providing therefore an original aspect to the research.

Part I

Flame Structure Study

Introduction

The global study of ammonia combustion envisaged in this work begins with a fundamental first part which concerns ammonia combustion at low pressure. In this first part, the detailed chemical processes which are encountered during the ammonia combustion are analyzed in details in order to understand the way ammonia is decomposed and, maybe more importantly, the way the burned gases are formed. The elaboration of a kinetic mechanism able to reproduce these phenomena is the main objective of this first part. The mechanism is then used to study the combustion of ammonia in more practical conditions such as the use of NH_3 in spark ignition engine conditions.

The ammonia combustion is therefore investigated experimentally and numerically at low pressure for ammonia-hydrogen-oxygen-argon (NH_3/ H_2/O_2/Ar) flames with several initial hydrogen contents, equivalence ratios, and at several pressures. After a review of the literature in order to identify the state of the art in the ammonia combustion area and to present the major nitrogen oxides formation and consumption pathways (**Chapter 1**), the experimental methods used to study the ammonia flames are presented in a second chapter (**Chapter 2**). Then, in a third chapter (**Chapter 3**), the software used to perform numerical simulation of the flames is described succintly before looking more deeply to the several ammonia combustion kinetic mechanisms available in the literature. Since none of those allow to reproduce satisfactorily the experiments performed, an improved mechanism is established before being reduced in order to allow simulations in more practical cases, such as CFD[1] codes where the fluid mechanics aspects must also be taken into account. The detailed

[1]Computational Fluid Dynamics

kinetic study is also the opportunity to understand the kinetic pathways involved in ammonia combustion and in the exhaust gases formation. Finally the experimental measurements and the numerical results obtained with the *reduced* ammonia mechanism are compared and discussed in a fourth chapter (**Chapter 4**). The ammonia flames which are investigated in this first part are low pressure (around 50 mbar) and argon diluted flames, in opposition with the ones investigated in the second and third part of this work which are atmospheric or higher pressure and air diluted flames. Therefore this fourth chapter is completed with a numerical study of the pressure impact (between 50 mbar and 1 bar) and of the difference between air and argon dilution on kinetics of ammonia combustion.

CHAPTER 1

Literature review on ammonia combustion in flames

In this first literature survey, main experimental and numerical studies performed in the past on ammonia combustion are presented before a short overview on kinetics of nitrogen oxides formation and consumption.

1.1 Ammonia combustion

Since the early 60's, several studies have been performed to investigate experimentally and theoretically the combustion of ammonia. Compositions of the analyzed flames were very wide. Neat rich, lean and stoichiometric ammonia flames burning with air or with oxygen as well as seeded ones with nitrogen monoxide or hydrogen have been the subject of investigations at various pressures. The main interest of those studies was to understand the function of hydrogen and ammonia in the formation and consumption of nitrogen oxides. However, from 1966, the possibility of the use of ammonia as a fuel in engines has been suggested, reinforcing thus the interest of ammonia combustion studies. An overview of these previous studies is proposed below in a chronological way, with a first part on experimental studies and a second one on numerical or theoretical studies.

Among the several experimental studies, the first one is the study realized by Fenimore and Jones [20] who investigated H_2/O_2 and H_2/N_2O flames seeded with ammonia or nitrogen monoxide in order to determine the kinetic impact of each constituent on the kinetic mechanism. Then, Mac Lean and Wagner [21]

analyzed at low pressure the sharp reaction zone of neat ammonia flames containing 40, 57 or 65% of ammonia in oxygen using mass spectrometry and optical spectrophotometry. Pratt and Starkman [22] studied the non-catalytic, gas-phase combustion reaction between ammonia and air in an adiabatic well-stirred reactor. They concluded that the overall reaction rate for ammonia-air combustion in a back-mixed combustion system can be well represented by an Arrhenius equation. However, the activation energy, pre-exponential factor, fuel and oxygen reaction orders obtained experimentally did not agree well with those reported from earlier investigations, giving thus the opportunity to various studies on kinetics of ammonia combustion as described further. Fisher [23] measured NH_3, NH_2, NH and OH concentrations as well as temperatures in three rich flames (ϕ = 1.5, 1.7, 1.8) of ammonia, oxygen and nitrogen at atmospheric pressure. The equilibrium of NH_2 and NH with NH_3 via reactions with OH and H, first steps in ammonia combustion, have been confirmed thanks to this study. In the early 80's, Dasch and Blint [24] investigated the major properties of lean to stoichiometric ammonia-oxygen-nitrogen atmospheric pressure flames to identify the reactions and conditions which control the conversion of the nitrogen contained in NH_3 to NO or N_2. These ammonia flames were investigated over a combustible range of initial dilutions (0.0-0.5 initial N_2 mole fraction) and equivalence ratios (ϕ = 0.5-1.1). They concluded that the conversion of the nitrogen from NH_3 to N_2 is mainly dependent on the NH_2 + NO reactions, the ratio of the products of this reaction (N_2 + H_2O or N_2 + H + OH) together with the reaction rate of NH+O_2, influencing the flame speed. Finally, important experimental studies on ammonia combustion at low pressure were performed by Bian, Vandooren and van Tiggelen. They performed a first study [25] on the determination of the flame structure of a neat ammonia, oxygen flame near stoichiometry using a molecular beam sampling technique coupled with a mass spectrometer. This study allowed to discuss the role of the conversion reactions of NO with NH_2 as well as the formation process of nitrogen monoxide via the reaction

$$NH \ + \ O_2 \ \rightarrow \ NO \ + \ OH \tag{1.1}$$

They also found that the reactions of NH_2 with H and OH radicals are the dominant steps for NH production. Furthermore, rate constants concerning some of these reactions were deduced. They performed a second experimental study [26] in 1990 on several lean and stoichiometric H_2-O_2-Ar premixed flat

flames seeded with NH_3 and/or NO to identify the main paths leading to NO and NO_2 formation. They concluded from a kinetic analysis of the experimental results that the reactions

$$NH_2 + O \rightarrow NO + H_2 \tag{1.2}$$

$$NH + O_2 \rightarrow NO + OH \tag{1.3}$$

are responsible for the nitrogen monoxide production and that the main reaction for nitrous oxide (N_2O) formation is

$$NH + NO \rightarrow N_2O + H \tag{1.4}$$

They also established a simplified kinetic mechanism in order to reproduce their experimental results. This model has then been used to simulate an NH_3-NO-Ar flame [27, 28] and an ammonia seeded rich hydrogen-oxygen-argon flame [29].

Concerning numerical or theoretical studies on kinetic mechanisms of ammonia combustion, a first mechanism of decay of ammonia from an NH_3/O_2 flame has been proposed by Kaskan and Hughes in 1973 [30]. This mechanism contained only 12 chemical species (H_2O, O_2, H_2, O, H, OH, N_2, NH_3, NH_2, NH, N and NO) and 26 elementary reactions and had as main objective to reproduce the rates of change of [NH_3], [NO] and [NH]. They concluded that the ammonia decay occurs through the combination of one set of reversible reactions that convert the various NH_i (i = 0-3) into each other, and another set of irreversible reactions that remove one or more of the NH_i permanently. Even if this mechanism was not sufficient to reproduce correctly all the phenomenons observed during ammonia combustion (for example, the model did not take into account important species like HNO or N_2O) it can be seen as a first interpretation of the ammonia combustion.
The first complete mechanism for ammonia combustion has been proposed by Miller et al. [31] and is based on several burner-stabilized and freely propagating NH_3/O_2 and $NH_3/H_2/O_2$ flames. The agreement on concentration between theory and experiments was generally good, excepted for very rich flames where it appeared that the kinetic model was missing important pyrolysis steps. Nevertheless, the important NO and N_2 formation reactions were identified as being in lean flames the production of nitrogen monoxide through the nitroxyl

(HNO) intermediate, itself formed either by the reactions of NH_2+O, NH+OH or NH+O_2. The conversion of NO in N_2 in these lean flames is supposed to occur by reaction with NH_2 or NH, forming NNH or N_2O as intermediates. Under rich conditions, NH_2 and NH were supposed to be rapidly converted to nitrogen atoms and the extended Zeldovich mechanism [32] was considered to become responsible for NO formation and the conversion of NO to N_2.

In order to complete this Miller et al. mechanism [31], ammonia combustion has then been investigated in other conditions of pressure and temperature. Dean et al. [33] analyzed three ammonia flames burning at atmospheric pressure. They highlighted the importance of reactions between various NH_i (i=1,2) species to form N-N bonds. The N_2H_j (j=1-3) species could then lose H atoms via dissociation to ultimately form N_2. Salimian et al. [34] studied ammonia oxidation, using N_2O as a thermal source of O atoms, in a shock tube in the temperature range of 1600-2100 K. They observed particularly reactions involving the HNO radical, which was supposed to be primarily produced through the reaction of O atoms with NH_2, concluding that those one were the major NO producing paths. The reactions of N and NH_2 with NO were considered to be the important NO removing steps. They also concluded that, under rich conditions, NH_i-NH_i interactions play a critical role in the fast removal of ammonia and production of N_2 through non-NO paths.

In 1989, Miller proposed an improved version of its mechanism with Bowman [35] focusing on nitrogen oxides formation, considering both thermal and prompt NO as well as fuel nitrogen conversion, thermal De-NO_x and RAPRENO$_x$ (Rapid Reduction of NO_x) processes. NO_2 and N_2O formation and removal processes were also considered.

This improved Miller mechanism [35] has been used by Davidson et al. [36] as a starting point to elaborate a pyrolysis mechanism for ammonia. Measurements of some NH reactions rates [37–39] which provided more confidence in the NH_2 and NH consumption reactions have been included. Even if this model presents ammonia degradation in conditions very different of combustion, some of its reactions and associated rate constants can be of particular interest.

Based on the Bian et al. model [26] elaborated thanks to their experiments and focused on the formation of NO and N_2O and completed by several H_2/O_2 mechanisms, Vandooren et al. [28, 29, 40] have elaborated a complete mecha-

nism for ammonia combustion providing valuable data on the reactions:

$$NH_2 + NO \rightarrow N_2 + H_2O \quad (1.5)$$

$$N_2H + OH \quad (1.6)$$

$$N_2 + H + OH \quad (1.7)$$

$$N_2O + H_2 \quad (1.8)$$

They deduced the branching ratio, $\beta = \mathrm{k}_{N_2+H+OH}/\mathrm{k}_{products}$, this one being a factor determining the operational conditions of the DeNO_x process. Furthermore they concluded that reaction (1.7) plays an essential role on the burning abilities of NH_3/NO mixtures by providing the essential hydrogen atoms and hydroxyl radicals for the primary attack of NH_3.

Starting with the Miller [35] and Vandooren [29] mechanisms, Lindstedt et al. [41] elaborated a reaction mechanism able of satisfactory predictions for a wide range of flat laminar premixed $NH_3/H_2/O_2$ and NH_3/O_2 flames. They found that the relative significance of the different NO formation channels depends entirely on the flame conditions: (a) reaction of NH_2 + O is found to be significant in all flames, (b) reaction NH + OH becomes important in neat ammonia flames, (c) the Zeldovich mechanism [32] becomes more and more important with increasing fuel concentrations in hydrogen flames with ammonia and ammonia flames with nitrogen monoxide. They concluded also that the conversion of NO in nitrogen is dominated by reactions involving the NH_2 and N radicals with NH providing a secondary path. Finally, they fixed the major NO conversion path as the reaction NO + NH_2 in neat ammonia and doped lean hydrogen flames and as the reaction NO + N in doped stoichiometric and rich hydrogen flames.

Other kinetic models which can be considered for ammonia combustion are those who were developed for methane or natural gas combustion but which contained also nitrogenous species in order to predict nitrogen oxides in the exhaust gases. The Gas Research Institute mechanism (GRI-mech) [42] is an example of such mechanisms and is an optimized kinetic scheme designed to model natural gas combustion, including NO formation and re-burn chemistry. Another example is the San Diego mechanism [43] which has been designed to focus on conditions relevant to flames, high temperature ignition and detonations. It was derived by beginning with simple chemical systems such as methane then proceeding gradually to more complex systems until n-heptane.

In these approaches, the numbers of species and reactions were kept to the minimum needed to describe the systems and phenomena addressed, thereby minimizing as much as possible the uncertainties in the rate parameters employed. The philosophy thus differs from that underlying a number of other databases, many of which seek completeness, attempting to include all potentially relevant elementary steps. Glarborg et al. [44] proposed also such a mechanism.They performed an experimental investigation of methane oxidation in the presence of NO and NO_2 in an isothermal plug-flow reactor at 750-1250K. Thanks to these experiments and based on a previously proposed reaction set [45], they suggested a complete low temperature oxidation mechanism for methane. However, they investigated also the specific part of this mechanism for ammonia oxidation under fuel rich conditions and moderate temperatures [46]. Such a study, performed at low temperature compared to combustion in flames, promoted the reaction path $NH_3 \rightarrow NH_2 \rightarrow N_2$ (directly or via NNH), rather than the sequence $NH_3 \rightarrow NH_2 \rightarrow NH \rightarrow N$ important in flames. They concluded that the major conversion of fuel-N species to N_2 occurs by reaction of amine radicals with NO, in particular NH_2 + NO. Finally, a more appropriated mechanism is the one proposed by Konnov et al. [1] developed for the combustion of small hydrocarbons but for which a detailed N/H reaction mechanism has been developed [47] and validated in comparison with experimental data for ammonia pyrolysis in shock waves [36]. They shown that incorporation of the reactions with N_2H_3 and N_2H_4 into the mechanism significantly influenced calculated rise-time and peak concentrations of the NH and NH_2 radicals. However, ammonia pyrolysis in shock waves does not occurs in same pressure and temperature conditions as ammonia combustion in flames.

In order to bring additional information to these complete mechanisms, several studies have been performed on specific reaction pathways and associated rate constants. Accuracy of the theoretical results depends mainly on the method used to obtained them. For example, the following reactions have been studied:

- $NH_2 + O$ investigated by a laser spectroscopy technique by Lozovsky et al. [48]

- NH_2 + *radicals* (NH_2, *NH, O)* studied in discharge flow system with laser magnetic resonance, electron spin resonance and laser induced fluorescence detection methods by Dransfeld et al. [39]

- $NH_2 + NO \rightarrow$ *products* and $NH + NO \rightarrow$ *products* studied theoretically by Melius and Binkley [49], using the quantum chemical method Bond Additivity Corrections with fourth order Moller-Plesset perturbation theory (BAC-MP4) which provides accurate thermochemical molecular heats of formation and thermodynamic partition functions. The results indicated that the NH_2 + NO reaction can form either N_2 + H_2O or NNH + OH and that for the reaction NH + NO the favored products should be H + N_2O rather than N_2 + OH. The branching fraction of the NH_2 + NO reactions has been determined in the temperature range 1210-1370K from flow reactor experiments on the $NH_3/NO/O_2$ system by Glarborg et al.[45]. The one for the NH + NO reactions, together with the associated rate constants has been calculated by Simonson et al.[50] using the Rice-Ramsperger-Kassel-Marcus (RRKM) theory. The potential energy surface of the reaction NH_2 + NO $\rightarrow$ H_2 +N_2O has then been studied at several high levels of ab initio molecular orbital theory by Baker and Su [51] giving useful information on the reaction barrier for this path.

- $NH_3 + OH \rightarrow NH_2 + H_2O$ investigated at low pressure and under high temperature by Zabielski and Seery [52] in CH_4/O_2/Ar flames seeded with NH_3 using a molecular beam sampling mass spectrometer to obtain NH_3 concentration profiles and determining the net rate of NH_3 loss rate with correction for the reaction NH_3 + O $\rightarrow$ NH_2 + OH using the measured values of O and the rate constant value given by Salimian et al. [53] for this reaction.

- *NH + NO, NO_2* studied using laser induced fluorescence by Harrison et al. [54] leading to a mechanism involving an intermediate HNNO or $HNNO_2$ complex.

- *NH_2 + HO_2, O_2, O* investigated by energized complex quantum Rice-Ramsperger-Kassel analysis by Bozzelli and Dean [55].

- *NH_3 + H → NH_2 + H_2* for which the temperature dependence of the rate coefficients has been measured by the high-temperature photochemistry technique by Ko et al. [56].

- *NH + NO, O_2* studied by Miller and Melius [57] using potential energy surface information from BAC-MP4 calculations and statistical dynamical methods. They determined the branching fraction for the NH + NO → N_2 + OH or N_2O + H reactions and the rate coefficients of the two-channel process NH + O_2 → HNO + O or NO + OH.

- *NH_2 + NH_2 → N_2H_2 + H_2* which has been experimentally investigated by Stothard et al. [58] measuring NH_2 profiles in a discharge flow reactor at ambient temperature and low pressure by monitoring reactants and products with an electron impact mass spectrometer.

- *H_2 + NO, NH_2 + O, NH + OH* and *H + HNO*, i.e. reactions occurring on the multichannel lowest doublet potential energy surface of the [H_2NO] system containing H_2NO, HNOH and NOH_2 intermediates, probed using an unrestricted coupled-cluster formalism by Sumathi et al. [59]. The energetic and molecular parameters derived from this study were then used to compute the apparent rate constant of the different competitive channels.

- *HNO + HNO* and *HNO + NO* investigated by intracavity laser spectroscopy by Cheskis et al. [60]

- *HNO + H,OH* theoretically investigated by Nguyen et al.[61] using ab initio calculations. They deduced the classical energy barrier for the H + HNO $\rightarrow$ H_2 + NO as 0.5 kcal/mol and the reaction path of the HNO + OH as OH + HNO $\rightarrow$ HNO(OH)-complex $\rightarrow$ Transition State $\rightarrow$ NO(H_2O)-complex $\rightarrow$ H_2O + NO with no energy barrier.

The combustion of ammonia has thus already been fundamentally investigated in the past but only few studies correspond to the ammonia flames composition envisioned in this work, i.e., ammonia-air flames around stoichiometric conditions as those presumed to occur in spark ignition engines. The kinetic mechanisms suggested to reproduce ammonia combustion will thus have to be tested and eventually improved in order to predict correctly ammonia consumption and exhaust gases composition in such conditions.

1.2 Nitrogen oxides

The only three nitrogen oxides that can be isolated at room temperature are nitrogen monoxide (NO), nitrous oxide (N_2O) and nitrogen dioxide (NO_2). Since those ones are the only pollutants produced during ammonia combustion, a short overview of their production and consumption in ammonia flames is presented below, based on some of the previously presented experimental and theoretical studies [20, 21, 25, 26, 28, 35, 36, 47, 62–64].

Nitrogen monoxide is formed in ammonia flames by two main paths:

The thermal-NO produced from the atmospheric nitrogen.
The thermal-NO formation pathway is the Zeldovich [32] mechanism. He has noted that the speed of nitrogen monoxide formation is much lower than the one of the combustion products and that mainly NO is produced in the burned gases where the temperature is the highest. Zeldovich deduced therefore that the nitrogen monoxide formation pathway is isolated of the main combustion process. The NO formation speed depends on the highly endothermic reaction

$$O + N_2 \rightarrow NO + N \qquad \Delta H_0^{298K} = +313.85\text{kJ/mole} \tag{1.9}$$

Then, atomic nitrogen reacts with molecular oxygen

$$N + O_2 \rightarrow NO + O \qquad \Delta H_0^{298K} = -133.21\text{kJ/mole} \tag{1.10}$$

And with hydroxyl radical according to

$$N + OH \rightarrow NO + H \qquad \Delta H_0^{298K} = -203.91\text{kJ/mole} \tag{1.11}$$

A lot of studies confirmed the validity of the Zeldovich mechanism.

The fuel-NO produced from nitrogenous fuels.
The formation of fuel-NO is highly faster than the thermal one, especially since diluted ammonia flames have a relatively low temperature leading to few thermal-NO formation. Furthermore, the quantity of nitrogen monoxide produced during combustion processes is superior to the one predicted by the thermodynamic equilibrium of the investigated system. Concerning its formation mechanism in an H/O/N system, it is generally schematized as:

$$NH_i + OX \rightarrow NO + H_iX \tag{1.12}$$

where OX is an oxygenated species and NH_i a radical. Nitrogen monoxide precursors in ammonia flames are thus nitrogenous radicals (mainly NH_2 and NH) and their formation occurs in the flame front.

There are two main strategies used to reduce nitrogen monoxide emissions during combustion processes; either the modification of the combustion conditions (reduction of the oxygen concentration, reduction of the temperature) or the further treatment of the exhaust gases. In this last case, reaction

$$NH_2 + NO \rightarrow N_2 + H_2O \tag{1.13}$$

is responsible for nitrogen monoxide to nitrogen conversion. The NH_2 radical is obtained in the flame by the following hydrogen abstraction reactions:

$$NH_3 + H\ (OH, O) \rightarrow NH_2 + H_2\ (H_2O, OH) \tag{1.14}$$

Thanks to this reaction with NH_2 (1.13), nitrogen monoxide concentration in the burned gases of ammonia flames is largely smaller than the one presumed

to occur.

Nitrous oxide is also formed in ammonia flames. It is not present in the exhaust gases of stoichiometric flames but remains in small concentration, approximately one tenth of the NO one, in exhaust gases of lean flames. Following reactions are responsible for its formation and consumption :

$$NH + NO \rightarrow N_2O + H \tag{1.15}$$

$$N_2O + H \rightarrow N_2 + OH \tag{1.16}$$

Nitrogen dioxide is in equilibrium with nitrogen monoxide following reactions

$$NO + O(HO_2) \rightarrow NO_2\ (+OH) \tag{1.17}$$

$$NO_2 + H \rightarrow NO + OH \tag{1.18}$$

In actual combustion processes, the above two reactions occur simultaneously. Based on the equilibrium concentrations, any NO formed at room temperature is converted to NO_2. At higher temperatures, the concentration of NO exceeds the concentration of NO_2. At conventional combustion temperatures (> 2500 K) appreciable amounts of NO formation is possible, with negligible amounts of NO_2 present.
NO_2 is also formed in lower atmosphere during the ozone formation performed by the reaction of NO with unburned hydrocarbons ($RO_2^{\bullet}$) in presence of oxygen and sunlight ($h\nu$) [65] :

$$NO + RO_2^{\bullet} \rightarrow NO_2 + RO^{\bullet} \tag{1.19}$$

$$NO_2 + h\nu \rightarrow NO + O^{(3\rho)} \tag{1.20}$$

$$O_2 + O^{(3\rho)} \rightarrow O_3 \tag{1.21}$$

These reactions are however not applicable to ammonia combustion since there is no unburned hydrocarbons.

Formation and consumption pathways of nitrogen oxides in ammonia flames are thus relatively well-known. However, kinetic parameters of some important reactions require to be validated against experimental data.

CHAPTER 2

Experimental methods

The aim of this chapter is to give an overview of the experimental techniques used to obtain flame structures. A presentation of the initial composition and of the operating conditions will be followed by a detailed description of the equipment, an explanation of the calibration method to convert signal intensities to mole fractions and a discussion of the measure of temperature profiles.

2.1 Presentation of the analyzed flames

Eight ammonia-hydrogen-oxygen-argon flames close to the stoichiometry with different initial composition or operating conditions have been investigated as illustrated in Table 2.1 where X_i are mole fractions.

	X_{NH_3}	X_{H_2}	X_{O_2}	X_{Ar}	V_0	ϕ	p
I	0.2548	0.0512	0.2129	0.4811	35.1	1.02	60
II	0.2400	0.0749	0.2132	0.4719	42.1	1.02	50
III	0.2247	0.1003	0.2132	0.4618	42.1	1.03	50
IV	0.2074	0.1259	0.2137	0.4529	42.0	1.02	50
V	0.2243	0.1001	0.2443	0.4312	42.2	0.89	50
VI	0.2226	0.0993	0.2008	0.4773	42.5	1.08	50
VII	0.2548	0.0512	0.2129	0.4811	23.4	1.02	90
VIII	0.2548	0.0512	0.2129	0.4811	17.6	1.02	120

Table 2.1: Flames inlet composition (mole fractions) and initial conditions. (V_0 = inlet flow $[cm.s^{-1}]$; ϕ = equivalence ratio ; p = pressure [mbar]).

If the initial composition of the fresh gases corresponds to the stoichiometric equation of the complete combustion reaction, the flame is named stoichiometric ($\phi = 1$). To describe the difference of the reactive mixture from this stoichiometry, the concept of the equivalence ratio is used and can be defined by the equation (2.1):

$$\phi = \frac{(X_{combustible}/X_{oxydizer})_{mixture}}{(X_{combustible}/X_{oxydizer})_{stoichiometry}} \tag{2.1}$$

A flame with an equivalence ratio above one is qualified as a rich flame while the one with an equivalence ratio smaller than one is qualified as a lean flame. Since in this work, a few quantity of ammonia has been replaced by hydrogen, the calculation of the equivalence ratio must take into account these two combustibles. The stoichiometric complete combustion of ammonia follows the equation:

$$2\ NH_3\ +\ \frac{3}{2}\ O_2\quad \rightarrow\quad N_2\ +\ 3\ H_2O. \tag{2.2}$$

The ratio $(X_{combustible}/X_{oxydizer})_{stoichiometry}$ is equal to 4/3, lets call us this ratio β. The stoichiometric complete combustion of hydrogen follows the equation:

$$H_2\ +\ \frac{1}{2}\ O_2\quad \rightarrow\quad H_2O. \tag{2.3}$$

The ratio $(X_{combustible}/X_{oxydizer})_{stoichiometry}$ is thus equal to 2, lets call us this ratio α. The equivalence ratio of a mixture with ammonia and hydrogen can thus be written as:

$$\phi\ =\ \frac{\frac{X_{NH_3}}{\beta}\ +\ \frac{X_{H_2}}{\alpha}}{X_{O_2}} \tag{2.4}$$

Flames composition has been chosen to be close to the one occurring in engines. This one is an ammonia air flame near stoichiometry, following the complete combustion equation (2.5)

$$2\ NH_3\ +\ \frac{3}{2}\ O_2\ +\ 5.64\ N_2\quad \rightarrow\quad 6.64\ N_2\ +\ 3\ H_2O \tag{2.5}$$

However, nitrogen has been replaced by argon to follow exclusively the formation of nitrogen from ammonia during the combustion and to better stabilize the flames thanks to the smaller molar heat capacity of argon ($C_{p_{Ar}}$ = 21 J.mole^{-1}.K^{-1} ; $C_{p_{N_2}}$ = 29 J.mole^{-1}.K^{-1}). Furthermore, it has been necessary to add a small quantity of hydrogen since an ammonia flame with such a composition cannot be stabilized at the low pressure applied in this work ($\approx$ 50 mbar). However hydrogen addition is not necessary in spark ignition engines thanks to the much higher pressure. These eight analyzed flames can be categorized in three series: in the first one (flames I–IV) only the initial hydrogen percentage is modified, keeping a constant equivalence ratio. It varies from 5 percent to 12.5 percent. The comparison of these flames will emphasize not only the role of hydrogen on the NO formation but also on the flame speed. In the second set (flames III, V and VI) the equivalence ratio is varied from 0.89 to 1.08. It leads to determine the optimal equivalence ratio condition to minimize NO formation around stoichiometry. Finally in the last set (flames I, VII and VIII) the working pressure is varied. Because of the experimental setup capabilities, a maximum pressure of only 120 mbar has been reached. Naturally, the ammonia flame burning in a spark ignition engine takes place at a pressure much higher than the one chosen in these experiments.

2.2 Molecular beam–mass spectrometer sampling system

As showed in figure 2.1, the experimental setup [66] consists of a molecular beam mass spectrometer system (MBMS) developed to determine the structure of one-dimensional laminar premixed flames burning at low pressure. Gases (NH_3, O_2, H_2 and Ar) arrive premixed in the combustion chamber thanks to an homogenization of the gas fluxes in the burner. The flame is ignited by an electrical arc of about 2 kV created between the burner surface and a retractile electrode facing this one. Once the flat flame is stabilized, the analysis is performed by sampling through a conical quartz nozzle. As the burner can be moved by translation along the axis of the quartz nozzle, sampling can be performed at different distances from the burner: in the preheated zone, in the flame front and in the burned gases region. The pressure decreases through three differentially pumped stages from the combustion chamber (50 mbar) to the mass spectrometer chamber (10^{-7} mbar). This strong pressure gradi-

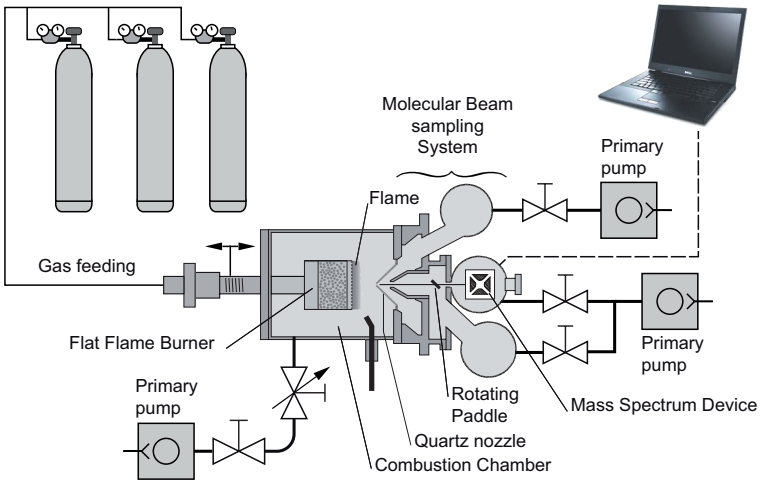

Figure 2.1: Experimental Setup

ent ensures the formation of a molecular beam that freezes the composition of the sample analyzed by the mass spectrometer. The internal energy of the molecules is transformed in kinetic energy. Because the total concentration in the molecular beam is very low, atoms, radicals and stable molecules cannot react together since the probability of collision is very low. Due to the intrusion of the conical probe in the flame, a high degree of stability is needed to avoid disturbances. Indeed its penetration deeply disturbs the flow field of a flame propagating at low burning velocity. The experience thus seeks the appropriate initial composition of the fresh gases and the pressure in the combustion chamber to obtain a stable flat flame, whatever the penetration degree of the probe in the flame is. The stability of the flame is controlled by the constant measurement of the burner temperature thanks to two chromium–alumel thermocouples included in the perforated plate at the burner mouth. One is located at the center, the other at 3 cm from the axis of the burner plate. To perform precise comparisons between ammonia flames belonging to a same series, signal intensities of a given species have been measured almost at the same time and with identical operating conditions. Complete description of the gas feeding system and of the several chambers can be found in appendix A.

2.3 Determination of species concentrations

Since the gas sample taken from the flame by the sampling cone is expanded into a molecular beam, the temperature and density are reduced sufficiently rapidly that all chemical reactions are quenched. In this way, the molecular beam composition includes both stable and unstable species, which remains in the collisionless flow up to the ionization chamber. The mass spectrometer signal therefore consists of electron multiplier current intensity at each ion mass to charge ratio produced from the sample stream in the ionization chamber. Signal intensities of a given species are measured by adjusting the electron beam energy above the ionization potential with an increment depending on the species under investigation in order to prevent fragmentation interferences from other species but also to keep a sufficiently high signal to noise ratio. In the investigated flames, the following 16 species were expected to be detected: NH_3, NH_2, NH, N_2H, N_2, NO, N_2O, HNO, H, H_2, H_2O, HO_2, O, OH, O_2, Ar. Table 2.2 presents the ionization (IP) and working potentials (WP) of these species [67].

Mass	Species	IP (eV)	WP (eV)
1	H	13.6	/
2	H_2	15.4	20
15	NH	13.1	27
16	NH_2	11.4	15.7
16	O	13.6	17
17	NH_3	10.2	13
17	OH	13.2	17.5
18	H_2O	12.6	26
28	N_2	15.6	16.5
29	N_2H	12	19.1
30	NO	9.3	15
31	HNO	10	15
32	O_2	12.1	26
33	HO_2	11.6	26
40	Ar	15.8	26
44	N_2O	12.8	26

Table 2.2: Potential of ionization and work potential

However some difficulties were encountered, disturbing the detection of species. The explanation of the experimental conditions and of these difficulties are presented below.

* The H atom cannot be measured with the mass spectrometer used; the ratio between mass and charge must be greater than two.

* H_2O, O_2, Ar, N_2O : For these four species, there is no other constraint than to work at a potential higher than the ionization one. Therefore the value of 26 eV has been chosen arbitrarily.

* H_2: The fragmentation of H_2O occurring at a potential of 20.7 eV must be avoided, therefore a potential of 20 eV has been chosen.

* NH: To avoid NH_3 fragmentation, occurring at a potential of 17.1 eV a work potential of 16.5 eV had been chosen. However, the NH radical is present in too small quantities to obtain a correct signal and a higher potential must be applied. (27 eV) Unfortunately, in doing so, ammonia split up in this radical, and even when a normalized profile of ammonia is subtracted, it does not give an acceptable result.

* NH_2: In this case too, the working potential was fixed below the fragmentation potential of ammonia at 15.73 eV but, ammonia being present in a such higher quantity, it still disturbed the NH_2 profile. Therefore, a potential of 15.7 eV has been used and an ammonia profile taken at the same potential has been subtracted.

* O: The fragmentation of N_2O (15.31 eV), O_2 (18.8 eV) and H_2O (19 eV) must be avoided. The N_2O contribution being really small and the atomic oxygen signal very low at 15 eV, a working potential of 17 eV has been fixed. However, since O have the same mass as NH_2 but a higher ionization potential, its profile is in any case disturbed by the one of NH_2. To obtain the atomic oxygen profile it is thus necessary to subtract a normalized NH_2 profile. This is unfortunately not possible due to the noise damaging the NH_2 profile. The signal of this species recorded at 17 eV follows exactly the ammonia profile due to the fragmentation giving NH_2 at such a potential. It has thus been concluded that ammonia contributes greatly to the atomic oxygen profile and a normalized ammonia profile has been subtracted but it does not give accurate results due to a low signal to noise ratio.

* $Mass$ 17: Since ammonia and hydroxyl radical have the same mass, precautions must be taken to discriminate the signals of these two species. The ammonia profile can be easily obtained by working at a potential lower than

the ionization potential of OH. However, to obtain the hydroxyl radical profile, the fragmentation of H_2O and the simultaneous ionization of NH_3 have to be taken into account. A working potential of 17.5 eV has thus been chosen and a normalized ammonia profile has been subtracted. However, only mole fractions in the burned gases where ammonia is not present can be measured accurately.
* N_2: A working potential of 16.5 eV is chosen to avoid fragmentation of N_2O occurring at 17.3 eV.
* N_2H: The presence of a nitrogen isotope at mass 29 is the origin of the difficulties to detect this species. This nitrogen isotope being present in a relatively high concentration, a higher potential has been fixed to obtain a better signal and then subtract a normalized nitrogen profile, but the N_2H signal is lost in the background noise and the obtained profile is not accurate enough.
* NO: The fragmentation of N_2O (13.75 eV) and NO_2 (12.34 eV) have to be avoided but for a working potential below 15 eV, the signal obtained is too low, therefore this potential has been chosen and the contributions of N_2O and NO_2 neglected due to very small quantities in comparison to the nitrogen monoxide.
* HNO: The signal obtained for this species is damaged by the presence of the isotope 15 of nitrogen in NO. In the burned gases, the entire signal at the mass 31 is due to this isotope of nitrogen monoxide. To obtain the contribution of HNO only, the profile at mass 31 is taken at the same potential as the one of NO and a normalized nitrogen monoxide profile is subtracted in the burned gases. However the obtained profile cannot be separated from the background noise.
* HO_2: The constrain for this species is the same than for HNO. The HO_2 signal is completely hidden by the oxygen isotope and is therefore not separated from the background noise. ($X_{HO_2} \leq 10^{-5}$) It is thus not possible to obtain an accurate profile of this species.
Table 2.3 presents, as a reminder, the isotopic abundance of the several elements present in the flame.

H	^{1}H	99.985%	N	^{14}N	99.63%	O	^{16}O	99.76%
	^{2}H	0.015%		^{15}N	0.37%		^{17}O	0.037%
							^{18}O	0.204%

Table 2.3: Isotopic abundance

The signal is recorded approximately twenty times for a given position of the burner and the statistical data are calculated to estimate the accuracy of the measurement. Random errors are estimated for each species. They are around 5% for hydrogen, amidogen radical and hydroxyl radical; 3% for ammonia, nitrogen monoxide, and nitrous oxide; and 1% for nitrogen, argon, oxygen, and water.

Finally, to convert the recorded intensity signal to mole fraction, an absolute calibration of species is achieved by direct comparison with the corresponding mole fraction profiles measured in a near stoichiometric ammonia flame studied previously [68]. The mole fraction X_i of a given species is directly linked to the intensity of the signal I_i by a proportional sensitivity factor S_i. Therefore the relation 2.6 can be written for both the flame studied previously and the flames analyzed in this work.

$$I_i = X_i * S_i \tag{2.6}$$

This sensitivity factor (S_i) depends on operational conditions like temperature, pressure and so on... However, since the calibration flame has been reproduced in the same experimental conditions as the analyzed one, it can be considered that the sensitivity factors are identical for a given species and therefore it can be written that:

$$(X_i)_{flame} = \frac{(I_i)_{flame}(X_i)_{ref}}{(I_i)_{ref}} \tag{2.7}$$

where X and I are mole fractions and signal intensities of a species i in the analyzed flame$_{(flame)}$ and in the reference flame$_{(ref)}$ respectively. This reference flame had the following composition:

NH_3: 24%; H_2: 7.5%; O_2: 21.35%; Ar: 47.15%

Dilution = $\alpha = X_{Ar} = 0.4715$

Equivalence ratio = 1.018

This technique is used for the following species: N_2, NO, H_2, H_2O, OH, O_2, NH_3, Ar and N_2O. For the five first species, this calibration is performed in the burned gases, at a distance of 20 mm from the burner. However, for the reactants, thus ammonia and oxygen, it is done in the fresh gases at 1 mm from the burner. For the argon calibration, a complete profile is taken to check the previous one and ensure that they are taken in the same operational conditions. Finally, as N_2O is an intermediate species, the calibration is performed at the distance corresponding to the maximum intensity of the species in the flame.

To calibrate species like NH_2 which is a radical species the comparison with a stable species (NH_3) and the estimation of the effective ionization sections (Q_i) are used:

$$I_i = Q_i * X_i \tag{2.8}$$

$$\frac{I_i}{I_{NH_3}} = \frac{Q_i}{Q_{NH_3}} * \frac{X_i}{X_{NH_3}} \tag{2.9}$$

$$X_i = X_{NH_3} * \frac{Q_{NH_3}}{Q_i} * \frac{I_i}{I_{NH_3}} \tag{2.10}$$

Care has to be taken that the electron impact potential used for each species has the same increment above the ionization potential of each species. The effective ionization sections of these species are 3.54 for ammonia and 2.89 for the amidogen radical [67]. Moreover, the constant mole fluxes from the fresh gases to the burned gases for each element, the normalization for a sum of the mole fractions equals to one all along the flame and the variation of the sensitivity factor with the temperature and the mean molecular weight are taken into account. The following chemical species are thus detected and calibrated:

$$NH_3,\ NH_2,\ NO,\ N_2O,\ N_2,\ H_2,\ H_2O,\ OH,\ O_2,\ Ar.$$

In any experimental procedure which requires the introduction of a physical measurement device into a high–temperature reacting flow there is the possibility of perturbation of the flow properties by the measurement device. In regions of steep concentration gradients, distortion of the profile due to the presence of the conical quartz probe is possible although it is not detectable visually in the flames investigated. Radical species may recombine on the quartz probe, but the major effect of the sampler is to decrease the local temperature. In previous studies using the molecular beam mass spectrometer technique [69, 70], measurements of the rate coefficients of well known reactions such as $CO + OH$ or $H + O_2$ have given good agreement with the accepted values published in the literature. This suggests that the effect of the probe on the concentration of radical species should be minimal.

2.4 Measure of temperature profiles

To obtain the temperature profiles, a Pt/PtRh 10% thermocouple as presented in figure 2.2 is used. Temperature measurements are made at the point of

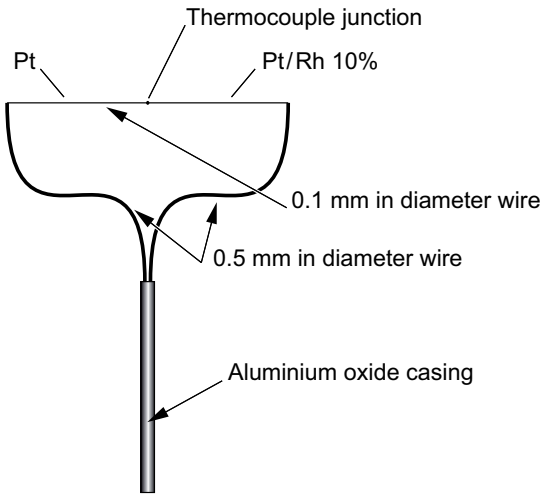

Figure 2.2: Thermocouple

sample collection immediately upstream of the sampling cone orifice. In this way the temperature and composition profiles should be directly comparable and can be modeled assuming a locally one dimensional flow field. The temperature increase produces an electromotive force at the junction of the two alloys of different compositions, force that can be measured and converted to temperature with an appropriate function [71]. To ensure the precision of the measurements, some precautions are taken:
1) The fork and the thermocouple being constituted of platinum, this latter could play a catalytic role in the flame [72]. Indeed, platinum is a catalist for the following reaction:

$$2H^{\bullet} \rightleftharpoons H_2.$$

If this exothermic reaction takes place, the temperature at the junction of the thermocouple will be higher than the real one in the flame. It is thus essential that the thermocouple is covered with an inert coating, which is in this case a Y_2O_3–BeO ceramic coating, to avoid this reaction. A second reason for this coating is the degradation of platinum and rhodium by some chemical

species found in each flame. This degradation decreases the life span of the thermocouple by weakening it and could damage its calibration.
2) The flames studied being one-dimensional, for a given distance from the burner the temperature is independent of the radial position in the flame. The thermocouple has therefore to be placed perpendicularly to the gas flow and thus parallel to the burner mouth plate. Doing this, because of being placed in an isothermal plan, the heat losses due to conduction in the wire because of a temperature gradient can be neglected.
3) The use of a thermocouple as thin as possible is an advantage for several reasons. First of all the spatial resolution is increased, secondly heat losses by radiation are minimized and finally it allows to minimize also the gas flow aerodynamic perturbations.
However, heat losses by radiation can not be totally neglected and they have to be taken into account. Indeed, it produces a decrease of the measured temperature compared to the real temperature of the flame. A correction has to be done to obtain the correct temperature profile. The electric compensation method is used for this purpose [71]. Considering the balance equation between the heat flux received by the thermocouple from the gas and the one lost by the thermocouple to the environment by radiation :

$$\begin{array}{rcl} Convection & & Radiation \\ \beta(T_g - T_c) & = & A(T_c^4 - T_0^4) \\ Where\ \beta = \alpha\pi d & and & A = \varepsilon\sigma\pi d \end{array} \tag{2.11}$$

α : *Heat exchange coefficient* $[W.m^{-2}.K^{-1}]$

d : *Wire diameter* $[m]$

ε : *Emissivity coefficient of the thermocouple*

σ : *Stefan − Boltzman constant* $[5.6998 * 10^{-8}\ W.m^{-2}.K^{-4}]$

T_g : *Gas temperature* $[K]$

T_c : *Thermocouple temperature* $[K]$

T_0 : *Wall temperature of the combustion chamber which absorbs the energy emitted by radiation* $[K]$

To determine the real gas temperature (T_g), a calibration curve has to be realized under high vacuum to link the thermocouple temperature measured in mV (T_c) to the intensity of an alternating current needed to heat it progressively. Under high vacuum, energy losses by thermocouple convection to the gas can be neglected, allowing to write the following equation:

$$(RI^2)_{vacuum} = A(T_c^4 - T_0^4) \tag{2.12}$$

where R is the thermocouple resistance per unit of length and I the intensity of the alternative current applied. The same experiment is then realized once the flame is turned on. The radiation losses are once again compensated by heating the thermocouple thanks to an alternative current. This experience suggests the following relation:

$$(RI^2)_{flame} + \beta(T_g - T_c) = A(T_c^4 - T_0^4). \tag{2.13}$$

These curves are plotted in graph 2.3. It can be seen that the curves realized in the flame (dashed lines) cut the one realized under high vacuum (line) for some value of the applied current.

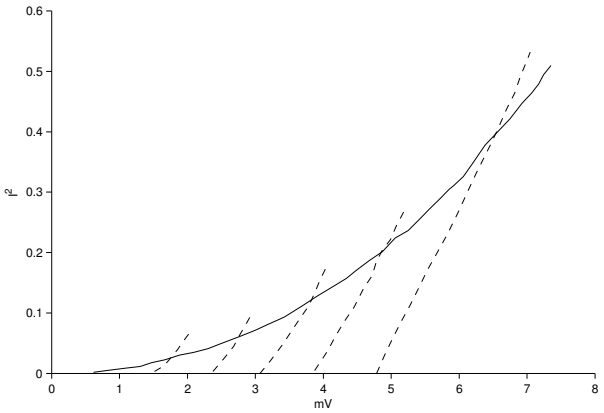

Figure 2.3: Electromotive forces curves of the thermocouple under vacuum and into the flame

And yet, for the intersection points:

$$(RI^2)_{flame} = (RI^2)_{vacuum} \quad (2.14)$$

$$(RI^2)_{flame} = A(T_c^4 - T_0^4) \quad (2.15)$$

$$\beta(T_g - T_c) = 0 \quad (2.16)$$

$$T_g = T_c. \quad (2.17)$$

It can thus be concluded that for the intersection points of the curves, the energy obtained from the alternative current corresponds exactly to the energy lost of the thermocouple by radiation. The real temperature of the flame (T_g) corresponds, for a given distance from the burner, to the abscissa of this intersection point. To realize this electric compensation method it is thus necessary to obtain a high vacuum. During the experiments performed in the laboratory, the vacuum obtained in the combustion chamber is not sufficient to apply directly this method. Therefore, the calibration of the temperature profiles obtained is done thanks to previous results obtained for the same thermocouple as the one used during these experiments [66]. The temperature profile can then finally be obtained by using the correlation between the corrected electromotive force and the temperature corresponding to a Pt/Pt-Rh 10% thermocouple. A random error on temperature measurement of less than 1% is estimated by taking the same profile several times.

Once the temperature profile is obtained it is important to ensure that it has been taken in the same conditions as the mole fractions profiles. According to the investigated flame, a species of which the formation is proportional to the temperature increase is chosen to allow the superposition of the temperature and mole fraction profiles [73]. For the ammonia flame, the temperature increase is proportional to the water mole fraction increase but also to the one of nitrogen. Therefore, the experimental profile is compared with a calculated one by using the water and nitrogen intensities profiles. The temperature profile calculated from the water mole fraction profile is obtained by the following relation (2.18):

$$T_z = [(\frac{(I_{H_2O})_z}{(I_{H_2O})_{max}})(T_{max} - T_0)] + T_0. \quad (2.18)$$

$(I_{H_2O})_z$: Intensity of the water signal measured at a distance z [mV]

$(I_{H_2O})_{max}$: Intensity of the water signal measured in the burned gases [mV]

T_{max} : Temperature in the burned gases [K]

T_z : Temperature at a distance z [K]

T_0 : Wall temperature [K]

Since the experimental and recalculated profiles are perfectly superimposed, it ensures that they have been taken in the same operational conditions. Fig. 2.4 presents the experimental and recalculated profiles with water and nitrogen for flame II.

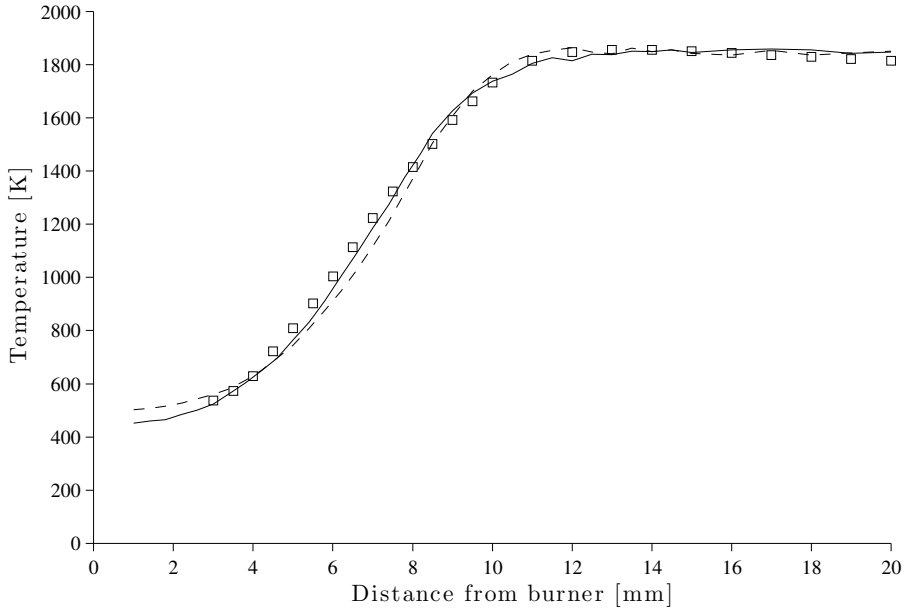

Figure 2.4: Temperature profiles of flame II. Squares: experiments, Line : Reconstructed profile with water concentration, Dashed line: Reconstructed profile with nitrogen concentration.

CHAPTER 3

Numerical simulations

This chapter presents first of all the software used to performed numerical simulation, i.e. Cosilab® [74]. Then, chemical kinetics of ammonia combustion is detailed more deeply by looking to the agreements reached by the kinetic mechanisms available in the literature with the experimental results obtained in this study. An improvement of these mechanisms is consequently proposed followed by a reduction of the improved model in order to fit the requirements of a potential integration of this one in a CFD simulation. This detailed kinetic study will also be the opportunity to understand the kinetic pathways involved in ammonia combustion and in burned gases formation.

3.1 Presentation of Cosilab®

Cosilab [74] is a comprehensive tool for the numerical simulation of a variety of industrially and scientifically relevant, laminar, chemically reactive flows including chemical equilibrium, freely propagating premixed flames and burner-stabilized premixed flames which are of a particular interest in this work. Typically, in Cosilab simulations, detailed mechanisms of gas phase chemical reactions are taken into account. A combustion or reactor problem to be solved with Cosilab is tackled step by step, which are:

* Step 1: Choose the type of flame – or reactor – appropriate to model the specific problem.
* Step 2: Prepare the chemistry input file, i.e., the reaction mechanism.
* Step 3: Acquire the databases of thermodynamic and molecular data.
* Step 4: Prepare a control document. A control document contains both problem–specific and solver–specific data for the Cosilab solvers, such as infor-

mation on the boundary conditions or on the desired accuracy of the numerical solution.
* Step 5: Prepare an initial profiles document or dataset. By definition, a profiles document, or dataset, contains flame or reactor profiles. Prior to a computation, a profiles document is needed to specify initial profiles or initial guesses for the solvers, which – based on them – will obtain an iterative solution of the problem.
* Step 6: Run the solver and post–process the results.

The following sections detail more deeply these steps by presenting important basic quantities and relationships along with governing equations, before looking more deeply to the several input files needed for the simulations.

3.1.1 The appropriate model for the simulations

The numerical simulations performed in this part of the work concern laminar, one–dimensional, burner–stabilized flames. It is thus this model which is chosen in Cosilab [74]. The chemical composition in such systems is variable mainly due to chemical reactions and species mass diffusion. Before presenting the principal governing equations of a one-dimensional, laminar, burner stabilized flame, a brief description of the main notions used to define the composition of a mixture is proposed. Indeed, to quantify the composition of a multicomponent system, various measures of concentration exist such as:
* The mass fractions Y_i, i=1,...,I; where, here and below, I represents the number of chemical species in the system. By definition,

$$\sum_{i=1}^{I} Y_i = 1. \tag{3.1}$$

* The mole fractions X_i, i=1,...,I; by definition,

$$\sum_{i=1}^{I} X_i = 1. \tag{3.2}$$

Mass and mole fractions are related by

$$Y_i = \frac{W_i}{W} X_i, \qquad i = 1, \ldots, I. \tag{3.3}$$

where W_i represents the molecular weight (molar mass) of species i, and W the mixture or mean molecular weight (molar mass), both of them in [kg.mol^{-1}],

$$W = (\sum_{i=1}^{I} \frac{Y_i}{W_i})^{-1} = \sum_{i=1}^{I} X_i W_i. \tag{3.4}$$

* The molar concentrations C_i, i=1,...,I; the sum of all C_i is the molar concentration of the mixture, both of them in [mol.m^{-3}],

$$C = \sum_{i=1}^{I} C_i. \tag{3.5}$$

Mass fractions and molar concentrations are related by

$$C_i = \frac{\rho Y_i}{W_i}, \qquad i = 1, \ldots, I. \tag{3.6}$$

where ρ denotes the density of the mixture.[kg.m^{-3}]
* The partial densities ρ_i, i=1,...,I, [kg.m^{-3}] given by $\rho_i = Y_i \rho$.
* The partial pressures p_i, i=1,...,I, [Pa] given by $p_i = X_i p$; here p denotes the pressure [Pa].
Even if in practical use it is often the mole fractions that are measured, the numerical simulations performed are based, in most cases, on mass fractions.
Generally, to simulate a combustion phenomena, the global form of the mass, momentum, species and energy conservation equations have to be solved. A complete description of these equations has been made by Poinsot and Veynante [75]. The brief description of these equations presented below is limited to the simplified form of those ones corresponding to a one-dimensional, burner stabilized, laminar flame with the hypothesis of a fixed known pressure, meaning that the momentum conservation equation does not need to be solved. The corresponding equation set is therefore composed of:

the mass conservation equation

$$D_m = \rho v A, \tag{3.7}$$

the species conservation equation

$$D_m \frac{\partial Y_i}{\partial x} + \frac{\partial}{\partial x}(\rho A Y_i V_i) - A \dot{\omega}_i W_i = 0 \qquad i = 1, \ldots, I, \tag{3.8}$$

the energy equation

$$D_m \frac{\partial T}{\partial x} - \frac{1}{c_p}\frac{\partial}{\partial x}(\lambda A \frac{\partial T}{\partial x}) + \frac{A}{c_p}\sum_{i=1}^{I} \rho Y_i V_i c_{p_i} \frac{\partial T}{\partial x} + \frac{A}{c_p}\sum_{i=1}^{I} \dot{\omega}_i h_i W_i = 0 \quad (3.9)$$

This equation is generally not solved since it is difficult to define correctly the heat losses. Thus, the experimental temperature profile has to be introduced as an input data.

the ideal-gas equation of state

$$p = \frac{\rho R T}{W}. \quad (3.10)$$

In eq. (3.7) to (3.10), in addition to previously defined symbols, x is the spatial coordinate [m]; D_m the mass flux [kg.s^{-1}]; A the cross section [m^2]; v the gas flow velocity [m.s^{-1}]; c_{p_i} and h_i the constant–pressure heat capacity and specific enthalpy, respectively, of species i [J.kg^{-1}K^{-1}] and [J.kg^{-1}], $\dot{\omega}_i$ the net molar reaction rate of species i per unit of volume [mol.m^{-3}s^{-1}]; c_p the constant pressure heat capacity of the mixture [J.kg^{-1}K^{-1}], λ its thermal conductivity [W.K^{-1}.m^{-1}] and V_i the species diffusion velocity [m.s^{-1}]. Following Oran and Boris [76], it is assumed that the diffusion velocity is composed of three parts, i.e.,

$$V_i = V_i^D + V_i^T + V_c \quad (3.11)$$

V_i^D is the ordinary–diffusion velocity for which an approximation recommended by Hirschfelder and Curtiss [77, 78] is adopted, viz.,

$$V_i^D = -\frac{D_i}{X_i}\nabla X_i, i = 1, \ldots, I. \quad (3.12)$$

Where X_i denotes the mole fraction of species i and D_i is its mixture–averaged diffusion coefficient.
V_i^T is the thermal diffusion velocity,

$$V_i^T = -\frac{D_i^T}{\rho Y_i T}\nabla T, i = 1, \ldots, I. \quad (3.13)$$

which is included only for the light species H and H_2. T is the temperature and D_i^T is the thermal–diffusion coefficient of species i.
Finally, V_c appearing in eq. (3.11) represents the global flow velocity.
Equations (3.7) to (3.10) represent a system of $I + 2$ equations for the $I + 2$

unknowns ρ, v and $Y_1, \ldots, Y_I$; hence the system is closed and can be solved, which is performed by an iterative method.

3.1.2 The reaction mechanism input file

As mentioned above, a reaction mechanism is necessary to perform a numerical simulation of a one–dimensional flame with Cosilab [74]. This section presents the general mathematical relations needed to understand the use of such a kinetic mechanism. A mechanism of K chemical reactions amongst I chemical species is written in the form

$$\sum_{i=1}^{I} \nu_{ik}^{'} M_i \rightleftharpoons \sum_{j=1}^{I} \nu_{jk}^{''} M_j. \tag{3.14}$$

Here M_i represents the chemical symbol of reactant species i, M_j represents the chemical symbol of product species j and $\nu_{ik}^{'}$ and $\nu_{jk}^{''}$ are their stoichiometric coefficients on the reactants and products side, respectively, of reaction k, $k = 1, \ldots K$. The net mass reaction rate of species i can be written as

$$\omega_i = W_i \sum_{k=1}^{K} \left(\nu_{ik}^{''} - \nu_{ik}^{'} \right) \left(r_{fk} - r_{bk} \right) \tag{3.15}$$

or alternatively, with $\nu_{ik} = \nu_{ik}^{''} - \nu_{ik}^{'}$ and $r_k = r_{fk} - r_{bk}$ as

$$\omega_i = W_i \sum_{k=1}^{K} \nu_{ik} r_k \tag{3.16}$$

Here ν_{ik} is the net stoichiometric coefficient of species i in reaction k; this quantity can be equals to zero, positive or negative. It will be positive if in reaction k there is a net production of species i, and negative, if there is a net consumption or destruction. It will be equals to zero in two cases, if either species i does not participate at all in the reaction, or if it acts in the reaction as an inert third body. r_k is the net reaction rate of the k reaction and the quantities r_{fk} and r_{bk} are its forward and backward rate, respectively. For elementary reactions, these quantities are given by the expressions:

$$r_{fk} = k_{fk} \prod_{i=1}^{I} C_i^{\nu_{ik}^{'}} \quad \text{and} \quad r_{bk} = k_{bk} \prod_{i=1}^{I} C_i^{\nu_{ik}^{''}}.$$

where k_{fk} and k_{bk} are the rate coefficients of the forward and backward reactions respectively.
Thus, the net reaction rate r_k can be written as

$$r_k = k_{fk} \prod_{i=1}^{I} C_i^{\nu_{ik}^{'}} - k_{bk} \prod_{i=1}^{I} C_i^{\nu_{ik}^{''}}, \tag{3.17}$$

or, if the equilibrium constant is introduced, $K_{Ck} = k_{fk}/k_{bk} = \prod_{i=1}^{I} C_i^{\nu_{ik}}$, as

$$r_k = k_{fk} \prod_{i=1}^{I} C_i^{\nu_{ik}^{'}} \left(1 - \frac{1}{K_{Ck}} \prod_{i=1}^{I} C_i^{\nu_{ik}} \right). \tag{3.18}$$

Equation (3.17) shows that for an elementary reaction as most of those found in a kinetic mechanism, the reaction order with respect to species i is always equal to the stoichiometric coefficient of that species. For non–elementary reactions this is not always the case, reaction orders are often encountered that differ more or less from the stoichiometric coefficients.
The forward, and eventually backward, rate constants are usually assumed to be of the Arrhenius form, i.e.,

$$k_{fk} = A_{fk} T^{\beta_{fk}} exp\left(\frac{-E_{fk}}{RT} \right), \tag{3.19}$$

where A_{fk} is the pre–exponential factor, β_{fk} the pre–exponential temperature exponent, and E_{fk} the activation energy [J.mol^{-1}], all of the forward step of reaction k. The equilibrium constant defined previously in 3.18 as the ratio of the forward and backward reaction rate constant is easier to evaluate in terms of partial pressures, K_{Pk}, which are defined as

$$K_{Pk} = \prod_{i=1}^{I} \left(\frac{p_i}{p^0}^{\nu_{ik}} \right); \tag{3.20}$$

where p^0 denotes atmospheric pressure [Pa]. It can easily be verified that the two equilibrium constants are related by $K_{Ck} = K_{Pk} \left(\frac{p_{atm}}{RT} \right)^{\sum_{i=1}^{I} \nu_{ik}}$. The equilibrium constant K_{Pk} is evaluated from

$$K_{Pk} = exp\left(\frac{\Delta S_k^0}{R} - \frac{\Delta H_k^0}{RT} \right), \tag{3.21}$$

where

$$\frac{\Delta S_k^0}{R} = \sum_{i=1}^{I} \nu_{ik} \frac{S_k^0}{R} \quad \text{and} \quad \frac{\Delta H_k^0}{RT} = \sum_{i=1}^{I} \nu_{ik} \frac{H_k^0}{RT},$$

ΔS_k^0 and ΔH_k^0 being the standard entropy and standard enthalpy of reaction k, respectively. Before closing this section concerning the reaction mechanism, two different effects observed sometimes in elementary reactions of a kinetic mechanism are discussed below. The first one is the fact that certain reactions between two molecules can take place only if in the collision leading to reaction a third, inert body – usually designated by M in the mechanism – is present. That third body can be any species molecule present in the system. This is often the case, for instance, in recombination and dissociation reactions. In formulating the reaction rate of a three–body reaction, naturally the concentration of the third body needs to be taken into account. Since principally each species present in the system can act as a third body – and can do so with a different effect or efficiency on the reaction – all species as well as their specific efficiencies in acting as a third body have to be included in the formulation. Considering this, the effective rate constant r_k for a three–body reaction can be written as the sum of all the individual rate constants in which the individual species act as a third body, i.e.,

$$r_k = \left(\sum_{i=1}^{I} z_{ik} C_i \right) \left(k_{fk} \prod_{i=1}^{I} C_i^{\nu_{ik}^{'}} - k_{bk} \prod_{i=1}^{I} C_i^{\nu_{ik}^{''}} \right), \tag{3.22}$$

where z_{ik} is the third–body efficiency of species i in reaction k. If all species act with equal third–body efficiency, then according to convention all z_{ik} are unity, and the effective third-body concentration $\sum_{i=1}^{I} z_{ik} C_i$ reduces to the mixture total molar concentration C. However this is not often the case and some species present in the mixture have a higher efficiency than other in acting as a third–body, therefore, the third–body efficiency z_{ik} of these species is specified in the kinetic mechanism.

The second effect observed in reaction mechanisms is the pressure dependence of some reactions. Indeed, in addition to temperature, the reaction rate of unimolecular reactions is equally found to depend on pressure and its definition has to take this influence into consideration. This question has been addressed by Lindemann and Hinshelwood [79, 80] who showed that a unimolecular reaction is rather a two step process than an elementary reaction. As depicted in the

following equations, Lindemann and Hinshelwood proposed that the reaction begins with the activation of the reactant A by collision with a non reacting partner M . The rate constant of this reaction is noted k_f . Then, the activated reactant A^* can either be deactivated by another collision with a rate constant k_b, or decomposes into final products with a rate constant k_p.

$$A + M \underset{k_f}{\overset{k_b}{\rightleftarrows\rightleftarrows}} A^* \ + \ M \tag{3.23}$$

$$A^* \overset{k_p}{\rightarrow} products \tag{3.24}$$

The reaction rate of a unimolecular reaction should therefore accounts for the concentration of nonreactive partners, which directly depends on the surrounding pressure. Lindemann showed that at low and infinite pressures the rate constant respectively corresponds to equations (3.25) and (3.26).

$$k_0 = k_f[M] \tag{3.25}$$

$$k_\infty = \frac{k_f k_p}{k_b} \tag{3.26}$$

In between these 2 regions, the rate constant is said in the fall-off regime and different formalisms have been proposed to model its behavior. The most popular is that of Troe which consists in an equation involving k_0, k_∞, $[M]$ and 4 additional parameters noted as a, T^*, T^{**} and T^{***} that represent the reaction fall-off [81–83].

3.1.3 Databases of thermodynamic and molecular data

As presented here above in sections 3.1.1 and 3.1.2, the transport properties required for the simulations performed in this work are the thermal conductivity λ of the gas mixture if the energy equation has to be solved and the mixture averaged and thermal diffusion coefficients D_i, and D_i^T, respectively, $i = 1, \ldots, I$. The thermodynamic data required are the specific heat capacities at constant pressure, enthalpies and entropies of the species i, c_{pi}, h_i and s_i and of the gas mixture, c_p, h and s. These data are present in a separated input file and are needed to perform the simulation as mentioned in step 3 of the introduction of this section. They are often available with the kinetic mechanism of a specific author, or if not, sources are specified. In combustion, the first unified approaches to detailed modeling of molecular transport and thermody-

namic data in a manner suitable for implementation into computer codes was initiated by Dixon-Lewis [84] and Warnatz [85]. However, these approaches were taken up, modified, improved and summarized by others. Therefore, the several models of these properties used in the simulations are essentially the ones summarized in a series of publication co-authored by Kee [77, 86].

Transport data The transport input file is constituted of six parameters needed for the characterization of the transport properties of the molecules, these are the molecule geometry (monoatomic molecule, linear or non-linear molecule); the Lennard-Jones potential ϵ_k [J]; the Lennard-Jones collision diameter σ [$\dot{A}$]; the dipole moment μ_k [D], the polarizability α [$\dot{A}^3$] and the collision frequency Z_{rot} [s^{-1}] at 298K.

Thermodynamic data For each species i, $i = 1, \ldots, I$, polynomial curve fits are used to calculate the thermodynamic properties. Specifically, the molar heat capacity at constant pressure [$J.K^{-1}.mol^{-1}$] is given by

$$\frac{C_{pi}}{R} = a_1 + a_2 T + a_3 T^2 + a_4 T^3 + a_5 T^4, \tag{3.27}$$

the molar enthalpy [$J.mol^{-1}$] is given by

$$\frac{H_i}{R} = a_6 + a_1 T + \frac{a_2}{2} T^2 + \frac{a_3}{3} T^3 + \frac{a_4}{4} T^4 + \frac{a_5}{5} T^5, \tag{3.28}$$

and the molar entropy [$J.K^{-1}.mol^{-1}$] is given by

$$\frac{S_i}{R} = a_7 + a_1 lnT + a_2 T + \frac{a_3}{2} T^2 + \frac{a_4}{3} T^3 + \frac{a_5}{4} T^4. \tag{3.29}$$

There are two sets of coefficients a_1 – a_7 in the thermodynamic data file, one for the temperature range between 300 K and 1000 K, and one for the range from 1000 K to 5000 K. The molar quantities C_{pi}, H_i and S_i are related to the respective mass–based quantities through $C_{pi} = c_{pi} W_i$, $H_i = h_i W_i$ and $S_i = s_i W_i$, where W_i is the molar mass of species i [$kg.mol^{-1}$]. The mass–based mixture specific heat capacity, enthalpy and entropy are given by

$$c_p = \sum_{i=1}^{I} Y_i c_{pi}, \qquad h = \sum_{i=1}^{I} Y_i h_i, \qquad s = \sum_{i=1}^{I} Y_i s_i. \tag{3.30}$$

3.1.4 The control document and initial profiles

Control Data Control data are required to communicate to the solvers essential details of a computation such as

* The mass flux, ρv, [kg.s^{-1}.m^{-2}] of the fresh gas mixture, calculated using eq. (3.31), where A is the burner surface area [m^2] ;

$$\rho v = \sum_i Dv_i \frac{pW_i}{RTA} \tag{3.31}$$

* The pressure in the combustion chamber;

* The experimental temperature profile; as detailed previously, the energy equation is not solved during the simulation and an experimental temperature profile is used as an input parameter;

* Initial or boundary conditions, such as the mole fractions of the fresh gases. Species produced by chemical reactions – in particular light species such as H and H_2 – diffuse from the flame zone upstream towards the burner surface. Therefore, unless the flame stabilizes far from the burner surface, the species concentrations and hence the mixture composition at the burner surface will be different from the composition further upstream, either in the burner or in the supply system. However, it is only the mixture composition far upstream of the burner surface that is measured. The fact that usually the unburned gas composition at the burner surface is unknown must therefore be reflected in proper boundary conditions.

* The desired output data such as the mole fractions or concentrations of chemical species, reaction rates, etc.

* Convergence criteria for the solvers and specifications for adaptive meshing or time-stepping methods.

Initial Profiles Initial guesses profiles for temperature, species concentrations and overall massflux are required for the solvers to start their computations. Such profiles can be imported into Cosilab [74], usually copied from a similar case and then modified, or they can be drawn directly in Cosilab.

3.2 Contribution calculation

An interesting tool of results post-processing to understand the combustion pathways of a fuel is the contribution calculation, based on the net reaction rates of each reaction. This analysis allows to underline the important kinetic pathways of formation and degradation for each species of the mechanism. In order to improve or to reduce a kinetic model, this gives a very useful information. The theory of such an analysis is presented below, while the results are presented in the next chapter.

An efficient routine has been developed in Excel [87] to calculate contributions of each reaction to the consumption and formation of every chemical species i of the kinetic model. The routine looks for all reactions that contain a definite compound i and stores their net reaction rate profiles into a separated spreadsheet. In order to assess the relative weight of a reaction k forming or consuming i, the macro compares the surface S_k under its curve of net reaction rate to the sum of all those involved in formation or consumption of i. This mean that it first calculates surfaces S_k under curves of each net reaction rate involving i by summing surfaces A_n of every rectangle n centered on a coordinate z_n, as presented in figure 3.1 and in Eq. (3.32).

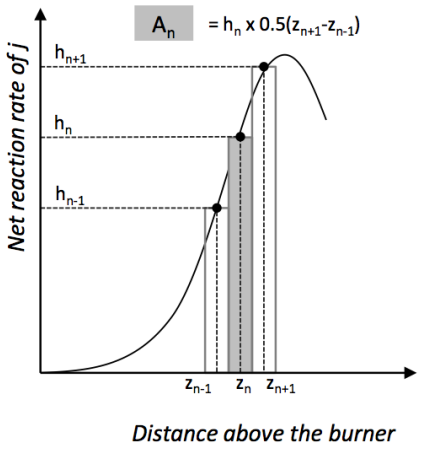

Figure 3.1: Calculation of the surface S_k under the curve of net reaction rates

$$S_k = \sum_n A_n = \sum_n h_n \text{ x } 0.5(z_{n+1} - z_{n-1}) \tag{3.32}$$

Equation (3.32) is a good approximation of S_k since the grid used for Cosilab [74] calculations has about 200 points, homogeneously spread along the 2 cm of the considered reaction zone and that therefore the distance z_n - z_{n-1} = z_{n+1} - z_n $\approx$ 0.01 cm. Afterwards, contributions C_k of each reaction k are calculated by dividing surfaces S_k by the sum on absolute values of all surfaces S_k , according to eq. (3.33).

$$C_k = \frac{S_k}{\sum_k |S_k|}. \tag{3.33}$$

These general contributions can be either positive or negative, depending on the direction taken by the considered reaction. Based on the sign of each contribution C_k and the position of the chemical species i compared with the arrow in the chemical reaction k, reactions are divided into formation and consumption reactions of species i. Finally, the sum on surfaces S_k are calculated inside each set of reactions and contributions of k to either i formation (Cf_k) or i consumption (Cc_k) by equations (3.34) and (3.35) .

$$Cf_k = \frac{|S_k|}{\sum_j |S_k|}, \qquad j \in Formation \tag{3.34}$$

$$Cc_k = \frac{|S_k|}{\sum_j |S_k|}, \qquad j \in Consumption \tag{3.35}$$

These contributions Cf_k and Cc_k are positive since absolute values of S_k are used. Practically, values of Cf_k and Cc_k are reported for each reaction in order to perform comparative analysis allowing to determine main reaction channels for formation and consumption of i.

3.3 Chemical kinetics of ammonia combustion

As presented in the previous section, the choice of an appropriate kinetic mechanism for the performed simulations is of high importance. When beginning with a new set of simulations, i.e., a new fuel or new conditions of pressure and temperature for the combustion, the search of mechanisms in the literature helps to find a starting point. However, when testing several mechanisms by comparing the numerical simulation results with the experimental ones, one can find that some of them are not appropriate, and that others are in good

agreement for the main species but need adjustements for some intermediate or minor species. Finally, when obtaining a kinetic mechanism estimated to give a good agreement between simulated and experimental results, the reduction in size of this one can help to use it in more complex cases such as the combustion in spark ignition engine in which fluids mechanic has also to be taken into account and for which the diminution of the number of chemical species implied in the simulation is of a critical importance for the computational time.

3.3.1 Mechanisms from the literature

A previous study on ammonia combustion [88] presented five mechanisms found in the literature [1, 41–43, 89]. These mechanisms can be consulted in appendix B and some details are given below.

* The Bian [89] model is specific to ammonia oxidation and has been tested for seeded H_2/O_2/Ar flames with ammonia and/or nitrogen monoxide and for ammonia flames burning in oxygen or in nitrogen monoxide [25, 26, 28, 29]. These laminar one-dimensional flames have been investigated experimentally by molecular beam mass spectrometry as in this work and their composition is presented in Table 3.1.

	H_2	O_2	Ar	NO	NH_3	ϕ	p [mbar]
LF1	0.1860	0.7650	0.0490	0	0	0.12	46
LF2	0.1860	0.7480	0.0320	0.0340	0	0.12	46
LF3	0.1350	0.7650	0.0660	0	0.0340	0.12	46
LF4	0.1605	0.7565	0.0490	0.0170	0.0170	0.12	46
SF1	0.2540	0.1270	0.6190	0	0	1.00	46
SF2	0.2540	0.1120	0.6040	0.0300	0	1.00	46
SF3	0.2090	0.1270	0.6340	0	0.0300	1.00	46
SF4	0.2315	0.1195	0.6190	0.0150	0.0150	1.00	46
FON	0	0.5100	0.0100	0	0.4800	0.71	47
FNN	0	0	0.0670	0.4720	0.4720	1.46	72

Table 3.1: Composition of flames investigated by Bian et al. [89]

This mechanism has thus not really been validated for flames as those presented in this work, namely, ammonia-oxygen-argon flames near stoichiometry and seeded with hydrogen. It takes into account 20 chemical species and con-

tains 73 reactions. Finally, as other mechanisms it can be decomposed into two parts, a first one considering the H_2/O_2 system, based on the Westbrook model [90], and the second peculiar to the ammonia oxidation.

* The Lindstedt [41] model is also specific to ammonia combustion and has been tested for the oxidation of ammonia in flat laminar premixed flames of $H_2/NH_3/O_2$, $NH_3/NO/H_2/O_2$ and NH_3/O_2. However, none of the flames simulated previously with this mechanism correspond to those of this work. Their compositions are presented in Table 3.2. Three ammonia-hydrogen-oxygen flames (1-3) have been studied but in opposition to this work they were hydrogen flames seeded with ammonia. This model takes into account 22 chemical species and contains 95 reactions.

	H_2	O_2	Ar	NO	NH_3	ϕ	p [mbar]	Ref.
1	0.2090	0.1270	0.6340	0	0.0300	1.00	46	[89]
2	0.3540	0.1040	0.5130	0	0.0290	1.91	47.5	[29]
3	0.1350	0.7650	0.0660	0	0.0340	0.12	46	[89]
4	0.2315	0.1195	0.6190	0.0150	0.0150	1.00	46	[89]
5	0.1605	0.7565	0.0490	0.0170	0.0170	0.12	46	[89]
6	0	0.3500	0	0	0.6500	1.40	27	[21]
7	0	0.6000	0	0	0.4000	0.50	27	[21]
8	0	0.4300	0	0	0.5700	1.00	27	[21]
9	0	0.5100	0.0100	0	0.4800	0.71	47	[89]

Table 3.2: Composition of flames tested by Lindstedt mechanism

* The Konnov [1] model is a mechanism for the combustion of small hydrocarbons ($C_1 - C_3$) tested satisfactorily for decomposition, oxidation, ignition, and flame structure of hydrogen, carbon monoxide, formaldehyde, methanol, methane, nitrous oxide, nitrogen monoxide, nitrogen dioxide and ammonia. From the complete model containing 1207 reactions and considering 127 chemical species, only reactions involving H, O, N containing species have been considered excluding carbon containing molecules to obtain a model with 245 reactions and 31 species.

* Similarly, the GRI [42] model is used to simulate natural gas flames burning in oxygen or in air but takes also into account nitrogenous species like ammonia, radical amidogen, nitrogen monoxide, etc.... This mechanism considers 45 species, but only 19 of those are of interest for this study, corresponding to 70 reactions involving H, O, N containing species.

* Finally, the part of the San Diego [43] model specific for the nitrogen chemistry is based on a previous work of Hewson and Bollig [91] and has been elaborated to predict nitrogen oxides concentration in flames. This mechanism is constituted of 74 reactions and takes into account 29 chemical species.

For each mechanism, transport and thermodynamic data provided by the authors were used. If some disagreements between experimental and numerical results can be due to a flow configuration somewhat different from the ideal simulation, they are definitely smaller than those coming from the individual kinetic parameters. The five mechanisms are systematically tested on each flame investigated in this work and figs. 3.2 to 3.9 present the comparison for flame II containing 24% of ammonia, 7.49% of hydrogen, 21.32% of oxygen and 47.19% of argon and stabilized at 50 mbar. As presented on these graphs, three mechanisms (Lindstedt, GRI and San Diego mechanisms) give always results completely in disagreement with the experimental ones. Indeed the disagreements of species concentrations as well as of the mole fraction gradients are well noticeable indicating a too slow consumption of ammonia. Concerning the choice between Konnov and Bian mechanisms, the second one give for all investigated flames underestimated values for the final nitrogen monoxide concentration (Fig. 3.4). This species being of critical importance to control the ammonia combustion, we elaborated a mechanism based on the Konnov model. Indeed, for this model, most of the calculated mole fraction profiles agree with the experimental ones but a significant divergence is observed for N_2O (Fig. 3.6) and NH_2 (Fig. 3.7). However, the trend of the maxima of these species in each series of flames is well reproduced by the simulation. It is thus necessary to update kinetic parameters of the formation and degradation reactions of these species to obtain an improved mechanism leading to a better agreement with all the detected species.

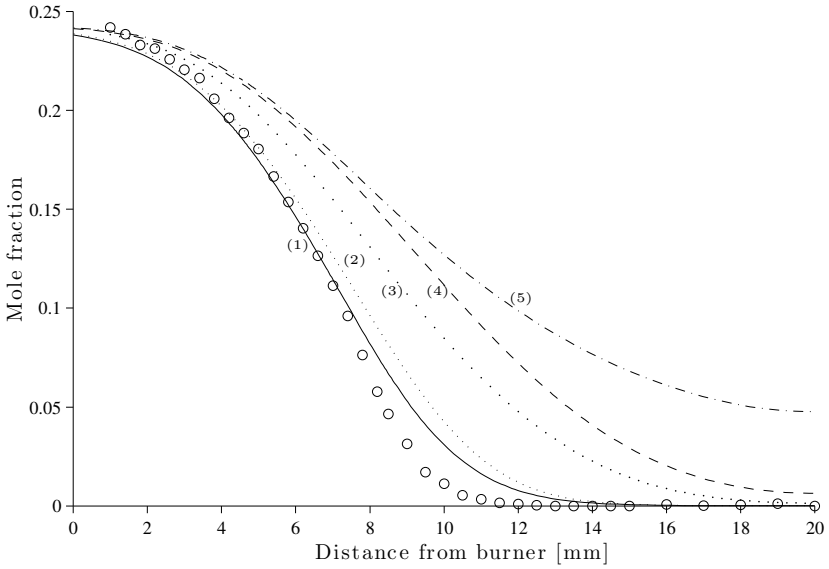

Figure 3.2: Ammonia mole fraction profiles.
○ : experiments ; Lines : numerical simulation. (1) : Konnov [1], (2) : Bian [89], (3) : San Diego [43], (4) : Lindstedt [41], (5) : GRI [42].

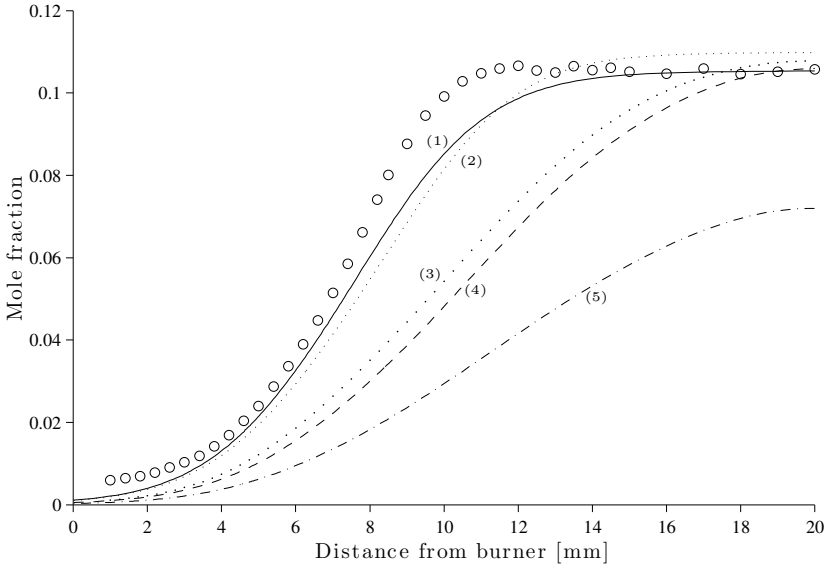

Figure 3.3: Nitrogen mole fraction profiles.
○ : experiments ; Lines : numerical simulation. (1) : Konnov [1], (2) : Bian [89], (3) : San Diego [43], (4) : Lindstedt [41], (5) : GRI [42].

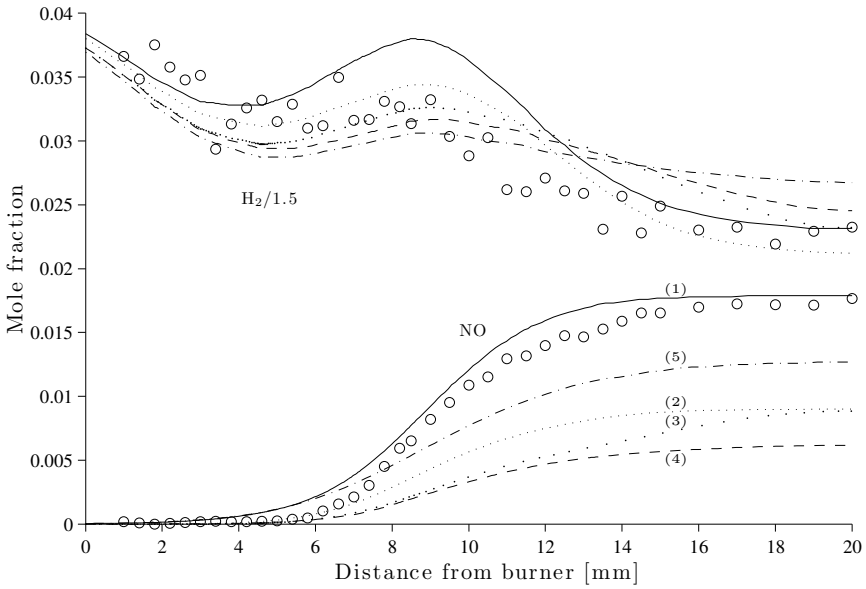

Figure 3.4: Hydrogen and nitrogen monoxide mole fraction profiles.
○ : experiments ; Lines : numerical simulation. (1) : Konnov [1], (2) : Bian [89], (3) : San Diego [43], (4) : Lindstedt [41], (5) : GRI [42].

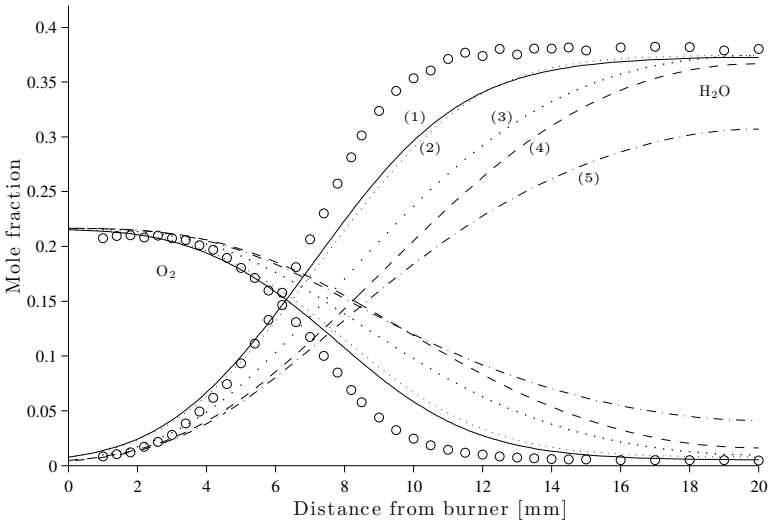

Figure 3.5: Oxygen and water mole fraction profiles.
○ : experiments ; Lines : numerical simulation. (1) : Konnov [1], (2) : Bian [89], (3) : San Diego [43], (4) : Lindstedt [41], (5) : GRI [42].

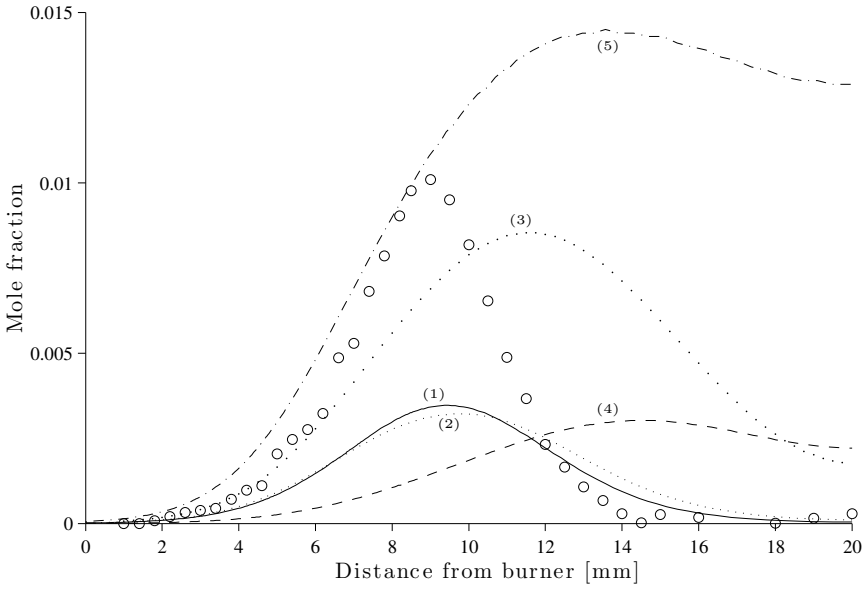

Figure 3.6: Nitrous oxide (N_2O) mole fraction profile. ∘ : experiments ; Lines : numerical simulation. (1) : Konnov [1], (2) : Bian [89], (3) : San Diego [43], (4) : Lindstedt [41], (5) : GRI [42].

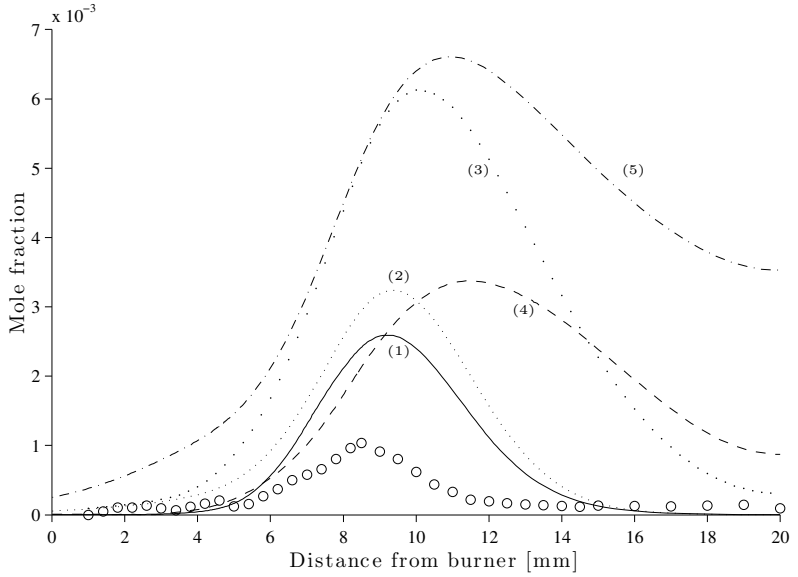

Figure 3.7: Amidogen radical (NH_2) mole fraction profile.
∘ : experiments ; Lines : numerical simulation. (1) : Konnov [1], (2) : Bian [89], (3) : San Diego [43], (4) : Lindstedt [41], (5) : GRI [42].

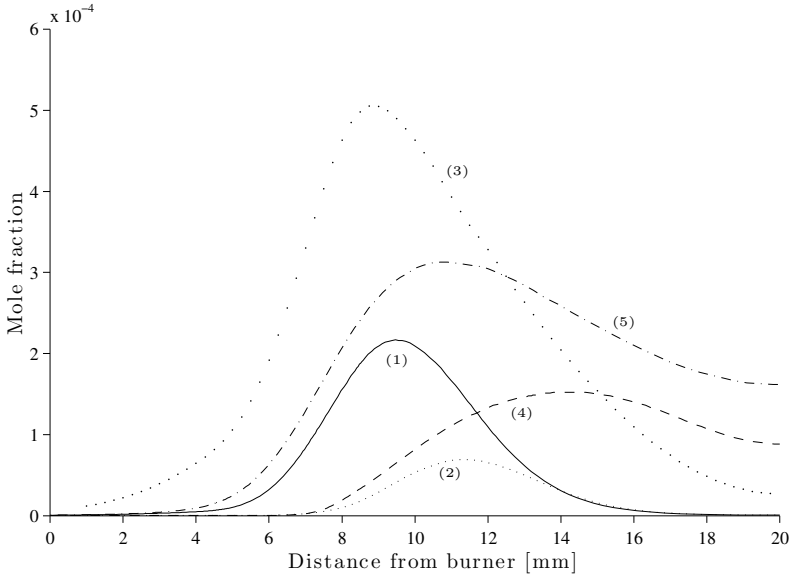

Figure 3.8: Nitroxyl (HNO) mole fraction profile. (1) : Konnov [1], (2) : Bian [89], (3) : San Diego [43], (4) : Lindstedt [41], (5) : GRI [42].

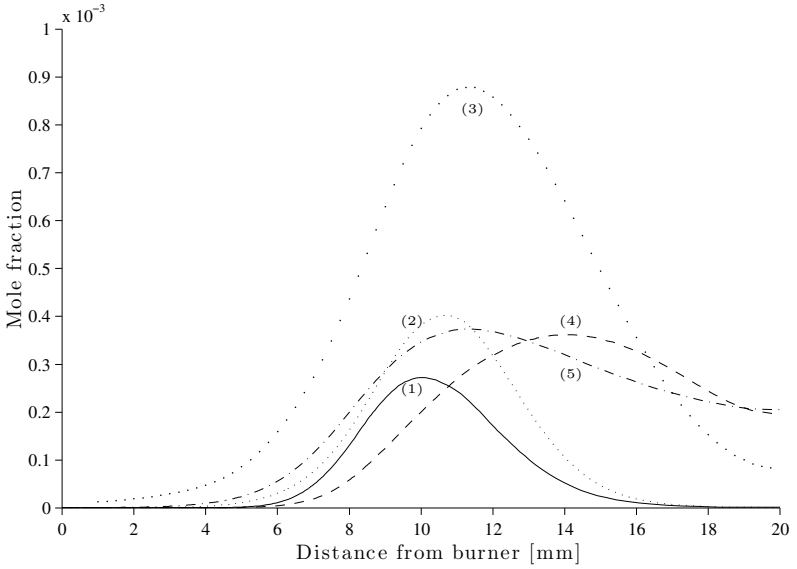

Figure 3.9: Imidogen radical (NH) mole fraction profile. (1) : Konnov [1], (2) : Bian [89], (3) : San Diego [43], (4) : Lindstedt [41], (5) : GRI [42].

3.3.2 Improvement of the Konnov mechanism

In order to improve the simulated profiles of NH_2 which is overestimated and of N_2O underestimated by the Konnov mechanism (figs. 3.6 and 3.7), four reactions were modified. The choice of those reactions comes out from the kinetic analysis of the main reactions involving these two chemical species.

For N_2O, Table 3.3 presents the two main reactions impacting this species among all the reactions where N_2O is considered together with their modifications. N_2O maximum mole fraction being underestimated by the Konnov mechanism, the aim was thus to accelerate its formation and to slow down its degradation. A search in the literature [35, 50, 57, 92–105] allowed to modify the kinetics parameters of these two reactions, in order to reach this goal.

		A ($cm^3mol^{-1}s^{-1}$)	n	E_a (cal/mole)	Ref
1. Konnov	NH+NO=N_2O+H	2.5x10^{16}	-1.03	835	[99]
This work	**NH+NO=N_2O+H**	**5x10^{14}**	**-0.4**	**0**	*
2. Konnov	N_2O+H=N_2+OH	2.2x10^{14}	0	16750	[99]
This work	**N_2O+H=N_2+OH**	**5x10^{13}**	**0**	**15200**	*

Table 3.3: Rate constant modifications performed to improve N_2O prediction. * = Estimated in this work

Reactions of imidogen (NH) play a role in many aspects of nitrogen chemistry in combustion [35]. Perhaps most importantly, in the case of ammonia combustion, the reaction of NH with nitrogen monoxide is believed to be the principal sources of nitrous oxide (N_2O). However, this reaction has two different possible routes :

$$\begin{aligned} NH+NO &\rightarrow N_2 + OH \quad (a) \\ &\rightarrow N_2O + H \quad (b) \end{aligned}$$

There are now many experimental and theoretical data focused on the determination of these rate constants. In general these fell into two categories, the measure of the overall rate constant, $k_a + k_b$ [92–95] and the measure of the branching ratio of the two paths, $f=k_a/(k_a + k_b)$ [50, 57, 96–98], a parameter that is critical in predicting N_2O levels in combustion systems. Most of

the overall rate constant measurements were performed at room temperature and there is a good agreement between the various results, ranging from 2.3 to 3.5x10^{13} cm^3/mol.s but to date the influence of temperature on this rate constant remains unclear. Moreover, there is significantly less agreement concerning the branching ratio between the two possible paths. It started with experiments where OH was not detected at all, then there were experiments where it was found to be the sole product, but it is now accepted, following several independent measurements, that the yield of N_2 + OH is in the range of 5-30%. All of this shows that the rate constant of the path (b) NH+NO = N_2O + H is not well known. Based on the most used rate constant calculated by Miller and Melius [57] (k_b = 2.3x10^{14} [cm^3/mol.s] T$^{-0.4}$) and in order to accelerate the formation of N_2O to be in agreement with the experimental results for the eight investigated flames this rate constant has been estimated to be k_b = 5x10^{14} [cm^3/mol.s] T$^{-0.4}$. Figure 3.10 presents several experimental and theoretical rate constants found in the literature [31, 35, 41, 42, 57, 99] together with the rate constant evaluated in this work [*].

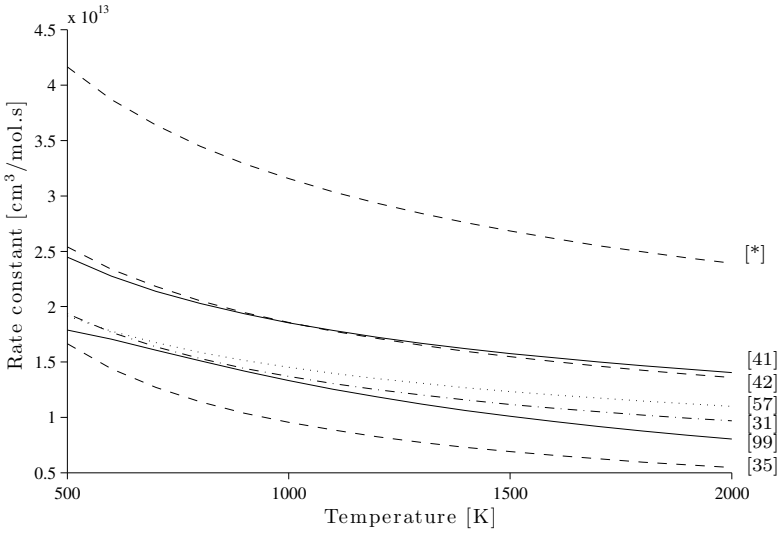

Figure 3.10: Rate constants of the reaction NH+NO=N_2O+H.

Concerning the reaction N_2O + H = N_2 + OH, Fig. 3.11 presents several experimental and theoretical rate constants found in the literature [99–105], showing that the exact value of this constant is not established but that an agreement has been reached concerning the global range of its value. Moreover, the kinetic

data estimated in this work [*] for this reaction is in the range of those found in the literature [99–105].

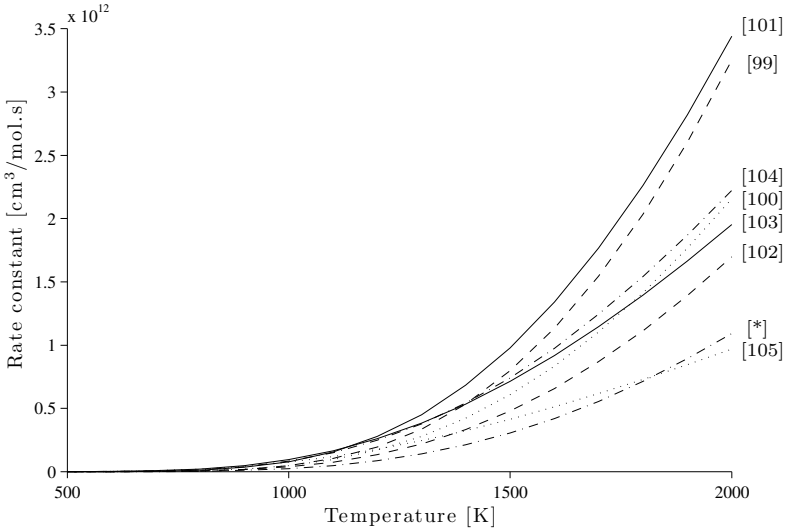

Figure 3.11: Rate constants of the reaction $N_2O+H=N_2+OH$

For NH_2 the problem is more complicated since this species is the main intermediate in the degradation of ammonia and thus also the precursor needed for the formation of approximately all the combustion products. As NH_2 concentrations are overestimated by the Konnov mechanism but that the concentration profiles of main species appear to be correctly simulated for all the analyzed flames, the consumption reactions of this species have to be accelerated. Based on the rate analysis of the main reaction pathways of NH_2 consumption, and avoiding to impact largely other species like H_2O, N_2 or NO correctly reproduced by the simulation, kinetic parameters of reactions presented in Table 3.4 have been adjusted.

		A ($cm^3mol^{-1}s^{-1}$)	n	E_a (cal/mole)	Ref
1. Konnov	NH_2+H=NH+H_2	6.3x10^{13}	0	8843	[106]
This work	**NH_2+H=NH+H_2**	**1x10^6**	**2.32**	**799**	*
2. Konnov	NH_2+NH_2=N_2H_2+H_2	10^{13}	0	1500	[107]
This work	**NH_2+NH_2=N_2H_2+H_2**	**5x10^{13}**	**0**	**1500**	*

Table 3.4: Rate constant modifications performed to improve NH_2 prediction. * = Estimated in this work

A search in the literature allowed to find the rate constant of reaction NH_2 + H = NH + H_2 improving as much as possible the numerical simulation of NH_2 profile. This was the one suggested by the theoretical work of Linder et al. [108]. Then, this constant has been adjusted in order to fit experimental NH_2 profiles gathered in all the investigated flames. Figure 3.12 presents several experimental and theoretical rate constants found in the literature [42, 89, 106, 108–110] together with the rate constant estimated in this work [*].

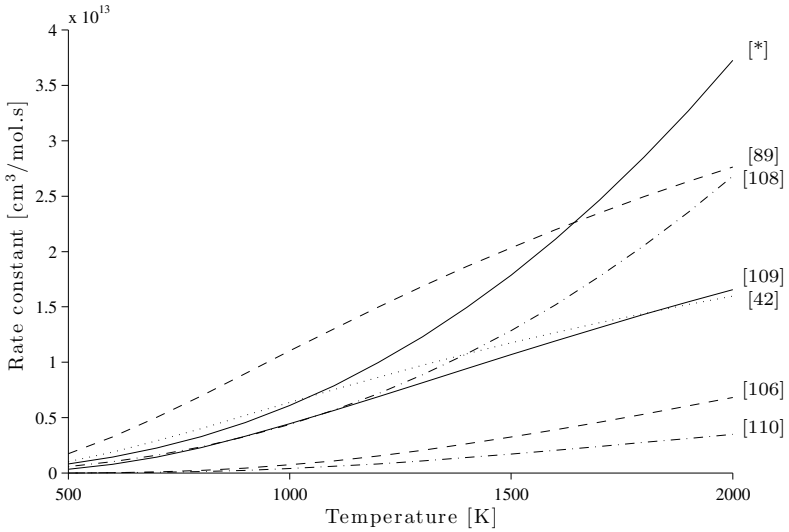

Figure 3.12: Rate constants of the reaction NH_2+H=NH+H_2

Concerning the reaction $NH_2 + NH_2 = N_2H_2 + H_2$, as presented in Fig. 3.13 its rate constant is only estimated and there are few references in the literature [35, 41, 46, 58, 107]. The Konnov mechanism (k = 10^{13} [cm^3/mol.s] x exp(-1500 [cal/mole]/RT))[107] suggests an estimated value based on the work of Stothard et al. [58] performed at low pressure but at room temperature. Therefore, this rate constant has been adjusted to k = 5x10^{13} [cm^3/mol.s] x exp (-1500 [cal/mole]/RT [*] in order to fit experimental NH_2 profiles gathered in all the investigated flames.

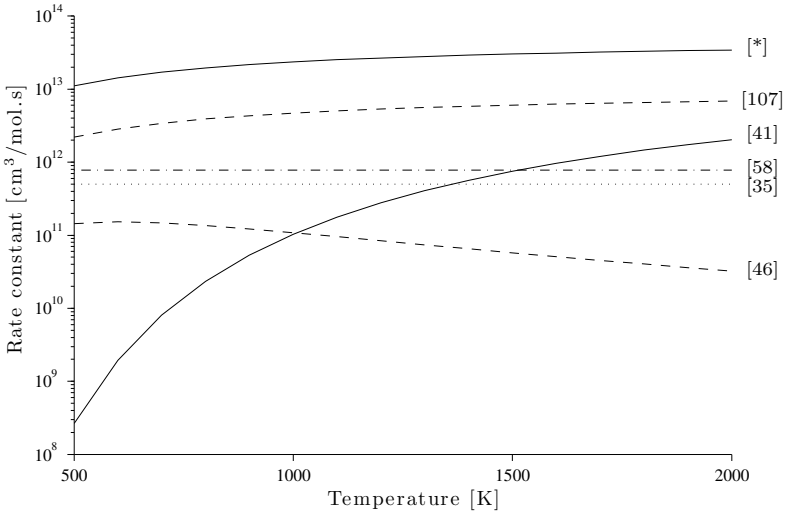

Figure 3.13: Rate constants of the reaction NH_2+NH_2=N_2H_2+H_2

The modified Konnov mechanism is validated at low pressure for the simulation of the structure of all the flames presented in Chapter 2 but also for the prediction of laminar burning velocities of ammonia-air flames burning at atmospheric pressure and room temperature which has been measured and will be presented in Chapters 5 to 7. The predicted species mole fraction profiles by the original Konnov mechanism and by the modified Konnov mechanism are compared in figs. 3.14 to 3.17 for an ammonia-oxygen-hydrogen flame stabilized at 50 mbar (Flame II : $\phi = 1.02$, 24% NH_3, 7.5% H_2, 21.3% O_2, 47.2% Ar). Concerning the major species, i.e., ammonia, oxygen, nitrogen, water and argon, they are all well simulated by both mechanisms (Fig. 3.14). For the minor species (figs. 3.15, 3.16, 3.17), the experimentally detected ones were also well reproduced by the Konnov mechanism, excepted nitrous oxide and the amidogen radical for which the predictions have been improved thanks to the modifications performed on the Konnov mechanism.

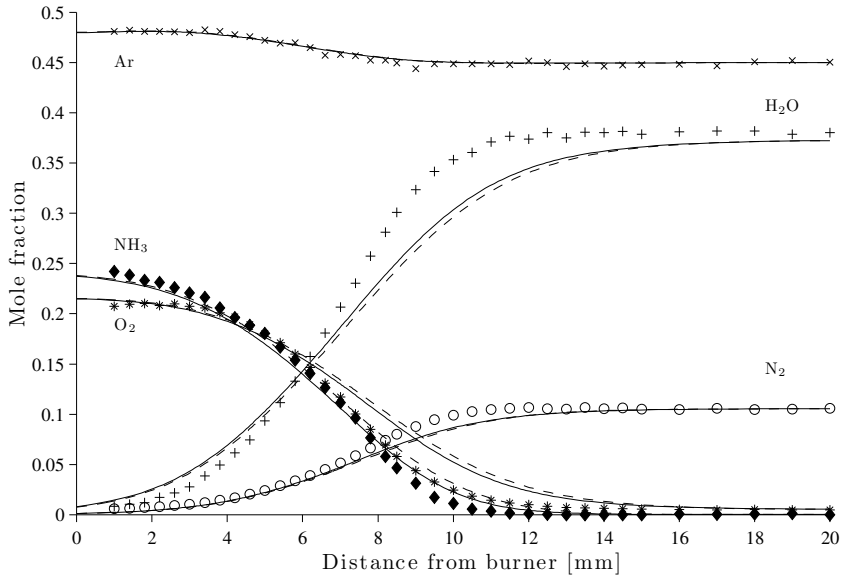

Figure 3.14: Comparison of the Konnov and *modified Konnov* mechanisms for the structure prediction of major species of flame II. Symbols: experiments, Solid lines: Modified Konnov mechanism, Dashed lines: Konnov mechanism [1]

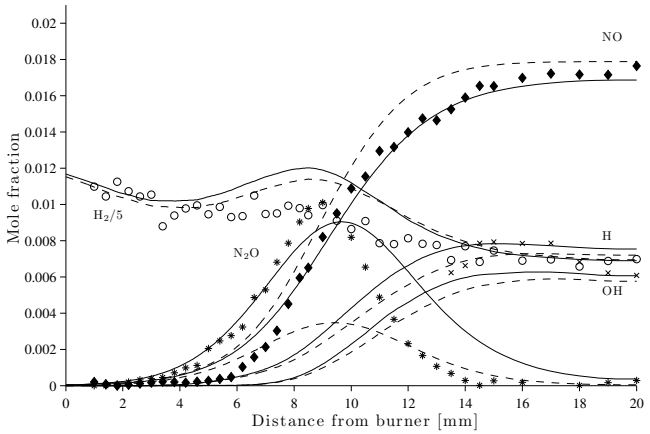

Figure 3.15: Comparison of the Konnov and *modified Konnov* mechanisms for the structure prediction of some minor species of flame II. ($1.5\text{x}10^{-3} < \text{X}_i < 2\text{x}10^{-2}$) Symbols: experiments, Solid lines: Modified Konnov mechanism, Dashed lines: Konnov mechanism [1]

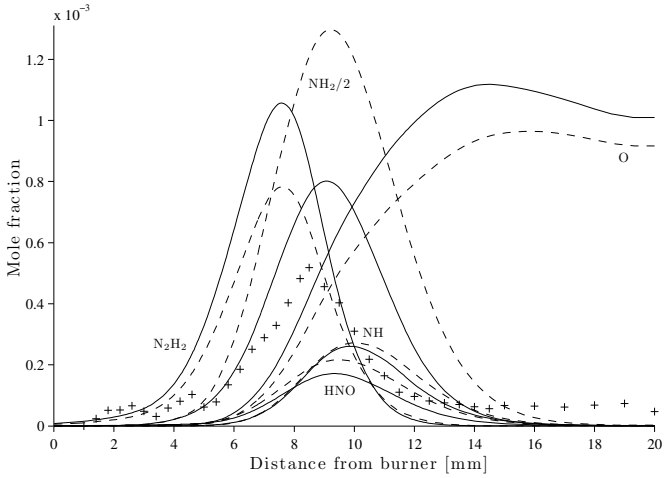

Figure 3.16: Comparison of the Konnov and *modified Konnov* mechanisms for the structure prediction of some minor species of flame II. ($1\text{x}10^{-4} < \text{X}_i < 1.5\text{x}10^{-3}$) Symbols: experiments, Solid lines: Modified Konnov mechanism, Dashed lines: Konnov mechanism [1]

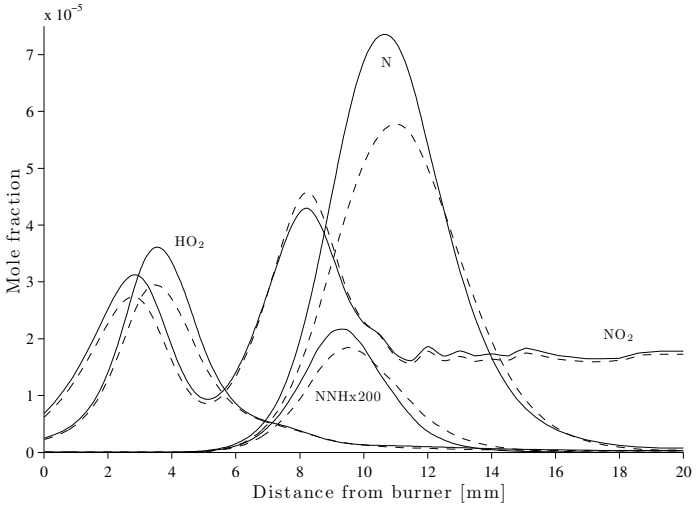

Figure 3.17: Comparison of the Konnov and *modified Konnov* mechanisms for the structure prediction of some minor species of flame II. ($X_i < 1x10^{-4}$) Solid lines: Modified Konnov mechanism, Dashed lines: Konnov mechanism [1]

Finally, the non detected minor species are similarly simulated by both mechanisms excepted N_2H_2 and N. The comparison of the formation and consumption kinetic pathways for the two mechanisms can help to understand these differences. Those ones are depicted in figs. 3.18 to 3.21. On these diagrams, the percentages represent the weight of the reaction on the global formation or consumption of a species. Since the several pathways involved in the formation of a species do not necessarily correspond to the pathways involved in its consumption, these diagrams must therefore be read separately.

N_2H_2 is formed in both mechanisms mainly by the reaction $NH_2 + NH_2 \rightarrow N_2H_2 + H_2$, reaction that has been accelerated in the model presented in this work in order to increase the NH_2 consumption. This explains why this species is present in much higher quantities in the new model.

The increase in the N radical concentration comes from the global changes in term of nitrogenous species applied to the Konnov mechanism.

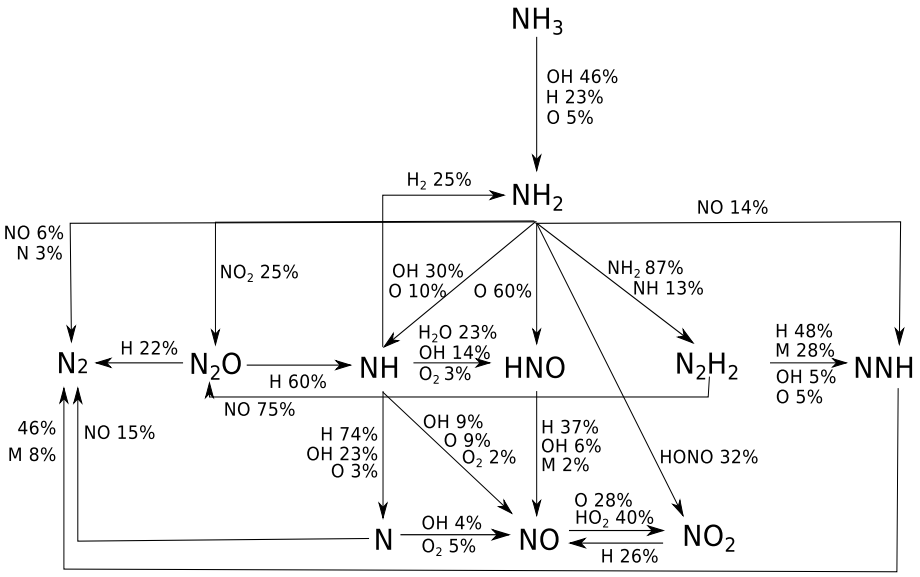

Figure 3.18: Formation reaction pathways for the *modified Konnov* mechanism in flame II

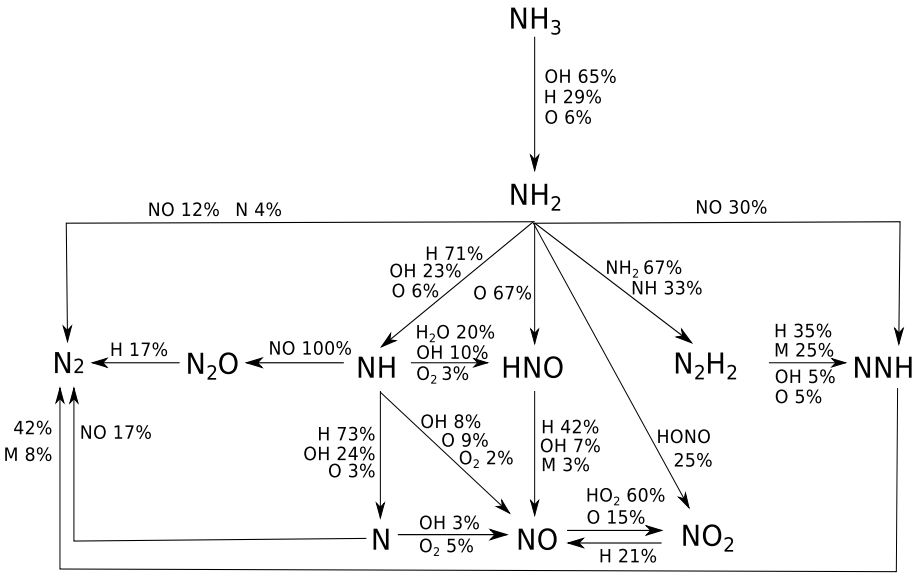

Figure 3.19: Formation reaction pathways for the Konnov mechanism in flame II

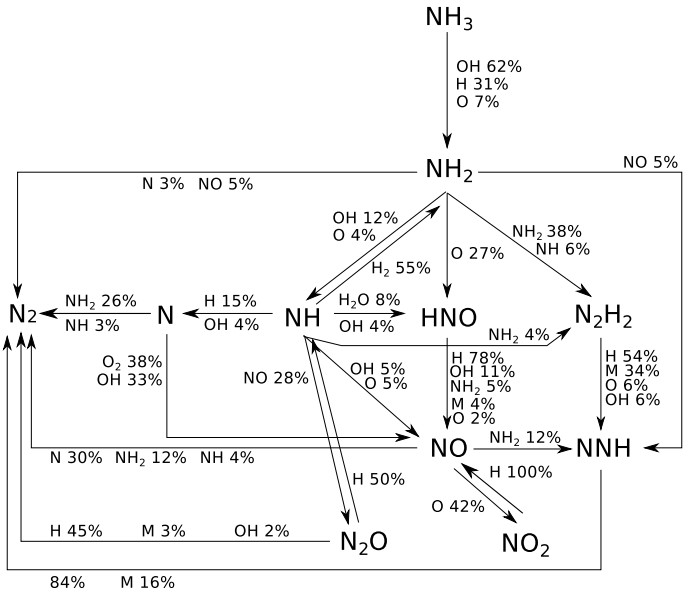

Figure 3.20: Consumption reaction pathways for the *modified Konnov* mechanism in flame II

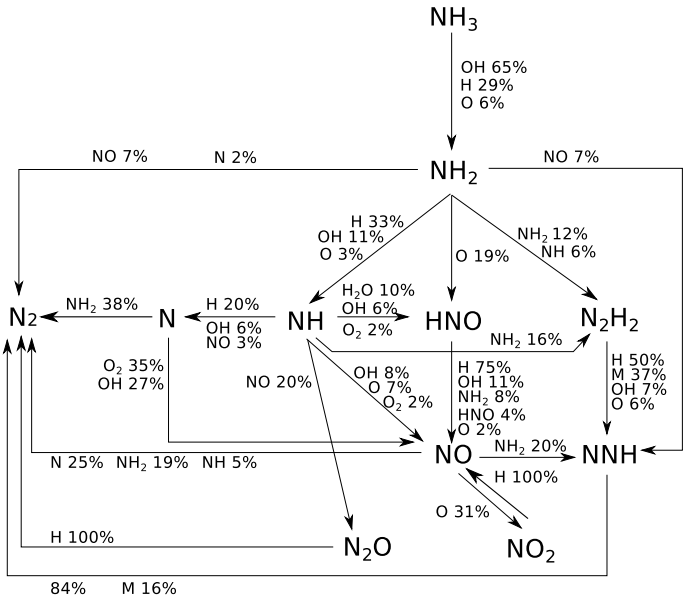

Figure 3.21: Consumption reaction pathways for the Konnov mechanism in flame II

The unusual aspect of the NO_2 profile comes from the several reactions involved in its formation and consumption. Indeed, this species is formed in the Konnov mechanism and in the *modified* Konnov mechanism by the reactions

$$NO + HO_2 = NO_2 + OH \ (1)$$
$$NH_2 + HONO = NO_2 + NH_3 \ (2)$$
$$NO + O \ (+M) = NO_2 \ (+M) \ (3)$$

and consumed by the reaction $NO_2 + H = NO + OH$ (4).

Reaction (1) takes place in the first part of the flame, near the burner surface, while the consumption reaction (4) begins around 3 mm from the burner surface and explains the first peak observed in the mole fraction profile. Then reactions (2) and (3) take place in the second part of the flame, in the flame front, and allow to explain the second peak observed at a distance of 8 mm from the burner surface. Finally, reaction (3) and (4) remain important in the burned gases and allow to explain the residual NO_2 mole fraction in the burned gases.

3.3.3 The *reduced* kinetic mechanism

To reduce the size of the modified Konnov mechanism, a contribution rates calculation has been performed with the Cosilab software [74] for all low pressure investigated flames. The result of this analysis showed that only 143 reactions contribute for at least one percent in the formation or the consumption of at least one chemical species. The same rate analysis has then been performed for laminar, freely propagating premixed flames burning at atmospheric pressure and room temperature at equivalence ratios of 0.5, 1 and 1.5. Consequently, 18 reactions have been added to the 143 first one. Finally, this freely propagating flame has been simulated for the same equivalence ratios but for higher pressure and temperature conditions corresponding to a spark ignition compression ratio of 20 needed for an efficient ammonia-air combustion (T $\approx$ 830 K ; P $\approx$ 55 atm). These last simulations showed that 10 reactions had to be added to the previous ones, giving a set of 171 reactions involving 31 species. Then, in order to decrease the number of chemical species, those present in very small quantities ($X_i < 10^{-8}$) and not necessary for the formation or consumption of main species, namely, N_2O_3, NO_3, HONO, HNO_3, N_2O_4, HNNO, N_2H_3, N_2H_4, H_2NO, HNOH, NH_2OH and H_2O_2, together with the corresponding reactions involving only these species, were removed to obtain the *reduced* mechanism presented in Table 3.5 and containing 80 reactions and 19 chemical species.

Elements	H	O	N	Ar
	H	H_2	O	O_2
	OH	HO_2	H_2O	N
Species	NH	NO	N_2O	NH_2
	HNO	NO_2	NNH	NH_3
	N_2H_2	AR	N_2	
Reactions	A	n	E_a(cal/mole)	Ref.
1. H+H+M=H_2+M	7.00E+17	-1.00E+00	0.00E+00	[111]
	H_2/0/	N_2/0/	H/0/	
	H_2O/14.3/			
2. H+H+N_2 = H_2+N_2	5.40E+18	-1.30E+00	0.00E+00	[111]
3. O+O+M = O_2+M	1.00E+17	-1.00E+00	0.00E+00	[112]
	O/71/	O_2/20/	NO/5/	
	N_2/5/	N/5/	H_2O/5/	
4. O+H_2 = OH+H	5.06E+04	2.67E+00	6.29E+03	[113]
5. H+O_2 = OH+O	9.75E+13	0.00E+00	1.49E+04	[114]
6. H+O_2(+M)=HO_2(+M)	1.48E+12	6.00E-01	0.00E+00	[115]
LOW	3.50E+016	-0.41	-1.12E+03/	
TROE	5.00E-01	1.00E+05	1.00E+01	
	AR/0/	H_2O/10.6/	H_2/1.5/	
7. H+OH+M = H_2O+M	2.20E+22	-2.00E+00	0.00E+00	[113]
	H_2O/6.4/	AR/0.38/		
8. H_2+OH = H_2O+H	1.00E+08	1.60E+00	3.30E+03	[113]
9. OH+OH = H_2O+O	1.50E+09	1.14E+00	1.00E+02	[113]
10. HO_2+OH = H_2O+O_2	2.89E+13	0.00E+00	-5.00E+02	[113]
11. HO_2+O = OH+O_2	1.63E+13	0.00E+00	-4.45E+02	[116]
12. H+HO_2 = H_2+O_2	4.28E+13	0.00E+00	1.41E+03	[113]
13. H+HO_2 = OH+OH	1.70E+14	0.00E+00	8.75E+02	[113]
14. H+HO_2 = H_2O+O	3.00E+13	0.00E+00	1.72E+03	[113]
15. NH_3+M = NH_2+H+M	2.20E+16	0.00E+00	9.35E+04	[36]
16. NH_3+H = NH_2+H_2	5.42E+05	2.40E+00	9.92E+03	[56]
17. NH_3+O = NH_2+OH	1.10E+06	2.10E+00	5.21E+03	[117]
18. NH_3+OH = NH_2+H_2O	5.00E+07	1.60E+00	9.50E+02	[117]
19. NH_3+NH = NH_2+NH_2	3.16E+14	0.00E+00	2.68E+04	[118]
20. NH_2+M = NH+H+M	3.16E+23	-2.00E+00	9.14E+04	[102]
21. NH_2+H = NH+H_2	1.00E+06	2.32E+00	7.99E+02	*
22. NH_2+N = N_2+H+H	6.90E+13	0.00E+00	0.00E+00	[119]
23. NH_2+NH = N_2H_2+H	1.50E+15	-5.00E-01	0.00E+00	[36]
24. NH_2+NH = NH_3+N	1.00E+13	0.00E+00	2.00E+03	[34]
25. NH_2+NH_2 = N_2H_2+H_2	5.00E+13	0.00E+00	1.50E+03	*
26. NH_2+O = H_2+NO	5.00E+12	0.00E+00	0.00E+00	[117]
27. NH_2+O = HNO+H	4.50E+13	0.00E+00	0.00E+00	[117]
28. NH_2+O = NH+OH	7.00E+12	0.00E+00	0.00E+00	[117]

29. NH_2+OH = NH+H_2O	9.00E+07	1.50E+00	-4.60E+02	[117]
30. NH_2+HO_2 = HNO+H_2O	5.68E+15	-1.12E+00	7.07E+02	[120]
31. NH_2+O_2 = HNO+OH	1.00E+13	0.00E+00	2.63E+04	[121]
32. NH_2+NO = NNH+OH	2.29E+10	4.25E-01	-8.14E+02	[122]
33. NH_2+NO = N_2+H_2O	2.77E+20	-2.65E+00	1.26E+03	[122]
34. NH_2+NO = H_2+N_2O	1.00E+13	0.00E+00	3.37E+04	[63]
35. NH_2+NO_2 = N_2O+H_2O	1.62E+16	-1.44E+00	2.70E+02	[123]
36. NH+H = N+H_2	3.20E+13	0.00E+00	3.25E+02	[38]
37. NH+N = N_2+H	9.00E+11	5.00E-01	0.00E+00	[107]
38. NH+NH = NNH+H	5.10E+13	0.00E+00	0.00E+00	[37]
39. NH+NO = N_2O+H	5.00E+14	-4.00E-01	0.00E+00	*
40. NH+O = NO+H	7.00E+13	0.00E+00	0.00E+00	[117]
41. NH+O = N+OH	7.00E+12	0.00E+00	0.00E+00	[117]
42. NH+OH = HNO+H	2.00E+13	0.00E+00	0.00E+00	[117]
43. NH+OH = N+H_2O	2.00E+09	1.20E+00	0.00E+00	[117]
44. NH+OH = NO+H_2	2.00E+13	0.00E+00	0.00E+00	[124]
45. NH+O_2 = HNO+O	4.00E+13	0.00E+00	1.79E+04	[114]
46. NH+O_2 = NO+OH	4.50E+08	7.90E-01	1.19E+03	[125]
47. NH+H_2O = HNO+H_2	2.00E+13	0.00E+00	1.39E+04	[106]
48. NH+N_2O = N_2+HNO	2.00E+12	0.00E+00	6.00E+03	[102]
49. NH+NO = N_2+OH	6.10E+13	-5.00E-01	1.20E+02	[99]
50. N+O_2 = NO+O	9.00E+09	1.00E+00	6.50E+03	[114]
51. N+OH = NO+H	2.80E+13	0.00E+00	0.00E+00	[114]
52. N_2+O = NO+N	1.80E+14	0.00E+00	7.61E+04	[114]
53. NO+O(+M) = NO_2(+M)	1.30E+15	-7.50E-01	0.00E+00	[100]
LOW	4.72E+24	-2.87E+00	1.55E+03	
TROE	9.62E-01	1.00E+01	7.96E+03	
	AR/0.6/	NO_2/6.2/	NO/1.8/	
	O_2 /0.8/	N_2O/4.4/	H_2O/10/	
54. NO+O = NO_2	1.30E+15	-7.50E-01	0.00E+00	[100]
55. H+NO(+M) = HNO(+M)	1.52E+15	-4.10E-01	0.00E+00	[100]
LOW	4.00E+20	-1.75E+00	0.00E+00	
	H_2O/10/	O_2/1.5/	AR/0.75/	
	H_2/2/			
56. N_2O(+M) = N_2+O(+M)	1.26E+12	0.00E+00	6.26E+04	[126]
LOW	4.00E+14	0.00E+00	5.66E+04	
	O_2/1.4/	N_2/1.7/	H_2O/12/	
	NO/3/	N_2O/3.5/		
57. N_2O+O = N_2+O_2	1.00E+14	0.00E+00	2.82E+04	[102]
58. N_2O+O = NO+NO	6.92E+13	0.00E+00	2.66E+04	[102]
59. N_2O+NO = N_2+NO_2	2.75E+14	0.00E+00	5.00E+04	[127]
60. N_2O+H = N_2+OH	5.00E+13	0.00E+00	1.52E+04	*
61. N_2O+OH = N_2+HO_2	1.00E+14	0.00E+00	3.00E+04	[128]

62. NO_2+O = NO+O_2	3.91E+12	0.00E+00	-2.38E+02	[100]
63. NO_2+H = NO+OH	1.32E+14	0.00E+00	3.62E+02	[129]
64. NO_2+OH = HO_2+NO	1.81E+13	0.00E+00	6.68E+03	[100]
65. HNO+H = NO+H_2	4.46E+11	7.20E-01	6.55E+02	[130]
66. HNO+OH = NO+H_2O	1.30E+07	1.88E+00	-9.56E+02	[131]
67. HNO+O = OH+NO	5.00E+11	5.00E-01	2.00E+03	[132]
68. HNO+NH_2 = NH_3+NO	2.00E+13	0.00E+00	1.00E+03	[35]
69. NNH = N_2+H	3.00E+08	0.00E+00	0.00E+00	[133]
70. NNH+M = N_2+H+M	1.00E+13	5.00E-01	3.06E+03	[133]
71. NNH+O = NH+NO	2.00E+14	0.00E+00	4.00E+03	[134]
72. NNH+O_2 = N_2O+OH	2.90E+11	-3.40E-01	1.50E+02	[133]
73. NNH+NO = N_2+HNO	5.00E+13	0.00E+00	0.00E+00	[135]
74. N_2H_2+M = NNH+H+M	5.00E+16	0.00E+00	5.00E+04	[31]
	H_2O/15/	O_2/2/	N_2/2/	
	H_2/2/			
75. N_2H_2+H = NNH+H_2	8.50E+04	2.63E+00	-2.30E+02	[136]
76. N_2H_2+NH_2 = NH_3+NNH	8.80E-02	4.05E+00	-1.61E+03	[136]
77. N_2H_2+O = NH_2+NO	1.00E+13	0.00E+00	0.00E+00	[35]
78. N_2H_2+O = NNH+OH	2.00E+13	0.00E+00	1.00E+03	[35]
79. N_2H_2+OH = NNH+H_2O	5.92E+01	3.40E+00	-1.36E+03	[136]
80. N_2H_2+NO = N_2O+NH_2	3.00E+10	0.00E+00	0.00E+00	[63]

Table 3.5: The *reduced* ammonia combustion mechanism
(* = Estimated in this work)

This *reduced* kinetic mechanism has been tested at low pressure for the simulations of the structure of all flat flames investigated but also for the prediction of burning velocities of ammonia-air flames propagating at atmospheric pressure and room temperature as it has been measured and will be presented in Chapters 5 to 7. The results of this *reduced* mechanism for the simulation of the flame structure together with the comparison with those coming from the *modified* Konnov mechanism are depicted in figs. 3.22 to 3.25 for the ammonia-oxygen-hydrogen flame II.

Concerning main species, i.e., ammonia, oxygen, nitrogen, water and argon, the reduction of the *modified* Konnov mechanism does not lead to any change in their predictions. (Fig. 3.22).

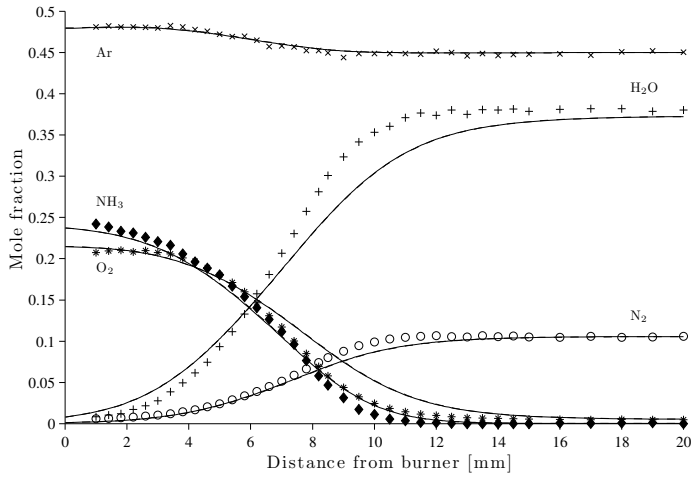

Figure 3.22: Experimental and simulated flame structure for major species in flame II. Symbols: experiments, Solid line: *Reduced mechanism*, Dashed line : *modified* Konnov mechanism

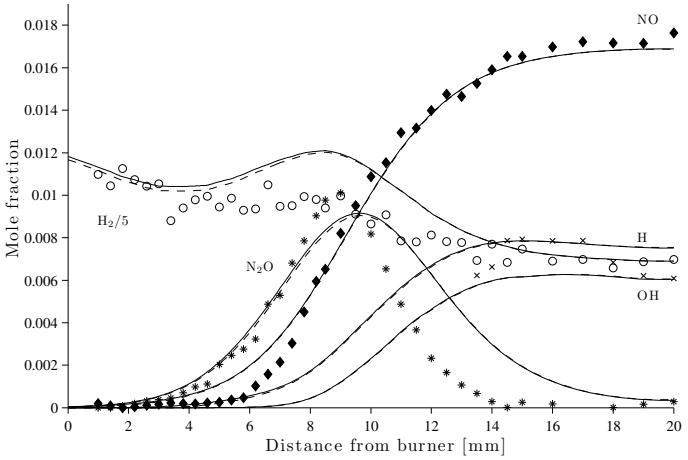

Figure 3.23: Experimental and simulated flame structure of some minor species of flame II. ($1.5\text{x}10^{-3} < \text{X}_i < 2\text{x}10^{-2}$) Symbols: experiments, Solid line: *Reduced mechanism*, Dashed line : *modified* Konnov mechanism

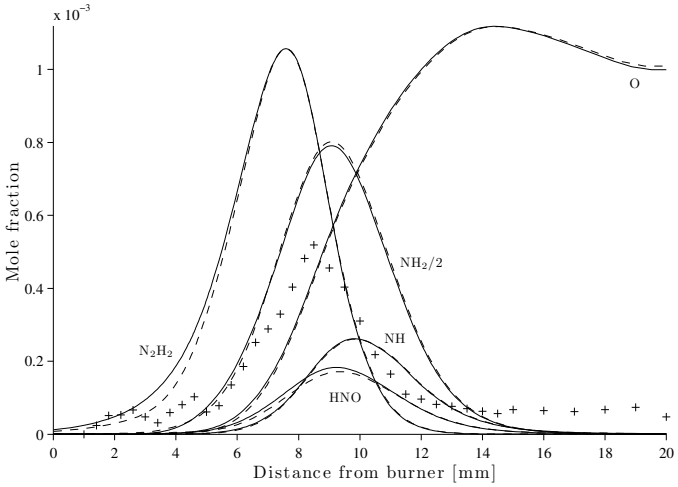

Figure 3.24: Experimental and simulated flame structure of some minor species of flame II. ($1x10^{-4} < X_i < 1.5x10^{-3}$) Symbols: experiments, Solid line: *Reduced mechanism*, Dashed line : *modified* Konnov mechanism

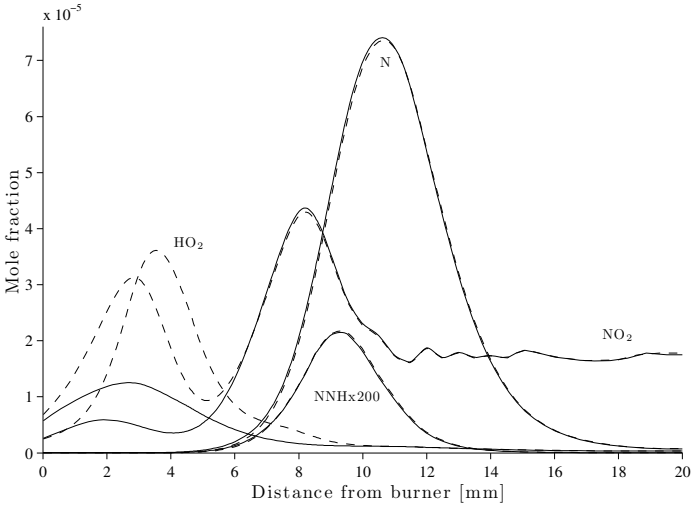

Figure 3.25: Simulated flame structure of some minor species of flame II. ($X_i < 1x10^{-4}$) Solid line: *Reduced mechanism*, Dashed line : *modified* Konnov mechanism

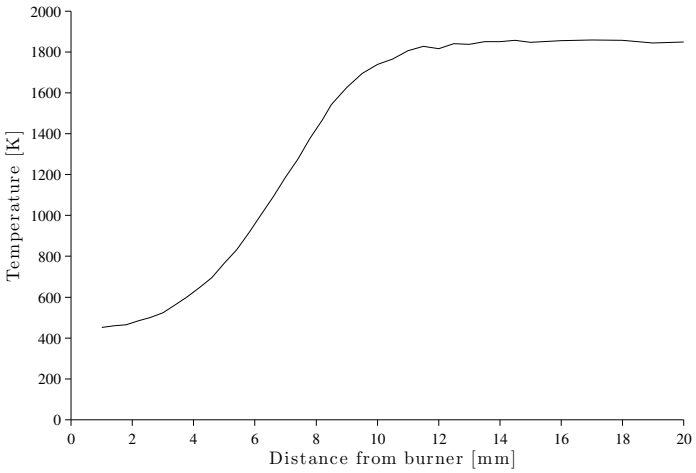

Figure 3.26: Experimental temperature profile of flame II

For the minor species (figs. 3.23, 3.24, 3.25), their predictions are identical for both mechanisms excepted for NO_2 and HO_2. The comparison of the formation and consumption kinetic pathways for the two mechanisms can help to understand these differences. They are depicted in figs. 3.27 to 3.30.

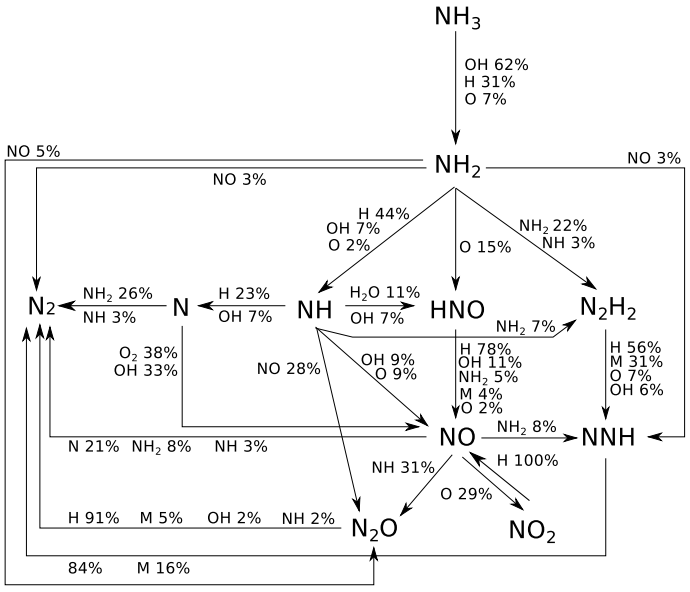

Figure 3.27: Consumption reaction pathways for the *reduced* ammonia combustion mechanism in flame II

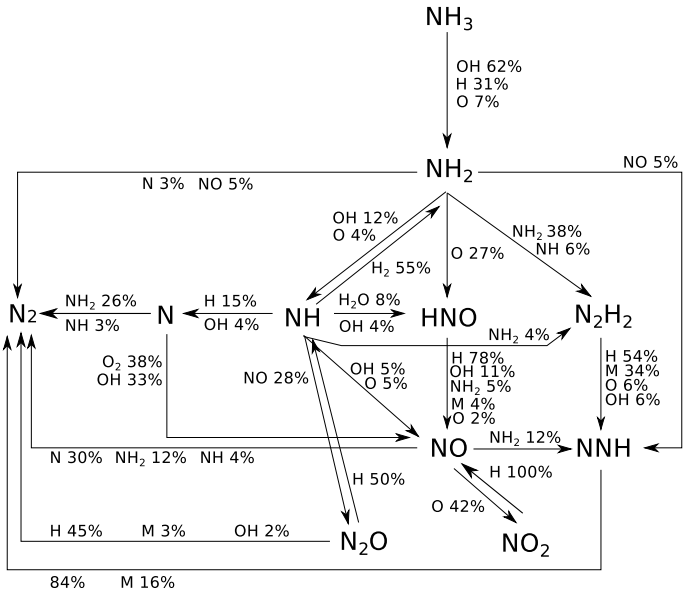

Figure 3.28: Consumption reaction pathways for the modified Konnov mechanism in flame II

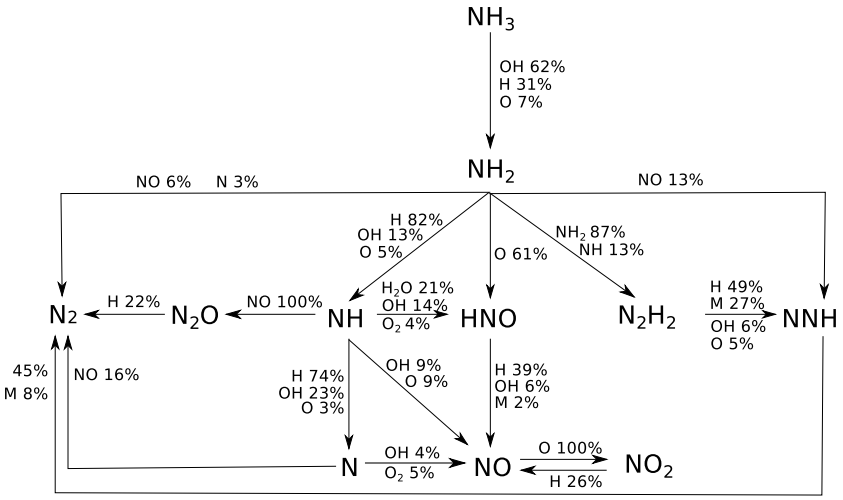

Figure 3.29: Formation reaction pathways for the *reduced* ammonia combustion mechanism in flame II

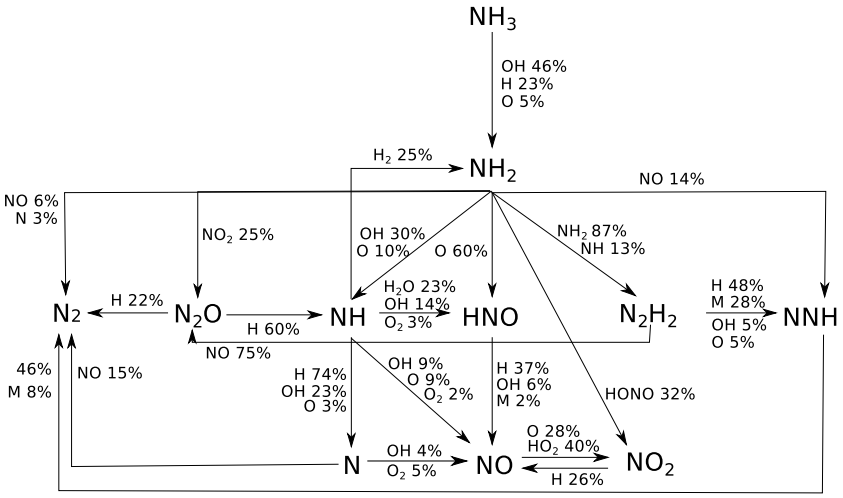

Figure 3.30: Formation reaction pathways for the modified Konnov mechanism in flame II

In the *modified* Konnov mechanism, NO_2 is formed thanks to three reactions:

$$NO + HO_2 = NO_2 + OH \ (1)$$
$$NH_2 + HONO = NO_2 + NH_3 \ (2)$$
$$NO + O \ (+M) = NO_2 \ (+M) \ (3)$$

while it is only produced by the third reaction in the *reduced* model since HONO is not taken into consideration in this mechanism and HO_2 mole fraction is strongly lowered. Reaction (1) produces NO_2 mainly in the first part of the flame where the temperature is lower and explains the difference in the NO_2 profile between the two mechanisms.

The persistence of NO_2 in the burned gases, which is observed in the Konnov mechanism, in the *modified* Konnov mechanism and in the *reduced* mechanism, can be explained by its equilibrium with NO. Indeed, as mentioned here above, NO_2 is produced mainly by the reaction NO+HO_2 = NO_2+OH in the Konnov and the *modified* Konnov mechanism and by the reaction NO+O (+M) = NO (+M) in the *reduced* mechanism while it is consumed mainly by the reaction NO_2+H = NO+OH in the three mechanisms. All of these reactions suggest an equilibrium with the nitrogen monoxide which is persistent in the burned gases for all the investigated flames.

Finally, HO_2 is formed in both mechanisms by the reaction $H+O_2+M = HO_2+M$, mainly in the first part of the flame front and consumed mainly by the reaction $H+HO_2 = OH+OH$. Figure. 3.31 presents the comparison of the reaction speed for these two reactions in each mechanism. The increase of the consumption reaction speed and the decrease of the formation reaction speed in the *reduced* mechanism compared to the *modified* Konnov mechanism explain the reduction of the HO_2 mole fraction in the *reduced* mechanism.

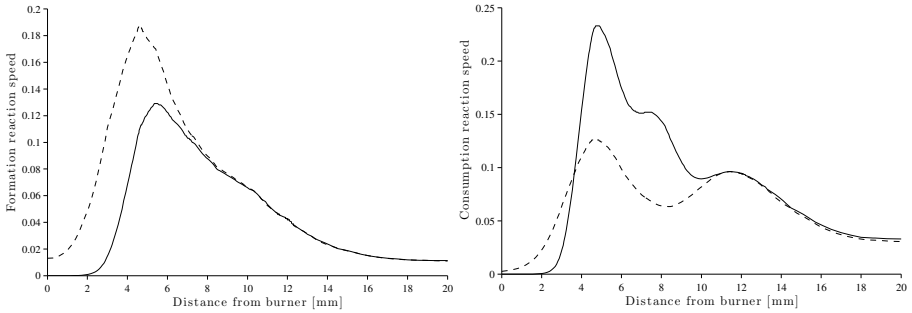

(a) $H+O_2+M = HO_2+M$ **(b)** $H+HO_2 = OH+OH$

Figure 3.31: HO_2 formation and consumption reactions speed in the *modified* Konnov mechanism (dashed lines) and in the *reduced* mechanism (solid lines)

CHAPTER 4

Ammonia flames structure at low pressure

With the *reduced* ammonia combustion mechanism presented in the previous Chapter, several simulations have been performed. First of all, the structures of the eight measured ammonia flames have been predicted. The comparison between the experimental and the numerical results is presented in the first section of this Chapter, along with a discussion on the individual impact of several initial parameters (initial hydrogen content, equivalence ratio, pressure) on species concentrations and on kinetic reaction pathways. Other numerical simulations of a stoichiometric ammonia flame with 7.5% of hydrogen have been performed to study separately the effects of pressure and temperature. These results are presented in the second section of this Chapter. Finally, to emphasize the role of nitrogen in the formation of the combustion products of ammonia, the numerical simulation of an ammonia-air flame burning at low pressure is reported in the third section. These numerical simulations allow also to create a link between the flame structure study, realized at low pressure with argon, with the study of ammonia combustion in a spark ignition engine, presented in the third part of this thesis and realized at elevated pressures and temperatures with air.

4.1 Flame structure study at low pressure

The comparisons of ammonia, nitrogen monoxide, nitrogen, oxygen, water, nitrous oxide, hydrogen, hydroxyl and amidogen radicals and temperature profiles are presented for each series of flames in Figs 4.1 to 4.24. Experimental results presented on these figures are mean species concentrations averaged from multiple measurements. Error bars are not added to ensure more legible graphs,

but random errors are estimated for each chemical species by the probability Student theory (4.1),

$$x = \overline{x} \pm \frac{ts}{\sqrt{n}} \tag{4.1}$$

where $\overline{x}$ is the average of measurements, s the standard deviation and t the Student's coefficient chosen for a given confidence interval of 95% and a population of size n. These random errors are around 5% for hydrogen, hydroxyl and amidogen radicals, 3% for ammonia, nitrogen monoxide and nitrous oxide and 1% for oxygen, nitrogen, water and temperature. Concerning systematic errors, they do not affect the comparison between the different flames because concentration profiles have been taken in the same conditions and consecutively.

4.1.1 Effect of the initial hydrogen content

As a reminder, Table 4.1 presents the initial composition and operating conditions of the four flames of this series. These flames have the same equivalence ratio ($\phi = 1.02$).

	X_{NH_3}	X_{H_2}	X_{O_2}	X_{Ar}	V_0	ϕ	p
I	0.2548	0.0512	0.2129	0.4811	35.1	1.02	60
II	0.2400	0.0749	0.2132	0.4719	42.1	1.02	50
III	0.2247	0.1003	0.2132	0.4618	42.1	1.03	50
IV	0.2074	0.1259	0.2137	0.4529	42.0	1.02	50

Table 4.1: Flames compositions and inlet conditions. (V_0 = inlet flow velocity $[cm.s^{-1}]$; ϕ = equivalence ratio ; p = pressure [mbar]).

Since the initial flow velocities of the fresh gases of all the flames of this series are similar, the displacement of the position of the flame front towards the burner by about 2.5 mm when the initial hydrogen percentage is increased from 5% to 12.5%, as depicted in Fig. 4.1, indicates indirectly the promoting effect of hydrogen on the adiabatic burning velocity of the ammonia flame. Furthermore, the flame with more hydrogen contains less argon leading to an increase of the adiabatic burning velocity due to a lower dilution. The small difference in distance observed between flames I and II is attributed to the pressure difference. Indeed flame I has been analyzed at 60 mbar in place of

50 mbar in order to stabilize it on the burner. This increase of pressure moves the flame closer to the burner.

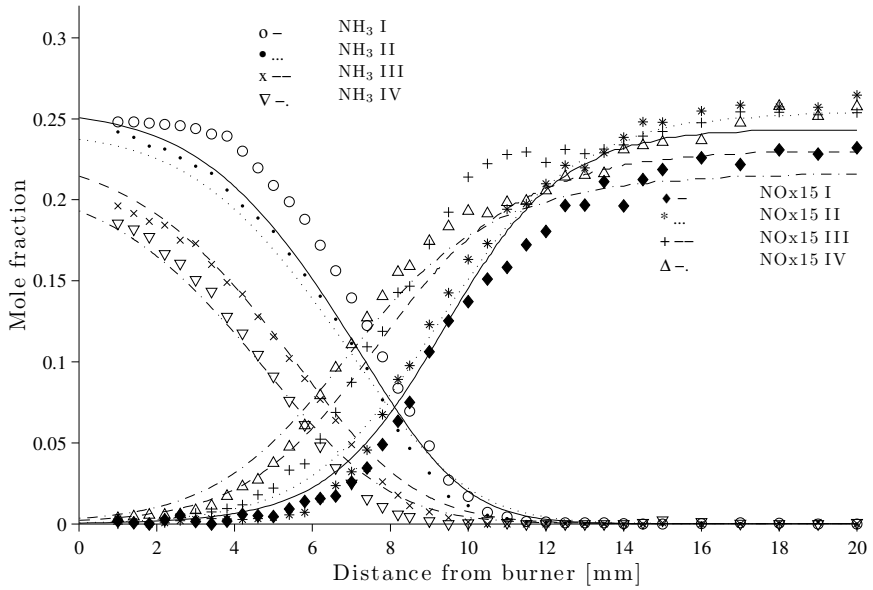

Figure 4.1: Comparison of the simulated (line) and experimental (symbols) mole fraction profiles of NH_3 and NO for different hydrogen percentages (I: 5%; II: 7.5%; III: 10%; IV: 12.6%).

The temperature profiles of the flames are presented in Fig. 4.2. Burned gases temperatures being 1874 K, 1850 K, 1781 K and 1741 K for flames I to IV, respectively. They all exhibit the three main flame zones: a preheating zone where temperature slowly increases, the flame front where the heat release is maximum, and the burned gas region where the temperature slowly decreases. These experimental burned gases temperatures can be compared to the adiabatic flame temperatures as presented in Table 4.2. The difference between the experimental and the adiabatic temperatures is about 300 K and can be explained by heat losses mainly on the burner mouth.

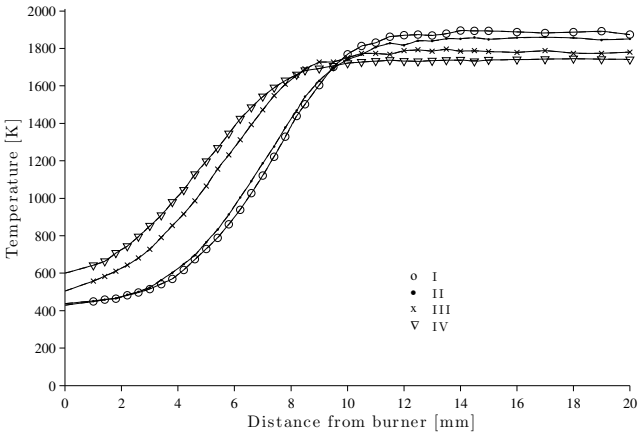

Figure 4.2: Comparison of the temperature profiles for different hydrogen percentages (I: 5%; II: 7.5%; III: 10%; IV: 12.6%).

% H_2	T_{exp}	T_{ad}
5%	1874 K	2125 K
7.5%	1850 K	2130 K
10%	1781 K	2105 K
12.6%	1741 K	2085 K

Table 4.2: Experimental and adiabatic flame temperatures for the four initial hydrogen percentages (I: 5%; II: 7.5%; III: 10%; IV: 12.6%).

Fig. 4.1 shows that the initial hydrogen content does not have an important impact on the final nitrogen monoxide concentration in the burned gases, the difference observed for flame I being attributed to a pressure effect that will be described later. Indeed, this flame has been stabilized at 60 mbar in place of 50 mbar for the three other ones. However, to maintain a constant equivalence ratio, an increase of the initial hydrogen content implies a lower ammonia initial concentration. Therefore, the $(X_{NO})_{max}$ / $(X_{NH_3})_{initial}$ ratio increases when the initial hydrogen content raises (flame I: 0.062 < flame II: 0.074 < flame III: 0.077 < flame IV: 0.082) even if the peak temperature decreases (Fig. 4.2). Since the thermal NO must decrease and that the fuel NO must decrease too, the increase of nitrogen monoxide proportionally to the decrease of the initial ammonia content observed experimentally is quite surprising and the effect ob-

served with the numerical simulations is more reasonable. Table 4.3 presents the importance of main reaction pathways for nitrogen monoxide formation and consumption according to the initial hydrogen content. Since flame I has been stabilized at 60 mbar experimentally, the second column of the table presents the same flame simulated at 50 mbar in order to eliminate a potential pressure effect. The increase of the initial hydrogen content leads to a change in the main NO consumption reaction pathways. Indeed, the contribution of the NO+O = NO_2 reaction is increased and the one of NO+NH_i reactions is decreased. Furthermore, variation of the initial H_2 content leads to a modification in the two main nitrogen monoxide formation pathways, i.e., reactions HNO+H = NO+H_2 (65) and NO_2+H = NO+OH (63). The increase of the weight of reaction (63) when the hydrogen percentage increases is due to higher NO_2 concentrations and the decrease of the importance of reaction (65) to lower HNO concentration. Indeed, HNO is produced from NH_2, itself produced from NH_3 and to maintain a constant equivalence ratio, an increase of the initial hydrogen content implies a lower ammonia initial concentration.

% H_2	5%	5%	7.5%	10%	12.6%
NO formation					
65. HNO+H = NO+H_2	39	40	39	35	32
63. NO_2+H = NO+OH	24	21	26	34	41
40. NH+O = NO+H	8	9	9	8	7
44. NH+OH = NO+H_2	9	10	9	7	6
51. N+OH = NO+H	4	5	4	4	3
50. N+O_2 = NO+O	5	5	5	5	4
66. HNO+OH = NO+H_2O	6	6	6	5	4
NO consumption					
54. NO+O = NO_2	27	24	29	38	45
39. NO+NH = N_2O+H	32	33	31	28	25
52. NO+N = N_2+O	20	23	21	18	15
33. NO+NH_2 = N_2+H_2O	9	8	8	7	7
32. NO+NH_2 = NNH+OH	9	9	8	7	6
49. NO+NH = N_2+OH	3	3	3	2	2

Table 4.3: Variation of main reaction pathways relative importance (%) with the initial hydrogen content according to the *reduced* ammonia mechanism for NO

Despite different initial mole fractions of H_2, the hydrogen concentration in the burned gases remains quite similar. Fig. 4.3 shows that the H_2 concentration profiles present a plateau which results from two opposite processes: the hydrogen consumption due to its oxidation and its formation due to the ammonia degradation.

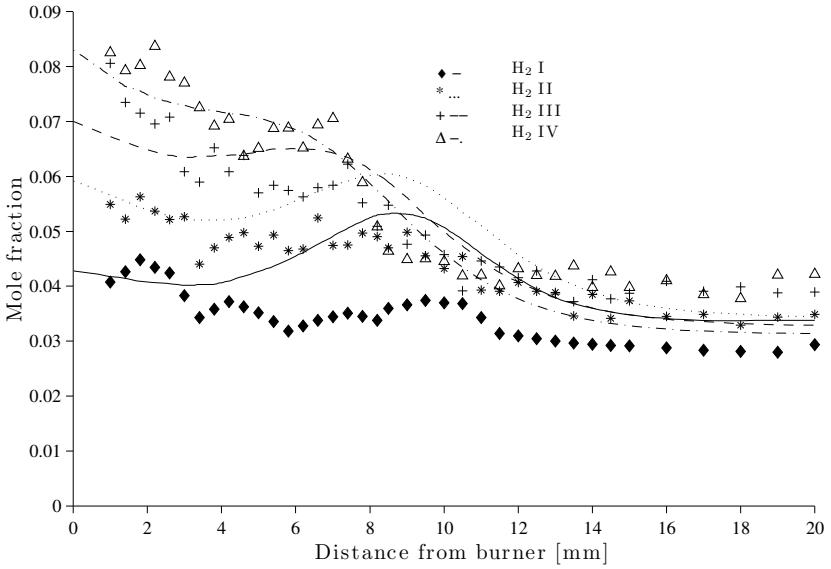

Figure 4.3: Comparison of the simulated (line) and experimental (symbols) mole fraction profiles of H_2 for different hydrogen percentages (I: 5%; II: 7.5%; III: 10%; IV: 12.6%).

Examining the NH_2 profiles in Fig. 4.4, it appears that their maxima depend mainly on the initial ammonia concentration and to a minor extent to the pressure difference for the profile of flame I. Table 4.4 shows the formation and consumption reactions of the NH_2 radical. Its formation is directly linked to ammonia consumption. Concerning its degradation, for all the conditions the main reaction is $NH_2+H = NH+H_2$. The initial hydrogen percentage does not have any impact on the weight of this reaction nor on the other ones.

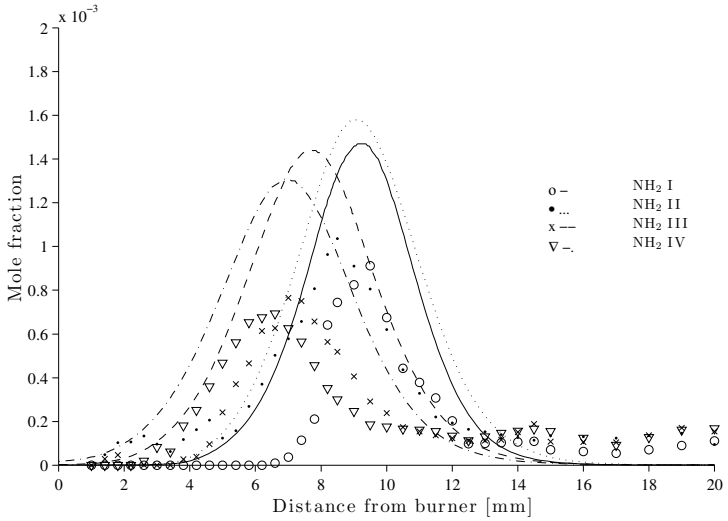

Figure 4.4: Comparison of the simulated (line) and experimental (symbols) mole fraction profiles of NH_2 for different hydrogen percentages (I: 5%; II: 7.5%; III: 10%; IV: 12.6%).

% H_2	5%	5%	7.5%	10%	12.6%
NH_2 formation					
18. NH_3+OH = NH_2+H_2O	64	62	63	63.5	65
16. NH_3+H = NH_2+H_2	30	31.5	30.5	30	29
17. NH_3+O = NH_2+OH	6	6.5	6.5	6.5	7
NH_2 consumption					
21. NH_2+H = NH+H_2	41	42	41	41	41
25. NH_2+NH_2 = N_2H_2+H_2	22	21	21	20	20
27. NH_2+O = HNO+H	13	13	14	14	15
29. NH_2+OH = NH+H_2O	7	7	7	6	6
28. NH_2+O = NH+OH	2	2	2	2	2
23. NH_2+NH = N_2H_2+H	3	3	3	3	3
33. NH_2+NO = N_2+H_2O	3	3	3	3	4
32. NH_2+NO = NNH+OH	3	3	3	3	3

Table 4.4: Variation of main reaction pathways relative importances (%) with the initial hydrogen content according to the *reduced* ammonia mechanism for NH_2

Looking at N_2O profiles (Fig. 4.5), it can be seen that the variation of the initial hydrogen content does not have a major influence on the formation of this species, the maxima increasing only from 9‰ to 12‰ when the initial H_2 concentration increases from 5% to 12.5%. Table 4.5 shows that independently of the conditions, this species is always formed by the reaction NH+NO = N_2O+H and mainly consumed by N_2O+H = N_2+OH.

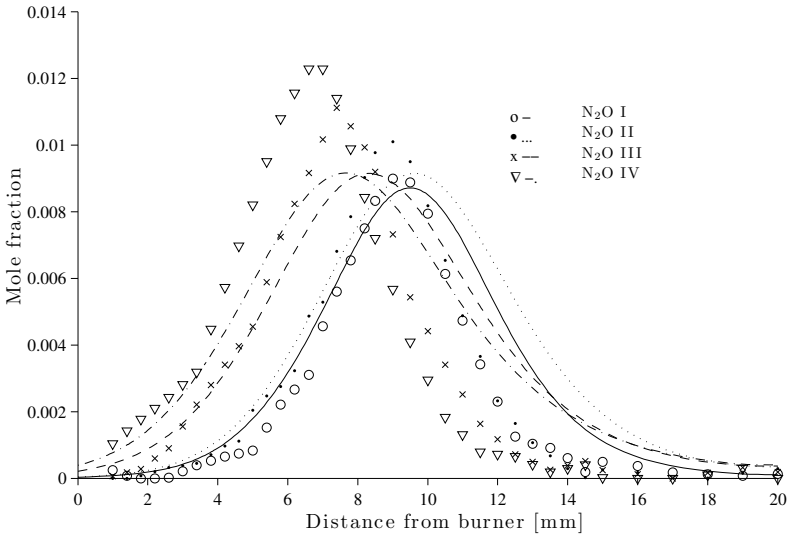

Figure 4.5: Comparison of the simulated (line) and experimental (symbols) mole fraction profiles of N_2O for different hydrogen percentages (I: 5%; II: 7.5%; III: 10%; IV: 12.6%).

% H_2	5%	5%	7.5%	10%	12.6%
N_2O formation					
39. NH+NO = N_2O+H	100	100	100	100	100
N_2O consumption					
60. N_2O+H = N_2+OH	88	88	90	92	93
56. N_2O(+M) = N_2+O(+M)	7	7	5	4	3
61. N_2O+OH = N_2+HO_2	2	2	2	2	1
48. N_2O+NH = N_2+HNO	2	2	2	2	2

Table 4.5: Variation of main reaction pathways relative importances (%) with the initial hydrogen content according to the *reduced* ammonia mechanism for N_2O

As shown in Fig. 4.6, the difference between the final concentrations of molecular nitrogen in the burned gases for each flame depends mainly on the initial ammonia concentration and to a lesser extent on some experimental errors on N_2 profiles in the flame front. The variation of the initial hydrogen content does not have any important impact on the nitrogen formation pathways as presented in Table 4.6.

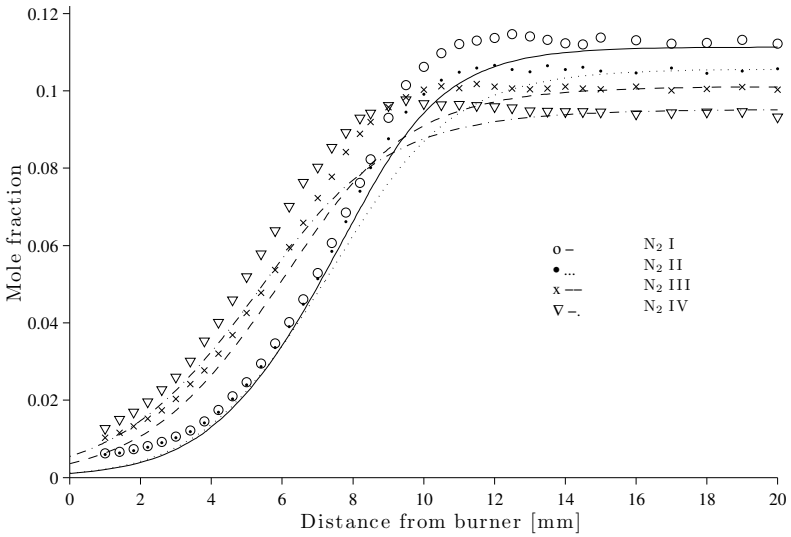

Figure 4.6: Comparison of the simulated (line) and experimental (symbols) mole fraction profiles of N_2 for different hydrogen percentages (I: 5%; II: 7.5%; III: 10%; IV: 12.6%).

% H_2	5%	5%	7.5%	10%	12.6%
69. NNH = N_2+H	42	43	42	42	40
60. N_2O+H = N_2+OH	20	20	21	22	23
52. N+NO = N_2+O	14	15	15	15	15
70. NNH(+M) = N_2+H(+M)	10	8	8	8	7
33. NH_2+NO = N_2+H_2O	6	6	6	6	7
22. NH_2+N = N_2+H+H	3	3	3	3	3

Table 4.6: Variation of main reaction pathways relative importances (%) with the initial hydrogen content according to the *reduced* ammonia mechanism for N_2

Finally, the only difference observed in the oxygen, water and hydroxyl radical profiles is the increase of the burning velocity of the ammonia flame when the hydrogen percentage increases (Figs. 4.7 and 4.8) as it has already been observed for the NH_3 and temperature profiles (Figs. 4.1 and 4.2). The oxygen concentration in the burned gases is very low ($\approx 5x10^{-3}$) and is ascribed to the $H/O/OH/H_2/O_2/H_2O$ partial equilibrium in stoichiometric conditions.

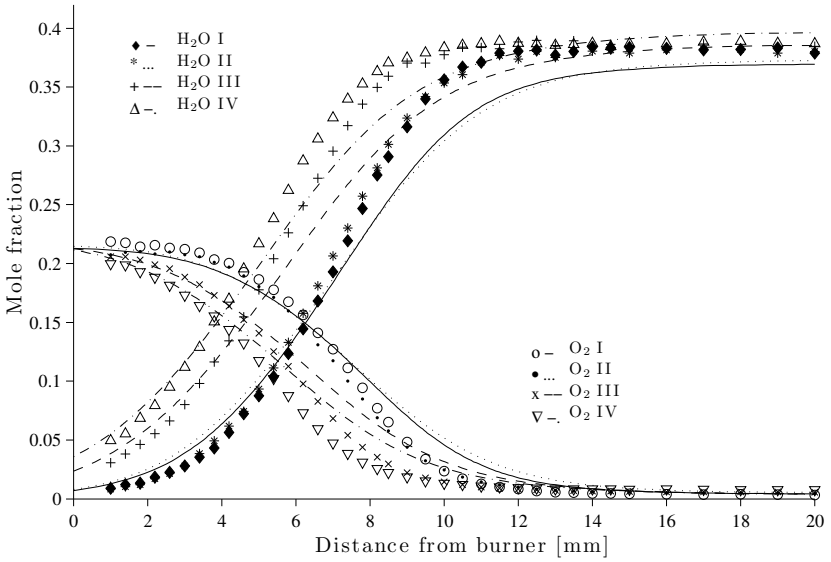

Figure 4.7: Comparison of the simulated (line) and experimental (symbols) mole fraction profiles of O_2 and H_2O for different hydrogen percentages (I: 5%; II: 7.5%; III: 10%; IV: 12.6%).

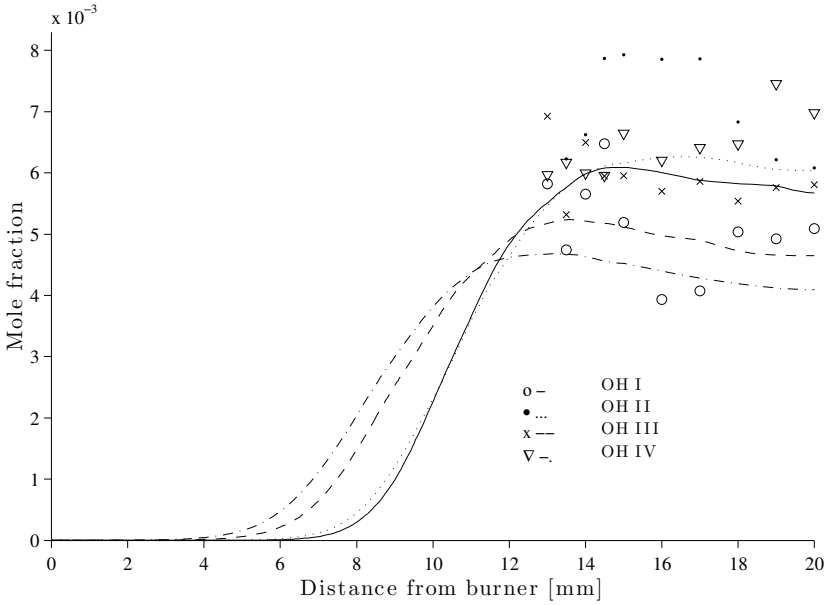

Figure 4.8: Comparison of the simulated (line) and experimental (symbols) mole fraction profiles of OH for different hydrogen percentages (I: 5%; II: 7.5%; III: 10%; IV: 12.6%).

4.1.2 Effect of the equivalence ratio

As a reminder, Table 4.7 presents the initial composition and operating conditions of the three flames of this series.

	X_{NH_3}	X_{H_2}	X_{O_2}	X_{Ar}	V_0	ϕ	p
V	0.2243	0.1001	0.2443	0.4312	42.2	0.9	50
III	0.2247	0.1003	0.2132	0.4618	42.1	1.0	50
VI	0.2226	0.0993	0.2008	0.4773	42.5	1.1	50

Table 4.7: Flames composition and inlet conditions. (V_0 = inlet flow velocity $[cm.s^{-1}]$; ϕ = equivalence ratio ; p = pressure [mbar]).

Figure 4.9 shows that for a same initial hydrogen content, the ammonia profile of the stoichiometric flame (III) lies between those of rich (VI) and lean (V) ones indicating that the latter has a larger adiabatic burning velocity than the rich and the stoichiometric one. This is due to the difference in the diluent concentration (Argon) for these three flames as shown in Table 4.7.

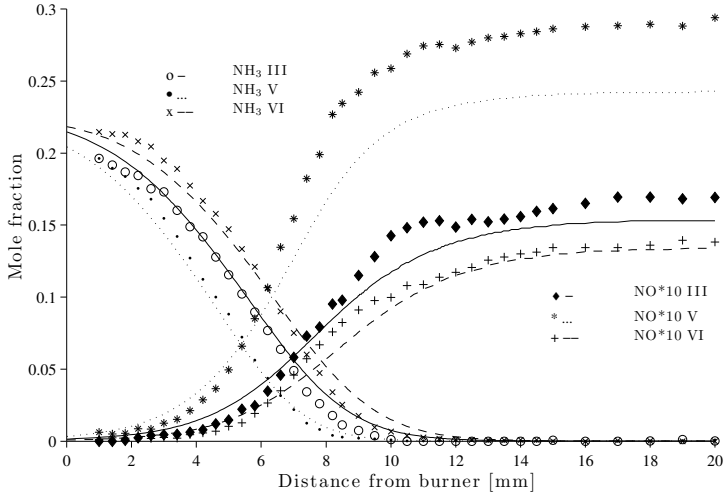

Figure 4.9: Comparison of the simulated (line) and experimental (symbols) mole fraction profiles of NH_3 and NO for different equivalence ratios (III: $\phi = 1.0$; V: $\phi = 0.9$; VI: $\phi = 1.1$)

The effects of the equivalence ratio on the main consumption reaction pathways of ammonia are presented in Table 4.8. As expected, the consumption reaction of ammonia with atomic hydrogen is more important when the flame is rich, the reaction with the hydroxyl radical is more important when the flame is lean and the reaction with atomic oxygen is not sensitive to the equivalence ratio.

ϕ	0.9	1.0	1.1
18. NH_3+OH = NH_2+H_2O	71	63	59
16. NH_3+H = NH_2+H_2	22	30	34
17. NH_3+O = NH_2+OH	7	7	7

Table 4.8: Variation of main reaction pathways relative importances (%) with the equivalence ratio according to the *reduced* ammonia mechanism for NH_3.

As depicted in Figure 4.9 the equivalence ratio has an important impact on the NO yield. This impact is more important between the lean (ϕ=0.9) and the stoichiometric flames where the ratio $(X_{NO})_{lean}$ / $(X_{NO})_{stoich}$ = 1.73 while it is only 1.22 for $(X_{NO})_{stoich}$ / $(X_{NO})_{rich}$. This can be explained by the temperature profiles presented in Fig. 4.10. Indeed, the burned gases temperature of the lean flame (T = 1920K) is higher than the stoichiometric and rich one (T $\approx$ 1800K). Such a result illustrates the strong effect of the equivalence ratio on the nitrogen monoxide formation which means that this is an important factor to take into account for the control of NO in exhaust gases in practical devices. The differences between the experimental burned gases temperatures and the adiabatic temperatures for these three flames are presented in Table 4.9. They can be attributed once again to the heat losses to the burner surface.

flame	ϕ	T_{exp}	T_{ad}
V	0.9	1920 K	2130 K
III	1.0	1781 K	2105 K
VI	1.1	1820 K	2095 K

Table 4.9: Experimental and adiabatic flame temperatures for the equivalence ratio variation.

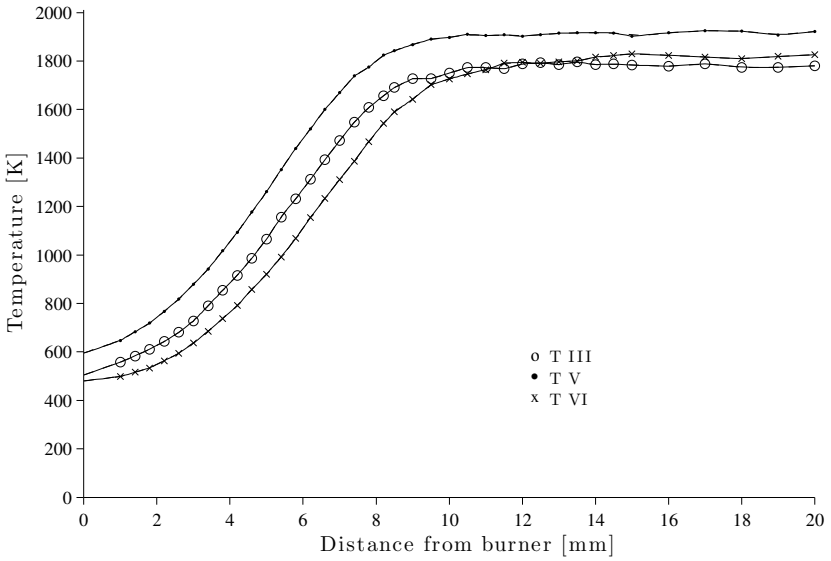

Figure 4.10: Comparison of the measured temperature profiles for different equivalence ratios (III: $\phi = 1.0$; V: $\phi = 0.9$; VI: $\phi = 1.1$)

As in the case of an initial hydrogen content variation, reactions HNO+H = NO+H_2 (65) and NO_2+H = NO+OH (63) represent approximately 70% of the nitrogen monoxide formation pathways (Table 4.10). When the equivalence ratio increases, the hydrogen atom concentration increases but the NO_2 one decreases leading to a less consequent impact of reaction (63) and a larger effect of reaction (65). Finally, nitrogen monoxide consumption reactions affected by the equivalence ratio are mainly reactions with atomic oxygen, atomic nitrogen and imidogen (NH) radical. As expected, the importance of the first one decreases for a richest flame due to lower oxygen atoms concentration in the flame and the contribution of the two others raises with an increasing NH_3 content.

ϕ	0.9	1.0	1.1
NO formation			
65. HNO+H = NO+H_2	32	35	39
63. NO_2+H = NO+OH	35	34	27
40. NH+O = NO+H	8	8	9
44. NH+OH = NO+H_2	8	7	8
51. N+OH = NO+H	3	4	5
50. N+O_2 = NO+O	3	5	6
66. HNO+OH=NO+H_2O	8	5	4
NO consumption			
54. NO+O = NO_2	42	38	29
39. NO+NH = N_2O+H	26	28	31
52. NO+N = N_2+O	13	18	23
33. NO+NH_2 = N_2+H_2O	9	7	7
32. NO+NH_2 = NNH+OH	8	7	7
49. NO+NH = N_2+OH	2	2	3

Table 4.10: Variation of main reaction pathways relative importances (%) with the equivalence ratio according to the *reduced* ammonia mechanism for NO

Since independently of the equivalence ratio conditions, N_2O is always formed mainly by the reaction NH+NO = N_2O+H and consumed by N_2O+H = N_2+H, its maximum concentration is as expected higher in the lean flame with a higher nitrogen monoxide content while those in the rich and stoichiometric ones are very similar. (Fig 4.11)

The opposite effect is observed for the final concentrations of molecular nitrogen $(X_{N_2})_{lean} < (X_{N_2})_{stoich.} \approx (X_{N_2})_{rich}$ (Fig. 4.12). This can be easily explained by a higher oxygen concentration in the leaner flame leading to more oxygenated combustion products like NO and N_2O. The equivalence ratio does not have a significant impact on the main formation reaction pathways of molecular nitrogen.

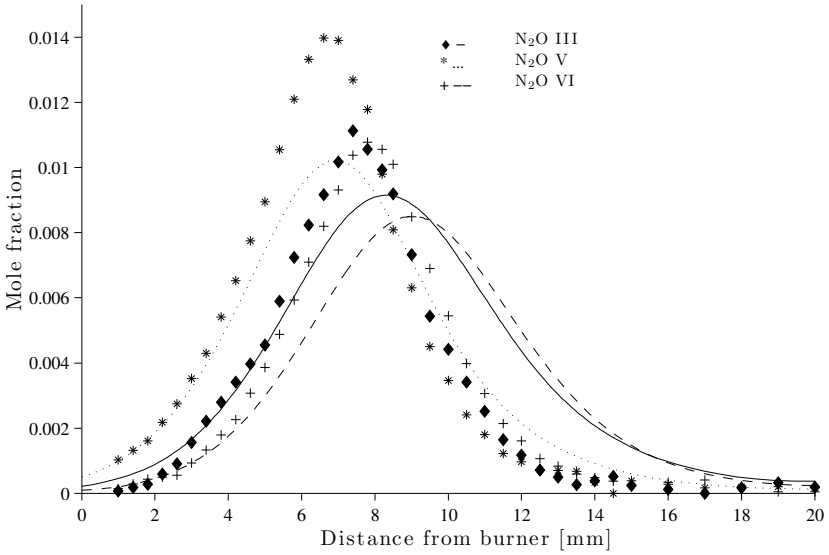

Figure 4.11: Comparison of the simulated (line) and experimental (symbols) mole fraction profiles of N_2O for different equivalence ratios (III: $\phi = 1.0$; V: $\phi = 0.9$; VI: $\phi = 1.1$)

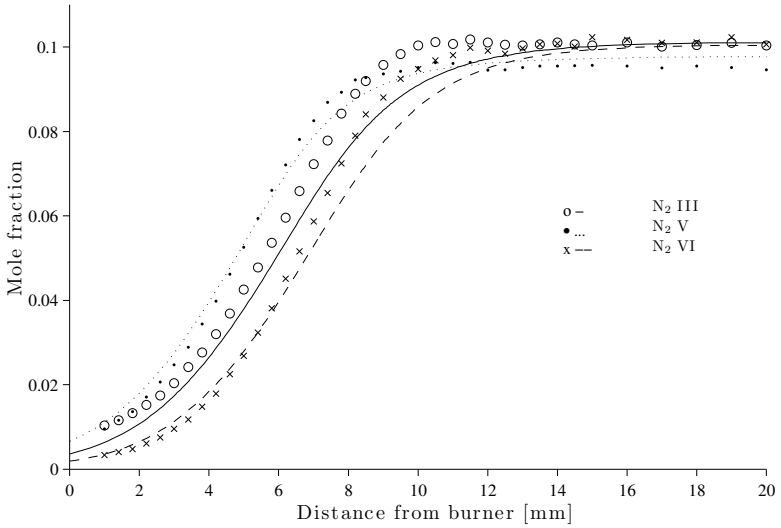

Figure 4.12: Comparison of the simulated (line) and experimental (symbols) mole fraction profiles of N_2 for different equivalence ratios (III: $\phi = 1.0$; V: $\phi = 0.9$; VI: $\phi = 1.1$)

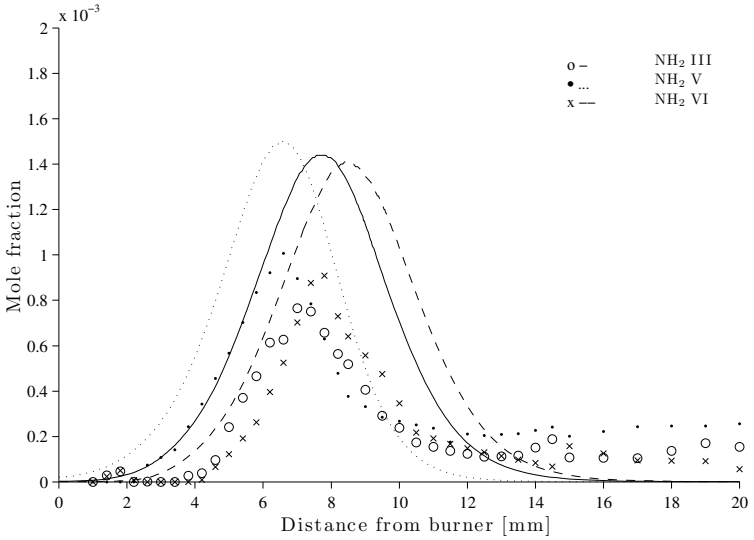

Figure 4.13: Comparison of the simulated (line) and experimental (symbols) mole fraction profiles of NH_2 for different equivalence ratios (III: $\phi = 1.0$; V: $\phi = 0.9$; VI: $\phi = 1.1$)

ϕ	0.9	1.0	1.1
NH_2 formation			
18. NH_3+OH = NH_2+H_2O	71	63	59
16. NH_3+H = NH_2+H_2	22	30	34
17. NH_3+O = NH_2+OH	7	7	7
NH_2 consumption			
21. NH_2+H = NH+H_2	35	41	45
25. NH_2+NH_2 = N_2H_2+H_2	19	20	20
27. NH_2+O = HNO+H	18	14	13
29. NH_2+OH = NH+H_2O	9	6	5
28. NH_2+O = NH+OH	3	2	2
23. NH_2+NH = N_2H_2+H	2	3	3
33. NH_2+NO = N_2+H_2O	4	3	3
32. NH_2+NO = NNH+OH	4	3	3

Table 4.11: Variation of main reaction pathways relative importance (%) with equivalence ratio according to the *reduced* ammonia mechanism for NH_2

Since the investigated range of equivalence ratios is not very wide, the NH_2 profiles (Fig. 4.13) are very similar in the three flames indicating a correct combustion in each case. Nevertheless, Table 4.11 shows the impact of the equivalence ratio on NH_2 main formation and consumption reactions. Its formation is directly linked to ammonia consumption. Concerning its degradation, for all the conditions the main reaction is $NH_2+H = NH+H_2$ but its importance increases with the equivalence ratio due to a higher atomic hydrogen content.

Finally, in comparison to a stoichiometric ammonia flame, a leaner flame leads to larger concentrations of oxygen, hydroxyl radical and water, but less hydrogen in the burned gases. A richest flame leads to approximately the same quantities of oxygen and hydroxyl radical but less water and more hydrogen. This can be observed in figures 4.14 to 4.16.

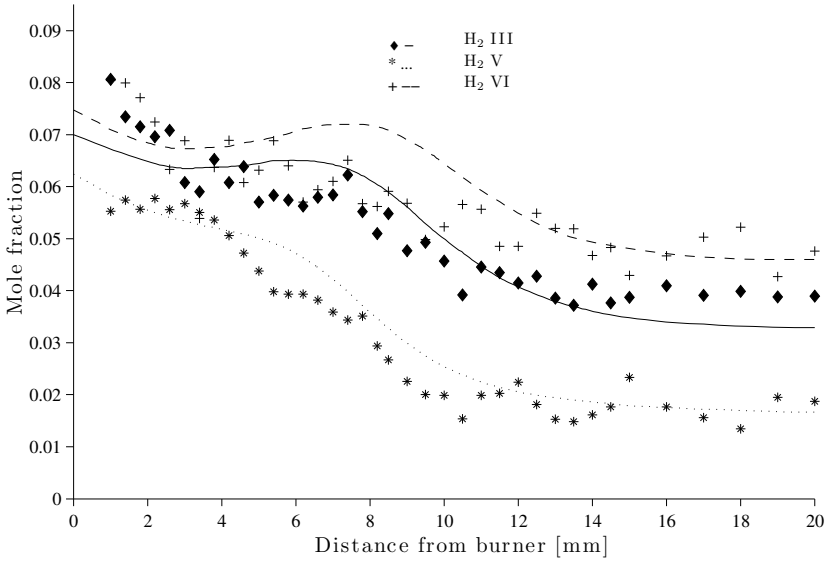

Figure 4.14: Comparison of the simulated (line) and experimental (symbols) mole fraction profiles of H_2 for different equivalence ratios (III: $\phi = 1.0$; V: $\phi = 0.9$; VI: $\phi = 1.1$)

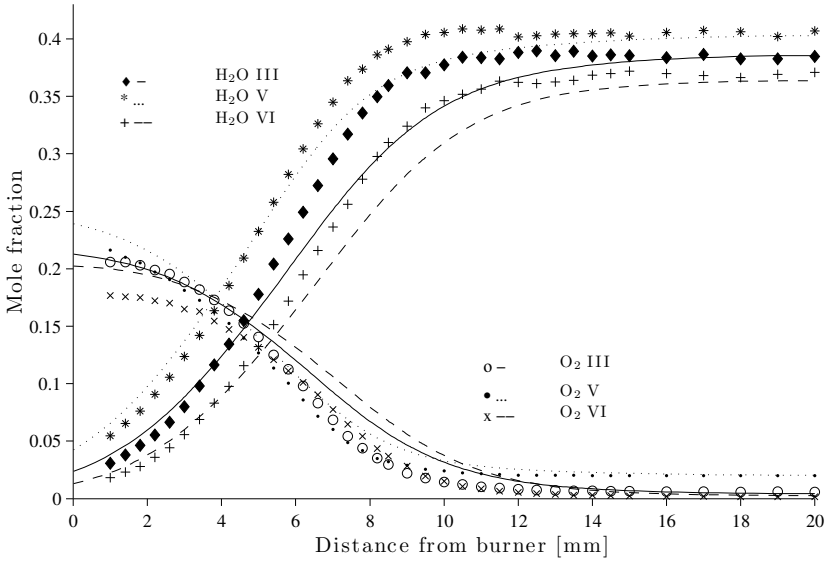

Figure 4.15: Comparison of the simulated (line) and experimental (symbols) mole fraction profiles of O_2 and H_2O for different equivalence ratios (III: $\phi = 1.0$; V: $\phi = 0.9$; VI: $\phi = 1.1$)

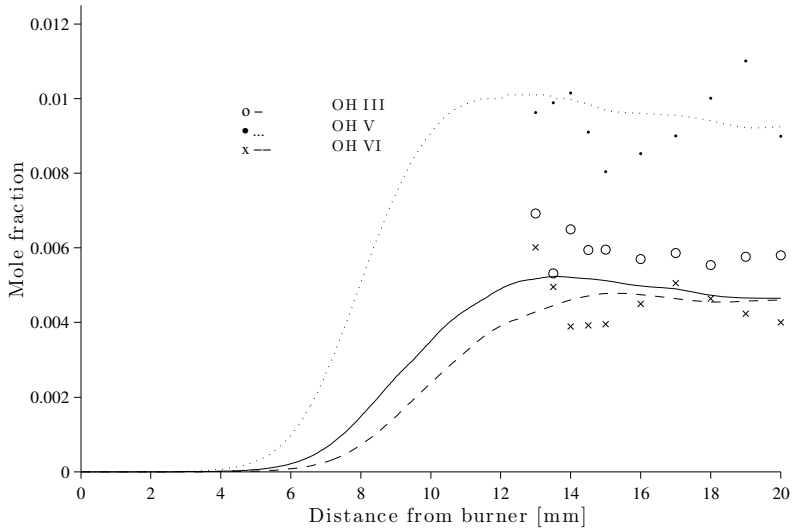

Figure 4.16: Comparison of the simulated (line) and experimental (symbols) mole fraction profiles of OH for different equivalence ratios (III: $\phi = 1.0$; V: $\phi = 0.9$; VI: $\phi = 1.1$)

4.1.3 Effect of the pressure

As a reminder, Table 4.12 presents the initial compositions and operating conditions of the three flames of this series.

	X_{NH_3}	X_{H_2}	X_{O_2}	X_{Ar}	V_0	ϕ	p
I	0.2548	0.0512	0.2129	0.4811	35.1	1.02	60
VII	0.2548	0.0512	0.2129	0.4811	23.4	1.02	90
VIII	0.2548	0.0512	0.2129	0.4811	17.6	1.02	120

Table 4.12: Flame compositions and inlet conditions. (V_0 = inlet flow velocity [$cm.s^{-1}$]; ϕ = equivalence ratio ; p = pressure [mbar]).

The effect of the pressure has been studied between 60 and 120 mbar. The initial flow velocities are 35.1, 23.4 and 17.6 cm.s^{-1} for flames I, VII and VIII, respectively. Because these flames must have a very similar adiabatic burning velocity, the flame stabilized at the highest pressure is located closer to the burner as shown in Fig. 4.17. Table 4.13 presents the impact of pressure on the main consumption pathways of ammonia. When the pressure increases, the reaction with atomic hydrogen is disadvantaged and the one with hydroxyl radical favored. However, this is most probably due more to a temperature effect than to a pressure one. Indeed, the flame located closer to the burner looses more heat to this one leading to a lower flame temperature.

p [mbar]	60	90	120
18. NH_3 + OH = NH_2+H_2O	64	68	70
16. NH_3 + H = NH_2+H_2	30	26	24
17. NH_3 + O = NH_2+ OH	6	6	6

Table 4.13: Variation of main reaction pathways relative importances (%) with the pressure according to the *reduced* ammonia mechanism for NH_3

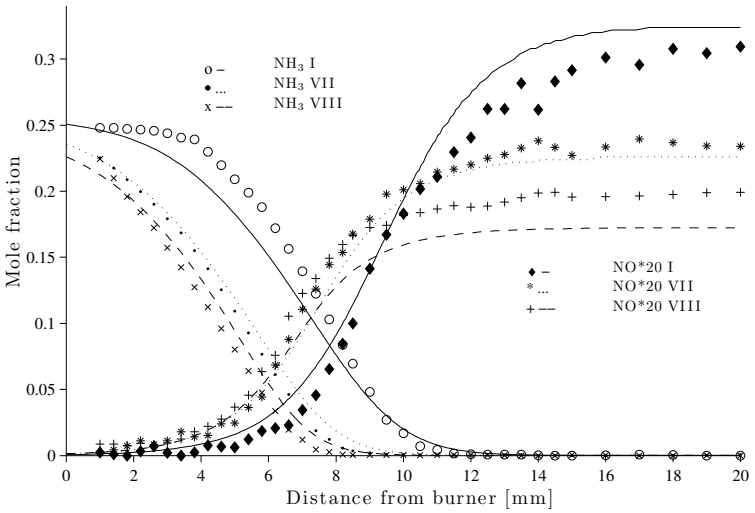

Figure 4.17: Comparison of the simulated (line) and experimental (symbols) mole fraction profiles of NH_3 and NO for different pressures (I: P = 60 mbar; VII: P = 90 mbar; VIII: P = 120 mbar)

For the nitrogen monoxide, the final value depends on the final temperature which varies from 1866 K (60 mbar) to 1727 K (90 mbar) and finally 1670 K (120 mbar) (Fig. 4.18). The higher the temperature, the higher the final NO mole fraction (Fig. 4.17). The differences between the experimental burned gases temperatures and the adiabatic flame temperatures for these three flames are presented in Table 4.14 and can be attributed to heat losses to the burner surface.

p [mbar]	T_{exp}	T_{ad}
60	1866 K	2125 K
90	1727 K	2080 K
120	1670 K	2050 K

Table 4.14: Experimental and adiabatic flame temperatures for the pressure variations

It is thus difficult to discriminate between temperature and pressure effects. Therefore the next section presents the simulation of the same ammonia flame (flame II) for several conditions of pressure (from 50 to 1000 mbar) with the same temperature profile as an input data in order to evaluate the pressure effect only on the major products and main reaction pathways of ammonia

combustion.

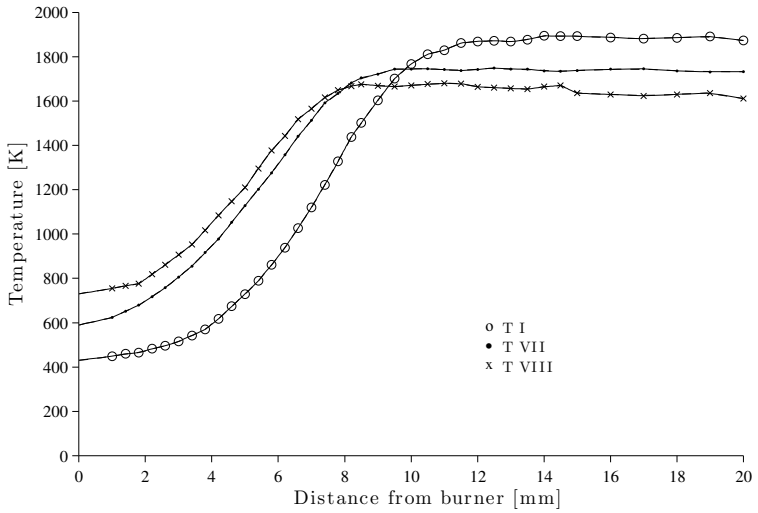

Figure 4.18: Comparison of the temperature profiles for different pressures (I: P = 60 mbar; VII: P = 90 mbar; VIII: P = 120 mbar)

An increase of the pressure coupled with a decrease of the temperature leads to a diminution of the N_2O peak, as shown in Fig. 4.19. This is due to a smaller nitrogen monoxide content reducing the N_2O formation by the NH+NO = N_2O+H reaction.

For molecular nitrogen (Fig. 4.20) no difference is observed in the burned gases region. Moreover, pressure does not have any impact on the main formation pathways of this species as presented in Table 4.15.

p [mbar]	60	90	120
69. NNH = N_2+H	42	42	40
60. N_2O+H = N_2+OH	20	20	20
52. N+NO = N_2+ O	14	11	9
70. NNH(+M) = N_2+H(+M)	10	14	18
33. NH_2+NO = N_2+H_2O	6	7	7
22. NH_2+N = N_2+H+H	3	2	2

Table 4.15: Variation of main reaction pathways relative importances (%) with the pressure according to the *reduced* ammonia mechanism for N_2

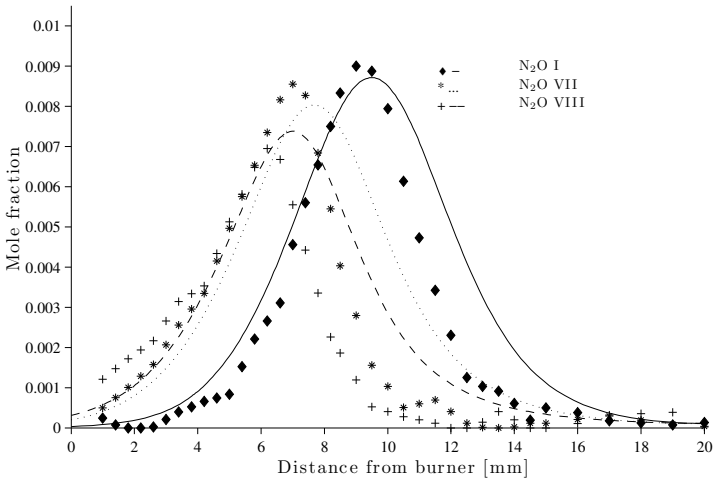

Figure 4.19: Comparison of the simulated (line) and experimental (symbols) mole fraction profiles of N_2O for different pressures (I: P = 60 mbar; VII: P = 90 mbar; VIII: P = 120 mbar)

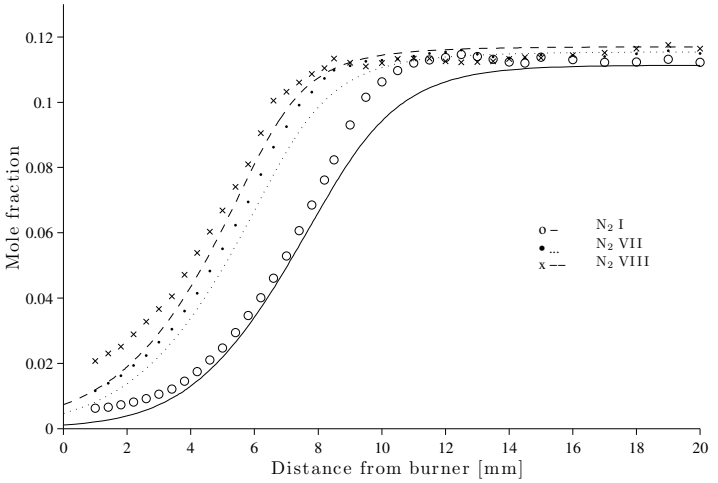

Figure 4.20: Comparison of the simulated (line) and experimental (symbols) mole fraction profiles of N_2 for different pressures (I: P = 60 mbar; VII: P = 90 mbar; VIII: P = 120 mbar)

The hydrogen consumption is faster and its final value is lower in the 90 and 120 mbar flames. Such a result, observed in Fig. 4.21, indicates an increase of the impact of termination reactions of the H_2 / O_2 system at higher pressure.

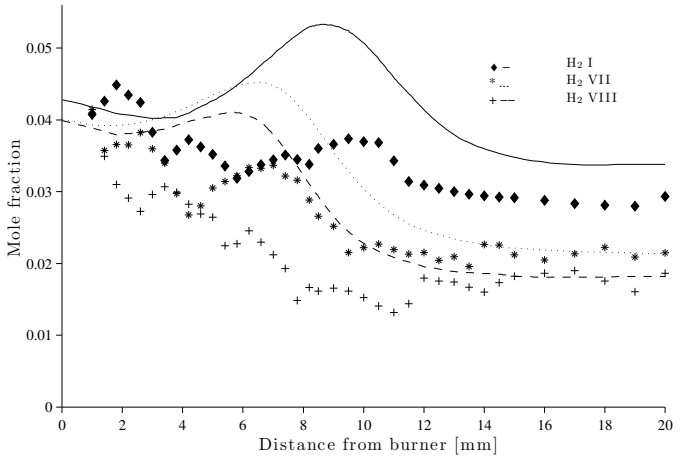

Figure 4.21: Comparison of the simulated (line) and experimental (symbols) mole fraction profiles of H_2 for different pressures (I: P = 60 mbar; VII: P = 90 mbar; VIII: P = 120 mbar)

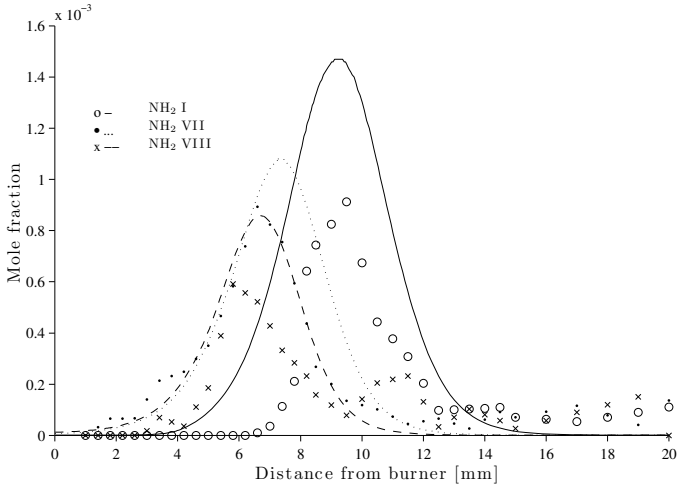

Figure 4.22: Comparison of the simulated (line) and experimental (symbols) mole fraction profiles of NH_2 for different pressures (I: P = 60 mbar; VII: P = 90 mbar; VIII: P = 120 mbar)

Due to an ammonia consumption gradient higher for the flame stabilized at a higher pressure, the NH_2 maximum is lower in the highest pressure flame (Fig. 4.22). However, the studied pressure domain is too narrow to change its main consumption reaction which remains NH_2+H = NH+H_2.

Finally, with the increasing pressure, the increase of the burned gases water mole fraction, the decrease of the hydroxyl radical mole fraction and the constant oxygen concentration can be attributed to the $H/O/OH/H_2/O_2/H_2O$ partial equilibrium. (Figs. 4.23 and 4.24)

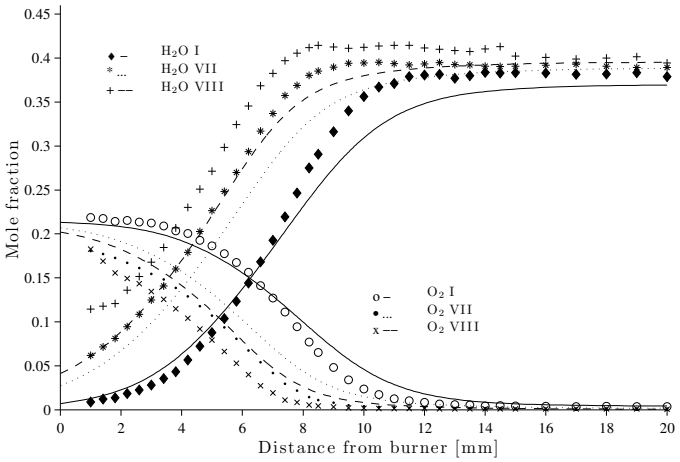

Figure 4.23: Comparison of the simulated (line) and experimental (symbols) mole fraction profiles of O_2 and H_2O for different pressures (I: P = 60 mbar; VII: P = 90 mbar; VIII: P = 120 mbar)

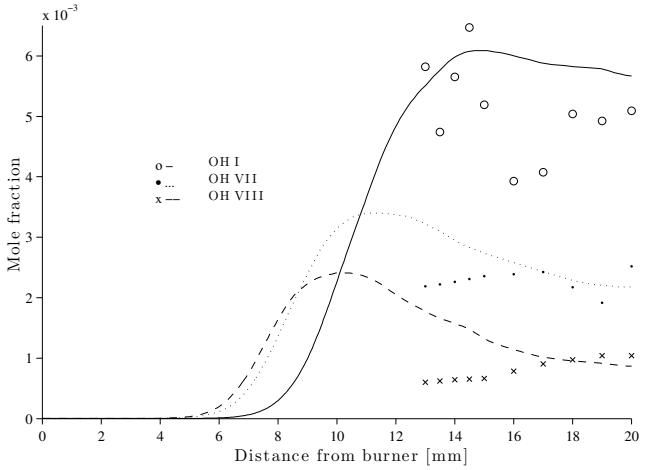

Figure 4.24: Comparison of the simulated (line) and experimental (symbols) mole fraction profiles of OH for different pressures (I: P = 60 mbar; VII: P = 90 mbar; VIII: P = 120 mbar)

4.2 Discussion on pressure variation

As discussed previously, it is difficult, based on the experiments, to discriminate between the effects of pressure or temperature changes. In order to separate these two effects, the flame structure of flame II has been simulated in several conditions of pressure, from 50 mbar to 1 bar, with the same experimental temperature profile as input data. As a reminder, flame II has the following initial composition:

$$X_{NH_3} : 0.24; X_{H_2} : 0.07; X_{O_2} : 0.21; X_{Ar} : 0.47; \phi : 1.02$$

Figures 4.25 to 4.28 present the effect of the pressure on the important species to consider in practical devices, i.e., ammonia and oxygen consumption, nitrogen monoxide, nitrogen and water formation and other nitrogen oxides, i.e. NO_2 and N_2O. An increase of pressure leads to a raise of the radicals recombination reactions and of the efficiency of reactions with a third body. Therefore, the combustion is more complete, leading in this case to more H_2O and N_2 and less products from an incomplete combustion like NO, HNO, N_2O and NO_2.

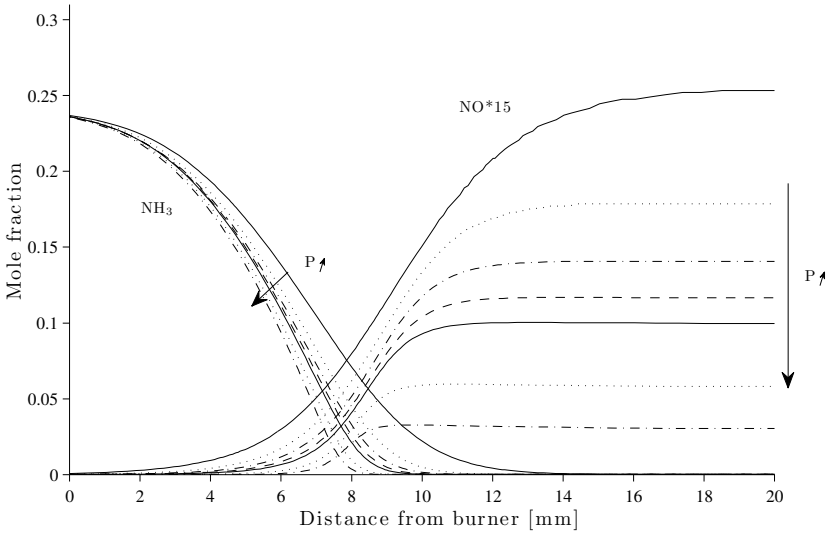

Figure 4.25: Effects of the pressure on ammonia consumption and nitrogen monoxide formation according to the *reduced* ammonia mechanism

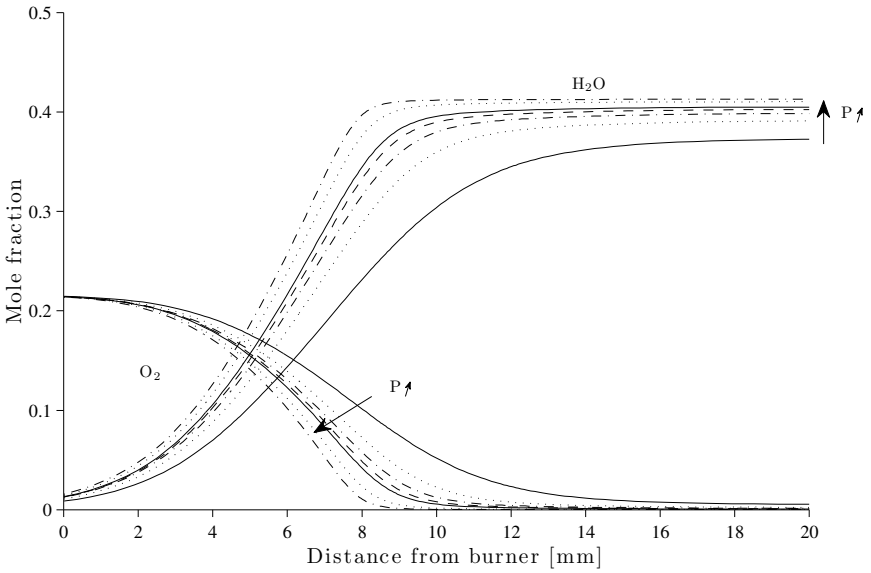

Figure 4.26: Effects of the pressure on oxygen consumption and water formation according to the *reduced* ammonia mechanism

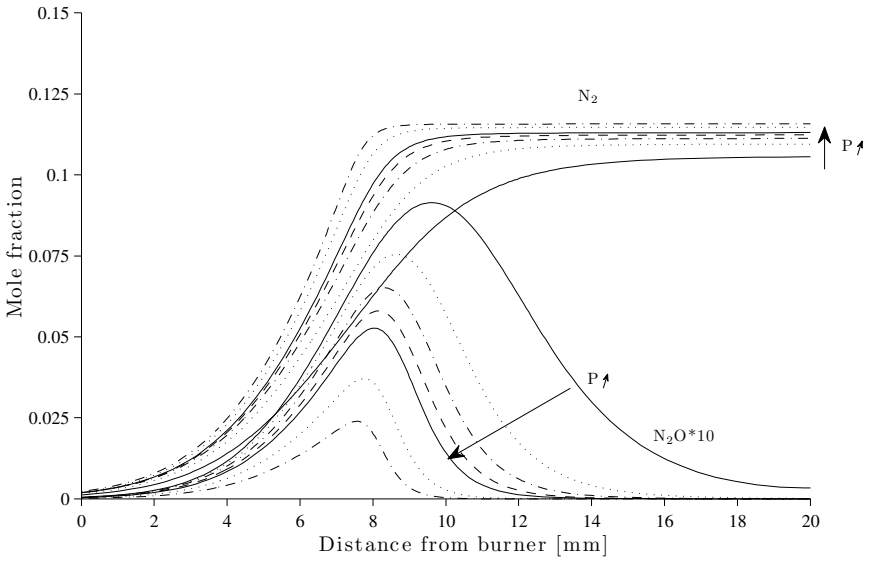

Figure 4.27: Effects of the pressure on nitrogen and nitrous oxide formations according to the *reduced* ammonia mechanism

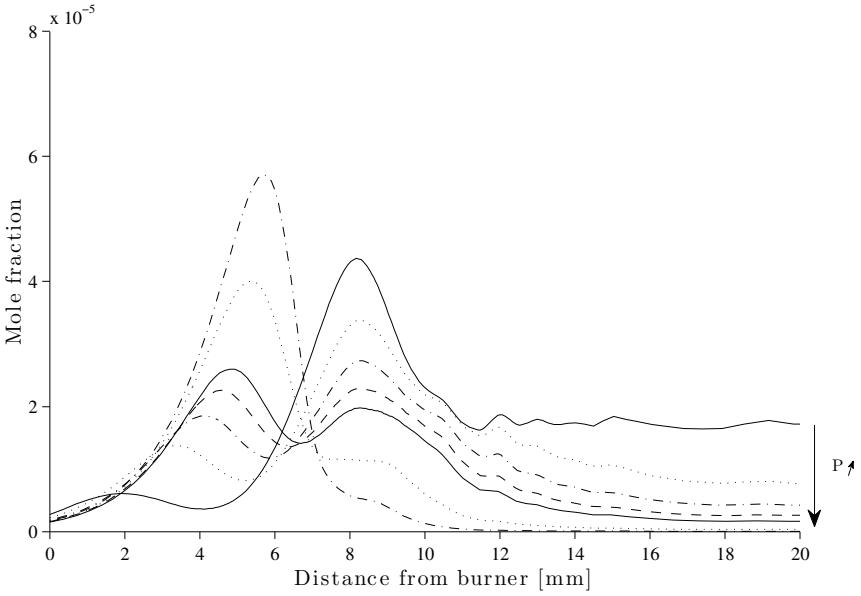

Figure 4.28: Effects of the pressure on nitrogen dioxide formation according to the *reduced* ammonia mechanism

Impact of pressure on NO_2 mole fraction profile as presented in Fig. 4.28 needs some explanations. Indeed, while the main consumption reaction remains the same for the investigated range of pressure (NO_2+H = NO+OH), the nitrogen dioxide formation reaction varies with an increasing pressure. At low pressure (50mbar), this species is mainly formed by the reaction NO+O(+M) = NO_2+OH (a) which presents a peak velocity at 8 mm from the burner surface, while this reaction is gradually replaced by HO_2+NO = NO_2+OH (b), presenting a peak velocity at 5.5 mm from the burner surface, with an increasing pressure until being the only one involved in NO_2 formation at a pressure of 1 bar. Reaction (a) persists in the burned gases at low pressure but an increased pressure tends to reduce this persistence. By opposition, reaction (b) does never persists in the burned gases.

4.3 Ammonia-air combustion at low pressure

Ammonia combustion with air in a spark ignition engine occurs at elevated pressures. These conditions are different of those used to perform the flame structure analysis presented in the first part of this thesis. Indeed, first of all, in the flame structure analysis, the pressure is strongly lower than the one encountered in engines, secondly argon has been used as diluent instead of nitrogen, thirdly hydrogen has been added to stabilize the flame at low pressure and finally dilutions do not correspond to the one of an ammonia air flame. Therefore, to conclude this first part on ammonia combustion at low pressure, an ammonia air flame (F_{NN}) with an equivalence ratio equals to one has been simulated at a pressure of 125 mbar using the previously established *reduced* ammonia combustion mechanism. Mole fraction profiles have been compared to those of the same flame with argon in place of nitrogen (F_{NAr}) in order to check the effect of the diluent change. Since, as already mentioned before, an ammonia-air flame is difficult to stabilize at low pressure, the value of 125 mbar is the lowest pressure that could be reached to perform the simulations. These flames have thus the following compositions:

$$F_{NN} : X_{NH_3} = 0.2188;\ X_{O_2} = 0.1641;\ X_{N_2} = 0.6171$$
$$F_{NAr} : X_{NH_3} = 0.2188;\ X_{O_2} = 0.1641;\ X_{Ar} = 0.6171$$

The comparison of these two flames emphasizes the role of nitrogen in the nitrogen oxides formation and on the kinetic pathways of formation and consumption of the chemical species present in an ammonia flame. No temperature profile has been introduced as an input data and the results presented in Figs. 4.30 to 4.33 correspond to an adiabatic flame calculation.

Since nitrogen has a higher heat capacity than argon, the nitrogen diluted flame has a lower temperature than the argon diluted one as depicted in Fig. 4.29. This explains also that the argon diluted flame is located closer to the burner and that reactions are faster for this flame than for the nitrogen diluted one (Fig. 4.30). This shift in the stabilization position is an illustration of the diluent impact on the laminar burning velocity, indeed these two flames have the same equivalence ratio and dilution and therefore Fig. 4.29 illustrates the higher laminar burning velocity of the argon diluted flame. Excepted this displacement in stabilization position, the replacement of argon by nitrogen does not have an important impact on the concentration of major

species in the burned gases as presented in Fig. 4.30. Moreover, the formation and consumption kinetic pathways of these species remain unchanged with such a diluent variation and still correspond to the previously presented diagrams (figs. 3.27 and 3.29).

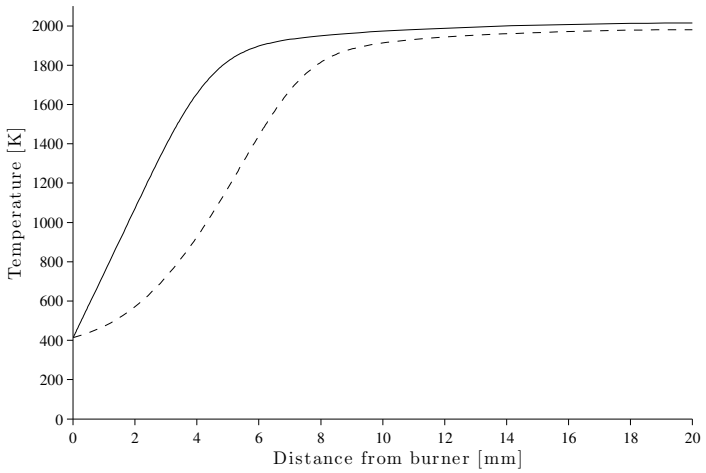

Figure 4.29: Effects of the dilution on adiabatic temperature of ammonia combustion (solid : F_{NAr} - dashed line : F_{NN})

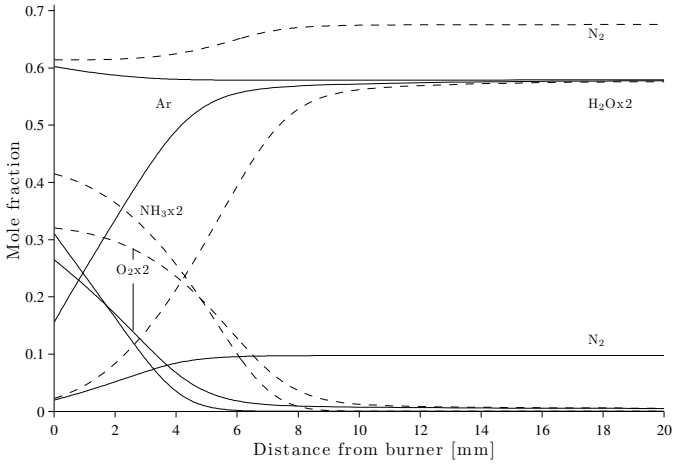

Figure 4.30: Effects of the dilution on major species concentration of ammonia combustion (solid : F_{NAr} - dashed line : F_{NN})

Even if the final adiabatic temperature is not very different for the two flames (F_{NN}: 1980K - F_{NAr}: 2000K), the replacement of argon by nitrogen leads to a small increase of the final nitrogen monoxide concentration (Fig. 4.31), this effect being explained by a larger N_2 concentration to perform the thermal nitrogen monoxide formation reactions:

$$N_2 + O \rightarrow NO + N \tag{4.2}$$

$$N + O_2 \rightarrow NO + O \tag{4.3}$$

$$N + OH \rightarrow NO + H \tag{4.4}$$

However, this impact is limited since for temperatures below 2000 K there is relatively few thermal nitrogen monoxide formation and furthermore these are stoichiometric flames leading to a complete oxygen consumption in the burned gases and therefore limited possibilities of NO formation.

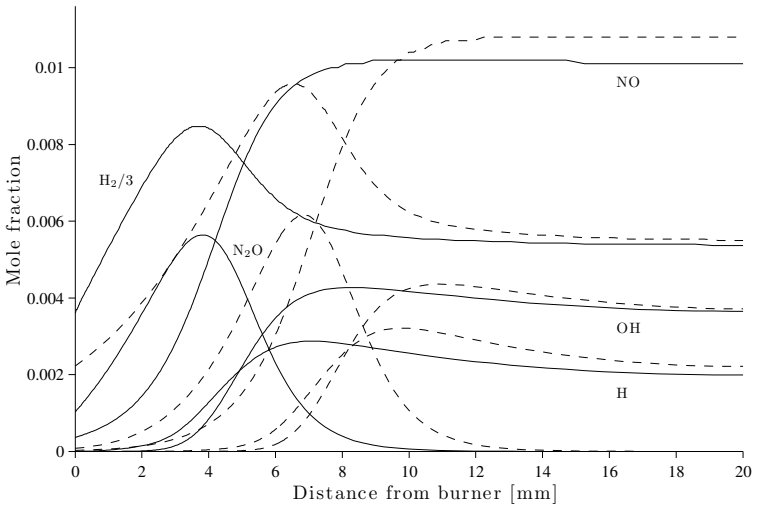

Figure 4.31: Effects of the dilution on some minor species concentration of ammonia combustion (solid : F_{NAr} - dashed line : F_{NN})

Finally, for all the minor species presented in Figs. 4.31 to 4.33, the increase of nitrogen concentration implied by a nitrogen dilution leads to a small increase of all the nitrogenous intermediate species and even to an increase of the H, O and OH radicals and H_2 concentrations since these ones are formed by the reactions presented in Table 4.16 for both argon and nitrogen diluted flames. The difference between the nitrogen and argon diluted flames for N_2H_2, HNO,

NH, N and NNH follows the effect observed for NH_2 in Fig. 4.32.

H	N_2H_2+M = NNH+H+M (48%)
	NNH+M = N_2+H+M (41%)
	HNO(+M) = H+NO(+M) (7%)
	NH_2+N = N_2+H+H (4%)
O	NO+N = N_2+O (70%)
	N_2O(+M) = N_2+O(+M) (20%)
	NH+NO = NNH+O (10%)
OH	H+O_2 = OH+O (60%)
	H_2O+O = OH+OH (20%)
	O+H_2 = OH+H (20%)
H_2	NH_2+O = H_2+NO (86%)
	H+HO_2 = H_2+O_2 (12%)
	H+H+M = H_2+M (2%)

Table 4.16: Formation reactions of H, O and OH radicals according to the *reduced* ammonia combustion mechanism

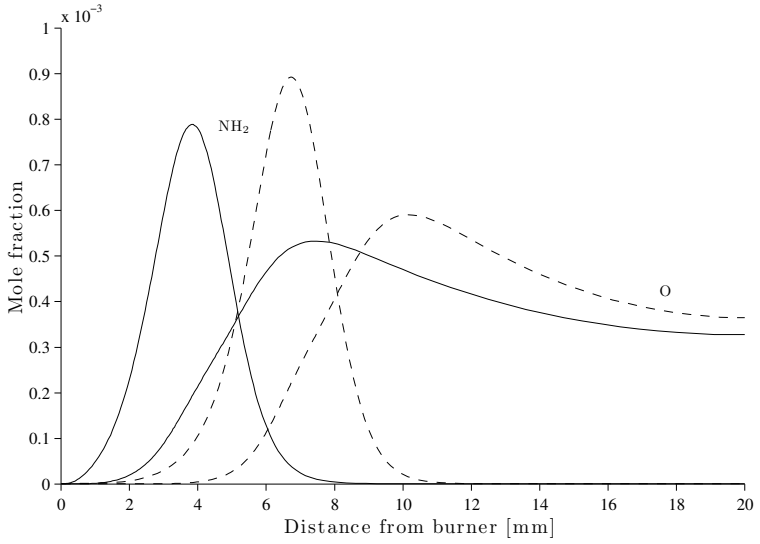

Figure 4.32: Effects of the dilution on some minor species concentration of ammonia combustion (solid : F_{NAr} - dashed lines : F_{NN})

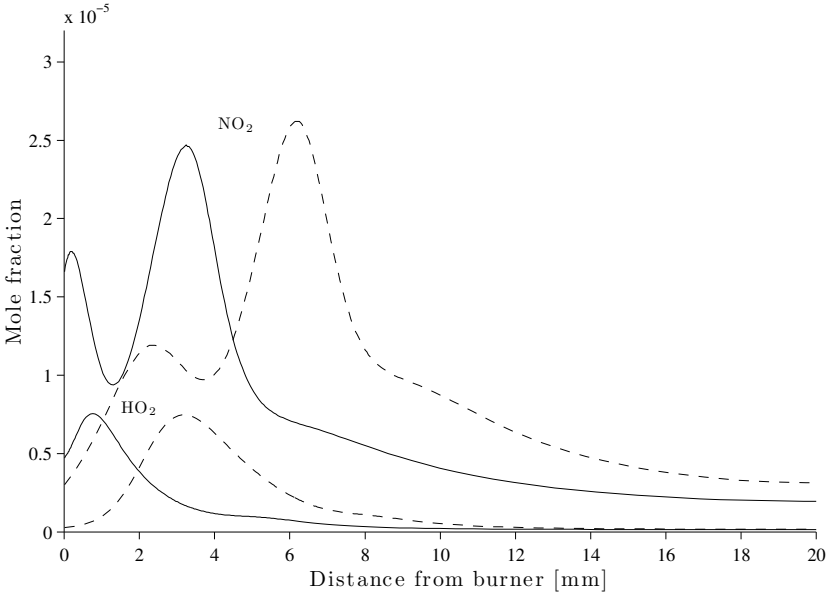

Figure 4.33: Effects of the dilution on some minor species concentration of ammonia combustion (solid : F_{NAr} - dashed lines : F_{NN})

Conclusions

In this first part, the ammonia combustion at low pressure has been experimentally and numerically investigated.

A literature review has shown that even if the combustion of ammonia has already been investigated in the past, only few results could be found for ammonia flames similar to those envisaged in this work, i.e., ammonia-air flames around stoichiometric conditions. Furthermore, the kinetic parameters of some important reactions involved in the formation and consumption of nitrogen oxides, the only pollutant formed during ammonia combustion, required to be validated against experimental data.

Eight $NH_3/H_2/O_2/Ar$ flames close to the stoichiometry with different initial compositions or operating conditions have thus been analyzed using a molecular beam mass spectrometer. Their compositions have been chosen to be close to the one presumed to occur in engines. However, it was necessary to add a small quantity of hydrogen since an ammonia flame with such a composition could not be stabilized on the low pressure burner ($\approx$ 50 mbar) used in this work. Furthermore, nitrogen has been replaced by argon to follow exclusively the formation of nitrogen from ammonia during the combustion and to better stabilize the flames thanks to the smaller molar heat capacity of argon. The effects of the variation of the initial hydrogen percentage, of the equivalence ratio and of the operation pressure have been investigated. Mole fraction profiles have been obtained for the following species : NH_3, NH_2, NO, N_2O, N_2, H_2, H_2O, OH, O_2 and Ar.

Numerical simulations of these experimentally analyzed flames have been done with five ammonia combustion kinetic mechanisms available in the literature. Since none of those ones allowed to reproduce satisfactorily the experiments performed, an improved mechanism has been established on the basis of the Konnov work [1]. Indeed, for this model, most of the calculated mole fraction profiles agreed with the experimental ones but a significant divergence was observed for N_2O and NH_2. Kinetic parameters of the formation and degradation reactions of these species have been modified to obtain an improved mechanism leading to a better agreement with all the detected species. This improved mechanism has then been reduced in order to fit the requirements of a potential integration in a CFD simulation. The *reduced* ammonia combustion mechanism contains 80 elementary reactions and 19 chemical species.

This detailed kinetic study has also been the opportunity to understand the kinetic pathways involved in ammonia combustion and in exhaust gases formation. Main ammonia combustion reaction pathways for the *reduced* ammonia combustion mechanism are schematized in the following figure.

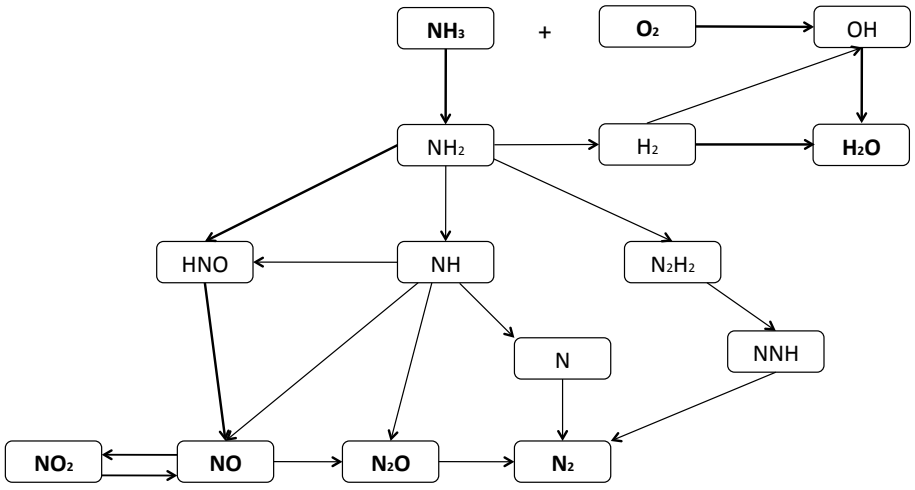

The *reduced* ammonia combustion mechanism has been used to simulate the eight analyzed ammonia flames leading to a good agreement between the experimental and the numerical results. This led also to a discussion on the impact of several parameters (initial hydrogen content, equivalence ratio, pressure) on species concentrations and on kinetic reaction pathways. Excluding a slight effect on the NO formation, the initial hydrogen content did not have a significant impact on the composition of the burned gases but an increase of its initial percentage increased the adiabatic burning velocity and therefore moved the position of the flame front closer to the burner surface. Around stoichiometric conditions, a decrease of the equivalence ratio strongly increased the NO formation. Furthermore, at high temperature, the NO formation was favored as it has been noticed in flames where, due to different heat losses, the maximum temperature increased with a decrease of pressure. This implies that the temperature and the equivalence ratio must be well controlled in practical devices such as spark ignition engines.

Other numerical simulations have also been performed on a stoichiometric ammonia flame with 7.5% of hydrogen to study the effect of a pressure increase (between 50 mbar and 1 bar) with a constant flame temperature. Results showed that a higher pressure leads to more products of a complete combustion, in this case H_2O and N_2 and less products from an incomplete combustion like NO, HNO, N_2O and NO_2. Finally, to emphasize the role of nitrogen in the formation of the combustion products of ammonia, the numerical simulation of an ammonia-air flame at low pressure has been performed. This allowed also to link the flame structure study, realized at low pressure with argon, with the study of ammonia combustion in a spark ignition engine, presented in the third part of this work and realized with air at elevated pressures and temperatures. Excepted a displacement of the flame front position, closer to the burner with argon, the replacement of argon by nitrogen does not have an important impact on the burned gases concentration of major species of ammonia combustion. Moreover, the formation and consumption kinetic pathways of these species remain unchanged. However, even if the final adiabatic temperature was not very different for the two flames, the replacement of argon by nitrogen led to a small increase of the final nitrogen monoxide concentration, this effect being explained by a larger N_2 concentration to perform the thermal nitrogen monoxide formation reactions.

Important things to keep in mind when reading the second and third part of this work are that:

- The equivalence ratio and the temperature must be well controlled in practical devices such as spark ignition engines in order to control the nitrogen oxides formation.
- The *reduced* ammonia combustion kinetic mechanism has now to be evaluated in other conditions of pressure and temperature than those in which it has been elaborated.

Part II

Burning Velocity

Introduction

Since ammonia combustion has been investigated in details at low pressure in the first part of this work, and in order to get closer to the high pressure and temperature conditions encountered during spark ignition engine combustion, this second part considers ammonia combustion at atmospheric pressure and initial room temperature thanks to a laminar flame speed experimental and numerical study. Furthermore, ammonia-air laminar burning velocities have not been widely investigated in the past. Yet they are important data for engine applications.

After a literature review presenting the various techniques used to measure burning velocities and a short survey on ammonia burning velocity measurements performed in the past (**Chapter 5**), the experimental method used in this work and the experimental conditions are presented in a next chapter (**Chapter 6**). The impact of equivalence ratio and dilution on ammonia flames laminar burning velocities is investigated, the knowledge of these effects being of great interest while keeping in mind the use of ammonia in spark ignition engines. However, since ammonia flame speed has not been widely studied in the past, the experimental device is firstly validated by the measure of the well known methane-air laminar burning velocities. Experimental results for ammonia are presented in a separate chapter (**Chapter 7**) together with those available in the literature and numerical results obtained with the *reduced* ammonia combustion mechanism. In order to link this atmospheric pressure laminar burning velocities study with the low pressure flame structure study performed in the first part of this work and the elevated pressure of the ammonia fueled engine experimental study presented in the third part of

this thesis, other numerical works are performed. To study the influence of a lower pressure on the laminar flame speed, the variation of the laminar burning velocity with the equivalence ratio, the initial hydrogen percentage and the dilution for several sub-atmospheric pressures are analyzed. Finally, the kinetic of ammonia combustion under pressures and temperatures corresponding to those encountered in spark ignition engines has been investigated.

CHAPTER 5

Literature review on ammonia burning velocity

This second literature survey presents in a first part the various techniques used to measure burning velocities in order to justify the choice of the method used in this work (i.e. for a low laminar flame speed). Then a short review on ammonia burning velocity is proposed.

5.1 Burning velocity measurements

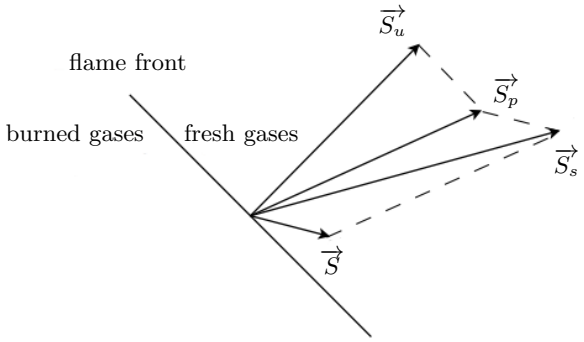

Figure 5.1: Schematic representation of the velocities for a flame front element

Every flame established in a mixture with adequate composition propagates with a speed noted S_s and named spatial speed or displacement speed. This velocity is defined in relation to a fixed axes system in space. Considering that the gaseous mixture can also be in movement, another velocity is defined in relation to an axes system relied to the fresh gases flow : S_p named propagation

speed of the flame. The laminar flame speed, S_u is finally the component of the propagation speed normal to the flame front area in laminar conditions. It is this speed, S_u, denoted S_u^0 in standard pressure and temperature conditions that is measured in this work. Unfortunately, although its theoretical definition is simple, its practical measurement is complex. Several methods are thus available to measure the laminar speed of flames. The choice of the method depends on several parameters as the precision, the reliability, and the simplicity of the experimental setup. There is no agreement on a standardized method to measure the laminar burning velocity since each one has its particularity, advantages and disadvantages. The following measurement methods description is based on a critical review of burning velocities determination proposed by Andrews and Bradley [137].

5.1.1 Methods with stationary flames

In these methods, a stream of premixed gas flows into a stationary flame with a velocity equal to the burning velocity.

Standard Bunsen burner method The conical flame has been used by the majority of workers. The gas velocity normal to the flame must be measured either directly or indirectly. It is assumed that all the premixed gas passes into the flame, that no air entrainment occurs, and that there are no heat losses to the burner rim. The laminar burning velocity follows the relation $S_u = F/A$ where F is the gas flow [$cm^3.s^{-1}$] and A the flame surface area [cm^2]. This latter must therefore be known accurately. The flame surface area of a conical flame, for a profiled burner or not, can be determined by the strioscopic schlieren method. Pictures reveal the flame front in its region closer to the fresh gases, where the variation of the gas refractive index, influenced by the temperature, contribute to a strioscopic picture, closer of the ideal cone than to the real luminous cone of the flame. One disadvantage of the method is that it is difficult to define the edge of the flame and so measure its area accurately. Furthermore, curvature effects are neglected when calculating the flame surface area.

Flat flame burner methods A uniform velocity profile of unburned gas issuing from a tube can also be obtained by using flow rectification [138]. At low velocities, with a suitable arrangement of stabilizing screens, a flat stationary flame can be obtained a short distance above the burner matrix; whereas at high gas velocities, a conical flame is produced [139]. Burning velocity may be obtained by dividing the gas volume flow rate by the flat flame area. This method, originally developed by Powling [138] was applicable only to mixtures having low burning velocities of the order of 15 cm.s^{-1} and less. However, Spalding and Botha [140] extended this method to higher flame speeds by cooling the plug. The cooling draws the flame front closer to the plug and stabilizes it. A plot of flame speed versus cooling rate is made and is extrapolated to zero cooling rate. At this point the laminar burning velocity, S_u, is obtained.

Slot Burner Methods By using a long, rectangular nozzle with a constant velocity profile, it is possible to form a flat–sided inverted "V" flame [141]; this has the advantage that any flame curvature effect is eliminated. However, this method introduces further complications into measurements insofar as it is possible for instabilities to develop and the flame front to wrinkle [142].

Measurement of Flame Thrust The pressure drop ΔP across a flame front can be obtained from an application of the momentum equation. For one–dimensional flow, with no expansion parallel to the flame front, it is easily shown that

$$\Delta P = \rho_u S_u^2 \left(\frac{\rho_u}{\rho_b} - 1 \right). \tag{5.1}$$

Since this ΔP goes around 0.1 Pa for a laminar burning velocity of 0.1 m.s^{-1}, it is not easy to measure this pressure drop with sufficient accuracy [143]. This technique is appropriated for burning velocities above 1 m.s^{-1}.

5.1.2 Methods with non stationary flames

In these methods of measurement, the flame moves through the initially quiescent mixture.

Soap bubble method In this method, the flammable mixture is contained in an enclosure constituted of a surfactant or an extensible plastic matter, the ignition being performed at the center of the mixture. The flame propagates

at constant pressure and the laminar burning velocity is deduced from the propagation speed S_s thanks to equation (5.2) presenting the mass conservation through the flame front,

$$\rho_b * S_s = \rho_u * S_u \rightarrow S_s = S_u * E. \tag{5.2}$$

For this method, two parameters must be determined: the linear flame front propagation speed thanks to a camcorder and the factor E evaluated with the measure of the initial and final diameter of the soap bubble or by measuring the ratio of temperatures T_u/T_b. This method presents several disadvantages like the difficulties to measure the factor E; the diffusion through the soap bubble; the convection effect of the burned gases leading to a non spherical form of the bubble implying that this method is inadequate for the measure of low flame speed and the presence of water in the soap bubble excluding the study of dry mixtures and affecting the water content of the mixture. By opposition, the advantages of this method are the facility of the experimental setup with small quantities of gases and the ideally spherical flame front, hypothesis which is quite well observed with high speed flames where the convection effect is reduced, the temperature and the pressure of the unburned mixture remaining constant during the progress of the flame front. The objective of this work being the measure of a low laminar speed flame, this method is not adequate and was therefore not used.

Spherical bomb method The flammable mixture is contained in a spherical enclosure ignited at the center. The propagation occurs at constant volume and leads to an increase of the pressure in the spherical bomb, burned gases at the center expanding and compressing fresh gases. Therefore the pressure must be measured with a high acquisition frequency to deduce the laminar flame speed from the linear flame propagation speed. The disadvantages of the spherical bomb method are that several hypothesis and simplification are necessary, the first one being the hypothesis of a spherical flame front centered around an ignition point with a negligible front thickness, the second the adiabatic consideration of the compression which is true only for high speed flames. Furthermore, for high speed flames, important instabilities can be formed, especially when the pressure is really high and for low speed flames, the convection effects leads to a flame front deformation. By opposition, the advantages of

this method are the use of a small quantity of gases, a good reproducibility and an easy control of the mixture composition, of its temperature and pressure. As for the soap bubble method, the spherical bomb method gives better results for mixtures with a relatively high laminar speed. This method was thus not appropriated for the measures performed in this work.

Tube method This is one of the earliest methods, first used by Mallard and Le Chatelier [144]. They ignited a mixture at the open end of a tube and photographed the flame front propagation toward the closed end. The deduction of the flame speed was straightforward. The tube was placed vertically to avoid convection effects and to obtain a symmetrical flame front. Mikhelson [145] realized that the measured flame speed was not equal to the burning velocity. The expression for the burning velocity S_u is obtained from the equation of mass conservation for the unburned gas. It follows from the definition of burning velocity that

$$\frac{\partial \rho_u V_u}{\partial t} = -\rho_u A_f S_u, \tag{5.3}$$

where A_f is the flame surface area [m^2]. This assumes that S_u is a constant value over the entire cross section of the tube. If ρ_u is also constant, then

$$\frac{\partial V_u}{\partial t} = -A_f S_u. \tag{5.4}$$

If the flame speed S_s is uniform over the tube cross section, then

$$\frac{\partial V_u}{\partial x} = -a, \tag{5.5}$$

where a is the area of the tube section. As $\partial x/\partial t = S_s$, it follows from Eqs. (5.4) and (5.5) that

$$S_u = \frac{a}{A_f} S_s. \tag{5.6}$$

This is the expression found experimentally by Coward and Hartwell [146]. Landau [147] has shown that a plane propagating flame is unstable, and the flow pattern relative to it has been discussed by Jost [148]. Such flows have been verified experimentally using the particle tracking technique [149, 150] and theoretically by Uberoi [151] and Maxworthy [152]. Unfortunately, the flame aerodynamic changes as the flame propagates along the tube and invalidate the assumption of a constant S_s over the cross section, which was made in deriving Eq. (5.5). The flame area A_f is also variable. Wheatley [137] observed variable

flame speeds and areas, while Neubert [137] has recorded periodic retardation and acceleration of the flame front as a result of pressure fluctuations in the gas column. Leyer [137] has studied the changes in flame front structure with variations in the frequency and amplitude of pressure oscillations for different tube lengths and mixtures.With high speed flames, the propagation can be accompanied with instabilities and important turbulences. Even if these effects can be reduced partially by the incision of small holes with variable diameters at the open extremity of the tube, these difficulties are secondary here since this work concerns the measure of low speed flames. The disadvantages of this method can be resumed by:
* Cooling and quenching effects along the tube wall.
* The flame surface area must be measured with very high precision.
* Instabilities and turbulences can occur for high speed and rich flames.
However, this method present several advantages:
* Appropriate technique for low laminar flame speed since in this case the propagation is regular and the flame front symmetrical.
* Experiments easily and quickly performed using a small quantity of gases.
* Good reproducibility.
* With appropriate techniques the surface area ratio can be calculated with high precision.
For all these reasons, this method has been chosen for the measure of the laminar burning velocity of ammonia flames. Furthermore, this was an available technique in our laboratory. In other cases, the choice of the spherical bomb method would have been more appropriated in the context of this thesis where we try to get closer to the elevated pressure and temperature conditions encountered in spark ignition engines.

5.2 Laminar burning velocity of ammonia

As mentioned by Ausloos and van Tiggelen in their experimental study performed in 1951 [153], "... Even if the scientific literature proposes several data on laminar burning velocities measurements in gaseous mixtures, only few data are reported on the particular case of ammonia for which the interest is more academic than for practical purposes ..." However, with the potential use of ammonia as an alternative fuel suggested in the early 60's some measurements were performed in order to determine ammonia burning velocity in oxygen or

in air.

Ausloos and van Tiggelen [153] measured the flame propagation speed in several mixtures ($NH_3/O_2/N_2$, $NH_3/O_2/CO_2$, $NH_3/O_2/H_2$ and $NH_3/N_2O/N_2$) using the burner method and direct photography of the flame. The ammonia, oxygen, nitrogen flames investigated spanned equivalence ratios between 0.5 and 1.3 and dilutions between 0 and 17% of nitrogen. They concluded that :
- the propagation speed reaches a maximum for slightly lean mixtures ($\phi = 0.9$) in $NH_3/O_2/N_2$ and $NH_3/N_2O/N_2$ mixtures.
- The dilution with an indissociable inert gas (N_2) leads to a linear decrease of the propagation speed in function of the diluent concentration. However there is a higher impact of a dissociable diluent in the flame, like CO_2 for example, and the variation of the flame propagation speed in this case is not a linear function of the dilution.
- In mixtures of NH_3/O_2 where hydrogen is added, the propagation speed is increased, however when the oxygen concentration becomes too small, the propagation speed decreases and ammonia must be considered as a diluent of the flammable mixture H_2/O_2.

Murray and Hall [154] measured the flame speed of ammonia-oxygen mixtures at 20 °C and 150 °C with the burner method, stabilizing a flame cone on a circular orifice, for equivalence ratios between 0.7 and 1.5. They concluded that these oxygenated mixtures show flame speed maxima on the slightly ammonia lean side as presented by Ausloos and van Tiggelen.

Van Wonterghem and van Tiggelen [155] measured flame propagation speed of various ammonia, oxygen, nitrogen mixtures with several equivalence ratios ($0.5 < \phi < 1.1$) and dilutions ($0\% < X_{N_2} < 40\%$) using the strioscopic Schlieren method. In this case too, they found a maxima for slightly lean mixtures and a linear decrease of the propagation speed in function of the diluent concentration.

Andrews and Gray [156] performed experimental measurements of burning velocity in binary mixtures of ammonia with oxygen, nitrous oxide and nitric oxide at sub-atmospheric pressures. Mixtures were ignited in a closed vessel and flame speeds (S_s) measured by schlieren photography with a drum cam-

era. To obtain flame speeds relative to unburned gases (S_u), the adiabatic flame temperatures and the equilibrium compositions of the hot products were calculated for mixtures corresponding to complete combustion and maximum burning velocity. For ammonia-oxygen flames, under the conditions of these experiments (0.092 atm and 60°C), flames could be propagated in mixtures containing between 23 and 61.5% of ammonia ($0.2 < \phi < 1.2$). Maximum laminar flame speed occurred at near stoichiometric proportions (ϕ=0.9). They also investigated the effect of dilution on flame speed between 0 and 36% of nitrogen for a stoichiometric mixture concluding to a linear decrease of the laminar flame speed in function of the dilution.

Ronney [157] measured flame propagation properties at microgravity for ammonia, methane, propane and hydrogen-air mixtures. This study at microgravity was performed in order to improve the understanding of the causes of flammability limits at earth gravity by eliminating the complicating factors associated with buoyancy-induced natural convection. The experimental apparatus consisted of a constant-volume cylindrical combustion vessel, a spark generator, a data acquisition system for measuring and recording the gas temperature profiles and a motion picture camera. Microgravity was obtained during 2.2 s of free-fall. The measurements for ammonia-air mixtures were performed at several pressures (from 0.07 until 2 atm) and equivalence ratios ($0.7 < \phi < 1.6$). They concluded that investigated initial pressure range has a little effect on the burning velocities of these mixtures. Furthermore they obtained a maximum laminar flame speed for an equivalence ratio equals to 1.1.

More recently, Pfahl et al. [158] measured ammonia-air mixtures laminar flame speed using the schlieren visualization technique with a 400-L closed vessel for equivalence ratios between 0.5 and 1.1. They observed an increase of the laminar flame speed with an increasing equivalence ratio for the investigated range.

Jabbour [159] performed his PhD Thesis on the classification of refrigerant fluids flammability based on laminar flame speed. He considered ammonia among others refrigerants. Laminar flame speed were measured using the tube method and direct photography of the flame propagation in the tube. Range of equivalence ratios between 0.7 and 1.3 were investigated for ammonia-air

mixtures and he obtained a maximum burning velocity for an equivalence ratio equals to 1.06.

A similar study to the one of Jabbour has been performed by Takizawa et al. [160] using the spherical-vessel method. In addition, flame propagation was directly observed by the schlieren photography method. They measured the burning velocity of nitrogen-containing compounds, i.e., ammonia, methylamine, ethylamine and propylamine to assess the flammability of potential natural refrigerants. Ammonia-air mixtures were investigated for $0.9 < \phi < 1.2$. They obtained a maximum laminar flame speed at $\phi = 1.1$.

Finally, in their theoretical study on the use of ammonia as a fuel for spark ignition engine, Checkel et al. [161] calculated the laminar burning velocity of ammonia-air mixtures at standard temperature and pressure (STP) by simulating freely propagating adiabatic, premixed, planar flames with the CHEMKIN^{TM} code and the Lindstedt mechanism [41]. They investigated equivalence ratios between 0.8 and 1.6 and found a maximum value for $\phi = 1.1$. They also performed numerical simulations to determine combustion characteristics of ammonia-air flames under pressure and temperature conditions encountered in engines. They concluded that the highest burning speed is obtained at an equivalence ratio equals to 1.1 while the flame temperature reaches a maximum under stoichiometric conditions. They suggested also that ammonia was consumed faster under elevated compression ratios. Nitrogen monoxide formation profiles were estimated for several equivalence ratios concluding that rich ammonia flames produce less NO, probably due to a lack of oxygen. This study presents interesting results on processes taking place during ammonia combustion in such conditions and on parameters to take into account in order to optimize the combustion and reduce as much as possible the production of NO_x.

This literature review on ammonia laminar burning velocity has shown that, even if only few measurements were performed in the past, they all led to the conclusion that ammonia has a very low flame speed, much lower than conventional fuels, and that the maximum value is obtained for slightly lean mixtures in the case of neat ammonia-oxygen flames and for slightly rich mixtures in the case of ammonia-air flames. Furthermore these measurements emphasized

the linear decrease of ammonia flame speed with an increasing nitrogen dilution. However, only few measurements were performed for ammonia-air flames around stoichiometric conditions.

CHAPTER 6

Experimental and numerical methods

The propagation of a flame in a tube gives normally a curved front. Indeed, the expansion of the burned gases leads to their flow through the open extremity of the tube. From the frictional resistance, this flow is limited at the wall and important at the center. The difference between the atmospheric pressure and the pressure downstream the flame is thus different at the center or at the wall of the tube. The pressure behind the flame front becomes higher at the center than at the tube wall. Therefore, in the fresh gases, the pressure is higher at the center than at the wall. Since the gas cannot escape by the closed extremity, it is subjected to a flow to the wall as presented in figure 6.1, and the surface of the flame becomes curved.

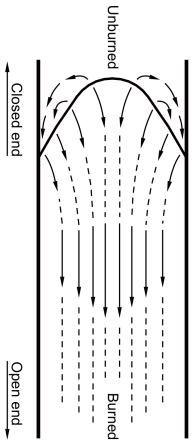

Figure 6.1: Laminar flame front propagating from the open extremity of a tube to the closed one.

When the effect of the burned gases on the fresh ones increases, the flame front becomes more and more elongated inducing an acceleration of the flame propagation. However, this acceleration is limited, the friction with the tube wall reduces the acceleration until a level dictated by the tube diameter. The acceleration of the flame propagation leads to a turbulent movement which succeeds the uniform propagation and flame front oscillations appear. Once these oscillations are coupled with the pressure oscillations in the gas column, a cellular structure favored by high speeds and rich mixtures may occur. With the amplitude and frequency amplification of these oscillations, the flame front is accelerated, leading to a turbulent regime and to high instabilities with a cellular front as depicted in Fig. 6.2. This happens only for high speed flames while for low speed flames the propagation is uniform all along the tube.

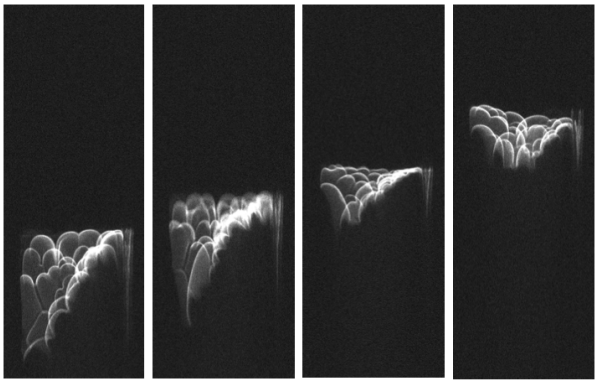

Figure 6.2: Flame front instabilities [159]

The principal sources of instabilities and turbulence are :
1. Turbulence in the initial mixture,
2. Concentration and temperature inhomogeneities,
3. Turbulence in the region of shear between the tube and the gas flow induced by the propagation,
4. Turbulence generated downstream and close to the accelerating flame front,
5. Fluctuations at the flame front caused by thermal and mass diffusions,
6. Interactions between the flame front and the acoustic wave generated by its propagation.
It is possible to reduce the effects of the first three causes by taking appropriate measures in the operating mode and by developing an adequate conception of

the tube. However, acoustic instabilities are sometimes very high with high speed and rich flames, which is not the case for the flames performed in this work.

The silica glass tube used in the experiments is 90 cm long and have an internal diameter of 39.6 mm. This diameter constitutes a compromise between smaller ones with elevated quenching effects and larger ones leading to more instabilities. The tube is placed vertically in order to ensure a symmetrical flame front with an ascending propagation. The global scheme of the experimental device is presented in Fig. 6.3. Ammonia, oxygen and nitrogen are premixed before entering into the tube by the lower end, extremity which is kept closed during the filling of the tube and opened right before the ignition of the flame. The higher end of the tube is kept closed during all the experiment but is opened between two successive measures in order to allow purging the tube.

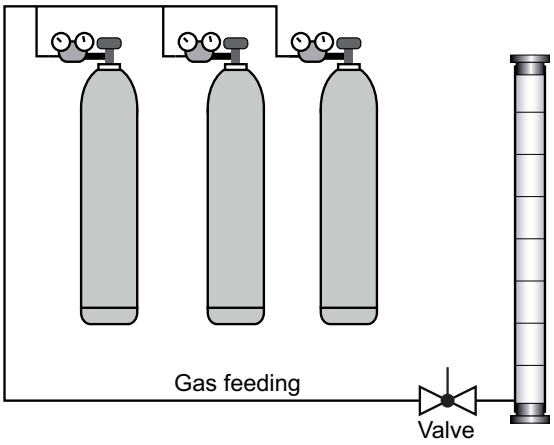

Figure 6.3: Experimental setup

The composition of the fresh gases is controlled by the same device than the one used for the study of ammonia flames at low pressure and presented in appendix A. The ignition of the flame is performed thanks to a lighter placed in the center of the lower open extremity of the tube.
If the uniform propagation is observed, with a flame front symmetrical and without wrinkles, S_u can be calculated with the propagation flame speed, S_s, and the ratio between flame and tube surface areas (Eq. 5.6). The flame prop-

agation speed in the tube is evaluated thanks to consecutive pictures obtained by direct photography of the flame in the tube. The time gap between two exposures is set to 10^{-1} ms. This short time satisfies a compromise between the reduction of the error caused by the displacement of the flame front during this time gap and the decrease of the admitted light leading to more uncertainties on the flame front outline. The flame front progression in these pictures, determined by marking a pixel with same brightness at the top of the flame front, and the knowledge of the acquisition frequency (1 kHz) allow to calculate S_s.

The ratio of the surface implies the measure of the flame front area (A_f) and of the tube section area (a). The A_f evaluation will be described in Section 6.2. Surface area a is calculated thanks to the reduced tube diameter, D, by $a = \pi D^2/4$. The tube diameter in these experiments is equal to 3.96 cm, and therefore $a = 12.32$ cm^2.

These measures of the laminar burning velocity are performed at room temperature and atmospheric pressure.

The relative uncertainty of the laminar flame speed measurement is calculated by relations (6.1) to (6.4).

$$S_u = \frac{a}{A_f} S_s \tag{6.1}$$

$$S_u = \frac{\pi D^2}{4A_f} S_s \tag{6.2}$$

$$dS_u = \frac{2\pi D}{4A_f} S_s dD + \frac{\pi D^2}{4A_f} dS_s + \frac{\pi D^2}{4A_f^2} S_s dA_f \tag{6.3}$$

$$RU_{S_u} = \frac{dS_u}{S_u} = \frac{2dD}{D} + \frac{dS_s}{S_s} + \frac{dA_f}{A_f} \tag{6.4}$$

The relative uncertainty on the tube diameter (dD/d) is equal to 0.25%, the one on flame propagation speed (dS_s/S_s) is estimated around 3% and the one on flame surface area (dA_f/A_f) around 6% giving a global relative uncertainty on the laminar burning velocity measurement of around 10%.

6.1 Experimental conditions and validation of the setup

Keeping in mind the use of ammonia in a spark ignition engine, the knowledge of equivalence ratio and dilution effects on ammonia flames laminar burning velocities is of great interest. In this context and based on ammonia flammability limits as described below, flames with composition presented in Tables 6.1 and 6.2 for the variation of equivalence ratio and dilution, respectively, have been performed. When varying the equivalence ratio, a constant dilution has been kept, i.e., 62% of nitrogen, and when varying the dilution, a constant equivalence ratio ($\phi = 1$) has been kept. Even if in practical purposes, where ammonia-air flames are considered, the dilution and the equivalence ratio will variate at the same time, these experimental conditions allow to study their effects separately.

ϕ	0.70	0.80	0.90	0.95	1.00	1.05	1.10	1.15	1.2
X_{NH_3}	0.185	0.198	0.209	0.214	0.219	0.223	0.228	0.232	0.236
X_{O_2}	0.198	0.185	0.174	0.169	0.164	0.160	0.155	0.151	0.147
X_{N_2}	0.617	0.617	0.617	0.617	0.617	0.617	0.617	0.617	0.617

Table 6.1: Flame compositions for the study of the equivalence ratio effect on the laminar burning velocity

Dilution (%)	35	40	45	50	55	60	62
X_{NH_3}	0.371	0.343	0.314	0.286	0.257	0.229	0.219
X_{O_2}	0.279	0.257	0.236	0.214	0.193	0.171	0.164
X_{N_2}	0.350	0.400	0.450	0.500	0.550	0.600	0.617

Table 6.2: Flame compositions for the study of the dilution effect on the laminar burning velocity

Considering a mixture constituted of fuel, air, and possibly a diluent, experience has shown that the flame propagation is only possible in a definite range of compositions. The lower flammable limit (LFL) and the upper flammable limit (UFL) are, by definition, the extreme percentages of fuel between which the system is flammable for a given diluent concentration. The existence of these limits can easily be interpreted from the global chain reactions scheme,

considering kinetic and thermal effects. Indeed, concentrations of reagents have to be fixed in order to keep propagation and ramification steps speeds higher than the termination reactions ones. Moreover, the thermal balance of these several elementary reactions must remain positive. The range of flammability varies substantially from one fuel to another. It is particularly wide for some components like hydrogen and acetylene. For ammonia, the LFL is equal to 16.5% ($\phi = 0.7$) and the UFL to 28.5% ($\phi = 1.4$) [162] for an ammonia-air dilution.

Flammable limits data are always affected by an uncertainties due to the ignition source used. Indeed, the flame ignition needs always a minimum amount of energy which increases near the boundaries of the flammable range. The narrower experimental range investigated in this work compared to the flammable range is thus due to the low ignition energy provided by the lighter. Furthermore, the aim was to study especially mixtures with a composition close to stoichiometry. The use of another ignition source was thus not necessary.

Finally, flammable limits vary also with the experimental conditions: temperature, pressure and dilution of the reactive mixture. An increase of temperature leads always to an increase of UFL and a decrease of LFL and thus to a globally wider flammable range. The influence of pressure is more complicated since for some fuels at elevated pressure, the flammable range is increased and for some others, the opposite effect is observed. However, for ammonia, despite very few experimental data, it seems that the first trend is observed [163]. Dilution, for example from pure oxygen to air, contributes always to reduce flammable range. Table 6.3 presents an illustration of these variations for ammonia.

Influence of pressure, T = 20 [°C], dilution = 62%, [163]		
P [atm]	LFL (%)	UFL (%)
1.02	15.5	26.0
6.81	15.0	29.0
Influence of temperature, p = 1 [atm], dilution = 62%, [162]		
T [°C]	LFL (%)	UFL (%)
20	16.5	29.0
150	15.0	32.5
300	12.5	35.5
400	11.0	37.1
500	11.0	38.5
Influence of dilution, p = 1 [atm], T = 20 [°C], [164]		
Dilution (% N_2)	LFL (%)	UFL (%)
0	15	80
30	15	55
60	16	28
65	16	22

Table 6.3: Influence of pressure, temperature and dilution on ammonia UFL and LFL

In order to validate the experimental device for the measure of ammonia laminar burning velocities, which are relatively unknown for the conditions relevant for this work, as presented in the literature survey, the same setup has been used for the measure of the well-known methane-air laminar burning velocities. The variation of the laminar flame speed with the equivalence ratio has been measured and the results have been compared with the one presented by Van Maaren et al. [165]. Composition of these flames are presented in Table 6.4.

ϕ	0.7	0.8	0.9	1.0	1.1	1.2	1.3
X_{CH_4}	0.068	0.078	0.086	0.095	0.104	0.112	0.120
X_{O_2}	0.196	0.194	0.192	0.190	0.188	0.187	0.185
X_{N_2}	0.736	0.729	0.722	0.715	0.708	0.701	0.695

Table 6.4: Methane flames composition for the validation of the experimental setup.

6.2 Flame surface area computation

The flame surface areas (A_f) have been retrieved from the successive pictures by a computational method.

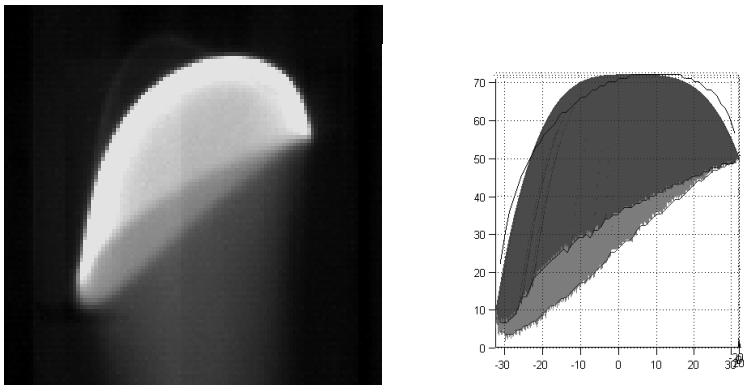

(a) Original picture **(b)** Reconstructed picture

Figure 6.4: Comparison of original and reconstructed pictures of the flame front.

On the typical original picture reproduced in Fig. 6.4a, one can easily distinguish the following three curves:

- Projection of the upper flame surface (curve C_{up}).
- Front intersection between the flame surface and the tube (curve C_{fi}).
- Back intersection between the flame surface and the tube (curve C_{bi}).

The summit of the flame surface is identified by taking into account the dissymmetry of the flame in both direction of the tube (width and depth) thanks to the curves C_{up}, C_{fi} and C_{bi}. The best power function curve, e.g. $y = 1.654\ 10^{-4}\ x^n$ with n equals to 3.5, fitting the upper flame surface, C_{up}, is then used to reconstruct the overall flame surface, using curves C_{fi} and C_{bi} to determine the lower limit of the domain. This domain is then discretized in several quadrilateral mesh elements.

Once the flame surface is numerically characterized, its area is calculated as the sum of the contributions of all the considered quadrilateral mesh elements,

each of them being divided into two elementary triangles.

Such a procedure has not been successful for every available picture. In some cases, the three main curves are not well defined, or the distinction between them is too challenging. Those cases were rejected. They only represented 5 to 10% of the available pictures depending on the effective velocity of the flame in the tube, a higher speed leading to more instabilities and ill-defined flame front outline.

6.3 Numerical determination of the burning velocity

Experimental results have been reproduced by numerical simulations with the Cosilab® [74] software and the *reduced* ammonia combustion mechanism presented in the first part of this work. Whilst under some circumstances a flame speed or burning velocity is impossible or hard to define, for the one–dimensional flames considered in this thesis the definition is straightforward. For freely propagating flames, S_u is the velocity at which the flame structure as a whole moves towards the fresh, unburned mixture. For a frame of reference fixed to the flame this is just the velocity with which the fresh, unburned mixture is provided far upstream of the flame. In both the steady and transient case, for a one–dimensional premixed, freely propagating flame, S_u cannot be prescribed but must be sought as part of the solution to the overall flame–propagation problem. The global equations used for this purpose have been presented in Section 3.1 in the first part of this work. The only difference with the low pressure flame structure simulation is that no temperature profile is provided for this laminar flame speed computation and therefore the energy conservation equation must be resolved.

The modifications performed on the Konnov mechanism to obtain the *reduced* ammonia combustion model, presented in Section 3.3.3, must also ensure a correct prediction of the laminar burning velocity. Therefore, the knowledge of the sensitivity of the laminar flame speed to the kinetic scheme rate constants is an important information. Sensitivity is the measure of the effect of the variation of a given rate constant, k_α, on a parameter like species concentration, laminar flame speed or adiabatic temperature. The following equations

(Eqs. 6.5 to 6.11) allow to calculate the relative sensitivity of the burning velocity.

For steady, one-dimensional premixed laminar flames – freely propagating or burner-stabilized – conservation of overall mass implies $\dot{m} = \rho v$. For freely propagating flames $\dot{m}$ is an eigenvalue to be determined as part of the solution, for burner-stabilized flames, $\dot{m}$ is a given constant. In either case, differentiation of this equation with respect to k_α gives

$$\frac{\partial \dot{m}}{\partial k_\alpha} = \rho \frac{\partial v}{\partial k_\alpha} + v \frac{\partial \rho}{\partial k_\alpha}, \tag{6.5}$$

since from the ideal gas equation,

$$\frac{p}{\rho} = RT \sum_{i=1}^{I} (\frac{Y_i}{W_i}) \tag{6.6}$$

and by considering the pressure as thermodynamically constant,

$$\frac{\partial \rho}{\partial k_\alpha} = -\rho [\sum_{i=1}^{I} (\frac{W}{W_i} \frac{\partial Y_i}{\partial k_\alpha}) + \frac{1}{T} \frac{\partial T}{\partial k_\alpha}] \tag{6.7}$$

equation (6.5) can be written as

$$\frac{\partial v}{\partial k_\alpha} = \frac{\dot{m}}{\rho} [\sum_{i=1}^{I} (\frac{W}{W_i} \frac{\partial Y_i}{\partial k_\alpha}) + \frac{1}{T} \frac{\partial T}{\partial k_\alpha}] + \frac{1}{\rho} \frac{\partial \dot{m}}{\partial k_\alpha}. \tag{6.8}$$

Thus, the relative velocity sensitivity is given by

$$S_v^\alpha = \frac{k_\alpha}{v} \frac{\partial v}{\partial k_\alpha} = \sum_{i=1}^{I} (X_i \frac{k_\alpha}{Y_i} \frac{\partial Y_i}{\partial k_\alpha}) + \frac{k_\alpha}{T} \frac{\partial T}{\partial k_\alpha} + \frac{k_\alpha}{\dot{m}} \frac{\partial \dot{m}}{\partial k_\alpha} \tag{6.9}$$

$$= \sum_{i=1}^{I} (X_i S_{Y_i}^\alpha) + S_T^\alpha + S_{\dot{m}}^\alpha. \tag{6.10}$$

The relative sensitivity of the burning velocity or flame speed with respect to rate constant k_α,

$$S_{S_u}^\alpha = \frac{k_\alpha}{S_u} \frac{\partial S_u}{\partial k_\alpha}, \tag{6.11}$$

is simply the value of S_v^α at the left boundary of the computational domain,

i.e., the value of S_v^α as x $\rightarrow$ -∞, i.e., at the first grid point. The relative importances of sensitivity factors on the laminar burning velocity for the *reduced* ammonia combustion model are presented in Fig. 6.5.

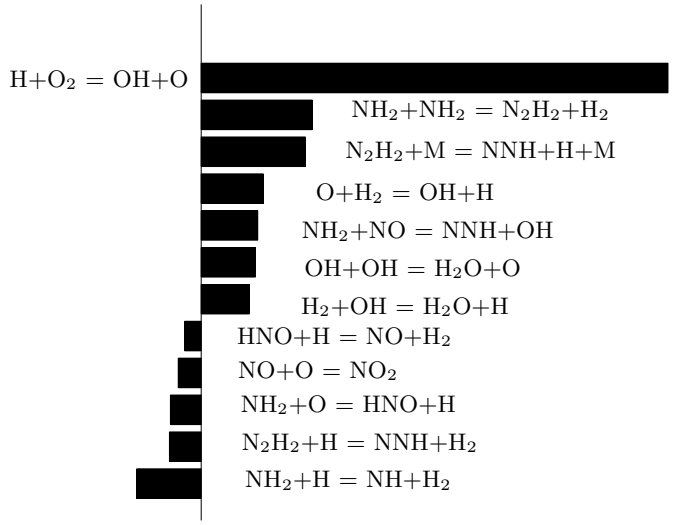

Figure 6.5: Sensitivities of laminar burning velocity to reactions of the *reduced* ammonia combustion model

Since reaction H+O_2 = OH+O is the most important chain branching step in every combustion process, it is not surprising that burning velocity is largely impacted by the rate constant of this reaction. This one, with reaction O+H_2 = OH+H convert O_2 and H_2 to two radicals and therefore increase the concentration of radicals and accelerate the combustion. Other important reactions are mainly chain branching and chain propagation reactions for the positive impact on laminar burning velocity, together with reactions accounting for a significant fraction of the heat release and thus linked to the increase of the heat and radicals diffusion into the flame front. The combustion reaction is mainly slowed down by chain termination reactions, however, compared to the H+O_2 = OH+O reaction, they do not have really an important impact.

CHAPTER 7

Ammonia burning velocities

In this chapter, the influence of the equivalence ratio and dilution on ammonia laminar flame speed will be experimentally and numerically investigated. However, the experimental device will firstly be validated for the measure of laminar flame speed thanks to methane-air flames well-known burning velocities measurements. The laminar flame speed experimental results will be compared to numerical simulation results obtained with the *reduced* ammonia combustion mechanism. Furthermore, these results will also be compared to available literature data. Finally, using the *reduced* kinetic model, other numerical simulations will be performed in order to analyze the influence of a lower and a higher pressure on the laminar flame speed. The variation of the laminar burning velocity with the equivalence ratio, the initial hydrogen percentage and the dilution for several sub-atmospheric pressures will be studied and the kinetic of ammonia combustion under pressure and temperature conditions encountered in spark ignition engines will be analyzed.

7.1 Validation of the experimental method

In order to validate the experimental method for the measure of ammonia laminar burning velocities, the effect of the equivalence ratio on a methane-air laminar flame speed has been measured and compared to literature data as depicted in Fig. 7.1. Indeed, methane air laminar flame speeds have been largely investigated in the past and a consensus has been reached concerning this property. Literature data are those of Van Maaren et al. [165] obtained using the heat flux method. This simple and accurate method allows to determine the flame temperature and the adiabatic burning velocity of laminar flat flames,

using a specially constructed flat flame burner. The heat loss of the flat flame to the burner is determined from the measurement of the temperature profile of the burner plate thanks to small thermocouples attached to the burner head plate. The adiabatic burning velocity is found when the burner plate temperature profile is uniform, implying that the net heat loss of the flame is zero. In the Van Maaren study, the results for methane/air mixtures were compared with experimental data found in the literature [166] and one-dimensional flame calculations, and close agreement was found. A very good agreement is reached between the experimental measurements of this work and those of Van Maaren.

The relative uncertainty on methane-air flames laminar burning velocities is higher than the one evaluated for ammonia flames since the laminar flame speeds of methane are higher, leading to a flame front profile which is less well-defined and therefore to a higher relative uncertainty on the flame surface area (around 10% in place of 6% in the case of ammonia flames).

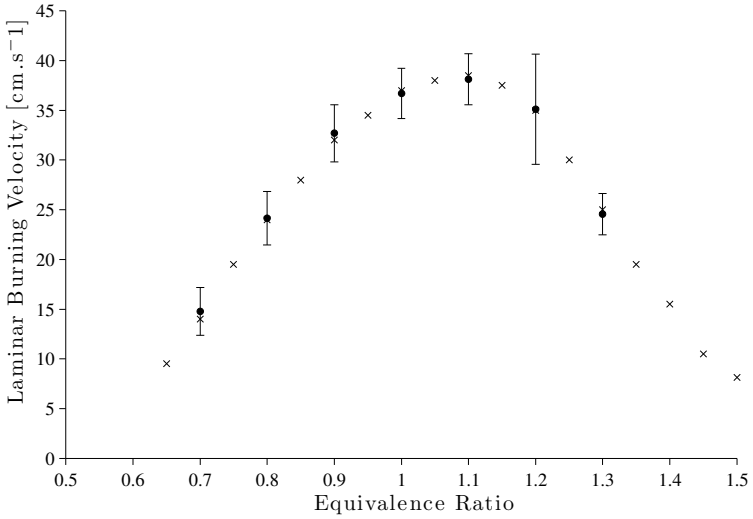

Figure 7.1: Comparison of experimental (circle) and literature data [165] (cross) for methane-air flames laminar burning velocities at several equivalence ratios.

These results allow to validate the experimental method for the measurement of ammonia flames burning velocities, especially as the velocities of ammonia flames are lower than those of methane and that the error in measuring the flame surface area is lower due to higher sharpness of the picture and therefore a more accurate flame front profile.

7.2 Laminar burning velocities at atmospheric pressure

The influence of the equivalence ratio and the dilution on ammonia laminar flame speed has been investigated experimentally and compared to numerical simulation results obtained with the *reduced* ammonia combustion mechanism. Furthermore, these results have also been compared to available literature data.

For the dilution effect, the experimental data of Ausloos and van Tiggelen [153] and Van Wonterghem and van Tiggelen [155] were obtained in the early 50's. These results were measured thanks to the direct flame photography method [153] and the strioscopic schlieren method [155] for reasonably high speed stoichiometric ammonia flames and therefore ammonia flames with lower dilution than in this work, the maximum dilution reached being 35% of nitrogen. The experimental conditions of these studies are presented in Tables 7.1 and 7.2.

Dilution (%)	0	3.7	6.65	10	13.4	16.8
X_{NH_3}	0.571	0.550	0.533	0.514	0.495	0.475
X_{O_2}	0.429	0.413	0.400	0.386	0.371	0.357
X_{N_2}	0.000	0.037	0.067	0.100	0.134	0.168

Table 7.1: Experimental conditions of the Ausloos and van Tiggelen measurements [153].

Dilution (%)	0	5	10	15	20	25	30	35
X_{NH_3}	0.571	0.543	0.514	0.486	0.457	0.429	0.400	0.371
X_{O_2}	0.429	0.407	0.386	0.364	0.343	0.321	0.300	0.279
X_{N_2}	0.000	0.050	0.100	0.150	0.200	0.250	0.300	0.350

Table 7.2: Experimental conditions of the Van Wonterghem and van Tiggelen measurements [155].

These low dilution ammonia flames were not investigated in this work with the tube method since, as presented in the previous chapter, this technique is not adapted for high speed flames due to an increased uncertainty in the flame surface area induced by a lower accuracy in the sharpness of the picture and therefore a less accurate flame front profile for such high speeds.

Results are depicted in Fig. 7.2 for the dilution variation. A global linear decrease of the laminar flame speed is observed with an increasing dilution. The laminar flame speed measured for an ammonia-air dilution is equal to 13.3 $cm.s^{-1}$. These results present a good agreement between the high dilution experimental results of this work and the numerical simulation results. However, a higher difference is observed for the low dilution experimental results obtained previously, even if the global dilution effect is quite well reproduced. Furthermore, the two literature data do not agree for the same dilution. This can be explained by the experimental methods used and the available techniques for these measurements in the 50's. Indeed, the use of a bunsen burner for the measure of the laminar burning velocity needs the determination of the flame surface area. This has been performed in the Ausloos and van Tiggelen study [153] by direct flame photography, leading to the evaluation of the surface area of the real luminous cone of the flame. However, the flame surface area of a conical flame, for a profiled burner or not, has been largely discussed and an agreement has been reached to say that this is not the surface area of the luminous cone but the one determined by the strioscopic schlieren method as in the study performed by Van Wonterghem and van Tiggelen [155]. These pictures reveal the flame front in its region closer to the fresh gases, where the variation of the gas refractive index, influenced by the temperature, contribute to a strioscopic picture, closer of the ideal cone than to the real luminous cone of the flame. The difference observed between the two experimental literature

data can be explained by such a definition of the flame surface area, smaller than the one of the luminous cone. Finally, it can be suggested that even with the strioscopic schlieren method used in the Van Wonterghem study [155], the evaluation of the flame surface area led to some errors and therefore to a smaller laminar flame speed.

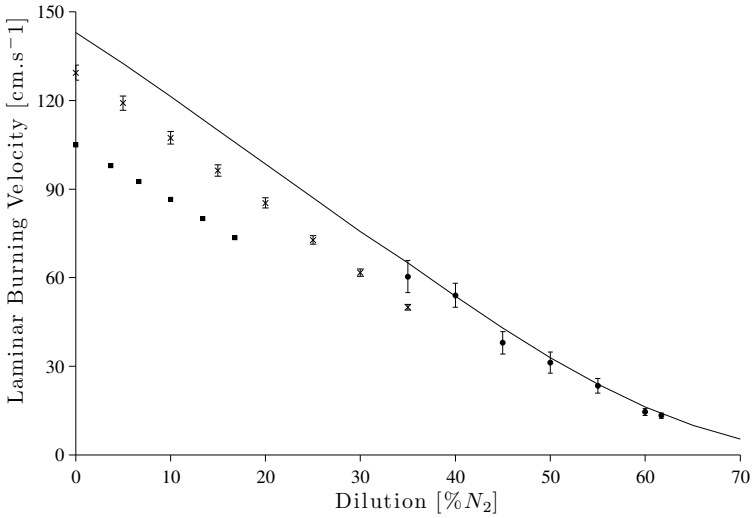

Figure 7.2: Experimental (symbols) and simulated (lines) laminar burning velocities of ammonia flames at several dilutions. Circles : this work ; squares : Ausloos and van Tiggelen [153]; cross : Van Wonterghem and van Tiggelen [155].

The effect of an equivalence ratio variation has been investigated for flames with a constant dilution and with compositions presented in Table 6.1. Figure 7.3 presents the comparison of the experimental results with the numerical simulation results obtained with the *reduced* ammonia combustion mechanism.

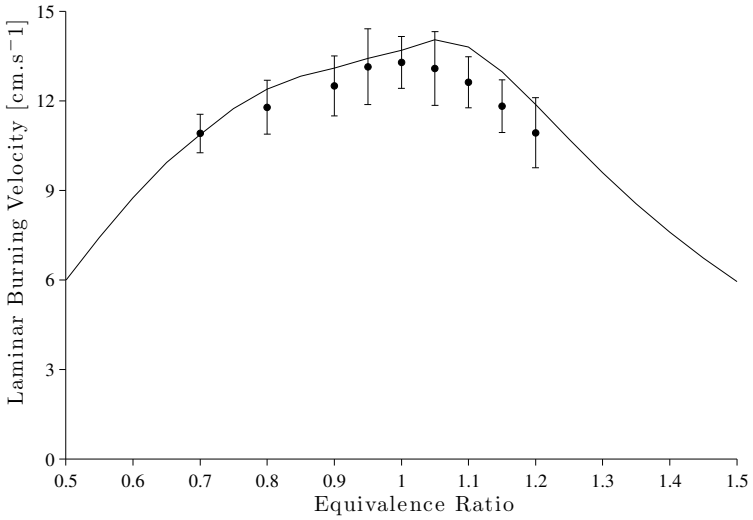

Figure 7.3: Experimental (symbols) and simulated (line) laminar burning velocities of ammonia flames at several equivalence ratios and 61.7% of nitrogen.

There is a quite good agreement between the experimental and the numerical results obtained in this work, excepted for the maximum laminar flame speed reached at an equivalence ratio equal to one in the experiments and of 1.05 in the numerical simulation. However, in both cases, this speed is approximately equal to 13.5 cm.s^{-1} which is quite lower than the 40 cm.s^{-1} of the traditionally used fuels. This is an important information to understand the engine parameters required to use ammonia in a spark ignition engine and developed in the third part of this work.

Since in the literature data [157–161], only ammonia-air flames were investigated, with variation at the same time of the dilution and the equivalence ratio, the conditions were not the same as in this work were the dilution has been kept constant during the equivalence ratio variation. The only point that can be compared is the one for a stoichiometric mixture of ammonia-air, on which the constant dilution of this work has been fixed. Results of those literature data are thus presented in a separated graph (Fig. 7.4) together with the simulated results obtained for the same conditions with the *reduced* ammonia combustion mechanism.

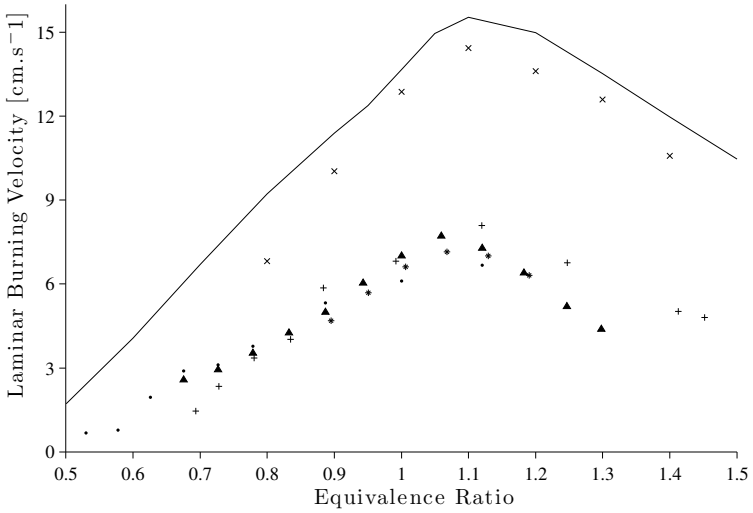

Figure 7.4: Simulated (line) and literature data (symbols) of ammonia air flames laminar burning velocities with several equivalence ratios. Dots : Pfahl et al. [158]; plus : Ronney [157]; stars : Takizawa et al. [160]; triangles : Jabbour [159]; cross : Checkel et al. [161]

Four of them [157–160] are experimental results obtained with various methods and the last one [161] is a theoretical result obtained by numerical simulation with the Lindstedt [41] mechanism. The global effect of the equivalence ratio seems to be the same as the one observed in this work, however the experimental laminar flame speeds obtained in these literature data are always lower than those obtained by numerical simulation with both the Lindstedt [41] and the *reduced* ammonia combustion mechanism.

This is more surprising for those obtained by Jabbour [159] using the same method as the one presented in this work. Since the experimental setup is the same in both cases, such a difference can only be explained by the flame surface area calculation, implicating that this area is always greater in the Jabbour results. In its work, Jabbour has calculated this area by reproducing the flame front profile thanks to selected points on the photographical contour and by dividing this profile in several horizontal sections. For each section, a polynomial trends curve is used and the surface area is calculated by considering that each elementary horizontal sub-section is cylindrical. It can be supposed that the difference in the flame surface area come from the difficulty of this technique to take the dissymmetry of the flame into consideration by opposition of the

numerical reconstitution performed in this work. The importance of the flame surface area calculation is particularly high for ammonia-air flames since those ones have a low flame speed and therefore a shape quite distorted from the perfect paraboloid one. However, the maximum laminar flame speed is reached for an equivalence ratio of 1.05 which is quite close to the value observed experimentally in this work and the same as the value predicted by the *reduced* ammonia combustion model.
For the numerical results presented by Checkel et al. [161], the maximum laminar burning velocity of 14.4 $cm.s^{-1}$ is reached at an equivalence ratio of 1.1 and is not so far from the one obtained using the *reduced* ammonia combustion mechanism elaborated in this work, i.e., 15.5 $cm.s^{-1}$ reached also at an equivalence ratio of 1.1.

7.3 Laminar burning velocities at sub-atmospheric pressure

Thanks to the validated *reduced* kinetic model for ammonia laminar flame speed predictions at atmospheric pressure, numerical simulations have been performed in order to analyze the influence of a lower pressure on the laminar flame speed. The variation of the laminar burning velocity with the equivalence ratio, the initial hydrogen percentage and the dilution has been studied for several sub-atmospheric pressures.

At sub-atmospheric pressures, typical combustion studies are usually limited to flame structure measurements, especially for ammonia where there are already only few measurements of laminar burning velocities at atmospheric pressure. This characteristic has never been measured under sub-atmospheric pressure to the best of our knowledge. Therefore, in order to understand the low-pressure effect on ammonia laminar flame speeds, the discussion on laminar burning velocities of methane-air flames at sub-atmospheric pressure by Bosschaart et al. [167] is first of all presented. They used the heat flux method for measuring laminar burning velocities of a stoichiometric methane/air mixture with an initial temperature of 295 K in the range 150-1000 mbar. Additionally, for a pressure of 200 mbar the burning velocity of methane/air flames has been measured as a function of the equivalence ratio. These experimental re-

sults were compared to several experimentally fitted correlations found in the literature and described below. Smith and Agnew [168] use

$$S_u/S_u^0 = exp(0.3 - 0.3(p/p_0)^{0.54}), \tag{7.1}$$

which is valid for the pressure range between 0.1 and 20 atm, where S_u^0 is the reference burning velocity at atmospheric pressure (p_0). Another correlation for the pressure in the range 0.5-20 atm is given by Agnew and Graiff [169]:

$$S_u = S_u^0 - 6.78ln(p/p_0). \tag{7.2}$$

Iijiama and Takeno [170] propose

$$S_u/S_u^0 = 1 + \beta_2 ln(p/p_0), \tag{7.3}$$

where the coefficient β_2 as well as the reference burning velocity S_u^0 depend on the equivalence ratio ϕ:

$$\beta_2 = -0.42 - 0.31(\phi - 1), \tag{7.4}$$

$$S_u^0 = 36.9 - 210(\phi - 1.12)^2 - 335(\phi - 1.12)^3. \tag{7.5}$$

The correlation is valid in the range 0.3-30 atm. Finally, Liao et al. [171] suggest the following relation for natural gas, constituted of 96% of methane, for the range 0.5-1.5 atm

$$\frac{S_u}{S_u^0} = (\frac{T_u}{T_{u^0}})^{\alpha_T} (\frac{p_u}{p_u^0})^{\beta_p}, \tag{7.6}$$

where α_T, β_p and S_u^0 depend on the equivalence ratio by:

$$\alpha_T = 5.75\phi^2 - 12.15\phi + 7.98, \tag{7.7}$$

$$\beta_p = -0.925\phi^2 + 2\phi - 1.473, \tag{7.8}$$

$$S_u^0 = -177.43\phi^3 + 340.77\phi^2 - 123.66\phi - 0.2297. \tag{7.9}$$

These correlations, depicted in Fig. 7.5, state that the burning velocity S_u increases when the pressure is reduced but show also significant differences, partly because these equations apply to different pressure ranges, but also be-

cause there still exists a quite large uncertainty on the pressure dependence of S_u today. As presented by Bosschaart et al. [167], none of these correlations are completely in agreement with the experimental results, only numerical results (obtained with the GRI mechanism [42] in their study) agree with the experiments.

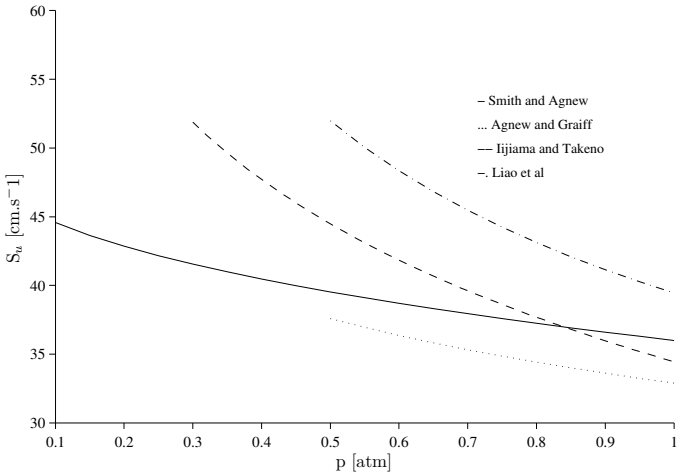

Figure 7.5: Correlations for methane burning velocity at sub-atmospheric pressures, ϕ=1, p_0=1 atm, $T_u = T_{u^0} = 298\ K$

Although no experiment has been performed at low pressure for ammonia, the numerical results obtained with the *reduced* ammonia combustion mechanism can help us to establish correlations valid for the investigated ranges of pressure, dilution, equivalence ratio and hydrogen percentage.

Figure 7.6 presents the global effect of a sub-atmospheric pressure on the laminar burning velocity of an ammonia-air flame at an equivalence ratio equal to one. These results suggest the following correlation for the pressure effect:

$$S_u = S_u^0 (\frac{p}{p_0})^\beta \tag{7.10}$$

where S_u^0 is the laminar burning velocity at atmospheric pressure for the previously defined dilution and equivalence ratio, in this case $S_u^0 = 13.7$ cm.s^{-1}, and β equals -0.09 in these conditions.

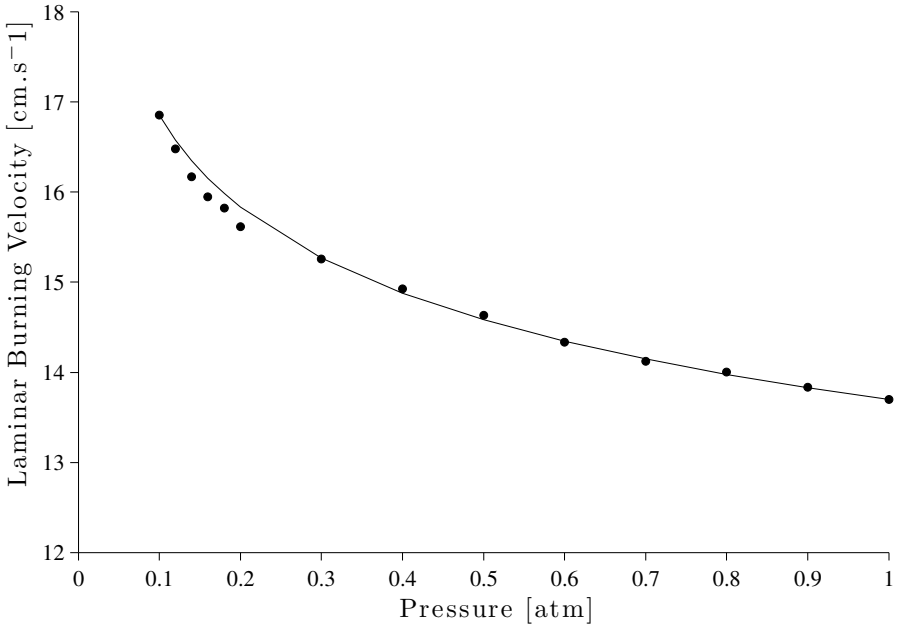

Figure 7.6: Influence of sub-atmospheric pressure on ammonia laminar burning velocity. Symbols : numerical results obtained with the *reduced* ammonia combustion model ; Line : Correlation results.

Keeping the equivalence ratio equal to one, the pressure effect for several dilutions is presented in Fig. 7.7.

When varying the dilution, i.e., the nitrogen mole fraction, the dependence of β and S_u^0 with the dilution must also be taken into consideration in the correlation. In equation (7.10), they become for an equivalence ratio equal to one:

$$S_u^0 = 77.474(X_{N_2})^2 - 260.04(X_{N_2}) + 145.71, \quad (7.11)$$

$$\beta = -0.125(X_{N_2})^2 - 0.0417(X_{N_2}) - 0.0187. \quad (7.12)$$

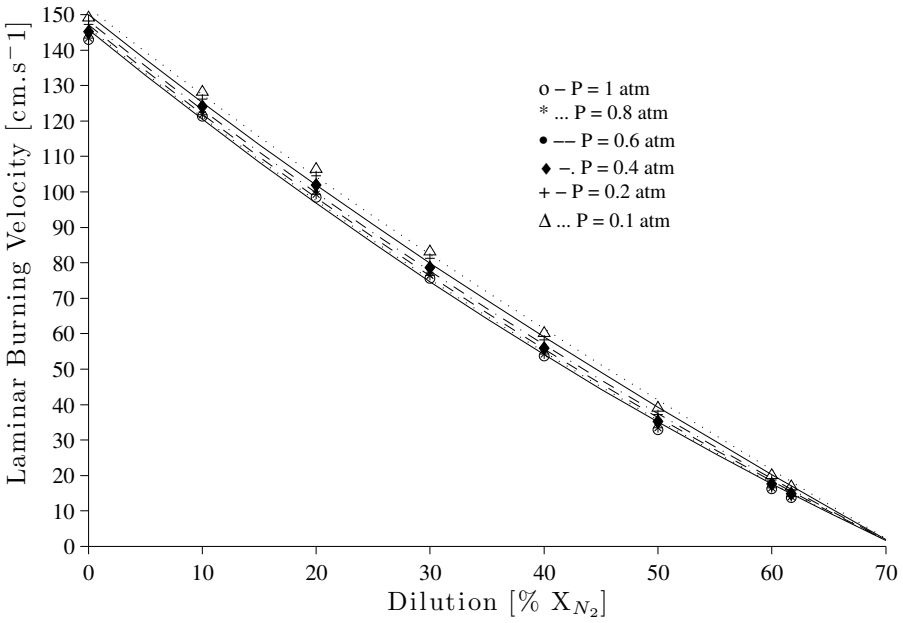

Figure 7.7: Influence of dilution on laminar burning velocity for ammonia flames at sub-atmospheric pressure. Symbols : numerical results obtained with the *reduced* ammonia combustion model ; Lines : Correlation results.

In the same way, when varying the equivalence ratio, for a fixed dilution equal to the air dilution, as presented in Fig 7.8, β does not vary with this parameter and is therefore always equal to -0.09. S_u^0 is defined by:

$$S_u^0 = -31.258\phi^2 + 61.695\phi - 16.979. \tag{7.13}$$

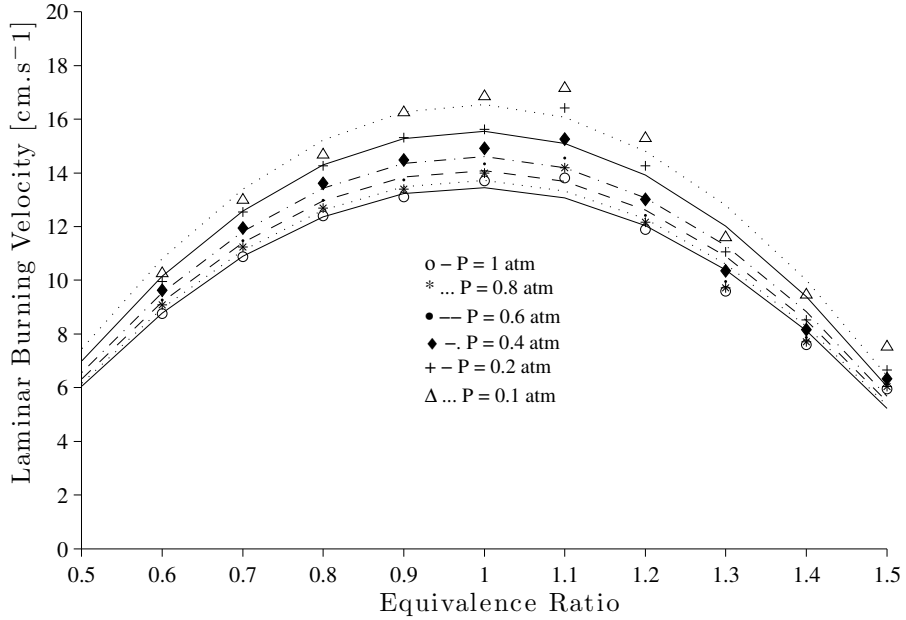

Figure 7.8: Influence of the equivalence ratio on laminar burning velocity for ammonia-air flames at sub-atmospheric pressure. Symbols : numerical results obtained with the *reduced* ammonia combustion model ; Lines : Correlation results.

Finally, when adding hydrogen in the ammonia-oxygen-nitrogen mixture, the laminar flame speed is increased and the effect of a pressure decrease is more important that for an ammonia flame, meaning a more negative β exponent. β varies also with the initial hydrogen percentage. For the investigated range from 5 to 12.5% of hydrogen, equation (7.14) follows:

$$\beta = -0.4X_{H_2} - 0.09. \tag{7.14}$$

S_u^0 is defined for the range of 5 - 12.5% of hydrogen by:

$$S_u^0 = 13.7 + 1.8235 \exp(16.105X_{H_2}). \tag{7.15}$$

Figure 7.9 presents the numerical results of the *reduced* ammonia combustion mechanism and the results of correlation (7.10) with adequate β and S_u^0.

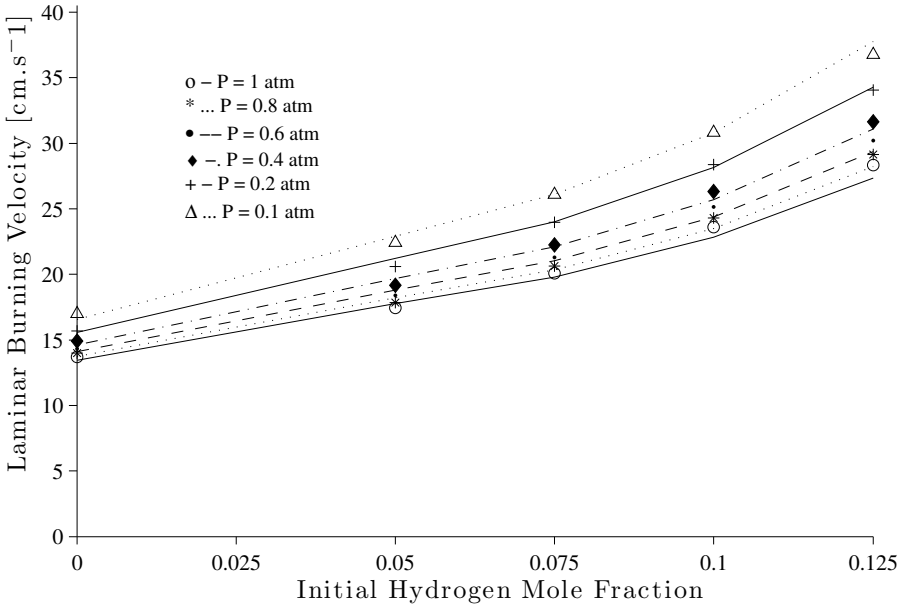

Figure 7.9: Influence of initial hydrogen percentage on laminar burning velocity for ammonia flames at sub-atmospheric pressure. Symbols : numerical results obtained with the *reduced* ammonia combustion model ; Lines : Correlation results.

7.4 Laminar burning velocities under elevated pressure conditions

The complete simulation of the ammonia combustion in spark ignition engines requires the integration of a proper ammonia combustion mechanism in a CFD code in order to take into account all the mechanical fluids aspects together with the kinetic ones. Such a simulation has not been performed during this thesis but is an interesting perspective of a future work to complete the knowledge on ammonia combustion. However, the aim of this Section is to simulate ammonia combustion at elevated pressure and temperature conditions such as those encountered in spark ignition engine combustion. Only the kinetic aspect of the combustion is thus taken into account. In nature, complex flames with wall effects are encountered. However, in the present flame simulations, we restricted ourselves to laminar, one dimensional, premixed and freely propagating flames. The adjective “freely” meaning that such flames are free from

wall effects. Although these flames are model flames that in reality rarely exist, they are valuable research "tools" and hence worthwhile to be considered for study.

The elevated pressure and unburned mixture temperature corresponding to those encountered in a SI engine before combustion have been determined for several compression ratios by assuming an isentropic compression process and an adiabatic and isobaric combustion process, this supposition being justified by the slow combustion process. The mixture was considered to be at Standard Temperature and Pressure Conditions (STP: 1 atm, 293.15 K) conditions before compression.

The initial composition of the flame has been chosen to be close to the one presumed to occur in a spark ignition engine, the equivalence ratio is thus close to 1.0. The chemical equation for the stoichiometric reaction of ammonia-air is

$$NH_3 + 0.75(O_2 + 3.76N_2) \rightarrow 3.32N_2 + 1.5H_2O \tag{7.16}$$

The ammonia-air equivalence ratio (ϕ) was determined according to eq. (7.16) here above and the mole fractions of each reactant are listed in Table 7.3 for equivalence ratio values from 0.7 to 1.2.

ϕ	X_{NH_3}	X_{O_2}	X_{N_2}
0.70	0.1639	0.1757	0.6604
0.80	0.1831	0.1716	0.6453
0.90	0.2013	0.1678	0.6309
0.95	0.2102	0.1659	0.6239
1.00	0.2188	0.1641	0.6171
1.05	0.2273	0.1623	0.6104
1.10	0.2356	0.1606	0.6038
1.15	0.2436	0.1589	0.5975
1.20	0.2516	0.1572	0.5912

Table 7.3: Ammonia-air mixtures (mole fractions) at several equivalence ratios.

The pressure and unburned temperature calculations corresponding to each compression ratio are summarized by the following isentropic process and ideal gas law equations:

$$PV^{\gamma} = constant \quad \Rightarrow \quad P_1 V_1^{\gamma} = P_2 V_2^{\gamma}, \tag{7.17}$$

$$P_1 V_1 / T_1 \quad = \quad P_2 V_2 / T_2. \tag{7.18}$$

P_1 and T_1 being the initial STP conditions, it can be written that:

$$V_2 \quad = \quad 1/CR, \tag{7.19}$$

$$P_2 \quad = \quad P_1 * (CR)^{\gamma}, \tag{7.20}$$

$$T_2 \quad = \quad (CR)^{\gamma - 1} * T_1. \tag{7.21}$$

The critical factor for the calculation of final pressures and temperatures is thus the ratio of specific heats, γ. The specific heat at constant pressure, C_p, is calculated from the mixture composition, expressed in mole fractions, X_i, and the individual specific heats, $C_{p,i}$: $C_p = \sum[X_i \ C_{p,i}]$. The mixture composition is calculated thanks to the equivalence ratio ranging from 0.95 to 1.2. The ratio of specific heats, γ then follows from $\gamma = C_p/(C_p\text{-}R)$. The ratio of specific heats is a function of temperature and look-up tables can be easily constructed relating this one to temperature for any mixture. Initial pressures and unburned mixture temperatures corresponding to every compression ratio are listed in Table 7.4.

To reproduce the conditions occurring in SI engines, initial pressure and temperature have been adjusted in order to correspond to compression ratios from 12:1 to 20:1. However, in a second part, these two parameters have been varied separately to study the effects of each one on the combustion characteristics of an NH_3-air mixture. The simulations were run at equivalence ratios listed in Table 7.3 for each compression ratio value except for 0.7, 0.8 and 0.9 for which it has only been done at STP conditions.

Compression ratio, CR	Pressure before combustion, P_2 (atm.)	Unburned mixture temperature, T_2 (K)
12	28	706
13	31	725
14	34	741
15	38	756
16	41	771
17	44	786
18	48	799
19	51	812
20	55	825

Table 7.4: Calculated pressures and unburned mixture temperatures for each compression ratio.

Finally, one of the critical elements needed for this simulation is a proper reaction mechanism which describes the essential fundamental reaction paths to be followed by the overall reaction. The *reduced* ammonia combustion mechanism elaborated in the first part of this thesis has been applied in these simulations. As a reminder, the reduction of the *modified* Konnov mechanism has been performed by taking into consideration elevated pressures and temperatures conditions as those encountered in spark ignition engines.

The computation yields the profiles of gases velocities, flames temperatures and species concentrations throughout the flame. The laminar burning velocity was obtained at the adiabatic flame boundary. Additionally, the flame temperature at the end of the computational domain was taken as the adiabatic flame temperature. Finally, to study the influence of the combustion characteristics such as the equivalence ratio and the initial temperatures and pressures on the exhaust gas composition, the maximum concentration of nitrogen monoxide and the final quantities at the end of the combustion process are plotted as a function of the equivalence and compression ratios.

7.4.1 Standard temperature and pressure conditions

Figs. 7.10 to 7.12 show the laminar burning velocities, NO mole fractions and adiabatic flame temperatures for fresh gas mixtures at STP for equivalence ratios ranging from 0.7 to 1.2.

As presented in Fig. 7.10, the maximum laminar burning velocity is reached in the rich side at an equivalence ratio of 1.12 and is equal to 15.5 cm.s^{-1}. This occurrence of peak laminar burning velocity agrees with the result of Checkel et. al [172] who measured a maximum pressure rise of ignited NH_3-air mixture at an ammonia volume concentration of approximately 23.5% ($\phi = 1.1$). Furthermore this is also in agreement with the experiences of Pfahl, Ronney, Jabbour and Takizawa [157–160] who measured a peak laminar burning velocity around $\phi = 1.1$ at STP conditions.

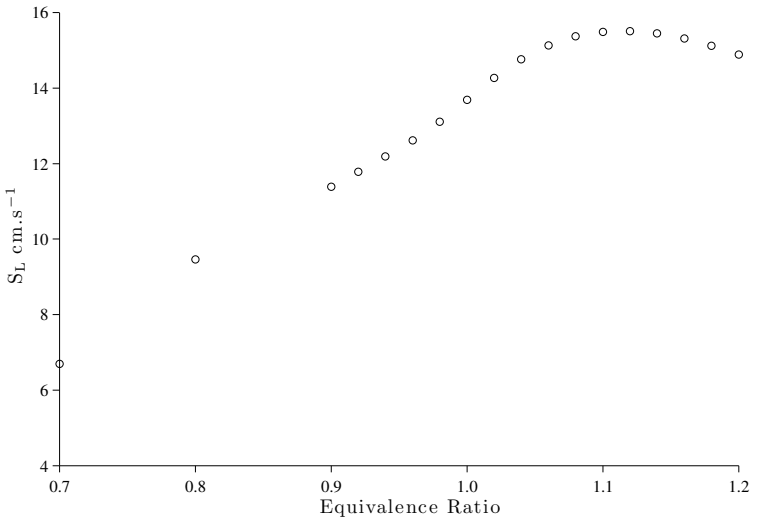

Figure 7.10: Laminar burning velocity of ammonia-air mixture at STP

Fig. 7.11 shows the maximum and the burned gases mole fractions of nitrogen monoxide in function of the equivalence ratio at STP. These two values reach a maximum and are identical at $\phi = 0.95$ ($X_{NO} = 8.6\text{x}10^{-3}$). For an equivalence ratio lower than 0.95, both values decrease and overlap and for ϕ higher than 0.95, they decrease too but the X_{NO} in the burned gases region falls more strongly. This indicates the importance to control the equivalence ratio in SI

engines operation to minimize the nitrogen monoxide formation.

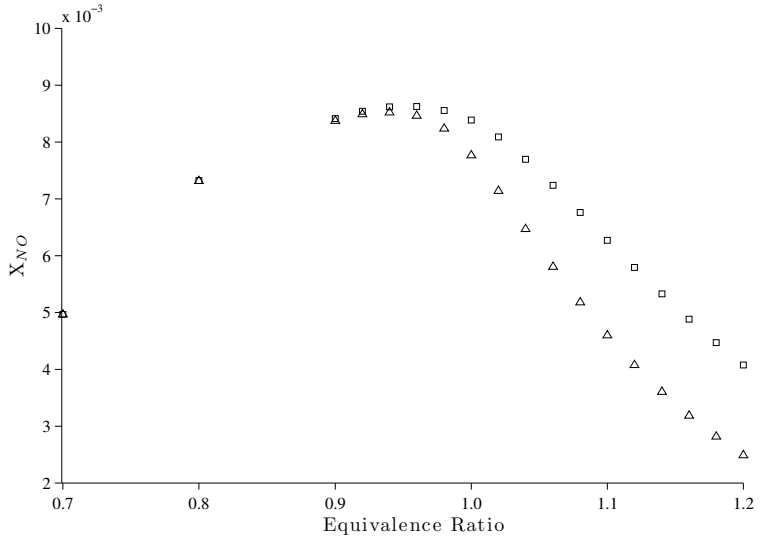

Figure 7.11: Highest (square) and burned gases (triangles) nitrogen monoxide mole fraction in ammonia-air mixture burning at STP.

Figure 7.12 illustrates the adiabatic flame temperature as a function of the equivalence ratio at STP. This graph shows a peak at an equivalence ratio equals to 0.99 instead of $\phi = 1.12$ as the laminar burning velocity. This is likely due to the maximum energy release and the dissociation of surplus ammonia into nitrogen and hydrogen at that equivalence ratio [161]. The decrease of the adiabatic flame temperature for equivalence ratios above one explains also the decrease of the thermal nitrogen monoxide formation.

The H_2 mole fraction profiles for stoichiometric and rich ($\phi = 1.1$) mixtures at STP are shown in Fig. 7.13. In rich mixtures, H_2 is produced in the flame front and reaches a partial equilibrium value in the burned gases region. Under stoichiometric conditions, H_2 is mainly an intermediate peaking in the flame front and declining in the post-combustion zone to reach an equilibrium state. Since the dissociation of NH_3 is endothermic, the adiabatic flame temperature of a rich mixture is expected to be lower than that of the leaner mixture as observed in Fig. 7.12.

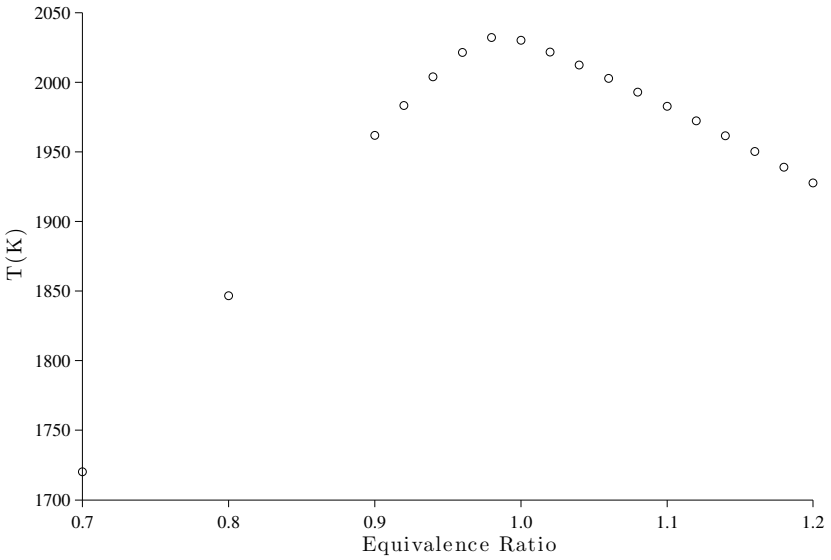

Figure 7.12: Adiabatic flame temperature for each equivalence ratio at STP.

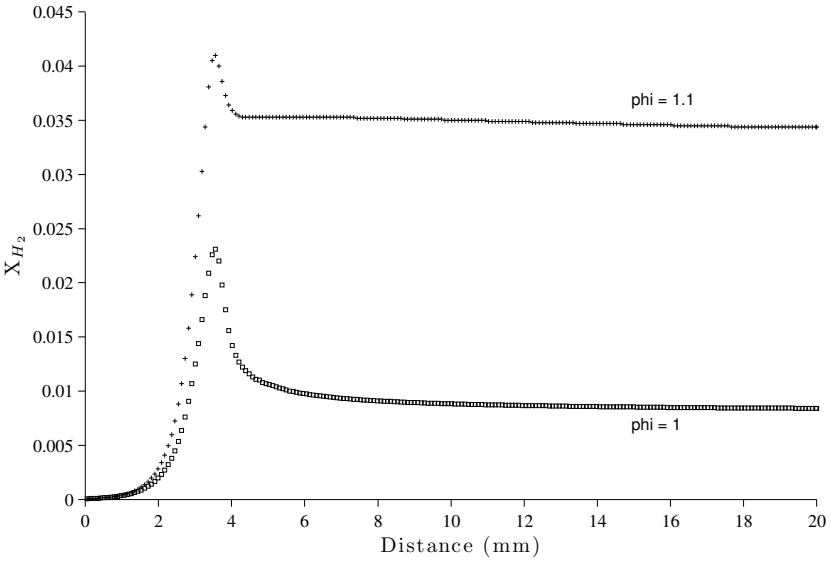

Figure 7.13: Hydrogen mole fraction profiles at equivalence ratio of 1.0 and 1.1 for STP.

7.4.2 Effects of the compression ratio

In Figs. 7.14 to 7.16, the influence of the compression ratio on the laminar burning velocity, the adiabatic flame temperature and the NO formation is illustrated for several equivalence ratios.

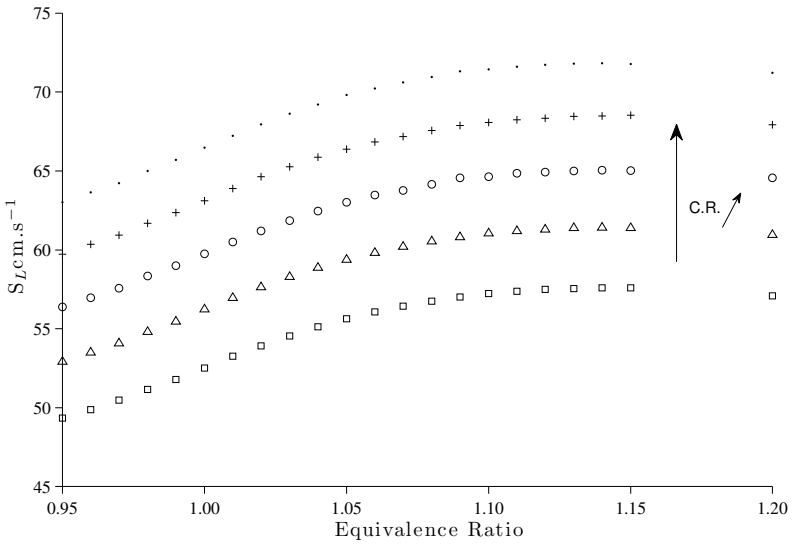

Figure 7.14: Laminar burning velocities at several compression ratios (C.R.). □ : C.R. = 12; △ : C.R. = 14; ○ : C.R. = 16; + : C.R. = 18; · : C.R. = 20.

In Fig. 7.14, it can be seen that the variation of compression ratio has no effect on the position of the maximum value of the laminar burning velocity. The maximum value for the laminar burning velocity is consistently found to be at an equivalence ratio of approximately 1.15. However, in the vicinity of stoichiometric mixtures, the variation of the compression ratio has a significant effect on the laminar burning velocity. An increase of the compression ratio from 12:1 to 20:1 leads to a 130% increase of the laminar burning velocity.

Fig. 7.15 presents the variation of the adiabatic flame temperature as a function of compression ratio and equivalence ratio. It was found that the adiabatic flame temperature increased slightly with the compression ratio. This implies thus an increase of the thermal nitrogen monoxide formation with an increase of the CR (Fig. 7.16). However, in this case too, a change in compression ratio does not have an impact on the position of the maximum value of the adiabatic

flame temperature, which is consistently found at an equivalence ratio around 1.00. The maximum adiabatic flame temperature varies from 2030K at STP to 2460K at 50 bars and 732K (CR=20). The decrease of the adiabatic flame temperature for equivalence ratios above one explains the decrease of the thermal nitrogen monoxide formation observed in Fig. 7.16 for all the investigated compression ratios.

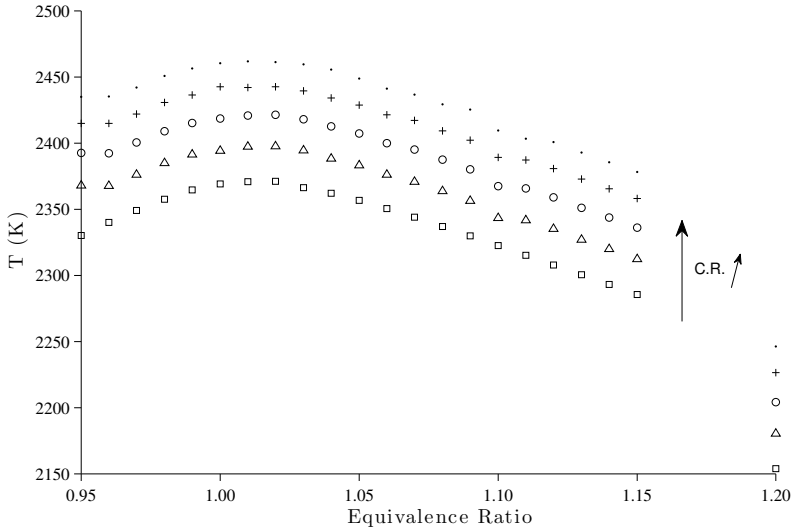

Figure 7.15: Adiabatic flame temperature at several compression ratios (C.R.). □ : C.R. = 12; △ : C.R. = 14; ○ : C.R. = 16; + : C.R. = 18; · : C.R. = 20.

Fig. 7.16 presents the variations of the highest NO mole fraction with the compression ratio and the equivalence ratio. Increasing the compression ratio does not have a significant impact on the NO formation for the range of CR investigated in this work because it leads only to a slight increase of the adiabatic temperature and as a consequence to a slight increase of the thermal NO formation. However, a huge decrease of the highest NO concentration is observed for rich mixtures ($\phi = 1.2$), with a NO maximum mole fraction of only 0.005. This is 50% less than the amount of NO found for an equivalence ratio of 0.95. This characteristic shows the advantage to use slightly rich mixtures as practical fuel to reduce NO production in SI engines. A similar trend is observed for the burned gas NO mole fraction.

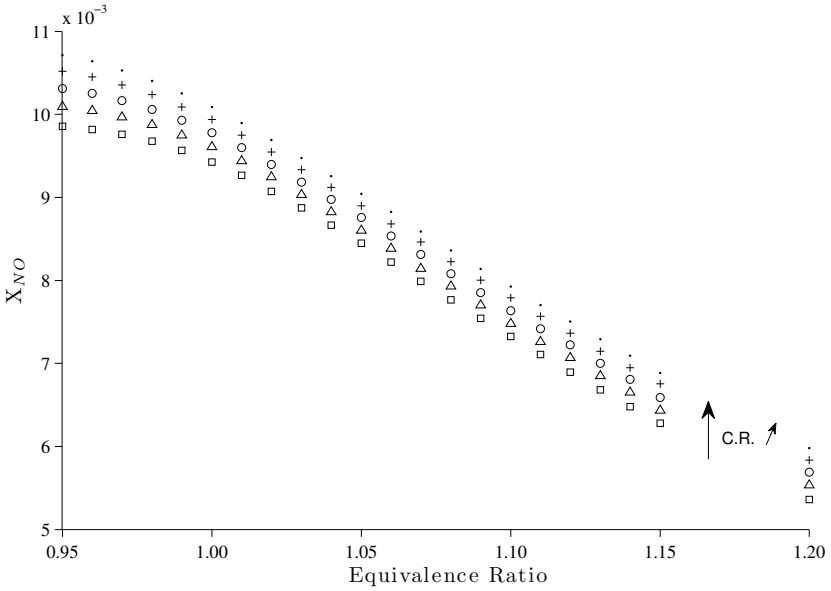

Figure 7.16: Highest nitrogen monoxide mole fraction at several compression ratios (C.R.). □ : C.R. = 12; △ : C.R. = 14; ○ : C.R. = 16; + : C.R. = 18; · : C.R. = 20.

In summary, at a given equivalence ratio (for $0.95 < \phi < 1.2$), the combined effects of a simultaneous increase in the initial temperature and pressure (effect of increasing the CR) contribute to an important increase of the laminar burning velocity but increase only slightly the adiabatic flame temperature and the NO formation.

A comparison of results obtained with Lindstedt and Konnov mechanisms [1, 41] has also been performed for several conditions of pressure, temperature and equivalence ratio. The burning velocities obtained with these mechanisms are 50% lower for the Lindstedt mechanism and 20% lower for the Konnov mechanism. The burned gases nitrogen monoxide mole fractions are 10% lower using the Lindstedt mechanism and equivalent of those obtained in this work with the Konnov mechanism. Finally, the adiabatic temperatures are identical for the three mechanisms.

7.4.3 Separated influences of temperature and pressure

In order to determine the impact of the initial pressure and temperature on the laminar burning velocity, adiabatic flame temperature and nitrogen monoxide formation, the initial pressure and temperature have been varied separately. In a first set of simulations, pressure was fixed at 1 atm. and temperatures ranged from 300 to 700 K, then temperature was fixed at 300 K and pressures ranged from 5 to 40 atm. in a second set. For all these numerical simulations, the flame considered had an equivalence ratio of 1.0.

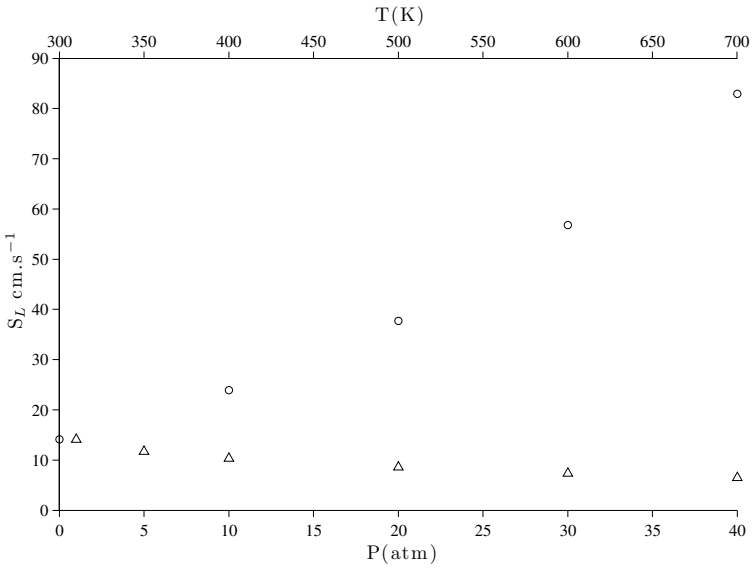

Figure 7.17: Separated effects of temperature (○) and pressure (△) variation on the laminar burning velocity.

As shown on Figs. 7.17 and 7.18, the increase of the unburned mixture temperature for a constant pressure has a positive effect on the laminar burning velocity and on the adiabatic flame temperature. However, the increase of pressure for a constant initial temperature has a rather slightly negative effect on the laminar burning velocity and almost no effect on the adiabatic flame temperature.

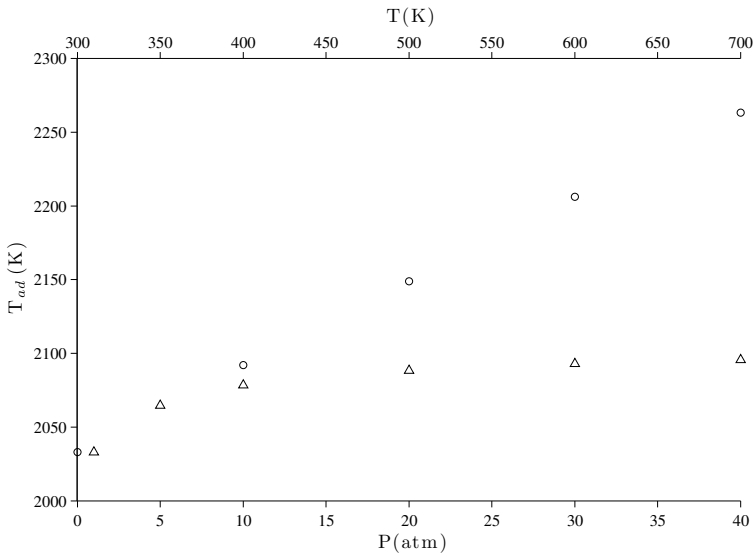

Figure 7.18: Separated effects of temperature (○) and pressure (△) variation on the adiabatic flame temperature.

Figure 7.19 illustrates the increase of the NO formation for an increase of the initial temperature (at a constant pressure of 1 atm.). This result is due to the increase of the final temperature of the flame as it can be seen in Fig. 7.18, and therefore the increase of the thermal NO formation. When only the initial pressure is increased, the final temperature of the flame is not really affected (Fig. 7.18). Unexpectedly, the maximum concentration and final NO mole fraction in the flame decrease. Such a result indicates that the temperature is not the only parameter to take into account for the NO formation. Indeed, for ammonia combustion, the NO formation is due to thermal NO but also to fuel NO. For an increase of the initial temperature at a constant initial pressure, the final flame temperature is increased and therefore the formation of the thermal NO. But for an increase in the initial pressure at a constant initial temperature, the final flame temperature remained unchanged, thus the thermal NO formation is the same. However, the nitrogen monoxide formation decreases with this pressure augmentation, therefore, it seems that pressure influences the kinetic reactions of the fuel NO formation pathways. This has already been observed in Chapter 4 when performing the simulation of an ammonia-hydrogen-oxygen-argon flame at several conditions of pressure (between 50 mbar and 1 bar). Indeed, an increase of pressure leads to a raise of the radicals recombination

reactions and of the efficiency of reactions with a third body. Therefore, the combustion is more complete, leading to more H_2O and N_2 and less products from an incomplete combustion like NO, HNO, N_2O and NO_2.

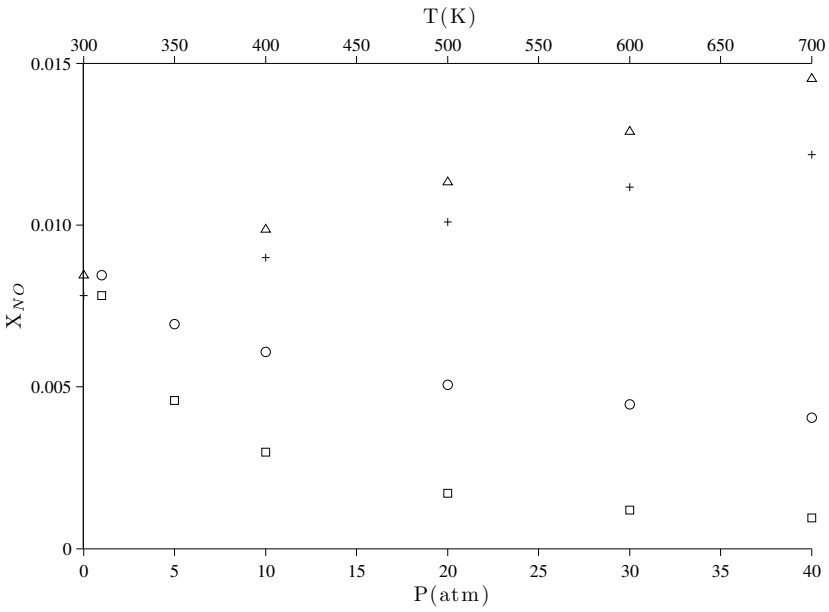

Figure 7.19: Separated effects of temperature and pressure variation on the maximum and the burned gases nitrogen monoxide mole fraction in the flame. Temperature variation: $\triangle$: $X_{NO_{max}}$; $+$: burned gases X_{NO}. Pressure variation: $\circ$: $X_{NO_{max}}$; $\square$: burned gases X_{NO}.

Conclusions

In this second part, ammonia laminar flame speed (S_u) has been experimentally and numerically investigated.

A literature survey has presented the various techniques developed to measure burning velocities in order to justify the choice of the tube method used in this work. Indeed, there is up to now no agreement on a standardized method to measure the laminar burning velocity since each one has its particularities, advantages and disadvantages. The choice of the method depends on several parameters as the precision, the reliability, and the simplicity of the experimental setup. A short review on ammonia burning velocity has then been proposed showing that even if only few measurements were performed in the past, they all led to the conclusion that ammonia has a very low flame speed, much lower than conventional fuels, and that the maximum value is obtained for slightly lean mixtures in the case of ammonia-oxygen flames and for slightly rich mixtures in the case of ammonia-air flames. Furthermore these measurements emphasized the linear decrease of ammonia flame speed with an increasing nitrogen dilution. However, only few measurements were performed for ammonia-air flames around stoichiometric conditions.

The influence of the equivalence ratio and the dilution on ammonia laminar flame speed have thus been investigated. The range of investigated equivalence ratios is $0.7 < \phi < 1.2$ at nitrogen dilution equals to 61.7% (this dilution corresponding to the air-dilution at $\phi = 1$). The range of dilutions equals to $35\% < X_{N_2} < 61.7\%$ for an equivalence ratio of one. The experimental values of the laminar flame speed have been obtained using the tube method. Before per-

forming laminar flame speed measurements for ammonia, which are relatively unknown, the experimental device has been successfully validated by performing well-known methane burning velocities measurements.

The experimental results for ammonia have been compared to numerical simulation results obtained with the *reduced* ammonia combustion mechanism. Furthermore, these results have also been compared to available literature data. An increased dilution led to a global linear decrease of the laminar flame speed. The numerical results were in agreement with the experimental ones and the literature data reproduced the same trend. For an equivalence ratio equals to one, the measured ammonia laminar flame speed at the air-dilution was equal to 13.3 $cm.s^{-1}$. The effect of an equivalence ratio variation for a constant dilution showed a peak value under stoichiometric conditions and a decrease of the laminar flame speed around this maximum. The numerical results were in agreement with the observed effect even if a slightly higher maximum value was obtained (14.1 $cm.s^{-1}$) for an equivalence ratio equals to 1.05. However the literature data were systematically lower than these experimental and numerical results by a factor of 2. This difference could not be explained but nevertheless these results showed a significantly lower ammonia laminar flame speed in comparison to the traditional fuels for which this one is around 40 $cm.s^{-1}$.

Using the *reduced* kinetic model, other numerical simulations were performed in order to analyze the influence of a lower and a higher pressure on the laminar flame speed. The variation of the laminar burning velocity with the equivalence ratio, the initial hydrogen percentage and the dilution for several sub-atmospheric pressures has been studied. A decrease of the pressure to sub-atmospheric values led to a slight increase of the laminar burning velocity (around 20% between 1 and 0.1 atm), but the effects of dilution and equivalence ratio variations are identical to those observed at atmospheric pressure. The addition of hydrogen led, as expected, to an increase of the laminar flame speed. Finally, numerical simulations of ammonia combustion at elevated pressure and temperature conditions such as those encountered in spark ignition engines have been performed. Only the kinetic aspect of the combustion has thus been taken into account. These simulations have shown that the maximum laminar burning velocity is reached in the rich side at an equivalence ratio of 1.1. In the vicinity of stoichiometric mixtures, the variation of the compression

ratio has a significant effect on increasing the laminar burning velocity. An increase of the compression ratio from 12:1 to 20:1 led to a 130% increase of the laminar burning velocity. The adiabatic flame temperature shows a peak at an equivalence ratio around 1.00. It was found that the adiabatic flame temperature increases slightly with the compression ratio. Finally, the nitrogen monoxide mole fraction reaches a maximum at $\phi = 0.95$. Increasing the compression ratio does not have a significant impact on the NO formation for the range of CR investigated in this work because it leads only to a slight increase of the adiabatic temperature and as a consequence to a slight increase of the thermal NO formation. However, a huge decrease of the highest NO concentration is observed for rich mixtures ($\phi = 1.2$), with a NO maximum mole fraction of 50% less than the amount of NO found for an equivalence ratio of 0.95.

Important things to keep in mind when reading the third part of this work are that:

- Ammonia laminar flame speed is much lower, by a factor of 3 to 4, than the one of conventional fuels which is around 40 cm.s^{-1}.
- The equivalence ratio has an impact on the laminar flame speed of ammonia with a maximum around stoichiometric conditions.

Part III

Combustion of ammonia in a SI engine

Introduction

In the first part of this thesis, ammonia combustion has been investigated under low pressure. Then, in the second part, ammonia combustion has been investigated under atmospheric pressure. Finally, in this third part, its combustion at elevated pressure and temperature conditions is investigated by performing an experimental study of ammonia combustion in spark ignition (SI) engines.

The use of ammonia as a fuel is quite surprising. Therefore, this introduction is the opportunity to compare this fuel with other conventional fuels. But before doing this, it seemed important to mention that we are not the only ones proposing this unusual idea. An annual ammonia fuel conference is even organized since 2004 in the USA. Technical and conceptual aspects of the use of ammonia as an alternative to fossil fuels are presented and discussed during this conference.

Why use ammonia as a fuel in spark ignition engines? As already mentioned in the introduction of this thesis, the search for alternatives to fossil fuels is an important concern of our society. Many studies are devoted to the evaluation of the energy efficiency and the environmental impact of alternative fuels. Among these, oxygenated fuels, biodiesel and hydrogen have been put forward. Even though hydrogen has been recognized as a promising fuel, implementing a global hydrogen-based economy is not a currently feasible approach unless a suitable storage medium can be found [2]. Indeed, while traditional forms of hydrogen can be sustainable, can be produced from any raw energy source, are environmentally friendly and, have the ability to be used in many prime movers (i.e. diesel engines, fuel cells, SI engines, gas turbines, etc.), the cost

effectiveness due to challenges in storing and delivering compressed and cryogenic hydrogen are huge barriers to near-term, wide-spread use of hydrogen in these traditional forms. Therefore, to bypass such difficulties, the use of ammonia in a modified spark ignition engine has been suggested. Since hydrogen must still be produced to obtain ammonia in large amount, it can be seen as a **hydrogen vector**. In the following discussion, ammonia is thus compared to gasoline, compressed natural gas (CNG), liquified petroleum gas (LPG), hydrogen and methanol. This latter represents an example of oxygenated fuels proposed as alternatives to gasoline or diesel. The table below presents the energetic and physicochemical properties of these fuels. Gasoline is taken as a reference to which other alternatives are compared.

Property/Fuel	Gasoline	Methanol	CNG	LPG	H_2	NH_3
Storage	Liquid	Liquid	Comp.	Liquid	Comp.	Liquid
Storage pressure $[bars]$	1	1	250	14	350-700	10
Density $[kg/m^3]$	725	786	188	543	31	608
Air/Fuel ratio (ϕ=1) $[kg_{air}/kg_{fuel}]$	14.5	6.44	15.44	15.51	34.3	6.05
LHV [MJ/kg]	43.5	20	45	46	121	18.7
$LHV_{mixture}$ $[kJ/kg_{mixture}]$	2800	2840	2740	2790	3420	2640
Energetic density $[GJ/m^3]$	31.54	15.72	9.4	24.98	3.75	11.3

Compressed Natural Gas (CNG). This is mainly methane stored at room temperature but at elevated pressure (250 bars). The lower heating value presented in the table here above must be explained further to avoid any confusion. Indeed, the energetic contain of a kilogram of CNG is higher than the one of gasoline. However, as specified by the air/fuel ratio, the energetic contain of a stoichiometric mixture CNG with air is lower than the one of a stoichiometric mixture of gasoline/air. The CNG engine is thus supposed to be slightly less powerful than a gasoline one. However, a higher effective efficiency could be obtained since CNG has a higher octane rating ($\approx$ 120) than gasoline leading thus to the opportunity to use higher compression ratios. Concerning the pollution, the smaller C/H ratio decreases the CO_2 production by 25% in comparison to gasoline.

Liquified Petroleum Gas (LPG). This is a widely used mixture of propane and butane, stored under slight pressure. This aspect is thus not an inconvenient. LPG is used in spark ignition engines and is vaporized and premixed with air before entering the cylinder. LPG has a lower heating value of the stoichiometric mixture very similar to the one of gasoline. The engine performances are thus supposed to be very similar. The density of LPG being quite smaller than gasoline, the energetic density of LPG is quite smaller, implying that the energetic contain of a same tank is reduced by 20%. Concerning its pollution, LPG combustion is less harmful than the one of gasoline leading to less unburned hydrocarbons and less CO_2. The flame temperature being lower, the thermal NO_x production is also decreased.

Methanol. This alcohol has a mixture lower heating value higher than the one of gasoline leading to more powerful engines. However, the fuel consumption is twice the one of gasoline, implying an energetic contain of the same tank twice lower. Furthermore, this fuel presents the risk of harmful methanol emissions.

Hydrogen As mentioned here above, hydrogen is an alternative to conventional fuels highly promoted since its combustion is environmentally friendly. However, its energetic density is very low and the main problem remains thus its on board storage and its distribution network.

Ammonia. The much lower air/fuel ratio of ammonia compared to gasoline appropriately compensates its lower LHV. The energetic contain of a stoichiometric mixture of ammonia-air is thus close to the one of a stoichiometric gasoline-air mixture. Same engine performances can thus be expected. However, its energetic density is three times lower indicating that fuel consumption will be three times that of gasoline. The toxicity of ammonia presented in the introduction of this thesis implies that a complete combustion must be ensured to avoid harmful ammonia emissions.

Considering this information, a short comparison of the cost of ammonia with gasoline can be performed. Indeed, for the same expected engine performances, gasoline consumption is equal to 7 l/100 km while ammonia consumption will be 21 l/100 km. Gasoline cost being currently 0.6971 €/l[1] and ammonia cost around 330 €/t[2], these fuels costs are:

Gasoline : 4.9 €/100 km and Ammonia : 4.7 €/100 km.

This calculation does not take into account the cost of distribution of ammonia nor the VAT and excise taxes on gasoline.

Finally, Zamfirescu et al. [173] performed an interesting comparison between the characteristics of an existing hydrogen internal combustion engine Ford Focus and the same vehicle converted to ammonia (see table below). In their calculations, they assumed that the cost of ammonia is \$0.33/kg and that the power-train performance is characterized by 1.19 MJ/km shaft power. They considered a similar efficiency of the ammonia engine and the hydrogen engine.

Parameter	Unit	H_2	NH_3
Storage tank volume	liter	217	76
Storage pressure	bar	345	10
Energy on-board	MJ	710	1025
Cost of full tank	\$	27	15
Driving range	km	298	430
Driving cost	\$/100 km	9.1	3.5
Tank compactness	l/100 km	73	18

As shown in the table here above, the driving range of the NH_3 vehicle is much higher and hence more economical as shows a driving cost of 3.5\$/100 km compared to 9.1\$/100 km for the H_2 ICE. Moreover, the tank compactness of the ammonia car is about 4 times better.

[1] 23/08/11, http://economie.fgov.be/fr/statistiques/chiffres/energie
13/05/11, http://www.petrolfed.be/french/chiffres/evolution_fiscalite.htm
[2] 19/07/11, http://www.terre-net.fr/cours_marches_agricoles/engrais/azote.html

In this third part, after a literature survey on the use of ammonia as a fuel in engines (**Chapter 8**), the experimental setup used to perform measurements of the engine efficiency and exhaust gases composition while using ammonia as a fuel is presented (**Chapter 9**). Finally, the experimental results are discussed in order to investigate the effects of the compression ratio, the spark advance and the equivalence ratio on the engine exhaust gases and performances (**Chapter 10**).

CHAPTER 8

Literature review on the use of ammonia in SI engines

Few studies investigated the use of ammonia as a fuel in spark ignition engines in the past. However, in recent years, with the oil reserves decrease and the pollution problems related to CO_2 emissions, the search for alternative to fossil fuels led to various studies on this subject.

The first time ammonia has been suggested as a potential alternative to fossil fuels was in 1941 by A. Macq [174]. In his opinion, ammonia was an excellent motor fuel and stood at the top of alternative fuels used at that time. This was demonstrated both in laboratory and on road, in light and heavy vehicles. Moreover, he concluded that ammonia is suitable to various conditions of use. Indeed, its condensed state is compatible with a lightweight and compact tank, compared to the one needed for compressed gases as hydrogen. Macq suggested that since ammonia was produced in large amount in Belgium, it was particularly indicated as an alternative fuel. It is important to note that at this time, the compression ratio of cars could not be increased. A problem of combustion initiation was thus encountered since, for conventional compression ratios used in spark ignition engines, ammonia does not ignite without a little boost. Therefore, a small part of ammonia was transformed into hydrogen which allowed the ignition when it was present in amounts greater than 5%. This hydrogen formation was performed using a catalyst composed of iron, aluminum oxide and potassium carbonate. Since ammonia decomposition is endothermic, the heat required for this reaction was supplied by the exhaust gases heat.

A second study has been performed in 1966 by Starkman et al. [175]. The objective was to extend the area of basic and applied information relative to successful substitution of hydrocarbons by anhydrous ammonia as a spark ignition engine fuel. On the one hand they predicted by thermodynamic calculations the relative performance to be expected when operating a SI engine on ammonia. Other theoretical calculations, relative to partial dissociation of NH_3 in H_2, prediction of exhaust gases composition and liquid ammonia evaporation (ammonia was introduced in the engine in the vapor phase an partly decomposed to H_2 and N_2 on a iron catalyst) were also performed. On the other hand, they operated such an engine under carefully calibrated conditions for comparison to theory. The aim of the experimental part was to point out the way to successfully operate the engine while keeping the modifications as small as possible. Therefore, the experiments were performed using nominal compression ratios between 6:1 and 10:1, normal ignition systems, atmospheric or throttled manifold pressures and dissociation or regeneration methods compatibles with domestic or military installations. They concluded that:

- The successful application of ammonia as a spark ignition engine fuel at conventional compression ratios in such engines needs its introduction as a vapor and its partial decomposition into H_2 and N_2 before introduction into the cylinder. Few engine modifications were necessary under such circumstances other than a means for ammonia flow control and adjustment of the spark timing.

- Since ammonia must be partly decomposed before introduction in the cylinder, the theoretical 77% performance of that with hydrocarbon cannot be accomplished. Experiments yielded a little over 70%.

- Specific fuel consumption is increased by a factor of 2 over that of hydrocarbon when compared at peak power and 2.5 when compared at maximum economy due to the smaller lower heating value of ammonia.

- The H_2 concentration in the fuel feed is a crucial factor for the successful use of ammonia as fuel. Minimum needed concentrations are 4-5% by weight for intermediate engine speeds of 1800 rpm. If less than minimum required hydrogen concentrations are used, engine performances rapidly fall.

- Performances are influenced by engine speed, spark timing and manifold pressure in a way not so different for ammonia than for hydrocarbons if minimum amounts of hydrogen are introduced as a part of the fuel flow.

More recently, in their theoretical study performed in 2003 and presented in the second literature survey of this thesis, Checkel et al. [161] gave interesting data on the engine itself. They concluded that using ammonia as a fuel, there is no loss of power, no more corrosion and no increase of the lubricating oil consumption than with conventional fuels. Finally they presented several ammonia characteristics placing it as an applicable alternative to fossil fuels for SI engines. Ammonia has, for example, a high octane rating (≈110) which allows to increase the compression ratio in order to reach higher engine efficiency.

Since 2006, Grannell et al. [176–179] perform research on the possibility to use ammonia in a dual fueled spark ignition engine with gasoline.
In a first paper [176], they investigated the operating features of a stoichiometric, ammonia and gasoline dual fueled SI engine using a single cylinder, variable compression ratio, supercharged Cooperative Fuel Research (CFR)[1] engine at varying ratios of gasoline to ammonia. Ranging from idle up to maximum load in the supercharge regime, the engine has been operated in order to obtain for all loads a combustion without knock and with minimal roughness. They observed a range of gasoline to ammonia ratios for which, for a fixed load, speed and compression ratio, knock-free, smooth firing was obtained. This range has been investigated until its roughness and knock limit. With too much ammonia, the engine fired with an excessive roughness, and with too much gasoline, knock-free combustion could not be obtained while keeping the maximum brake torque (MBT) spark advance. They also investigated stoichiometric operation on gasoline alone for comparison. They concluded that:

- A significant part of the gasoline used in SI engines can be replaced by ammonia.

- Near idling, the use of mainly gasoline is required while mainly ammonia can be used at high load.

[1] A cooperative fuel research engine is a standardized single-cylinder, overhead valve, variable-compression ratio engine used throughout the world for testing, research, and instruction in the performance of fuels and lubricants for the internal combustion engine.

- Higher compression ratios and higher loads can be obtained without knock using ammonia or ammonia with gasoline than with gasoline alone. A CR of 12:1 was allowed with 65% ammonia/ 35% gasoline, whereas the limit for gasoline alone was 9:1 and the engine could be operated at brake mean effective pressures that were more than 50% higher than those achieved with the use of gasoline alone.

- Operation at 10:1 compression ratio is the best mode from the standpoint of both efficiency and also the fuel replacement rate when ammonia and gasoline are used. The maximum brake thermal efficiency achieved with the use of ammonia/gasoline was 32.0% at a CR of 10:1 and with a brake mean effective pressure equals to 1025 kPa. The maximum brake thermal efficiency possible for gasoline was 24.6% at 9:1 and with a brake mean effective pressure equals to 570 kPa.

In 2007, to demonstrate the practical use of ammonia as an alternative automobile fuel, Grannell et al. converted a Chevy S-10 pick-up into an ammonia-powered vehicle and ran from Detroit to San Francisco (2500 miles) [177]. The truck was dual-fueled, meaning it could be switched seamlessly from 100% gasoline fuel to a mixture of 80% NH_3/ 20% gasoline. The truck ran the same, no matter which fuel it was burning. The technology that makes this NH_3 car possible is the control system that managed the perfect mixture of fuel for the amount of work the engine was doing (the load). At start and idle, the engine required the flammable properties of gasoline, but as the vehicle accelerated (increasing the load) the fuel mixture could be predominately ammonia.
Then, in order to refine their knowledge on the engine properties and capabilities, they investigated the fuel mix limits and efficiency of the engine [178]. They concluded that:

- Most of the gasoline burned by SI engines can be replaced by ammonia when the indicated mean effective pressure is higher or equal to 400 kPa. However, they suggested that a SI engine cannot generally give acceptable performance while fueled by ammonia alone.

- There is a fuel mix map, as a function of load, speed, and compression ratio, which specifies the proportion of gasoline that can be replaced by ammonia while keeping acceptable performance. This proportion goes up with increasing load, and down with increasing speed. A similar map

can be obtained when other fuels than gasoline are used as combustion promoters or when a different engine design is used.

- The compression ratio has a surprisingly weak effect on the combustion promoter requirement at the rough limit.
- A single, constant gasoline/ammonia ratio cannot be found to work appropriately for every combination of load and speed. Therefore, the combustion promoter and the ammonia should be stored in separated tanks and metered separately into the engine.
- A compression ratio of 10:1 is recommended for the ammonia and gasoline dual fueled engine. Indeed, they found a decrease of the thermal efficiency and of the proportion of ammonia that can be used for CR > 10:1. However, they suggested that an improved combustion chamber geometry should yield a slightly higher optimal compression ratio for efficiency, and also for the knock and rough limit crossovers, probably near 12:1 for both.
- Resistance of ammonia to knock allows engine operation at much higher indicated mean effective pressures than it is possible with the use of gasoline alone. The efficiencies at high load are also better, where comparable, when ammonia is used because MBT spark timing can be used with ammonia at high indicated mean effective pressure. The use of ammonia with gasoline enables the continued use of MBT spark timing at combinations of load and compression ratio, which are inaccessible to gasoline.

Finally in 2009 [179] Grannell et al. measured the engine-out and post-catalyst emissions of ammonia, hydrocarbons, nitric oxide, carbon monoxide, and nitrous oxide of the engine. They found that an ordinary three-way catalytic converter can be used to clean up these emissions but that lean operation must be absolutely avoided. The clean-up region has been found to occur between stoichiometric and 0.2% rich. The engine-out exhaust emissions reflected appropriately the proportion of ammonia in the intake fuel mixture when the engine was operating satisfactorily from the standpoint of combustion stability and overall thermal efficiency. The effect of rich and lean operation on post-catalyst NH_3, NO, and N_2O emissions becomes much stronger whenever any ammonia fuel is used. For that reason, they suggested that the inclusion of a post-catalyst oxygen sensor is necessary when ammonia is used.

Reiter et al. [180, 181] investigated also dual-fueled engines but in opposition to Grannell et al. who used gasoline engines, they investigated dual-fueled diesel- or biodiesel-ammonia engines.
In a first study [180] they demonstrated the feasibility of the use of ammonia in compression-ignition engines. Since ammonia has a high resistance to autoignition they chose a dual-fuel approach. A method has been developed to introduce ammonia into the intake manifold and to inject diesel fuel or biodiesel directly into the cylinder to ignite the mixture. They used a multi-cylinder, turbocharged diesel engine requiring only slight modification of the intake to implement the ammonia fuel line and keeping the existing diesel fuel injection system unchanged. The ammonia flow rate was regulated by a high pressure relief valve and a liquid ammonia tank was used for fuel storage. The diesel fuel injection was used to control the combustion onset (e.g., ignition). Both experiments and chemical kinetic studies were carried out for different diesel/ammonia ratios at various engine speeds and loads. Ammonia was used as an energy replacement for diesel fuel. The results showed that:

- The maximum engine torque could be achieved by using different proportions of diesel and ammonia. During the tests they measured a maximum energy replacement of 95%.
- The CO_2 emissions were reduced linearly as a function of the ammonia proportion increase in the fuel mixture, for the same engine torque output.
- Despite the fuel-bound nitrogen of ammonia, the NO_x emissions did not increased while burning ammonia. Lower levels of NO_x were even obtained as long as the energy substitution by NH_3 did not exceed 40%. They suggested that this was due to the lower combustion temperature of ammonia.
- The engine could be operated at different load conditions by using a small quantity of diesel fuel with the appropriate amounts of ammonia to achieve desirable loads.
- Using biodiesel in place of diesel gave same performances.

Then in a second study published recently [181] they investigated the effect of various ammonia/diesel proportions on the engine performances and exhaust gases composition. On the one hand, they used several combinations of ammonia and diesel to achieve a constant engine power. And, on the other hand,

they used a small fixed quantity of diesel and varied the amount of ammonia in order to reach variable engine power. For the constant engine power operation the optimized operation range to achieve favorable fuel efficiency was to use 40 to 60% of energy provided by diesel and 60 to 40% of energy supplied by ammonia. The CO and hydrocarbons exhaust gases emissions were generally higher using the dual fuel approach in place of using pure diesel for the same power output due to the lower combustion temperature of ammonia. Those of NO_x varied with the different fueling combinations. They were reduced if ammonia accounted for less than 40% in the total fuel energy, this was attributed to the lower combustion temperature resulting in lower thermal NO_x, and increased significantly if ammonia accounted for the majority of the fuel energy, this being attributed to the fuel-bond nitrogen. Soot emissions were reduced significantly if a large amount of ammonia was used. They explained this reduction by the lack of carbon present in the combination of fuels. Despite the overall high ammonia combustion efficiency, exhaust ammonia emissions ranged from 1000 to 3000 ppm and they suggested further after-treatment. The variable engine power operation resulted in relatively poor fuel efficiency and high exhaust ammonia emissions due to the lack of diesel energy to initiate the effective combustion of the lean ammonia-air mixture. The in-cylinder pressure history was also analyzed, and results indicated that ignition delays increased with increasing amounts of ammonia due to its high resistance to autoignition. The peak cylinder pressure also decreased because of the lower combustion temperature of ammonia. They suggested further combustion optimization using direct ammonia/diesel injection strategies to increase the combustion efficiency and reduce exhaust ammonia emissions.

Finally, Morch et al. [182] investigated the use of ammonia-hydrogen mixtures in a SI engine using metal amine complexes for ammonia storage. Ammonia and hydrogen were introduced into the intake manifold of a CFR-engine. They performed several experiments with varying excess air ratios and ammonia to hydrogen ratios. They found that, with respect to efficiency and mean effective power, a fuel mixture with 10 vol.% hydrogen was the optimum. This has been explained by the higher heat loss during combustion of the mixtures with high levels of hydrogen. In order to investigate the possibility of using $MgCl_2$ as an ammonia carrier in SI-engine, a fuel system was modeled. The model was used to analyze the possibility of using exhaust heat for the des-

orption and decomposition of ammonia. The investigation showed that it is possible to cover a major part of the needed heat for a metal amine complex based fuel system with the exhaust heat. They observed an important NO_x emission with the largest one occuring with a high hydrogen content and an excess air ratio between 1.1 and 1.4. In order to reduce these NO_x they proposed to use selective catalytic reduction (SCR) since ammonia is already onboard. They performed also a comparison with gasoline concluding to higher power and efficiency with NH_3/H_2 due to the possibility of achieve higher compression ratios. The overall emission levels of NO_x on ammonia/hydrogen and gasoline were the same.

All these studies show that ammonia combustion in spark ignition engines has been well investigated these last years but always with an additive to promote the reaction. The use of ammonia as envisioned in this work has thus never been investigated to the best of our knowledge.

CHAPTER 9

Experimental methods

In this chapter, each element presented in the Fig. 9.1 illustrating the experimental setup is described. This means the description of the Varimax engine, the ammonia injection system, the air intake, the exhaust gases analyses and the engine performances monitoring.

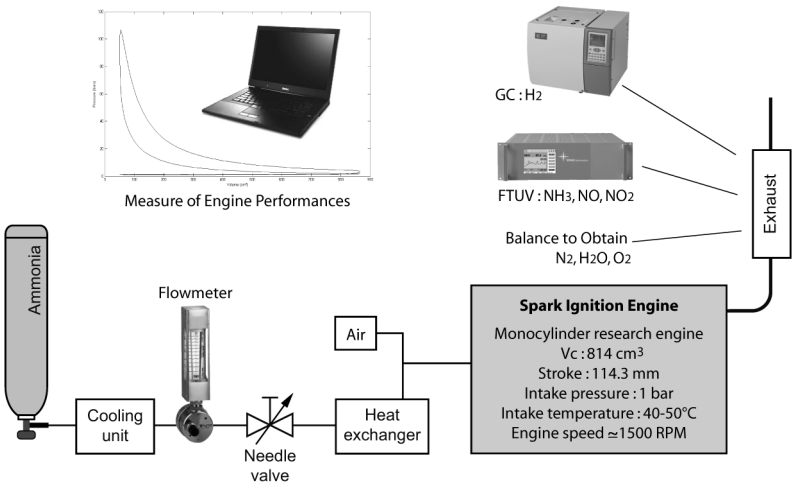

Figure 9.1: Experimental engine setup

9.1 The VARIMAX engine

The experiments have been performed on a VARIMAX test engine. This is a four-stroke single cylinder engine with a displacement of 814 cm^3. The cylinder bore is equal to 92.25 mm and the stroke to 114.3 mm. The compression ratio can be varied from 8 to 19 and the spark advance from -10° to 40° before top dead center (BTDC).

9.1.1 Valve adjustment

Before performing experiments on the engine, the valve timings (opening time and opening length) have been adjusted. The opening and closure parameters of the intake and exhaust valves are mentioned in Table 9.1 where EO/EC are the opening and the closure of the exhaust valve, IO/IC are the opening and the closure of the intake valve and TDC/BDC are the top and bottom dead centers. There is an overlapping (simultaneous opening of the two valves) of 10°. The intake opening phase is equal to 205°and the exhaust one to 195°.

EO	BDC	IO	TDC	EC	BDC	IC
170°	180°	-5°	0°	5°	180°	200°

Table 9.1: Opening and closing angles of intake and exhaust valves

9.1.2 Experimental determination of the compression ratio

From experimental observations, it has been noted that the compression ratio on the measuring system was not the actual one. Therefore, in order to determine the actual compression ratio, an experimental determination based on the in-cylinder pressure measurement has been performed [183, 184]. The first step consists to establish, in motoring conditions, the temperature-entropy diagram from the measure of the in-cylinder pressure as a function of the crank angle and from the volume occupied by the gas. Indeed, the entropic expression of the first principle of thermodynamic allows to write a differential relation between entropy, pressure and volume by the following reasoning:

$$TdS = dU + pdV, \tag{9.1}$$

or

$$\frac{dS}{d\theta} = \frac{mc_v}{T}\frac{dT}{d\theta} + \frac{p}{T}\frac{dV}{d\theta}. \tag{9.2}$$

where θ is the crank angle. The specific heat is the average for the range of temperature considered. The perfect gas relation allows to simplify this expression by eliminating the term $\frac{p}{T}\frac{dV}{d\theta}$ and to substitute the temperature differential by a sum of a pressure and a volume differential. Only this second aspect is described below. This substitution is based on a differential expression of the ideal gas equation which is then divided by itself. The expression

$$pV = mRT \tag{9.3}$$

becomes after differentiation and division

$$Vdp + pdV = mRdT, \tag{9.4}$$

$$\frac{Vdp + pdV}{pV} = \frac{mRdT}{mRT}, \tag{9.5}$$

$$\frac{dp}{p} + \frac{dV}{V} = \frac{dT}{T}. \tag{9.6}$$

By injecting expression 9.6 in the one derived for entropy here above (9.2) it gives

$$\frac{dS}{d\theta} = \frac{mc_v}{p}\frac{dp}{d\theta} + \frac{mc_p}{V}\frac{dV}{d\theta}. \tag{9.7}$$

In order to overcome parameters like the engine size and the mass admitted during the cycle, this equation can be written under a dimensionless form by relating each variable to its initial value (subscript 1 indicating the value at the bottom dead center during the intake phase).

$$\tilde{p} = \frac{p}{p_1}, \quad \tilde{V} = \frac{V}{V_1}, \quad \tilde{T} = \frac{T}{T_1}, \quad \tilde{S} = \frac{T_1 S}{p_1 V_1}. \tag{9.8}$$

The dimensionless expression of the angular evolution of entropy is derived from that obtained previously (9.7),

$$\frac{d\tilde{S}}{d\theta} = \frac{1}{(\gamma-1)\tilde{p}}\frac{d\tilde{p}}{d\theta} + \frac{\gamma}{(\gamma-1)\tilde{V}}\frac{d\tilde{V}}{d\theta}. \tag{9.9}$$

This one contains the average value of the isentropic coefficient, γ. The evolution of entropy is thus only function of the pressure, the volume and their derivatives in term of crank angle variation. The volume evolution is imposed

by the geometry and principally by the compression ratio which is not exactly known during the experiments. The pressure is thus the only experimental value needed. The evolution of entropy is illustrated in Fig. 9.2 based on a simple model of the cycle for the case with (line) and without (dashed line, motoring) combustion. This figure shows the great difference of the entropy evolution between the motoring and the case with combustion. Only the first case is relevant for the determination of the compression ratio. In a first stage, entropy increases as a result of a positive heat exchange with the cylinder walls. Then entropy decreases during most of the compression and expansion stages because of a higher gas temperature than the wall one. Finally, in the final stage of expansion, entropy increases again when the temperature drops sufficiently.

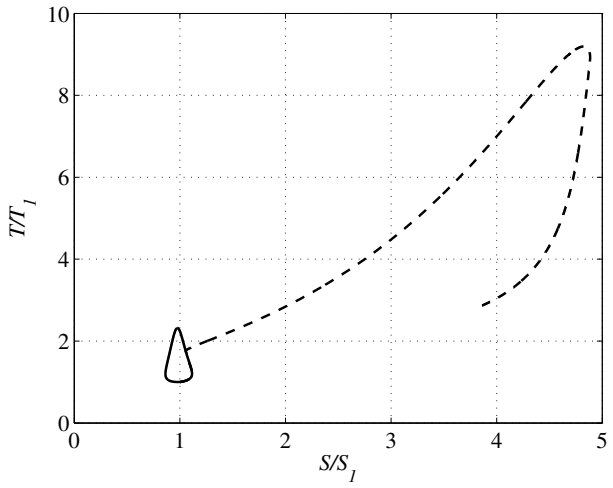

Figure 9.2: Evolution of entropy for the case with (line) and without (dashed, motoring) combustion.

Once the Temperature-Entropy diagram is obtained, it can be used to determine the effective compression ratio. Indeed, the case of monitoring is quite interesting since its graph presents a symmetry around the top dead center which can be used to verify the geometric characterization of the engine, especially its compression ratio. This symmetry is due to the constance of the entropy loss relied to the wall heat transfer, only source of entropy evolution around the top dead center. For a same measurement of the in-cylinder pressure, the aspect of the graph changes drastically according to the supposed

compression ratio. This one is symmetrical only for a value of this ratio very close to the real one. The following figure (Fig. 9.3) illustrates that point.

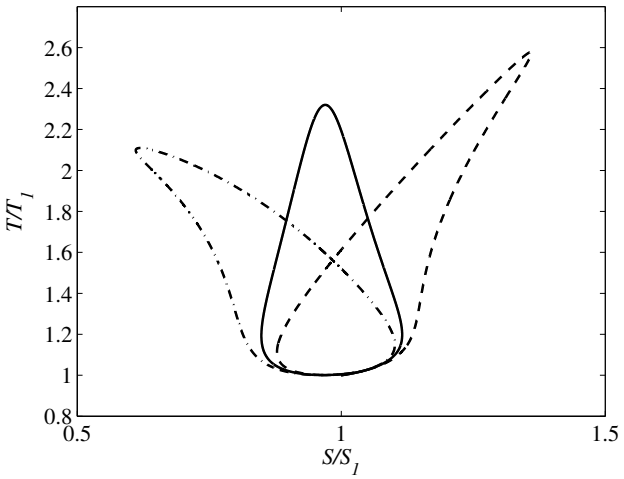

Figure 9.3: Evolution of entropy for the case of motoring for several supposed compression ratio: 10 (real CR, solid), 9 (dashed), 11 (dash-dotted).

The three evolutions have been obtained for a compression ratio of 11, 10 (real value) and 9 from left to right on this graph. An error of 10% in the compression ratio leads thus to an important distortion of the temperature-entropy diagram. This distortion to the left for higher compression ratios is explained by an increase of the influence of the term relied to the volume in the differential expression of entropy. The decrease of the maximum temperature can be explained by the factitious volume decrease for a same pressure since the mass is supposed constant. The opposite effect is observed for lower compression ratios. In order to support this visual analysis, it is preferable to consider the entropy derivative evolution according to the crank angle (θ). For the real value of the compression ratio, this derivative is constant and negative around the top dead center (TDC). In other cases, this one oscillates largely around TDC as illustrated in Fig. 9.4.

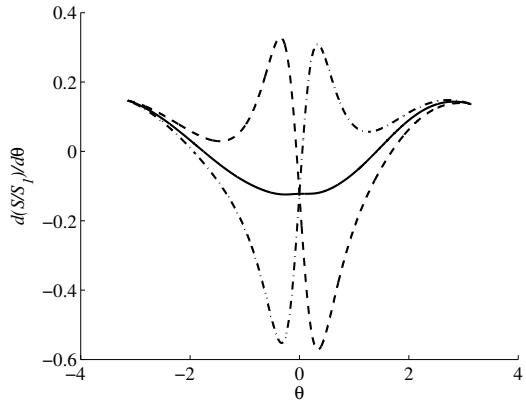

Figure 9.4: Evolution of the derivative of entropy for the case of motoring for supposed compression ratios of 10 (real CR, solid), 9 (dashed) and 11 (dash-dotted).

Even an error of 1% is clearly highlighted on the following figure (9.5) obtained for compression ratios of 10.1, 10 and 9.9.

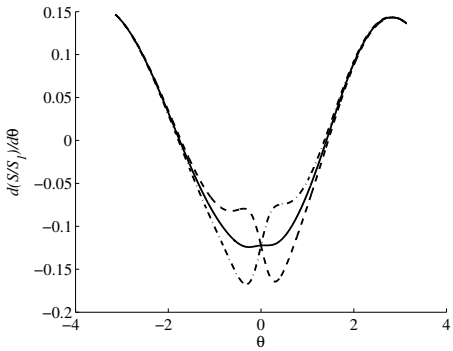

Figure 9.5: Evolution of the derivative of entropy for the case of motoring for supposed compression ratios of 10 (real CR, solid), 9.9 (dashed) and 10.1 (dash-dotted).

It is important to note that this approach does not require the evaluation of the wall heat transfer occurring during the motoring and therefore of the wall temperature nor of the exactly admitted mass.

9.2 Ammonia injection

Since liquid ammonia is corrosive for plastic constituting traditional injectors, a specific injection system was needed in order to bring ammonia from the tank to the engine. Figure 9.6 presents the fuel injection system design.

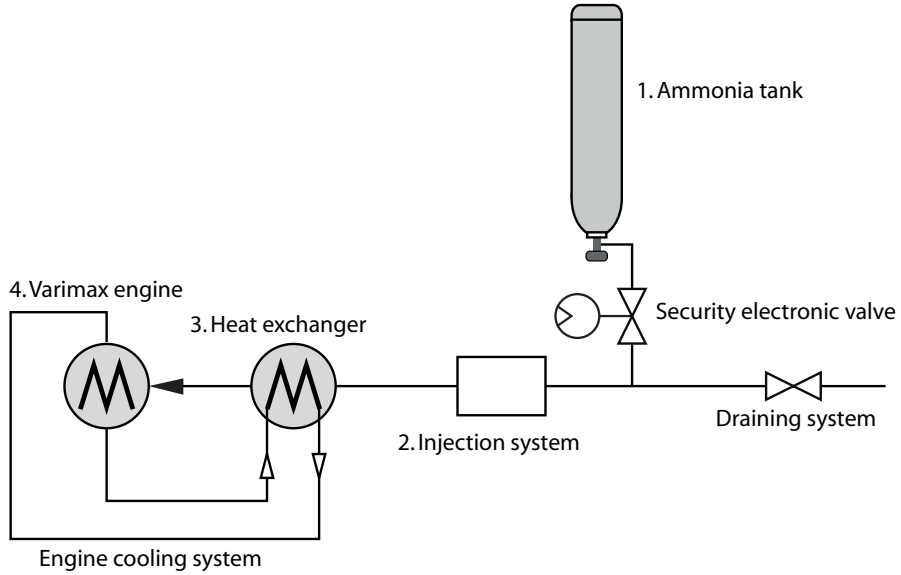

Figure 9.6: Ammonia injection system

1. *The ammonia tank:* The fuel is stored in a gas tank at its equilibrium pressure at atmospheric temperature which is around 10 bars. There is therefore coexistence of the gas and liquid phases. Ammonia extraction takes place at the bottom of the tank to retrieve the liquid only. A security electronic valve is placed after the regulator in order to be able to close the ammonia tank in case of emergency.

2. *The injection system:* In order to control the quantity of ammonia injected in the engine, preliminary tests were performed with a usual gasoline injector previously calibrated for ammonia. However, this led to several problems. On the one hand, the joints constituting the injectors were destroyed due to the corrosive nature of ammonia, leading to an obstruction of the injector after a few uses. On the other hand, an expansion of the liquid occured during the injection resulting in a sharp drop in temperature and therefore a variable

amount of ammonia injected. For these reasons, this method has not been kept for the experimental campaign.
A second method has therefore been chosen consisting of a mass flowmeter in series with a needle valve. The entrance of the mass flowmeter is immersed in water cooled to prevent evaporation of ammonia before the mass flow measurement. In order to prevent corrosive effects observed previously, all the components of the injection system in contact with ammonia are constituted of stainless steel and joints are in EPDM or PTFE.

3. *The heat exchanger:* As mentioned previously the heat of vaporization of ammonia is very high (1371.2 kJ/kg at 1 atm, -33.5 °C). It is therefore important to provide heat during the evaporation in order to avoid freezing of components at this place. For this purpose, the fuel flows through a heat exchanger recovering thereby the heat of the engine water cooling system. Once the engine reaches a stabilized regime, this cooling water achieves a temperature around 90 °C. Ammonia goes thus out of the exchanger in a gaseous state. This gaseous ammonia is premixed with air before entering the cylinder by the intake valve.

9.3 Air intake

The air flow is not imposed during the combustion but well measured thanks to a pressure drop in an admission diaphragm. In the case of the Varimax engine, the diameter of the aperture, d, is equal to 27.5 mm and according to the geometry, the flow coefficient, α, is equal to 0.6. The relation between the pressure drop [Pa] and the volume flow rate [$m^3.s^{-1}$] is:

$$V = \alpha \frac{\pi d^2}{4} \sqrt{\frac{\Delta p}{\rho}} \tag{9.10}$$

9.4 Exhaust gases analysis

For the purpose of exhaust gases analysis, the reaction of an incomplete ammonia combustion is considered to be:

$$aNH_3 + bO_2 + cN_2 \rightarrow dN_2 + eH_2O + fO_2 + gNH_3 + iNO + jNO_2 + kH_2 + lN_2O \tag{9.11}$$

where the several coefficients represent the mole fraction of each component in the fresh or burned gases. Since the equivalence ratio (ϕ) and the air composition (20.95% O_2 - 78.1% N_2) are known, the mixture composition, i.e. coefficients a, b and c, can be easily deduced from

$$a + b + c = 1 \tag{9.12}$$

$$\frac{4\phi b}{3} = a \tag{9.13}$$

$$3.73b = c \tag{9.14}$$

Exhaust gases composition has been determined by several methods detailed in the following subsections.

9.4.1 Gas chromatography, for H_2 and N_2O.

The column which has been used to analyze the exhaust gases is the Molsieve 5A provided by Varian inc. This column consists in a coated molecular sieve that allows a good separation of H_2, O_2, N_2 and N_2O at moderate temperatures. At the output of the column, detection of sample constituents is made by a Thermal Conductivity Detector (TCD). This detector compares the thermal conductivity of the eluent at the output of the column to that of the pure carrier gas and any difference caused by the presence of another compound having a different thermal conductivity results in a measurable signal. Since hydrogen has a thermal conductivity very different from that of oxygen, nitrogen and nitrous oxide as presented in Table 9.2, the choice of an appropriate carrier gas was very important in order to allow detection of small amount of hydrogen. Argon has been chosen as the carrier gas, since its thermal conductivity is low, leading to the best detection of hydrogen. Due to this choice, the precision on the oxygen and the nitrogen amounts was not sufficient to perform a quantitative study. The concentrations of these species have been obtained by a global combustion reaction balance as it will be presented later. Furthermore, by doing several tests with the engine in several conditions of compression ratios, equivalence ratios and spark advances, even when helium was used as a carrier gas, no nitrous oxide has been detected. Therefore, the choice of argon as a carrier gas was particularly appropriated.

Gas	H_2	O_2	N_2	N_2O	Ar	He
Th. Cond.	168.35	24.24	24	14.57	16.36	142.64

Table 9.2: Thermal Conductivity of the gases [mW/m.K].

In practice, a sample of 1 ml is taken in the exhaust pipe using a gas syringe and introduced in the Molsieve column by direct injection. A calibration has been performed in order to obtain the mole fraction of hydrogen in this sample.

9.4.2 UV Spectroscopy, for NH_3, NO and NO_2.

Fig. 9.7 presents the global scheme of the UV Spectroscopy analyzer used during the experiments.

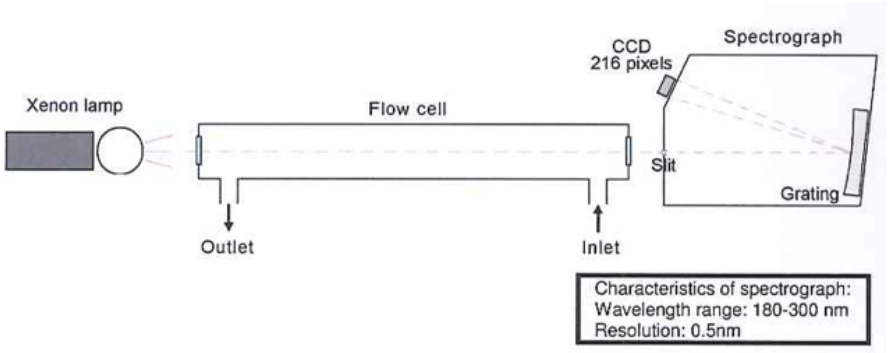

Figure 9.7: UV Spectroscopy analyze.

The first step of the measurement consists to set the blank by measuring the lamp emission on non absorbing gas (like air or nitrogen) as reference for zero. Then, when the gas to analyze circulates in the flow cell, the analyzer measures again the transmitted light to determine the absorption spectrum thanks to the following Lambert-Beer law:

$$[Abs] = log\frac{I_{in}}{I_{out}} \tag{9.15}$$

From this absorption spectrum and by using the appropriate algorithm, the analyzer can determine the concentration of the gas. Temperature and pressure are used to compensate their influences in the measurement. The device enables a high measurement selectivity thanks to the recognition of the specific UV

spectrum of gases by proprietary algorithms. Fig. 9.8 presents the absorption spectra of the three gases analyzed thanks to this method.

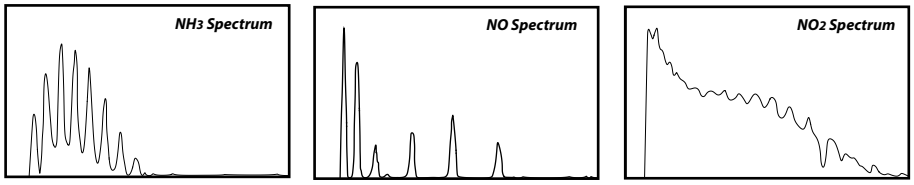

Figure 9.8: Absorption spectra.

The ranges of measurement for which the analyzer has been calibrated, defined in functions of the optical path corresponding to the length of the flow cell, are 0-2 % for ammonia, 0-5000 ppm for nitrogen monoxide and 0-1000 ppm for nitrogen dioxide.

9.4.3 Combustion balance, for N_2, H_2O and O_2.

From the previously described measurements methods, coefficients a, b, c, g, i, j, k and l from eq. (9.11) are known. Therefore, using the following species balance equations, concentration of exhaust gases in nitrogen (d), water (e) and oxygen (f) can be determined.

$$\mathbf{N}: \quad a + 2c = 2d + g + i + j + 2l \tag{9.16}$$

$$\mathbf{H}: \quad 3a = 2e + 3g + 2k \tag{9.17}$$

$$\mathbf{O}: \quad 2b = e + 2f + i + 2j + l \tag{9.18}$$

Finally, a normalization for a sum of the mole fractions equals to one has been performed, although in practice this amount was already close to one.

9.5 Engine performances monitoring

9.5.1 Basic quantities

This first paragraph presents a theoretical summary of several quantities that are important to characterize an engine.

The effective power P_e, represents the power available at the crankshaft. It depends on the effective torque (C_e) and the speed of rotation (rpm). This two quantities are measured during the experiments.

$$P_e = C_e * 2\pi * \frac{rpm}{60} \quad [W]. \tag{9.19}$$

The effective efficiency η_e, corresponds to the ratio between the effective power and the power provided by the fuel during the cycle.

$$\eta_e = \frac{P_e}{\dot{m}_c LHV}, \tag{9.20}$$

where LHV is the lower heating value of the fuel (equals to 18650kJ/kg for ammonia) and $\dot{m}_c$ the fuel mass flow rate.

The effective work W_e, available at the crankshaft depends on the effective torque only and corresponds to the work performed per operating cycle (4 stroke engine).

$$W_e = 4\pi C_e \quad [J]. \tag{9.21}$$

The brake mean effective pressure bmep is, by definition, the effective work divided by the engine displacement (V_c).

$$bmep = \frac{W_e}{V_c} = \frac{4\pi C_e}{V_c} \quad [Pa]. \tag{9.22}$$

The indicated work W_i, represents the work on the piston during an operating engine cycle.

$$W_i = \oint p dV \quad [J]. \tag{9.23}$$

During the experiments this quantity is calculated by integrating the Pressure-Volume diagram.

The indicated mean effective pressure imep, is obtained by dividing the indicated work by the engine displacement (V_c).

$$imep = \frac{W_i}{V_c} = \frac{\oint p dV}{V_c} \quad [Pa]. \tag{9.24}$$

The friction mean effective pressure fmep, is an indicator of the mean effective pressure lost to friction (or friction torque) and is just the difference between

imep and bmep.

$$fmep = imep - bmep \quad [Pa]. \tag{9.25}$$

The mechanical efficiency η_{mec}. In physics, mechanical efficiency is the effectiveness of a machine and is defined as the ratio of work output to work input. It is often expressed as a percentage. While the efficiency of an ideal machine is 100 percent, an actual machine's efficiency will always be less than 100% because of the second law of thermodynamics, which states that the quality of energy will decay, eventually becoming heat. This means that some of the work put into the system is transformed (lost) into thermal energy (heat). In a mechanical system, friction is the most common means by which work is lost to heat. In I.C. engine, the mechanical efficiency is defined by

$$\eta_{mec} = \frac{W_e}{W_i} = \frac{bmep}{imep} = \frac{imep - fmep}{imep} = 1 - \frac{fmep}{imep} \tag{9.26}$$

and is thus not a constant value, depending on the indicated mean effective pressure.

The indicated efficiency η_i, is representative of the ratio between the work on the piston and the power consumed by an engine cycle.

$$\eta_i = \frac{W_i}{m_c LHV} = \frac{\eta_e}{\eta_{mec}}, \tag{9.27}$$

where m_c is the fuel mass [kg] admitted during the cycle. This ratio takes into account the imperfections of the engine cycle together with the combustion efficiency.

The air volumetric efficiency r_{air}, is defined by

$$r_{air} = \frac{m_{air}}{\rho_0 V_c} \tag{9.28}$$

The combustion efficiency η_c, is the ratio between the real energy liberated by the combustion in the cylinder per cycle (Q_i) and the theoretical fuel energy contain.

$$\eta_c = \frac{Q_i}{m_c LHV}. \tag{9.29}$$

This can also be expressed as a function of the reactants and products Lower Heating Values (LHV):

$$\eta_c = 1 - \frac{LHV_{prod}}{LHV_{reac}}. \tag{9.30}$$

9.5.2 Evaluation of basic quantities for ammonia

This second paragraph presents a first evaluation of the effective power, P_e, developed by the spark ignition test engine described here above during the experiments.

The effective power can be deduced from:

$$P_e = bmep * \frac{\pi D^2}{4} * \frac{u}{s} \tag{9.31}$$

where u is the piston average linear speed, $u = rpm * stroke/30$ [m/s] and s is the number of strokes per cycle, equals to four for this engine. In these evaluations, the engine rotation speed is fixed to 1500rpm. The engine stroke is equals to 114.3 mm and the engine bore, D, equals 95.25 mm.

The brake mean effective pressure can be deduced from the indicated mean effective pressure by estimating the friction mean effective pressure around 300 kPa; bmep = imep - 300 [kPa] .

In the case of gaseous fuels, this indicated mean effective pressure can be estimated by the following relation:

$$imep = \eta_i * r_{air} * \frac{LHV}{(\frac{A}{F})_{\phi=1}} \rho_0 \quad [Pa] \tag{9.32}$$

where ρ_0 represents the air density at STP. $(\frac{A}{F})_{\phi=1}$ is the air fuel ratio under stoichiometric conditions, i.e. the quantity of air needed to burn one kilogram of ammonia on a stoichiometric combustion based, and is equals to 6.06 kg_{air}/kg_{NH_3}. The air volumetric efficiency, r_{air}, can be deduced from the global mixture volumetric efficiency r by:

$$r_{air} = r \frac{(\frac{A}{F})_{V,\phi=1}}{(\frac{A}{F})_{V,\phi=1} + 1} \tag{9.33}$$

where $(\frac{A}{F})_{V,\phi=1}$ is the volumetric definition of the air fuel ratio under stoichio-

metric conditions and is equal to 3.57 $m^3_{N\ air}/m^3_{N\ NH_3}$. The global mixture volumetric efficiency, r, is considered to be close to 0.8.

Finally, the highest supposition concerns the evaluation of the indicated efficiency, η_i. Since the experiments were conducted at full load in most of the cases and that the pumping losses can be neglected, this indicated efficiency can be matched to the internal thermodynamic efficiency, η_{ti} which corresponds, for a compression ratio of 15 to 0.46

From all these informations, for a compression ratio of 15, the imep is estimated to be equals to 1070 kPa, leading to a bmep equals to 770 kPa and en effective power around 7.5 kW.

CHAPTER 10

Ammonia combustion in SI engine conditions

In this last chapter, the ammonia combustion in spark ignition engine conditions will be experimentally investigated. Results of the compression ratio measurements, the analysis of the exhaust gases composition without combustion and finally the effects of the compression ratio, the spark timing and the equivalence ratio on the exhaust gases composition and the engine performances are presented.

10.1 Actual compression ratios

The actual compression ratios have been determined using the method presented in the previous Chapter. Figure 10.1 presents the experimental curve of the derivative of entropy evolution for three values of compression ratios, i.e., 13, 15 and 17. For the real value of the compression ratio, this derivative is constant and negative around the top dead center (TDC). In other cases, this one oscillates largely around TDC. Focus has thus been made around the top dead center in Fig. 10.1. Similar diagrams have been realized to reduce the range of the envisaged compression ratios until reaching, for this presented case, the actual value of 15.

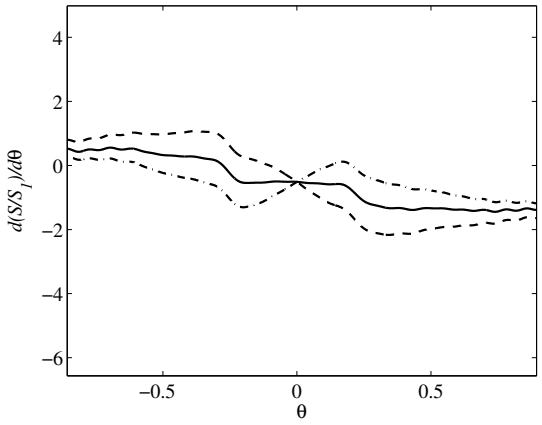

Figure 10.1: Evolution of the derivative of entropy for the experimental case of motoring for supposed compression ratios of 15 (real CR, solid), 13 (dashed) and 17 (dash-dotted).

10.2 Exhaust gases analysis without combustion

The temperatures reached at the end of the compression due to the high compression ratios applied in order to burn efficiently ammonia in a spark ignition engine suggest that ammonia could be partially or totally decomposed into hydrogen at the ignition timing, inducing a hydrogen combustion in place of or together with the ammonia combustion. This decomposition follows the equation:

$$2\ NH_3\ =\ N_2\ +\ 3\ H_2 \tag{10.1}$$

The value of the equilibrium constant of this reaction (K_x) at the appropriate temperatures and pressures conditions gives an information on the quantity of ammonia thermodynamically decomposed in hydrogen. This equilibrium constant is written as

$$K_x = \frac{[N_2][H_2]^3}{[NH_3]^2} = \frac{K_p}{p^2}, \tag{10.2}$$

where p is the pressure and $K_p = \exp\left(-\Delta_r G^\circ_{(T)}/RT\right)$. Figure 10.2 presents the evolution of this equilibrium constant as a function of temperature for several pressures in the range of these parameters obtained before combustion as pre-

sented in the section 7.4 of the second part of this thesis.

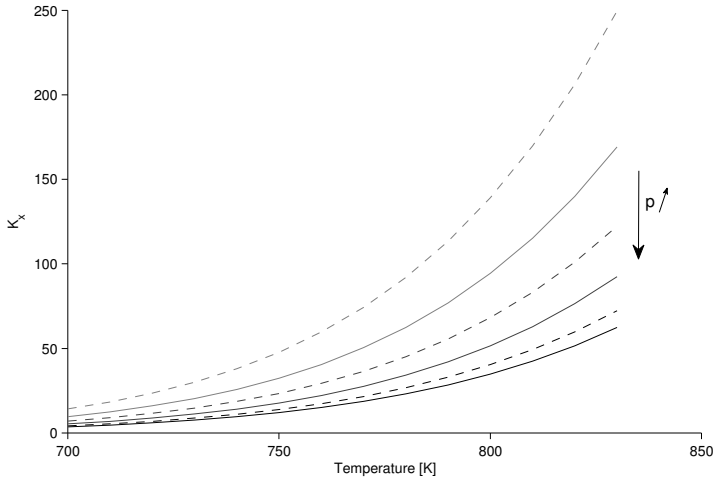

Figure 10.2: Evolution of the equilibrium constant as a function of temperature for several pressures from 28 atm until 56 atm.

According to this graph ammonia could be decomposed partially in hydrogen at such conditions. In order to check experimentally this possibility, the exhaust gases composition has been analyzed without combustion, i.e. without spark ignition, by driving the Varimax engine with an electrical engine.

No hydrogen has been found in the exhaust gases in such conditions, whatever the compression ratio, indicating that even if ammonia can be thermodynamically decomposed, kinetics of this reaction is not fast enough at the conditions prevailing in the engine.

10.3 Effect of the compression ratio

This first set of experimental measurements has been gathered to investigate the effects of the compression ratio on the exhaust gases composition and on the engine performances. In order to vary one parameter at a time only, the spark advance (30°) and the equivalence ratio (ϕ=1) have been kept constant during this set of experiments. The experimental results presented below are the mean measurements of several successive engine cycles.

CR	N_2 (%)	H_2O (%)	O_2 (%)	NH_3 (%)	NO (ppm)	NO_2 (ppm)	H_2 (ppm)
13	67.93	28.17	1.53	1.66	538	0	6554
15	67.82	27.81	1.72	1.96	434	0	6452
17	67.72	27.44	1.91	2.27	369	0	6101

Table 10.1: Exhaust gases composition for several compression ratios.

As presented in Table 10.1, an increase of the compression ratio leads to a higher quantity of ammonia and oxygen in the exhaust gases together with a decrease of the nitrogen monoxide and hydrogen percentages, all of this indicating a poorer combustion or an increase of the quenching effect. Indeed, the increase of the compression ratio leads to an increase of the in-cylinder pressure and therefore to more unburned fresh gases in the cylinder crevices. Furthermore, since ammonia has a low flame speed, the quenching effect at the cylinder wall, induced by a temperature gradient due to the engine cooling system, is particularly important.

Even if it has been experimentally proven in the previous paragraph that ammonia is not decomposed into hydrogen when the engine is driven without combustion, the important quantity of hydrogen in the exhaust gases in the case with combustion suggests that the residual ammonia is decomposed partially in hydrogen. Figure 10.3 presents the evolution of the previously defined equilibrium constant for a wider range of pressures and temperatures indicating that the ammonia decomposition is not surprising for the conditions encountered during combustion.

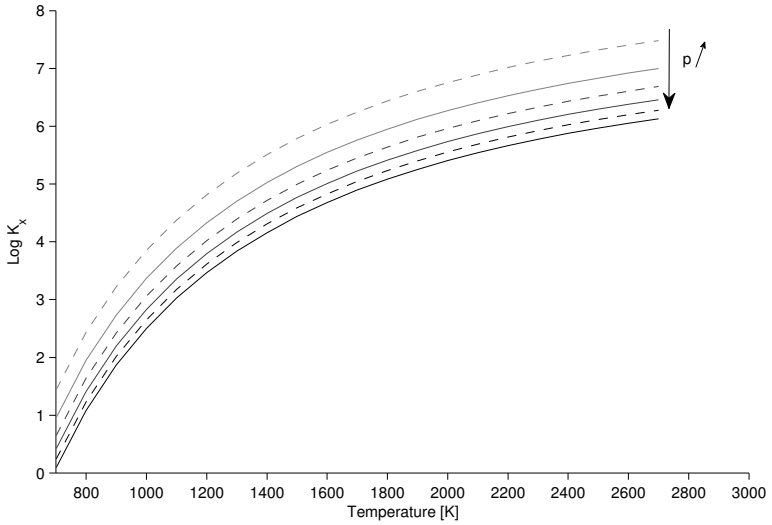

Figure 10.3: Evolution of the equilibrium constant for conditions reached during combustion (pressure ranges, from 20 atm until 95 atm).

Finally, when using ammonia as a fuel, one can imagine that the combustion will lead to important nitrogen oxides quantities in the burned gases. However, the nitrogen monoxide concentration is very low due to relatively low combustion temperatures and for these conditions of spark advance and equivalence ratio, there is no formation of nitrogen dioxide or nitrous oxide as for conventional fuels, where thermal NO_x which are formed are mainly nitrogen monoxide and very few NO_2 and N_2O. This latter species (N_2O) has never been detected in the experimental conditions investigated in this work, even if a measurement technique by gas chromatography was available as described previously. This observation is in agreement with the flame structure experimental results obtained at low pressure indicating that N_2O is an intermediate species in ammonia combustion formed initially by the reaction NH+NO = N_2O +H and then consumed to form nitrogen. Concerning nitrogen dioxide, NO_2, the numerical study performed in section 4.2 in order to investigate the pressure effect on ammonia combustion has shown that even if this species is present in the exhaust gases at low pressure (50 mbar), it disappears for increasing pressures until being totally consumed for the highest investigated

pressure of 1 bar (Fig. 4.28). The pressures reached in the engine being largely higher than this one, it is not surprising to find no or very small quantities of this species in the engine exhaust gases.

CR	13	15	17
$T°_e$ [°C]	481	528	505
Torque [Nm]	56	57	58
RPM	1488	1541	1504
bmep [kPa]	859	880	895
P_e [kW]	8.66	9.20	9.13
η_e	0.37	0.39	0.40
r_{air}	0.64	0.63	0.62
Friction torque [Nm]	14.95	15.35	15.07
fmep [kPa]	231	237	233
imep [kPa]	1089	1117	1128
η_{mec}	0.79	0.79	0.79
η_i	0.47	0.50	0.50
Unburned NH_3 (%)	7.53	8.90	10.29

Table 10.2: Engine performances monitoring for several compression ratios.

The highest effective power observed for the intermediate compression ratio of 15, is exclusively due to the higher engine speed in this case. Indeed, the effective power is not an appropriate indication to analyze the engine performances and the comparison in terms of brake mean effective pressure or effective efficiency is more appropriate.

As expected and presented in Table 10.2, an increase of the compression ratio improves the engine performances. This can be seen by the increase of the effective efficiency and of the brake mean effective pressure and can be explained by the definition of the engine thermodynamic efficiency (η),

$$\eta = 1 - \frac{1}{\tau^{\gamma-1}}. \tag{10.3}$$

This theoretical value indicates an increase of the efficiency with an increase of the compression ratio. It must be corrected by the wall losses that increase

with the compression ratio. The two combined effects justify the moderate benefit of an increase of the compression ratio above 15.

The equivalence of the mechanical efficiency in the three conditions shows that, for the investigated range of compression ratios, the proportion of the work furnished by the engine which is lost by friction is independent of the compression ratio. This means that friction losses depend slightly on the compression ratio for the Varimax engine.

The relatively high effective efficiencies (around 0.39) are due to the particular running conditions of the engine, with for example a low engine speed (around 1500 rpm) and high compression ratios. This demonstrates the interesting contributions of the use of ammonia as a fuel which allows the use of elevated compression ratios with spark ignition engines.

Finally, the fraction of ammonia remaining in the exhaust gases in comparison to the quantity admitted in the fresh gases , around 8 to 10%, is particularly high and cannot be explained only by the quenching effects as mentioned previously (wall quenching and unburned fresh gases in the cylinder crevices). For conventional fuels, this quantity is indeed around 3%. A hypothesis that could explain this important unburned fraction is the presence of bulk quenching as described by Smith et al. for lean natural gas combustion in an expanding chamber [185]. As lean fuel has a low flame speed, as it is the case for ammonia even for stoichiometric composition, the expansion during the combustion is too fast in comparison to the flame propagation. This means that the energy contained in the flame front is diluted and does not preheat the fresh mixture enough to allow a complete flame propagation during this expansion phase. This bulk quenching is influenced principally by the compression ratio and in a lesser extent by the engine rotating speed. However, by controlling the turbulence in the engine with an appropriate geometry or admission phase, one could reduce this effect. Since the Varimax engine is not optimized for ammonia combustion, this is absolutely not the case and bulk quenching could take place. In order to understand more deeply this phenomenon, fundamentals experiments would be needed, for example by investigating ammonia flame speeds in a tube as presented in the second part of this work but with a compression before combustion and an expansion during this one as in Smith et

al. [185]. Furthermore, bulk quenching seems to be influenced by the energy released by the spark. A deeper understanding of this phenomenon is thus an interesting perspective of this SI engine experimental study.

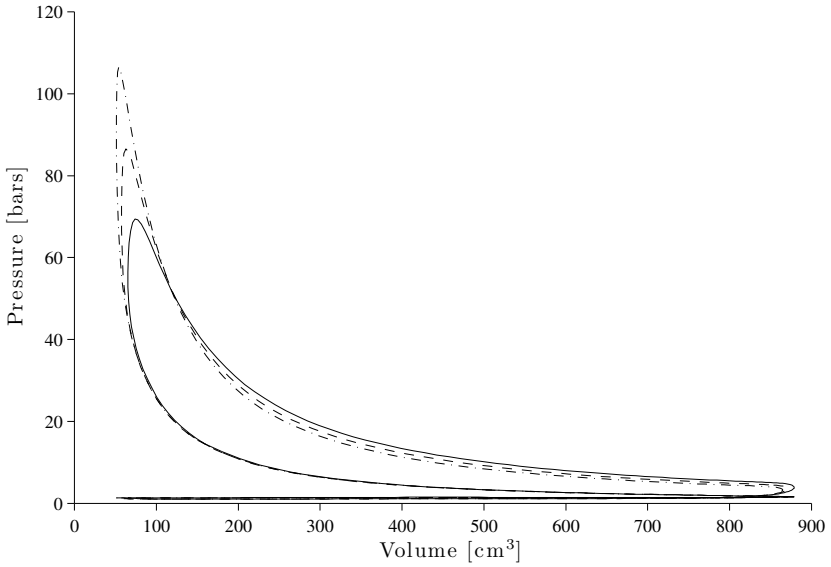

Figure 10.4: Pressure-Volume diagrams for several compression ratios: Line = CR 13; Dashed line = CR 15; Dash-dotted line = CR 17.

The pressure-volume diagrams presented in Figure 10.4 for the three compression ratios indicate as expected that the maximum pressure reached in the cylinder increases with the compression ratio. In order to prevent engine mechanical deterioration, and according to the results presented previously for this first parameter variation, an intermediate compression ratio around 15 seems to be a good trade-off. This choice is only based on the results obtained in this study, however, in practical cases with another and more efficient engine taking thus into account other parameters, this choice could be different.

10.4 Effect of the spark timing

This second set of experimental measurements has as objective to investigate the effect of the spark timing on the exhaust gases composition and on the engine performances. In order to vary only one parameter at a time, the com-

pression ratio (CR = 15.5) and the equivalence ratio (ϕ=1) have been kept constant for these experiments.

Since ammonia has a low flame speed and need therefore more time to burn, the use of this fuel requires a higher spark advance than gasoline. However, this parameter cannot be too high in order to avoid knock which has been experimentally observed starting from 40° before top dead center. The range of spark advances from 16° until 30° has thus been tested.

Spark advance [°]	N_2 (%)	H_2O (%)	O_2 (%)	NH_3 (%)	NO (ppm)	NO_2 (ppm)	H_2 (ppm)
16	66.92	25.29	2.93	3.79	400	0	10346
18	67.66	27.92	1.57	1.77	430	0	10324
20	67.87	27.90	1.66	1.76	527	0	7546
22	67.95	27.96	1.67	1.88	590	0	4730
24	67.86	27.71	1.79	1.95	587	0	6325
26	67.71	27.34	1.94	2.07	529	0	8824
28	67.79	27.66	1.81	2.21	424	0	4853
30	67.74	27.26	2.03	2.32	424	0	6192

Table 10.3: Exhaust gases composition for several spark advances.

Spark advance [°]	16	18	20	22	24	26	28	30
$T°_e$ [°C]	543	577	557	545	535	525	515	503
Torque [Nm]	40	52	54	54	54	54	54	54
RPM	1456	1510	1508	1513	1517	1512	1508	1500
bmep [kPa]	618	800	826	826	826	829	834	834
P_e [kW]	6.10	8.20	8.45	8.48	8.50	8.50	8.53	8.48
η_e	0.26	0.34	0.36	0.36	0.36	0.36	0.36	0.36
r_{air}	0.63	0.63	0.63	0.63	0.63	0.63	0.63	0.63
Friction torque [Nm]	14.71	15.12	15.10	15.14	15.16	15.13	15.10	15.04
fmep [kPa]	227	233	233	234	234	234	233	232
imep [kPa]	845	1033	1059	1060	1060	1062	1067	1066
η_{mec}	0.73	0.77	0.78	0.78	0.78	0.78	0.78	0.78
η_i	0.35	0.44	0.46	0.46	0.46	0.46	0.46	0.46
Unburned NH_3 (%)	16.88	7.93	8.00	8.59	8.89	9.40	10.00	10.54

Table 10.4: Engine performances monitoring for several spark advances.

As presented in Tables 10.3 and 10.4 for a spark advance of 16° the combustion is very poor and incomplete leading to important quantities of ammonia and hydrogen in the exhaust gases and modest engine performances. This can be explained by the bulk quenching effect described previously. The combustion is already more complete for a value of 18° but one can consider that a spark advance of at least 20° is needed to obtain a correct combustion.

From a theoretical point of view the engine efficiency should increase with an increasing spark advance before reaching a maximum. For conventional fuels, the aim is thus to increase the spark advance as much as possible while avoiding knock. However, in the case of ammonia which is very resistant to auto-ignition, the maximum efficiency is reached well before the apparition of knock. This can been seen in Tables 10.3 and 10.4 where, starting from the value of 20°, the spark advance has mainly an impact on the exhaust gases composition and less on the engine performances which are nearly identical between 20° and 30°. Only the maximum pressure reached in the engine cylinder increases with the spark advance (Fig. 10.5), which is not beneficial for the mechanical durability. Since there is no advantage to use a spark advance higher than needed, this one can be kept reasonably low (around 20°-22°). Furthermore this allows to set the advance for optimization purposes and not only to avoid knock.

Concerning the exhaust gases composition, an increase of the residual ammonia due to a higher spark advance is coupled with a decrease of the fuel NO, an increase of the thermal NO induced by a higher peak temperature and a decrease of the hydrogen as presented previously. The increase of the spark advance leads to an ignition at lower temperature and thus to a colder flame, increasing also the bulk quenching effects. The best trade-off between residual NH_3, NO and H_2 lies probably around 20°-22°. Once again in these conditions and for the same reasons as presented for the compression ratio variation, no nitrous oxide or nitrogen dioxide were detected.

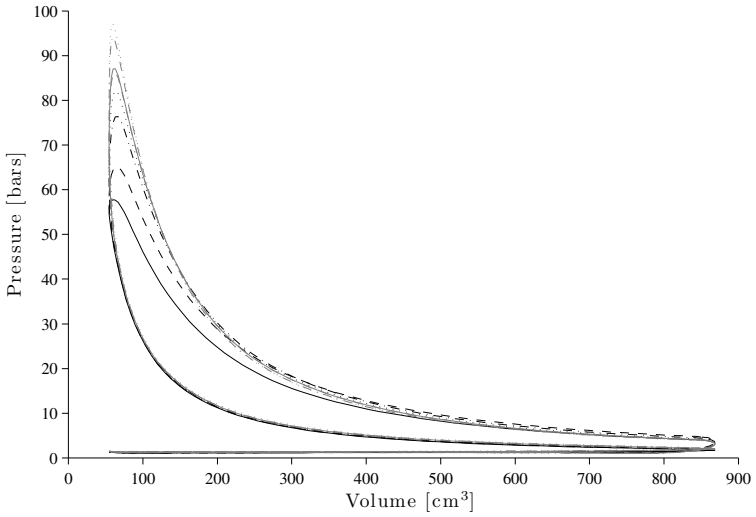

Figure 10.5: Pressure-Volume diagrams for several spark advances : Black line = 16° ; Black dashed line = 18° ; Black dash-dotted line = 20° ; Black dotted line = 22° ; Grey line = 24° ; Grey dashed line = 26° ; Grey dash-dotted line = 28° ; Grey dotted line = 30°.

10.5 Effect of the equivalence ratio

This last set of experimental measurements has as objective to investigate the effect of an equivalence ratio variation on the exhaust gases composition and on the engine performances. In order to vary only one parameter at a time, the compression ratio (CR = 15) and the spark advance (35°) have been kept constant during this set of experiments.

As already mentioned, the equivalence ratio has a huge impact on the engine performances and on the exhaust gases composition. Fresh gases compositions around stoichiometric conditions are an advantage for these two parameters. The investigated range of ϕ goes thus from 0.8 to 1.1

The residual quantity of oxygen presented in Table 10.5 is in agreement with the equivalence ratio evolution, indeed a leaner combustion leads to a higher quantity of oxygen in the exhaust gases since it is present in a higher quantity than needed to burn all the ammonia in the fresh gases.

By opposition, a richer combustion implies a higher residual ammonia fraction in the exhaust gases. It seems that using a slightly poor mixture is an advantage as observed for an equivalence ratio of 0.96, this ratio is minimizing the residual ammonia and leads to only small quantities of nitrogen monoxide and furthermore to lower quantities of hydrogen. The bulk quenching effect described previously allows once again to explain a lower residual ammonia for near stoichiometric conditions since the flame propagation speed is higher in these conditions and decreases for the richest and leaner sides as presented previously in the laminar burning velocities study.

As already observed for the low pressure flame structure study, leaner flames correspond to higher temperature than stoichiometric and rich ones inducing a higher thermal nitrogen monoxide formation (Table 10.5). Finally, the effect of the equivalence ratio on the hydrogen formation is also the same as the one observed at low pressure, a leaner flame inducing as expected a lower hydrogen content in the exhaust gases.

ϕ	N_2 (%)	H_2O (%)	O_2 (%)	NH_3 (%)	NO (ppm)	NO_2 (ppm)	H_2 (ppm)
0.81	69.55	24.17	4.30	1.70	2721	2	40
0.90	68.84	26.53	2.75	1.68	1716	2	296
0.96	68.42	27.65	1.99	1.62	794	96	2236
1.00	67.83	27.97	1.61	1.72	357	78	8259
1.06	67.39	29.25	0.76	1.83	212	0	7578
1.12	66.62	29.25	0.48	2.05	79	0	15977

Table 10.5: Exhaust gases composition for several equivalence ratios.

The engine performances are very similar for lean and stoichiometric conditions (Table 10.6). The maximum pressure reached in the cylinder (Fig. 10.6) are very similar excepted for the smaller value at an equivalence ratio of 1.12. The optimum effective power and efficiency are reached for an equivalence ratio of 0.96. This confirms the choice suggested by the composition of exhaust gases.

ϕ	0.81	0.90	0.96	1.00	1.06	1.12
$T°_e$ [°C]	468	480	502	520	523	523
Torque [Nm]	52	56	59	59	59	58
RPM	1445	1529	1552	1554	1519	1506
bmep [kPa]	803	865	911	911	904	895
P_e [kW]	7.87	8.97	9.59	9.60	9.32	9.15
η_e	0.42	0.42	0.42	0.41	0.38	0.36
r_{air}	0.67	0.64	0.63	0.63	0.62	0.62
Friction torque [Nm]	14.63	15.26	15.43	15.45	15.18	15.08
fmep [kPa]	226	236	238	238	234	233
imep [kPa]	1029	1100	1149	1149	1139	1128
η_{mec}	0.78	0.79	0.79	0.79	0.79	0.79
η_i	0.54	0.53	0.53	0.51	0.48	0.46
Unburned NH_3 (%)	9.18	8.26	7.65	7.80	7.91	8.51

Table 10.6: Engine performances monitoring for several equivalence ratios.

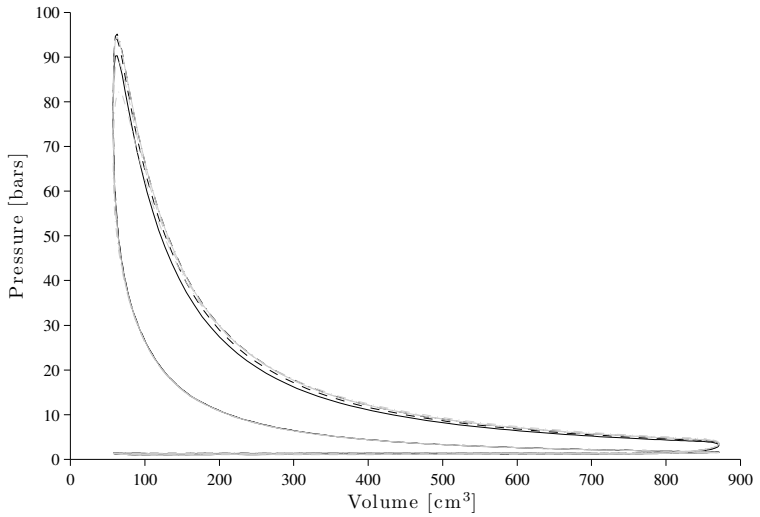

Figure 10.6: Pressure-Volume diagrams for several equivalence ratios: Black line = 0.81; Black dashed line = 0.90; Black dash-dotted line = 0.96; Grey line = 1.00; Grey dashed line = 1.06; Grey dash-dotted line = 1.12

To conclude, the optimum parameters for the use of ammonia in a spark ignition engine based on these experiments are a compression ratio of 15, a spark advance close to 20°-22° and an equivalence ratio of 0.96. The optimum equivalence ratio could be further refined with a specific study of the range $0.95 < \phi < 1$ for practical purposes.

This experimental study has shown that ammonia is a very interesting fuel to study because of its combustion properties very different from those of other conventional fuels. The study of this fuel can help to understand low flame speed combustion phenomenons as those encountered for lean flames. However, further interesting studies should be performed in an optimized engine for such low flame speeds.

Conclusions

In this third part, ammonia combustion in spark ignition engine conditions has been experimentally investigated.

A literature survey has shown that ammonia combustion in spark ignition engines has been well investigated these last years but always with an additive to promote the reaction. The use of ammonia as envisioned in this work (ammonia-air combustion) had thus never been investigated to the best of our knowledge.

The setup used to perform measurements of the engine efficiency and exhaust gases composition while using ammonia as a fuel has been presented. Experiments have been performed on a Varimax test engine. It has been noted that the observed compression ratio on the measuring system was not the actual one. Therefore, in order to determine the actual compression ratio, an experimental determination based on the in-cylinder pressure measurement has been performed [183, 184]. Ammonia was injected as a liquid in the cylinder using a mass flowmeter in series with a needle valve. The fuel flowed through a heat exchanger recovering thereby the heat of the engine water cooling system in order to avoid freezing of components during evaporation. Ammonia went thus out of the exchanger in a gaseous state and was premixed with air before entering the cylinder by the intake valve. Exhaust gases composition has been determined by several methods: gas chromatography for H_2 and N_2O, UV spectroscopy for NH_3, NO and NO_2 and combustion balance for N_2, O_2 and H_2O. Engine performances were monitored thanks to measurements of the in-cylinder pressure, the torque and the rotation speed. A theoretical evalu-

ation of the effective power developed by the spark ignition test engine while using ammonia as a fuel has been performed before experiments leading, for a compression ratio of 15, to a brake mean effective pressure equals to 770 kPa and an effective power around 7.5 kW.

In order to check experimentally the possibility of an ammonia decomposition into hydrogen before combustion, the exhaust gases composition has been analyzed without combustion, i.e. without spark ignition, by driving the Varimax engine with an electrical engine. No hydrogen has been found in the exhaust gases in such conditions, whatever the compression ratio, indicating that even if ammonia can be thermodynamically decomposed, kinetics of this reaction is not fast enough at the conditions prevailing in the engine.

The effects of the compression ratio, the spark timing and the equivalence ratio on the exhaust gases composition and the engine performances have then been analyzed.

When using ammonia as a fuel, one can imagine that the combustion will lead to important nitrogen oxides quantities in the burned gases. However, the nitrogen monoxide concentrations were very low due to relatively low combustion temperatures and there was nearly no formation of nitrogen dioxide or nitrous oxide. However, the fraction of ammonia remaining in the exhaust gases in comparison to the quantity admitted in the fresh gases, around 8 to 10%, was particularly high and could not be explained only by the quenching effects (wall quenching and unburned fresh gases in the cylinder crevices). For conventional fuels, this quantity is indeed around 3%. A hypothesis of bulk quenching has been made to explain this important unburned fraction [185] and a deeper understanding of this phenomenon is an interesting perspective of this SI engine experimental study. The important quantity of hydrogen in the exhaust gases suggested that the residual ammonia was decomposed partially into hydrogen. Indeed, the evolution of the

$$2\ NH_3\ \rightarrow\ 3\ H_2\ +\ N_2$$

equilibrium constant for a wider range of pressures and temperatures indicated that the ammonia decomposition was not surprising for the conditions encountered during combustion.

Based on these results, the optimum running conditions are :

$$\text{Compression ratio} = 15$$
$$\text{Spark timing} = 20°\text{- } 22\ °\text{BTDC}$$
$$\text{Equivalence ratio} = 0.95 < \phi < 1$$

These conditions are the best trade-off to reduce the ammonia ($\approx$ 8% of the quantity admitted in the fresh gases), the nitrogen monoxide ($\approx$ 800 ppm) and the hydrogen ($\approx$ 4000 ppm) contained in the exhaust gases while reaching the best engine performances by reducing the friction losses and increasing the effective efficiency (bmep $\approx$ 850 kPa, $P_e \approx 9$ kW, $\eta_e \approx 0.39$).

This experimental study has shown that ammonia is a very interesting fuel to investigate because of its combustion properties very different from those of other conventional fuels. The study of this fuel can help to understand low flame speed combustion phenomena as those encountered for lean flames. However, further interesting investigations should be performed with an optimized engine for such low flame speeds.

Epilogue

The successful application of ammonia (NH_3) as an alternative transportation fuel should be based on a detailed understanding of its combustion characteristics. The main objective of this thesis was thus the study of the ammonia combustion reaction in several conditions of pressure and temperature :

$$2\ NH_3 + \tfrac{3}{2}\ (O_2 + 3.76\ N_2) \rightarrow \ldots$$

In a first part, ammonia combustion at low pressure has been experimentally and numerically investigated in order to deepen the comprehension of ammonia-air combustion kinetics. Eight $NH_3/H_2/O_2/Ar$ flames close to the stoichiometry with different initial composition or operating conditions have thus been analyzed using a molecular beam mass spectrometer. The effects of the variation of the initial hydrogen percentage, of the equivalence ratio and of the operation pressure have been investigated. Mole fraction profiles have been obtained for the following species : NH_3, NH_2, NO, N_2O, N_2, H_2, H_2O, OH, O_2 and Ar. Numerical simulations of these experimentally analyzed flames have been done with five ammonia combustion kinetic mechanisms available in the literature. Since none of those ones allowed to reproduce satisfactorily the experimental results, an improved mechanism has been established on the basis of the Konnov work [1]. Indeed, for this model, most of the calculated mole fraction profiles agreed with the experimental ones but a significant divergence was observed for N_2O and NH_2. Kinetic parameters of the formation and degradation reactions of these species have been modified to obtain an improved mechanism leading to a better agreement with all the detected species. This improved mechanism has then been reduced in order to fit the requirements of a potential integration in a CFD simulation. The *reduced* ammonia combustion mechanism contains 80 elementary reactions and 19 chemical species. This

reduced ammonia combustion mechanism has been used to simulate the eight analyzed ammonia flames leading to a good agreement between the experimental and the numerical results. This led also to a discussion on the impact of the several parameters (initial hydrogen content, equivalence ratio, pressure) on the species concentrations and on the kinetic reaction pathways. Excluding a slight effect on the NO formation, the initial hydrogen content did not have a significant impact on the composition of the burned gases but an increase of its initial percentage increased the adiabatic burning velocity and therefore moved the position of the flame front closer to the burner surface. Around stoichiometric conditions, a decrease of the equivalence ratio strongly increased the NO formation. Furthermore, at high temperature, the NO formation was favored as it has been noticed in flames where, due to different heat losses, the maximum temperature increased with a decrease of pressure. This implies that the temperature and the equivalence ratio must be well controlled in practical devices such as spark ignition engines.

In a second part, ammonia laminar flame speed has been numerically and experimentally investigated using the tube method. Indeed, ammonia-air laminar burning velocities had not been widely investigated in the past. The influence of the equivalence ratio and the dilution on ammonia laminar flame speed have thus been investigated. The experimental results have been compared to numerical simulation results obtained with the *reduced* ammonia combustion mechanism. An increased dilution led to a global linear decrease of the laminar flame speed. For an equivalence ratio equal to one, the measured ammonia laminar flame speed at the air-dilution was equal to 13.3 $cm.s^{-1}$. This value is significantly lower than the one for traditional fuels for which it is around 40 $cm.s^{-1}$. The effect of an equivalence ratio variation for a constant dilution showed a peak value under stoichiometric conditions and a decrease of the laminar flame speed around this maximum. The numerical results were in agreement with the observed effect and allowed to validate the *reduced* mechanism at atmospheric pressure. Finally, using this mechanism, numerical simulations of ammonia combustion at elevated pressure and temperature conditions such as those encountered in spark ignition engine combustion have been performed. Only the kinetic aspect of the combustion has thus been taken into account. These simulations have shown that the maximum laminar burning velocity is reached in the rich side at an equivalence ratio of 1.1. In the vicinity of sto-

ichiometric mixtures, the variation of the compression ratio has a significant effect on increasing the laminar burning velocity. An increase in compression ratio from 12:1 to 20:1 led to a 130% increase in laminar burning velocity. The adiabatic flame temperature shows a peak at an equivalence ratio around 1.00. It was found that adiabatic flame temperature increases slightly with the compression ratio. The nitrogen monoxide mole fraction reaches a maximum at ϕ = 0.95. Increasing the compression ratio does not have a significant impact on the NO formation for the range of compression ratios investigated in this work because it leads only to a slight increase of the adiabatic temperature and as a consequence to a slight increase of the thermal NO formation. However, a huge decrease of the highest NO concentration is observed for rich mixtures (ϕ = 1.2), with a NO maximum mole fraction of 50% less than the amount of NO found for an equivalence ratio of 0.95.

In a third part, ammonia combustion in spark ignition engine conditions has been experimentally investigated. Ammonia combustion in spark ignition engines had been well investigated these last years but always with an additive to promote the reaction. The use of ammonia as envisioned in this work (ammonia-air combustion) had thus never been investigated to the best of our knowledge. The effects of the compression ratio, the spark timing and the equivalence ratio on the exhaust gases composition and the engine performances have been analyzed. When using ammonia as a fuel, one can imagine that the combustion will lead to important nitrogen oxides quantities in the burned gases. However, the nitrogen monoxide concentration was very low due to relatively low combustion temperatures and there was nearly no formation of nitrogen dioxide or nitrous oxide. However, the fraction of ammonia remaining in the exhaust gases in comparison to the quantity admitted in the fresh gases, around 8 to 10%, was particularly high and could not be explained only by the quenching effects (wall quenching and unburned fresh gases in the cylinder crevices). For conventional fuels, this quantity is indeed around 3%. A hypothesis of bulk quenching has been made to explain this important unburned fraction [185]. The important quantity of hydrogen in the exhaust gases suggested that the residual ammonia was decomposed partially in hydrogen. Indeed, the evolution of the 2 $NH_3 \rightarrow 3\ H_2 + N_2$ equilibrium constant for a wide range of pressures and temperatures indicated that the ammonia decomposition was not surprising for the conditions encountered during combustion.

Based on these results, the optimum spark ignition engine running conditions has been obtained for a compression ratio of 15, a spark timing around 20°- 22 °before top dead center and an equivalence ratio between 0.95 and 1. These conditions are the best trade-off to reduce the ammonia ($\approx$ 8% of the quantity admitted in the fresh gases), the nitrogen monoxide ($\approx$ 800 ppm) and the hydrogen ($\approx$ 4000 ppm) contained in the exhaust gases while reaching the best engine performances by reducing the friction losses and increasing the effective efficiency (bmep $\approx$ 850 kPa, $P_e \approx 9$ kW, $\eta_e \approx 0.39$). This experimental study has shown that ammonia is a very interesting fuel to investigate because of its combustion properties very different from those of other conventional fuels. The study of this fuel can help to understand low flame speed combustion phenomena as those encountered for lean flames.

These conclusions show that ammonia is an interesting fuel to study because of its unusual combustion properties. But they raise also the following question: ***Is ammonia a potential alternative fuel for the future?*** Answer this question is not obvious and some food for thought are given below by describing which properties an alternative fuel should have. Following Olson and Holbrook [186], this can be resumed by the following items.

1. *Produced from any raw energy source (i.e. wind, solar, biomass, coal, nuclear, hydro etc.).* A huge benefit associated with a hypothetical "ideal fuel" would be the ability to produce this fuel from any and all primary energy sources. Over time the primary energy sources of choice will change, but the ideal alternative fuel and, most importantly, the storage and delivery infrastructure associated with the ideal fuel would remain in place. There is a very short list of alternative fuels which can be made from all primary energy sources: hydrogen. But the storage and transportation of hydrogen lead to problems that have already been discussed earlier in this thesis. The use of ammonia as a hydrogen vector is thus a potential alternative. As discussed in the foreword of this thesis, it takes a relatively small amount of additional energy to produce NH_3 once hydrogen has been produced via electrolysis or other means.

2. *Cost effective.* The ideal fuel must be cost effective and not become an unaffordable luxury to the majority of the world's population. Energy costs must not inhibit reasonable economic development and industrial production. The cost of energy influences the cost of every product produced and

delivered. The opportunity to produce this fuel from any raw energy source helps to maintain an affordable price.

3. *Significant and practical storage and delivery systems already in place.* The ideal fuel would make use of existing fuel delivery infrastructure. Hydrogen in the form of NH_3 is annually in the top three chemicals in terms of volume transported worldwide. It is shipped by truck, rail, trans-oceanic ship and barge. More importantly, since ammonia can be shipped and stored in mild steel pipelines, any natural gas or petroleum pipeline could be cost effectively converted to carry NH_3.

4. *Environmentally friendly (No Carbon, Low Emissions).* The ideal fuel would not produce any greenhouse gas emissions nor air and water pollution of any type. Environmental issues are becoming increasingly important as global warming concerns become increasingly expressed. The use of hydrogen as a fuel becomes the standard by which all other alternative fuels are measured. As presented in this thesis, a huge effort has to be made if ammonia is used to avoid ammonia emissions in the exhaust gases. However, NH_3 has an ozone depletion potential of zero and a global warming potential of zero.

5. *The ability to be used in any prime mover (i.e. diesel engines, fuel cells, SI engines, gas turbines, etc.).* The ability to use one fuel in all types of combustion engines, gas turbines, burners and directly in efficient fuel cells is an undeniable advantage. Even if ammonia seems to be a potential candidates for several types of combustion engines, further investigations are needed to confirm this hypothesis.

6. *A proven, acceptable safety history.* This is maybe the weakness of ammonia, not really because of safety issues but mainly because of ideas people have on ammonia. Current usage of ammonia is limited to industrial applications and in rural farming communities. Would broader usage of ammonia in high density urban environments be accepted by society? As noted above, ammonia odor is detected at concentrations as low as 5 ppm. Small leaks, spills, etc... in and around filling stations should be expected and these could have a cumulative effect on airborn ammonia levels in the immediate vicinity. Similarly, high traffic concentrations in downtown areas and on traffic-clogged urban freeways might also result in odor-detectable concentration levels in the air if ammonia was used for onboard storage.

> Although the low detectability level may be cited as a positive safety factor in detecting leaks, a pervasive odor in the vicinity of high use areas may be against the perception of a "clean" fuel. However, ammonia used as a fertilizer and refrigerant has an excellent, decades-long safety record. Making ammonia "acceptably safe" from a statistical standpoint is an easily solved engineering design issue. There are risks associated with the use of ammonia as a fuel however all fuels have inherent dangers associated with their use.

This thesis has brought some learnings and ideas on the potential use of ammonia as a fuel for spark ignition engines, but there is still work to do. First of all, a more complete energetic balance should be performed in order to confirm or not the real possibility of the use of ammonia as an alternative fuel. This balance should be completed by a more technical approach taking into account transport, distribution and storage networks. Furthermore, several investigations should be performed to improve engine performances and decrease residual ammonia in the burned gases. First of all, an engine optimized for low speed flames should be used. Then the impact of the spark energy should be investigated. Finally, the potential bulk quenching phenomenon observed experimentally should be deeper understood, for example by investigating ammonia flame speeds in a tube as presented in the second part of this work but with a compression before combustion and an expansion during this one as in Smith et al. [185]. At the same time, the laminar flame speed of ammonia should be determined under higher pressures for example by using a closed vessel. This could help to understand the low speed flame phenomenons observed in the engine. Finally, numerical simulations should be performed to reproduce ammonia combustion in the engine. The *reduced* ammonia combustion mechanism elaborated in this thesis should be integrated in a CFD code in order to perform these simulations.

Bibliography

[1] A. Konnov, "Development and validation of a detailed reaction mechanism for the combustion of small hydrocarbons," *28-th Symposium (Int.) on Combustion*, p. Abstr. Symp. Pap. 317, Edinburgh, 2000.

[2] G. Kalghatgi, "Sustainable automotive fuels for the future," in *Third European combustion meeting*, (Chania, Greece), 2007.

[3] J. McKee and H. Wolf, *Water quality criteria*, vol. 3A. Sacramento, CA: State Water Quality Control Board, 2nd ed., 1963.

[4] R. Train, *Quality criteria for water*. Washington, DC: U.S. Environmental Protection Agency, 1976.

[5] G. Thomas and G. Parks, "Potential roles of ammonia in a hydrogen economy," *U.S. Department of Energy*, 2006.

[6] Air Liquide, "Air liquide encyclopedia.", *www.encyclopedia.airliquide.com*.

[7] R. Luebs and A. Laag, "Ammonia and related gases emanating from a large dairy area," *Calif. Agric.*, vol. 27, no. 2, p. 10, 1973.

[8] C. Delwiche, *Chemistry in the environment*, ch. The nitrogen cycle. San Francisco, CA: C.L. Hamilton, 1973.

[9] S. Kimball and K. Salazar, "Mineral commodity summaries," tech. rep., U.S. Department of the Interior and U.S. Geological survey, 2009.

[10] A. Standen, *Kirk-Othmer encyclopedia of chemical technology*, vol. 1. New York, NY: Interscience Publishers, 2nd ed., 1969.

[11] G. Taplin, S. Chopra, R. Yanda, and D. Elam, "Radionuclide lung-imaging procedures in the assessment of injury due to ammonia inhalation," *Chest*, vol. 69, no. 5, p. 582, 1976.

[12] P. van Blarigan, "Advanced internal combustion engine research," *Proceeding of the 2000 DOE hydrogen program review*, vol. NREL/CP-570-28890, 2000.

[13] J. Martin and J. Vanhemelryck, "Les combustibles et carburants d origine agricole," *Rapport dans le cadre de la convention de la Region Wallonne*, Universite catholique de Louvain, Belgium, 1992.

[14] European Fertilizer Manufacturers Association, "Production of ammonia," *Best Available Techniques for Pollution Prevention and Control in the European Fertilizer Industry*, 2000.

[15] New York State Energy Research and Development Authority, "Hydrogen fact sheet," *www.getenergysmart.org/files/hydrogeneducation 6hydrogen-productionsteammethanereforming.pdf*, 04/08/2011.

[16] F. Joseck, "Distributed hydrogen production via steam methane reforming," *www.hydrogen.energy.gov/docs/cs_distr_steam_methane_reform.doc*, 04/08/2011.

[17] U. Bossel, B. Eliasson, and G. Taylor, "The future of the hydrogen economy: Bright or Bleak," *Journal of KONES Internal Combustion Engines*, vol. 11, no. 1-2, 2004.

[18] H. Li, H. Hong, H. Jin, and R. Cai, "Analysis of a feasible polygeneration system for power and methanol production taking natural gas and biomass as materials," *Applied Energy*, vol. 87, pp. 2846–2853, 2010.

[19] D. Barranon, "Methanol and Hydrogen Production, Energy and Cost Analysis," Master's thesis, Lulea University of Technology, Sweden, 2006.

[20] C. Fenimore and G. Jones, "Oxidation of ammonia in flames," *Journal of Physical Chemistry*, vol. 65, no. 2, pp. 298–303, 1961.

[21] D. Maclean and H. Wagner, "The structure of the reaction zones of ammonia-oxygen and hydrazine decomposition flames.," *Eleventh Symposium (International) on Combustion/ The Combustion Institute*, pp. 871–878, 1967.

[22] D. Pratt and E. Starkman, "High-temperature kinetics of ammonia-air combustion," *Twelfth Symposium (International) on Combustion/ The Combustion Institute*, pp. 891–899, 1969.

[23] C. Fisher, "A study of rich ammonia/oxygen/nitrogen flames," *Combustion and Flame*, vol. 30, pp. 143–149, 1977.

[24] C. Dasch and R. Blint, "A mechanistic and experimental study of ammonia flames," *Combustion Science and Technology*, vol. 41, pp. 223–244, 1984.

[25] J. Bian, J. Vandooren, and P. van Tiggelen, "Experimental study of the structure of an ammonia-oxygen flame," *Twenty-first Symposium (International) on Combustion/ The Combustion Institute*, pp. 953–963, 1986.

[26] J. Bian, J. Vandooren, and P. van Tiggelen, "Experimental study of the formation of nitrous and nitric oxides in H_2-O_2-Ar flames seeded with no and/or NH_3," *Twenty-Third Symposium (International) on Combustion/ The Combustion Institute*, pp. 379–386, 1990.

[27] J. Bian, J. Vandooren, and P. van Tiggelen, "Etude expérimentale de la structure d'une flamme NH_3-NO-Ar," *Bulletin des Societes Chimiques Belges*, vol. 99, no. 7, pp. 467–472, 1990.

[28] J. Vandooren, J. Bian, and P. van Tiggelen, "Comparison of experimental and calculated structures of an ammonia-nitric oxide flame. importance of the NH_2+NO reaction," *Combustion and Flame*, vol. 98, pp. 402–410, 1994.

[29] J. Vandooren, "Comparison of the experimental structure of an ammonia seeded rich-hydrogen-oxygen-argon flame with the calculated ones along several reaction mechanisms," *Combustion Science and Technology*, vol. 84, pp. 335–344, 1992.

[30] W. Kaskan and D. Hughes, "Mechanism of decay of ammonia in flame gases from an NH_3/O_2 flame," *Combustion and Flame*, vol. 20, pp. 381–388, 1973.

[31] J. A. Miller, M. D. Smooke, R. M. Green, and R. J. Kee, "Kinetic modeling of the oxidation of ammonia in flames," *Combustion Science and Technology*, vol. 34, pp. 149–176, 1983.

[32] Y. Zeldovich, "The oxidation of nitrogen in combustion and explosions," *Acta Phys. Chim. USSR*, vol. 21, pp. 577–628, 1946.

[33] A. Dean, M. Chou, and D. Stern, "Kinetics of rich ammonia flames," *International Journal of Chemical Kinetics*, vol. 16, pp. 633–653, 1984.

[34] S. Salimian, R. Hanson, and C. Kruger, "Ammonia oxidation in shock-heated NH_3-N_2O-Ar mixtures," *Combustion and Flame*, vol. 56, pp. 83–95, 1984.

[35] J. Miller and C. Bowman, "Mechanism and modelling of nitrogen chemistry in combustion," *Prog. Energy Combust. Sci.*, vol. 15, pp. 287–338, 1989.

[36] D. F. Davidson, K. Kohse-Hoinghaus, A. Y. Chang, and R. K. Hanson, "A pyrolysis mechanism for ammonia," *Int. J. Chem. Kinet.*, vol. 22, pp. 513–535, 1990.

[37] J. Mertens, A. Chang, R. Hanson, and C. Bowman, "Reaction kinetics of NH in the shock tube pyrolysis of HNCO," *Int. J. Chem. Kinet.*, vol. 21, pp. 1049–1067, 1989.

[38] D. Davidson and R. Hanson, "High temperature reaction rate coefficients derived from N-atom aras measurements and excimer photolysis of NO," *Int. J. Chem. Kinet.*, vol. 22, pp. 843–861, 1990.

[39] P. Dransfeld, W. Hack, H. Kurzke, F. Temps, and H. Wagner, "Direct studies of elementary reactions of NH_2-radicals in the gas phase," *Twentieth Symposium (International) on Combustion/ The Combustion Institute*, vol. 20, pp. 655–663, 1984.

[40] J. Vandooren, O. Sarkisov, V. Balakhnin, and P. van Tiggelen, "Discussion on the formation and removal of NO_x in ammonia flames," *Chemical Physics Letters*, vol. 184, no. 4, pp. 294–300, 1991.

[41] S. M. Lindstedt RP, Lockwood FC, "Detailed kinetic modeling of chemistry and temperature effects on ammonia oxidation," *Combustion Science and Technology*, vol. 99, pp. 253–276, 1994.

[42] G. Smith, D. Golden, M. Frenklach, N. Moriarty, B. Eiteneer, M. Goldenberg, C. Bowman, R. Hanson, S. Song, J. W.C. Gardiner, V. Lissianski, and Z. Qin, "Gri-mech 3.0," *www.me.berkeley.edu/gri-mech/*, 1999.

[43] The combustion division of the Center for Energy Research at the University of California, "San diego," *www.maeweb.ucsd.edu/combustion/cermech/index.html*, 2005.

[44] A. Bendtsena, P. Glarborg, and K. Johansen, "Low temperature oxidation of methane: the influence of nitrogen oxides," *Combustion Science and Technology*, vol. 151, pp. 31–71, 2000.

[45] P. Glarborg, P. Kristensen, and K. Johansen, "Branching fraction of the NH_2 + NO reaction between 1210 and 1370k," *Journal of Physical Chemistry A*, vol. 101, pp. 3741–3745, 1997.

[46] O. Skreiberg, P. Kilpinen, and P. Glarborg, "Ammonia chemistry below 1400k under fuel-rich conditions in a flow reactor.," *Combustion and Flame*, vol. 136, pp. 501–518, 2004.

[47] A. Konnov and J. Deruyck, "Kinetic modeling of the thermal decomposition of ammonia," *Combustion Science and Technology*, vol. 152, pp. 23–37, 2000.

[48] V. Lozovsky, M. Ioffe, and O. Sarkisov, "On the reaction of the NH_2 radical with oxygen," *Chemical Physics Letters*, vol. 110, no. 6, pp. 651–654, 1984.

[49] C. Melius and J. Binkley, "Energetics of the reaction pathways for NH_2+NO $\rightarrow$ products and NH+NO $\rightarrow$ products," *Twentieth Symposium (International) on Combustion/ The Combustion Institute*, vol. 20, pp. 575–583, 1984.

[50] M. Simonson, K. Bradley, and G. Schatz, "RRKM studies of product branching in the NH+NO reaction," *Chemical Physics Letters*, vol. 244, pp. 19–26, 1995.

[51] L. Baker and S. Su, "An ab inition molecular orbital study of the reaction NH_2 + NO = H_2 + N_2O," *Chemical Physics*, vol. 228, pp. 9–16, 1998.

[52] M. Zabielski and D. Seery, "High temperature measurements of the rate of the reaction of OH with NH_3," *International Journal of Chemical Kinetics*, vol. 17, pp. 1191–1199, 1985.

[53] S. Salimian, R. Hanson, and C. Kruger, "High temperature study of the reactions of O and OH with NH_3," *International Journal of Chemical Kinetics*, vol. 16, pp. 725–739, 1984.

[54] J. Harrison, A. Whyte, and L. Phillips, "Kinetics of reactions of NH with NO and NO_2," *Chemical Physics Letters*, vol. 129, no. 4, pp. 346–352, 1986.

[55] J. Bozzelli and A. Dean, "Energized complex quantum rice-ramsperger-kassel analysis on reactions of amidogen with hydroperoxo, oxygen and oxygen atoms," *Journal of Physical Chemistry*, vol. 93, no. 3, pp. 1058–1065, 1989.

[56] T. Ko, P. Marshall, and A. Fontijn, "Rate coefficients for the H+NH_3 reaction over a wide temperature range," *Journal of Physical Chemistry*, vol. 94, pp. 1401–1404, 1990.

[57] J. Miller and C. Melius, "The reactions of imidogen with nitric oxide and molecular oxygen," *Proceedings of the Combustion Institute*, vol. 24, pp. 719–726, 1992.

[58] N. Stothard, R. Humpfer, and H. Grotheer, "The multichannel reaction NH_2 + NH_2 at ambient temperature and low pressures," *Chemical Physics Letters*, vol. 240, pp. 474–480, 1995.

[59] R. Sumathi, D. Sengupta, and M. Nguyen, "Theoretical study of the H_2 + NO and related reactions of [H_2NO] isomers," *Journal of Physical Chemistry A*, vol. 102, no. 18, pp. 3175–3183, 1998.

[60] S. Cheskis, V. Nadtochenko, and O. Sarkisov, "Study of the HNO+HNO and HNO+NO reactions by intracavity laser spectroscopy," *International Journal of Chemical Kinetics*, vol. 13, pp. 1041–1050, 1981.

[61] H. Nguyen, S. Zhang, J. Peeters, T. Truong, and M. Nguyen, "Direct ab initio dynamics studies of the reactions of HNO with H and OH radicals," *Chemical Physics Letters*, vol. 388, pp. 94–99, 2004.

[62] M. Allen, R. Yetter, and F. Dryer, "Hydrogen/nitrous oxide kinetics – implications of the N_xH_y species.," *Combustion and Flame*, vol. 112, no. 3, pp. 302–311, 1998.

[63] A. A. Konnov and J. De Ruyck, "Upper limit rate constants for the reactions of NH and NH_2 radicals with N_2O derived from the kinetic modeling of hydrogen oxidation by nitrous oxide," *Mediterranean Combustion Symposium*, vol. Antalya, Turkey, pp. 679 – 690, 1999.

[64] A. Konnov and J. Deruyck, "Kinetic modeling of nitrogen oxides decomposition at flame temperatures," *Combustion Science and Technology*, vol. 149, pp. 53–78, 1999.

[65] J. Guibet, *Carburants et moteurs*, vol. 2. Institut francais du petrole, 1997.

[66] J. Vandooren, M. Branch, and P. van Tiggelen, "Comparisons of the structure of stoichiometric $CH_4/N_2O/Ar$ and $CH_4/O_2/Ar$ flames by molecular beam sampling and mass spectrometric analysis," *Combustion and Flame*, vol. 90, pp. 247–258, 9 1992.

[67] H. M. Rosenstock, K. Draxl, B. Steiner, and J. T. Herron, "Energetics of gaseous ions," *Journal of Physical and Chemical Reference Data*, vol. 6, no. Supplement 1, 1977.

[68] C. Duynslaegher, H. Jeanmart, and J. Vandooren, "Kinetics in ammonia-containing premixed flames and a preliminary investigation of their use as fuel in spark ignition engines," *Combustion Science and Technology*, vol. 181, no. 8, pp. 1092–1106, 2009.

[69] J. Vandooren, J. Peeters, and P. van Tiggelen, "Rate constant of the elementary reaction of carbon monoxide with hydroxyl radical," *Symposium (International) on Combustion*, vol. 15, no. 1, pp. 745 – 753, 1975.

[70] J. Vandooren, F. N. da Cruz, and P. van Tiggelen, "The inhibiting effect of CF_3H on the structure of a stoichiometric $H_2/CO/O_2/Ar$ flame," *Symposium (International) on Combustion*, vol. 22, no. 1, pp. 1587 – 1595, 1989.

[71] G. Mahnen, *Contribution à l'étude du mécanisme des déflagrations*. PhD thesis, Université Catholique de Louvain, Belgium, 1973.

[72] J. Kent, "A noncatalytic coating for platinum-rhodium thermocouples," *Combustion and Flame*, vol. 14, pp. 279–284, 1970.

[73] R. Ancia, J. Vandooren, and P. van Tiggelen, "Experimental study of the structure of rich ethane flames," *Twenty-Sixth Symposium (International) on Combustion*, vol. 1, pp. 1009–1016, 1996.

[74] Rotexo, "Cosilab, the combustion simulation laboratory, version 3.1," *www.rotexo.com*, 2007.

[75] T. Poinsot and D. Veynante, *Theoritical and Numerical Combustion*. Edwards, 2nd ed., 2005.

[76] E. Oran and J. Boris, "Detailed modelling of combustion systems," *Prog. Energy Combust. Sci.*, vol. 7, pp. 1–72, 1981.

[77] R. Kee, J. Warnatz, and J. Miller, "A fortran computer code package for the evaluation of gas-phase viscosities, conductivities, and diffusion coefficients," Tech. Rep. SAND-8209, Sandia National Labs., 1983.

[78] J. Hirschfelder and C. Curtiss, "Theory of propagation of flames. part i: General equations.," *Third Symposium on Combustion and Flame and Explosion Phenomena, Baltimore*, pp. 121–127, 1949.

[79] P. Lindemann, P. Arrhenius, D. Langmuir, D. Dhar, P. Perrin, and P. Lewis, "Discussion on the radiation theory of chemical action," *Trans. Faraday Soc.*, vol. 17, pp. 598–606, 1922.

[80] C. Hinshelwood, "On the theory of unimolecular reactions," *Proc. Roy. Soc. (London) Ser. A*, vol. 113, no. 763, pp. 230–233, 1926.

[81] J. Troe, "Predictive possibilities of unimolecular rate theory," *Journal of Physical Chemistry*, vol. 83, no. 1, pp. 114–126, 1979.

[82] J. Troe, "Theory of thermal unimolecular reactions in the fall-off range. i. strong collision rate constants.," *Berichte der Bunsengesellschaft fur physikalische Chemie*, vol. 87, no. 2, pp. 161–169, 1983.

[83] R. Gilbert, K. Luther, and J. Troe, "Theory of thermal unimolecular reactions in the fall-off range. ii. weak collision rate constants.," *Berichte der Bunsengesellschaft fur physikalische Chemie*, vol. 87, no. 2, pp. 169–177, 1983.

[84] G. Dixon-Lewis, *Combustion Chemistry*, ch. 2, Computer Modeling of Combustion Reactions in Flowing Systems with Transport, pp. 21–125. New York: Springer, 1984.

[85] N. Peters and J. Warnatz, *Numerical Methods in Flame Propagation*, ch. Influence of Transport Models and Boundary Conditions on Flame Structure, pp. 87–111. Braunschweig/Wiesbaden: Vieweg Verlag, 1982.

[86] R. Kee, M. Coltrin, and P. Glarbourg, "Chemically reacting flow," *Wiley-Interscience*, 2003.

[87] V. Detilleux, *Experimental and kinetic modeling investigation of benzene and toluene combustion in premixed, laminar and one-dimensional flames*. PhD thesis, Universite Catholique de Louvain, Belgium, 2011.

[88] C. Duynslaegher, "Etude des flammes a base d'ammoniac et de leur utilisation potentielle en tant que combustible dans les moteurs," Master's thesis, Universite Catholique de Louvain, Belgium, 2006.

[89] J. Bian, *Mecanisme de formation et de disparition des oxydes d'azote dans les flammes*. PhD thesis, Universite Catholique de Louvain, Belgium, 1990.

[90] C. Westbrook, "Numerical modeling of flame inhibition by CF_3Br," *Combustion Science and Technology*, vol. 34, no. 1, pp. 201–225, 1983.

[91] J. C. Hewson and M. Bollig, "Reduced mechanisms for NO_x emissions from hydrocarbon diffusion flames," *Twenty-Sixth Symposium (International) on Combustion/The Combustion Institute*, vol. 26, pp. 2171–2179, Pittsburgh, Pennsylvania, 1996.

[92] W. DeMore, S. Sander, D. Golden, R. Hampson, M. Kurylo, C. Howard, A. Ravishankara, C. Kolb, and M. Molina, "Chemical kinetics and photochemical data for use in stratospheric modeling. evaluation number 12," *JPL Publication 97-4*, pp. 1–266, 1997.

[93] H. Lillich, A. Schuck, H. Volpp, and J. Wolfrum, "Kinetics studies of the reactions NH+NO and NH+O_2 at elevated temperatures," *Proceedings of the Combustion Institute*, vol. 25, pp. 993–1001, 1994.

[94] W. Hack, H. Wagner, and A. Zaspykin, "Elementary reactions of NH with N, O and NO," *Berichte der Bunsengesellschaft fur physikalische Chemie*, vol. 98, pp. 156–164, 1994.

[95] K. Yokoyama, Y. Sakane, and T. Fueno, "Formations of OH in the reaction of NH with NO in incident shock waves," *Bull. Chem. Soc. Jpn.*, vol. 64, pp. 1738–1742, 1991.

[96] S. Okada, A. Tezaki, A. Miyoshi, and H. Matsui, "Product branching fractions in the reactions of NH with NO," *Journal of Chemical Physics*, vol. 101, pp. 9582–9588, 1994.

[97] H. Szichman, M. Baer, H. Volpp, and J. Wolfrum, "Comparison between experimental and three dimensional quantum mechanical rate constants for the NH(d) + NO reactions," *Journal of Physical Chemistry A*, vol. 102, pp. 10455–10459, 1998.

[98] H. Szichman and M. Baer, "A three dimensional quantum mechanical study of the NH+NO reactions," *Journal of Chemical Physics*, vol. 105, pp. 10380–10386, 1996.

[99] J. Bozzelli, A. Chang, and A. Dean, "Analysis of the reactions H + N_2O and NH + NO : Pathways and rate constants over a wide range of temperature and pressure," *25th Symp. (Int.) on Combustion/The Combustion Institute*, vol. 25, pp. 965–974, 1994.

[100] W. Tsang and J. Herron, "Chemical kinetic data base for propellant combustion. i. reactions involving NO, NO_2, HNO, HNO_2, HCN and N_2O," *Journal of Physical and Chemical Reference Data*, vol. 20, pp. 609–663, 1991.

[101] Y. Hidaka, H. Takuma, and M. Suga, "Shock tube studies of N_2O decomposition and N_2O-H_2 reaction," *Bull. Chem. Soc. Jpn.*, vol. 58, pp. 2911–2916, 1985.

[102] R. Hanson and S. Salimian, *Combustion Chemistry*, ch. Survey of rate constants in the N/H/O system. New York: Springer-Verlag, 1984.

[103] H. Henrici and S. Bauer, "Kinetics of the nitrous oxide-hydrogen reaction," *Journal of Chemical Physics*, vol. 50, pp. 1333–1342, 1969.

[104] V. Balakhnine, J. Vandooren, and P. van Tiggelen, "Reaction mechanism and rate constants in lean hydrogen-nitrous oxide flames," *Combustion and Flame*, vol. 28, pp. 165–173, 1977.

[105] G. Dixon-Lewis, M. Sutton, and A. Williams, "Some reactions of hydrogen atoms and simple radicals at high temperatures," *Proceedings of the Combustion Institute*, vol. 10, pp. 495–502, 1965.

[106] M. Rohrig and H. Wagner, "The reactions of NH(x3s-) with the water gas components CO_2, H_2O, and H_2," *25th Symp. (Int.) on Combustion/The Combustion Institute*, vol. 25, pp. 975–981, 1994.

[107] A. A. Konnov and J. Deruyck, "Kinetic modeling of the decomposition and flames of hydrazine," *Combustion and Flame*, vol. 124, pp. 106–126, 2001.

[108] D. Linder, X. Duan, and M. Page, "Ab initio variational transition state theory calculations for the H + NH_2 = H_2 + NH hydrogen abstraction reaction on the triplet potential energy surface," *Journal of Physical Chemistry*, vol. 99, pp. 11458–11463, 1995.

[109] J. Dove and W. Nip, "A shock tube study of ammonia pyrolysis," *Canadian Journal of Chemistry*, vol. 57, pp. 689–701, 1979.

[110] M. Yumura and T. Asaba, "Rate constants of chemical reactions in the high temperature pyrolysis of ammonia," *Eighteenth Symposium (International) on Combustion/ The Combustion Institute*, pp. 863–872, 1981.

[111] N. Cohen and K. R. Westberg, "Chemical kinetic data sheets for high-temperature chemical reactions," *Journal of Physical and Chemical Reference Data*, vol. 12, pp. 531–590, 1983.

[112] J. Warnatz, *Rate coefficients in the C/H/O system combustion chemistry.* New York: Springer-Verlag, 1984.

[113] D. Baulch, C. Cobos, R. Cox, C. Esser, P. Frank, T. Just, M. Pilling, J. Troe, R. Walker, and W. J., "Evaluated kinetic data for combustion modelling," *Journal of Physical and Chemical Reference Data*, vol. 21, pp. 411–734, 1992.

[114] D. Baulch, C. Cobos, R. Cox, P. Frank, G. Hayman, T. Just, J. Kerr, T. Murrells, M. Pilling, J. Troe, R. Walker, and W. J., "Summary table of evaluated kinetic data for combustion modelling: Supplement 1.," *Combustion and Flame*, vol. 98, pp. 59–79, 1994.

[115] C. J. Cobos, H. Hippler, and J. Troe, "High-pressure falloff curves and specific rate constants for the reactions H + O_2 = HO_2 = HO + O," *Journal of Physical Chemistry*, vol. 89, pp. 342–349, 1985.

[116] R. Atkinson, D. Baulch, R. Cox, R. Hampson, J. Kerr, M. Rossi, and J. Troe, "Evaluated kinetic and photochemical data for atmospheric chemistry: supplement vi. IUPAC subcommittee on gas kinetic data evaluation for atmospheric chemistry," *Journal of Physical and Chemical Reference Data*, vol. 26, pp. 1329–1499., 1997.

[117] N. Cohen and K. Westberg, "Chemical kinetic data sheets for high-temperature reactions. part ii," *Journal of Physical and Chemical Reference Data*, vol. 20, pp. 1211–1311, 1991.

[118] M. Rohrig, H.-J. Romming, and H. Wagner, "A direct measurement of the reaction NH_3 + NH = $2NH_2$," *Berichte der Bunsengesellschaft fur physikalische Chemie*, vol. 98, pp. 1332–1334, 1994.

[119] P. Dransfeld and H. Wagner, "Investigation of the gas phase reaction N+NH_2=N_2+2H at room temperature," *Z. Phys. Chem. (Munich)*, vol. 153, pp. 89–97, 1987.

[120] R. Sumathi and S. D. Peyerimhoff, "A quantum statistical analysis of the rate constant for the HO_2 + NH_2 reaction," *Chemical Physics Letters*, vol. 263, pp. 742–748, 1996.

[121] G. Hennig, M. Klatt, B. Spindler, and H. Wagner, "The reaction of NH_2 + O_2 at high temperatures," *Berichte der Bunsengesellschaft fur physikalische Chemie*, vol. 99, pp. 651–657, 1995.

[122] J. A. Miller and P. Glarborg, "Modeling the thermal de-nox process: Closing in on a final solution," *Int. J. Chem. Kinet.*, vol. 31, pp. 757–765, 1999.

[123] J. Park and M. C. Lin, "A mass spectrometric study of the NH_2 + NO_2 reaction," *Journal of Physical Chemistry A*, vol. 101, pp. 2643–2647, 1997.

[124] J. Miller, R. Mitchell, M. Smooke, and R. Kee, "Toward a comprehensive chemical kinetic mechanism for the oxidation of acetylene: Comparison of model predictions with results from flame and shock tube experiments,"

in *19th Symp. (Int.) on Combustion* (T. C. Institute, ed.), pp. 181–196, 1982.

[125] H. Romming and H. Wagner, "A kinetic study of the reactions of NH(x3 sigma) with O_2 and NO in the temperature range from 1200 to 2200 k," *26th Symp. (Int.) on Combustion/The Combustion Institute*, vol. 26, pp. 559–566, 1996.

[126] M. Rohrig, E. Petersen, D. Davidson, and R. Hanson, "The pressure dependence of the thermal decomposition of N_2O," *Int. J. Chem. Kinet.*, vol. 28, pp. 599–608, 1996.

[127] A. Borisov, G. Skachkov, and A. Oguryaev, "Ignition of mixtures N_2O + NO at high temperatures," *Kinetics and Catalysis*, vol. 14, pp. 294–300, 1973.

[128] T. Rutar, J. Kramlich, P. Malte, and P. Glarborg, "Experimental and modeling study of N_2O destruction by reburning," *Combustion and Flame*, vol. 107, pp. 453–463, 1996.

[129] T. Ko and A. Fontijn, "High-temperature photochemistry kinetics study of the reaction H + NO_2 = OH + NO from 296 to 760 K," *Journal of Physical Chemistry*, vol. 95, pp. 3984–3987, 1991.

[130] M. Soto and M. Page, "Ab initio variational transition-state-theory reaction-rate calculations for the gas-phase reaction H + HNO = H_2 + NO," *J. Chem. Phys*, vol. 97, pp. 7287–7296, 1992.

[131] M. Soto, M. Page, and M. McKee, "Theoretical study of the reaction of OH with HNO," *Chemical Physics*, vol. 153, pp. 415–426, 1991.

[132] T. Etzkorn, S. Muris, J. Wolfrum, C. Dembny, H. Bockhorn, P. Nelson, A. Attia-Shahin, and J. Warnatz, "Destruction and formation of NO in low pressure stoichiometric CH_4/O_2 flames," *24th Symp. (Int.) on Combustion/The Combustion Institute*, vol. 24, pp. 925–932, 1992.

[133] J. Bozzelli and A. Dean, "O + nnh : A possible new route for NO_x formation in flames," *Int. J. Chem. Kinet.*, vol. 27, pp. 1097–1109, 1995.

[134] A. A. Konnov and J. De Ruyck, "Temperature dependent rate constant for the reaction NNH + O = NH + NO," *Combustion and Flame*, vol. 125, no. 4, pp. 1258–1264, 2001.

[135] P. Glarborg, J. Miller, and R. Kee, "Kinetic modelling and sensitivity analysis of nitrogen oxide formation in well-stirred reactors," *Combustion and Flame*, vol. 65, pp. 177–202, 1986.

[136] D. Linder, X. Duan, and M. Page, "Thermal rate constants for R+N_2H_2 = RH+N_2H (R=H, OH, NH_2) determined from multireference configuration interaction and variational transition state theory calculations," *J. Chem. Phys*, vol. 104, pp. 6298–6306, 1996.

[137] G. Andrews and D. Bradley, "Determination of burning velocities: A critical review," *Combustion and Flame*, vol. 18, pp. 133–153, 1972.

[138] J. Powling, "A new method for the determination of low burning velocities and limits of inflammability," *Fuel*, vol. 28, pp. 25–28, 1949.

[139] J. Chase and F. Weinberg, "The acetylene decomposition flame and the deduction of reaction mechanism from "global" flame kinetics," *Proc. Roy. Soc. (London) Ser. A*, vol. 275, pp. 411–430, 1963.

[140] D. Spalding and J. Botha, "The laminar flame speed of propane/air mixtures with heat extraction from the flame," *Proc. R. Soc. Lond. A*, vol. 225, pp. 71–96, 1954.

[141] J. Singer, "Burning velocity measurements on slot burns; comparison with cylindrical burner determination," in *Fourth Symposium (International) on Combustion* (Williams and Wilkins, eds.), (Baltimore), pp. 352–358, 1953.

[142] J. Singer, J. Grumer, and E. Cook, "Burning velocities by the bunsen-burner method i. hydrocarbon-oxygen mixtures at one atmosphere. ii. hydrocarbon-air mixtures at subatmospheric pressures.," in *Proc. Gas Dynamics Symposium on Aerothermochemistry* (N. University, ed.), (Evanston, Illinois), pp. 139–150, 1956.

[143] R. Fristrom and A. Westenberg, *Flame Structure*, vol. 129-131. New York: McGraw-Hill, 1st ed., 1965.

[144] E. Mallard and H. Le Chatelier, "Sur les temperatures de combustion," *Ann. Mines*, vol. Sec. IV, no. 8, pp. 261–274, 1883.

[145] V. Mikhelson, "Physics of combustion and explosion," *Israel Program for Scientific Translations*, pp. 138–140, 1962.

[146] H. Coward and F. Hartwell, "Studies in the mechanism of flame movement—part ii.," *Journal of chemical Society*, pp. 2676–2684, 1932.

[147] L. Landau, "On the theory of slow combustion," *Acta Phys. Chim. USSR*, vol. 19, pp. 77–85, 1944.

[148] W. Jost, *Explosion and Combustion Processes in Gases.* New York: McGraw-Hill, 1st ed., 1946.

[149] B. Lewis and G. von Elbe, *Combustion, Flames and Explosion of Gases.* New York: Academic Press, 2nd ed., 1961.

[150] M. Uberoi, "Flowfield of a flame in a channel," *Phys. Fluids*, vol. 2, pp. 72–78, 1959.

[151] M. Uberoi, "Flow fields of flame propagating in channels based on the source sheet approximation," *Phys. Fluids*, vol. 6, pp. 1104–1109, 1963.

[152] T. Maxworthy, "Flame propagation in tubes," *Phys. Fluids*, vol. 5, pp. 407–417, 1962.

[153] P. Ausloos and A. van Tiggelen, "Vitesse de propagation de la flamme dans les mélanges gazeux contenant de l'ammoniac," *Bulletin des Societes Chimiques Belges*, vol. 60, pp. 433–445, 1951.

[154] R. Murray and A. Hall, "Flame speeds in hydrazine vapor and in mixtures of hydrazine and ammonia with oxygen," *Trans. Faraday Soc.*, vol. 47, pp. 743–751, 1951.

[155] J. V. Wonterghem and A. van Tiggelen, "Energie d'activation dans la propagation de la flamme," *Bulletin des Societes Chimiques Belges*, vol. 64, pp. 99–121, 1955.

[156] D. Andrews and P. Gray, "Combustion of ammonia supported by oxygen, nitrous oxide or nitric oxide: laminar flame propagation at low pressures in binary mixtures," *Combustion and Flame*, vol. 8, pp. 113–126, 1964.

[157] P. Ronney, "Effect of chemistry and transport properties on near limit flames at microgravity," *Combustion Science and Technology*, vol. 59, pp. 123–141, 1988.

[158] U. Pfahl, M. Ross, J. Shepherd, K. Pasamehmetoglu, and C. Unal, "Flammability limits, ignition energy and flame speeds in H_2-CH_4-NH_3-N_2O-O_2-N_2 mixtures," *Combustion and Flame*, vol. 123, pp. 140–158, 2000.

[159] T. Jabbour, *Classification de l'inflammabilité des fluides frigorigènes basée sur la vitesse fondamentale de flamme*. PhD thesis, Ecole de mines de Paris, 2004.

[160] K. Takizawa, A. Takahashi, K. Tokuhashi, S. Kondo, and A. Sekiya, "Burning velocity measurements of nitrogen-containing compounds," *Journal of Hazardous Materials*, vol. 155, pp. 144–152, 2008.

[161] D. Checkel, R. Liu, and D. Ting, "Ammonia as a fuel for SI engine," *SAE technical paper series*, vol. 2003-01-3095, pp. 1–7, 2003.

[162] G. Ciccarelli, D. Jackson, and J. Verreault, "Flammability limits of NH_3-H_2-N_2-air mixtures at elevated initial temperatures," *Combustion and Flame*, vol. 144, no. 1-2, pp. 53 – 63, 2006.

[163] W. Buckley and H. W., "Combustion properties of ammonia," *Chemical Engineering Progress*, vol. 58, pp. 81–84, 1962.

[164] Y. Shebeko, A. Trunev, S. Tsarichenko, and A. Zaitsev, "Investigation of concentration limits of flame propagation in ammonia-based gas mixtures," *Combustion, Explosion and Shock Waves*, vol. 32, no. 5, pp. 477–480, 1996.

[165] A. van Maaren, D. Thung, and L. De Goey, "Measurements of flame temperature and adiabatic burning velocities of methane air mixtures," *Combustion Science and Technology*, vol. 96, pp. 327–344, 1994.

[166] C. Law, N. Peters, and B. Rogg, *Reduced Kinetic Mechanisms for Application in Combustion*, ch. A compilation of experimental data on laminar burning velocities, pp. 15–26. Springer-Verlag, 1993.

[167] K. Bosschaart and L. de Goey, "Extension of the heat flux method to subatmospheric pressures," *Combustion Science and Technology*, vol. 176, pp. 1537–1564, 2004.

[168] D. Smith and J. Agnew, "The effect of pressure on the laminar burning velocity of methane oxygen nitrogen mixtures," *Proceedings of the Combustion Institute*, vol. 6, pp. 83–90, 1956.

[169] J. Agnew and L. Graiff, "The pressure dependence of laminar burning velocity by the spherical bomb method," *Combustion and Flame*, vol. 5, pp. 209–219, 1961.

[170] T. Iijiama and T. Takeno, "Effects of temperature and pressure on burning velocity," *Combustion and Flame*, vol. 65, pp. 35–43, 1986.

[171] S. Liao, D. Jiang, and Q. Cheng, "Determination of laminar burning velocities for natural gas," *Fuel*, vol. 83, pp. 1247–1250, 2004.

[172] D. Checkel, D. Ting, and W. Bushe, "Flammability limits and burning velocities of ammonia-nitric oxide mixtures," *Journal of Loss Prevention in the Process Industries*, vol. 8, pp. 215–220, 1995.

[173] C. Zamfirescu and I. Dincer, "Ammonia as a green fuel and hydrogen source for vehicular applications," *Fuel Processing Technology*, vol. 90, pp. 729–737, 2009.

[174] A. Macq, "Emploi de l'ammoniac comme combustible de remplacement," in *Compte rendu des journees d'etudes sur les combustibles et carburants nationaux*, (Louvain), pp. 286–309, 1941.

[175] E. Starkman, H. Newhall, R. Sutton, T. Maguire, and L. Farbar, "Ammonia as a spark ignition engine fuel: Theory and application," *SAE technical paper series*, vol. 660155, pp. 765–784, 1966.

[176] S. Grannell, D. Assanis, S. Bohac, and D. Gillespie, "The operating features of a stoichiometric, ammonia and gasoline dual fueled spark ignition engine," in *Proceedings of IMECE2006*, vol. 13048, (Chicago, Illinois, USA), ASME International Mechanical Engineering Congress and Exposition, 5-10 November 2006.

[177] J. Mathis, "Mr. clean hits the road ammonia-gas blend to fuel a drive to San Francisco," *The Ann Arbor News*, 01 August 2007.

[178] S. Grannell, D. Assanis, S. Bohac, and D. Gillespie, "The fuel mix limits and efficiency of a stoichiometric, ammonia, and gasoline dual fueled

spark ignition engine," *Journal of engineering for gas turbines and power*, vol. 130, pp. 0428021–0428028, July 2008.

[179] S. Grannell, D. Assanis, S. Bohac, and D. Gillespie, "Exhaust emissions from a stoichiometric, ammonia and gasoline dual fueled spark ignition engine," in *Proceedings of the ICES2009*, vol. 76131, (Milwaukee, Wisconsin, USA), ASME Internal Combustion Engine Division Spring Technical Conference, 3-6 May 2009.

[180] A. Reiter and S. Kong, "Demonstration of compression-ignition engine combustion using ammonia in reducing greenhouse gas emissions," *Energy and Fuels*, vol. 22, pp. 2963–2971, 2008.

[181] A. Reiter and S. Kong, "Combustion and emissions characteristics of compression-ignition engine using dual ammonia-diesel fuel," *Fuel*, vol. 90, no. 1, pp. 87–97, 2011.

[182] C. Morch, A. Bjerre, M. Gottrup, S. Sorenson, and J. Schramm, "Ammonia/hydrogen mixtures in an SI engine: Engine performance and analysis of a proposed fuel system," *Fuel*, vol. 90, no. 2, pp. 854–864, 2011.

[183] M. Tazerout, O. L. Corre, and A. Ramesh, "A new method to determine the start and end of combustion in an internal combustion engine using entropy changes," *International Journal of Applied Thermodynamics*, vol. 3, no. 2, pp. 49–55, 2000.

[184] M. Tazerout, O. L. Corre, and S. Rousseau, "TDC determination in IC engines based on the thermodynamic analysis of the temperature-entropy diagram," *SAE technical paper series*, vol. 1999-01-1489, pp. 1–9, 1999.

[185] O. Smith, C. Westbrook, and R. Sawyer, "Lean limit combustion in an expanding chamber," *Seventeenth Symposium (International) on Combustion/ The Combustion Institute*, pp. 1305–1313, 1979.

[186] N. Olson and J. Holbrook, "NH3 – The other hydrogen," *Paper presented at the National Hydrogen Association Annual Conference*, 30 March 2009.

[187] M. Barrere, "Rocket propulsion," *Elsevier*, 1960.

[188] G. Sanna and G. Tomassetti, *Introduction to molecular beam gas dynamics*. Imperial College Press, 2005.

[189] P. Atkins and L. Jones, *Chimie: Molécules, matière, métamorphoses*. De Boeck, 3e ed., 1998.

Publications associated to this work

Journal articles

- *"Kinetics in ammonia containing premixed flames and a preliminary investigation of their use as a fuel in spark ignition engines"*, Combustion Science and Technology, 181(8):1092-1106, 2009. doi:10.1080/00102200903074006

- *"Flame Structure Studies of Premixed Ammonia/Hydrogen/Oxygen/Argon Flames: Experimental and Numerical Investigation"*, Proceedings of the Combustion Institute, 32:1277-1284, 2009. doi:10.1016/j.proci.2008.06.036

- *"Ammonia combustion at elevated pressure and temperature conditions"*, Fuel, 89(11):3540-3545, 2010. doi:10.1016/j.fuel.2010.06.008

Oral presentations in conferences

- *"Effects of the equivalence ratio, the hydrogen initial content and the pressure on the structure of ammonia flames"*, 20^{th} Journees d'Etude of the Belgian Section of the Combustion Institute, Gand, Belgium, 2008.

- *"Experimental and Numerical Investigation of the Structure of Premixed Ammonia/Hydrogen/Oxygen/Argon flames"*, 32^{nd} International Symposium on Combustion, Montreal, Canada, 2008.

- *"Experimental and Numerical Study of the Ammonia Combustion in Flames and Spark Ignition Engines"*, PhD Student's Day, Louvain la Neuve, Belgium, 2009.

- *"Laminar Burning Velocity of Ammonia-Air-Diluent Mixtures"*, 21^{st} Journees d'Etude of the Belgian Section of the Combustion Institute, Liege, Belgium, 2010.

- *"Ammonia Combustion in spark ignition engine conditions"*, 7^{th} Annual NH3 Fuel Conference, Romulus, MI, USA, 2010.

Posters

- *"Study of ammonia containing premixed flames and possibility of their use as fuel in spark ignition engines"*, 3^{rd} European Combustion Meeting, Chania, Crete, 2007.

- *"Effects of the equivalence ratio, the hydrogen initial content and the pressure on the structure of ammonia flames"*, PhD Student's Day, Louvain la Neuve, Belgium, 2008.

- *"L'ammoniac, carburant du futur ?"*, 3^{rd} Strategic Energy Forum, Bruxelles, Belgium, 2008.

- *"Use of Ammonia as a Fuel for SI engine"*, 4^{th} European Combustion Meeting, Vienna, Austria, 2009.

- *"Experimental and Numerical Study of Ammonia Laminar Burning Velocity"*, 33^{rd} International Symposium on Combustion, Beijing, China, 2010.

- *"Modeling of $NH_3/H_2/O_2/Ar$ flames at low pressure"*, 5^{th} European Combustion Meeting, Cardiff, Wales, 2011.

Appendix

Appendix A

The gas feeding system

To fix the individuals gas flow rates entering the burner and to be able to adjust the composition of the flame, the sonic throat technique has been used. This technique allows to determine the mass flow rate of a gas passing through a small hole by measuring the pressure and temperature upstream the sonic throat [187]. The flow rate of the gas flowing through a Laval nozzle will be proportional to the upstream pressure only if the following conditions are fulfilled:

$$\frac{P_{up}}{P_{down}} \geq (\frac{2}{1+\gamma})^{\gamma/1-\gamma}.$$

Where γ represents the ratio of the specific heats at constant pressure and constant volume of the gas : $\gamma = C_p/C_v$. For the gases used in this work, critical ratios of the upstream (P_{up}) and downstream (P_{down}) pressures are presented in the table below.

Gas	$\gamma = C_p/C_v$	P_{up}/P_{down}
NH_3	1.3096	1.8383
H_2	1.3843	1.8834
O_2	1.3934	1.8889
Ar	1.6640	2.0512

Critical pressure conditions

Care must be taken to ensure that the pressure upstream the capillary nozzle is at least twice the pressure downstream, namely the pressure in the combustion chamber. When this condition is ensured, the gas flows through the nozzle at the sound speed and the mass flow rate can be calculated thanks to:

$$D_m = AP_{up}\sqrt{\frac{\gamma M}{RT}(\frac{2}{\gamma+1})^{\frac{\gamma+1}{\gamma-1}}}$$

where D_m is the mass flow rate $[kg/s]$, A the area of the sonic throat $[m^2]$, γ the specific heat ratio, M the molar mass of the gas $[kg/mol]$, R the perfect gas constant and T the temperature [K]. For a given nozzle, gas and temperature, this equation can be written as follows:

$$D_m = cste.P_{up}$$

Since the volume flow rate is obtained by dividing the mass flow rate by the density of the gas, this can also be written as:

$$D_v = cste'.P_{up}$$

Following this equation, volume flow calibration curves have been established for oxygen, hydrogen and argon. The corresponding volume flow rates have been measured by using a calibrated flowmeter for several upstream pressures. However, since ammonia is corrosive for brass, material constitutive of the flowmeter, the flow rate can not be calibrated directly by this method. But using previously presented equations, ammonia flow rate has been calculated from a corresponding flow rate of methane which has similar mass and specific heat ratio values. The following equations have been used:

$$D_{m(NH_3)} = A.P_{up}\sqrt{\frac{\gamma M}{RT}(\frac{2}{\gamma+1})^{\frac{\gamma+1}{\gamma-1}}} = A.P_{up}.0.055$$

$$D_{m(CH_4)} = A.P_{up}\sqrt{\frac{\gamma M}{RT}(\frac{2}{\gamma+1})^{\frac{\gamma+1}{\gamma-1}}} = A.P_{up}.0.054$$

$$\frac{D_{m(NH_3)}}{D_{m(CH_4)}} = 1.03$$

$$\frac{D_{v(NH_3)}}{D_{v(CH_4)}} = \frac{D_{m(NH_3)}\rho_{CH_4}}{D_{m(CH_4)}\rho_{NH_3}}$$

$$D_{v(NH_3)} = 0.97 D_{v(CH_4)}$$

The combustion chamber

The combustion chamber is constituted of a stainless steel cylinder with a water cooling system. The chamber is airtight and a low pressure is ensured by a rotary vacuum pump. The pressure in the combustion chamber is very low (in these experiments between 50 and 120 mbar) to enlarge the flame front. Indeed, at atmospheric pressure, the flame front is excessively narrow (about 10^{-4} m) and consequently difficult to investigate with a sufficient spatial resolution. Fortunately, the thickness of the flame front is a function of the inverse of the working pressure and it can therefore be enlarged by stabilizing flames at lower pressures. As presented in the figure below, a burner, a quartz nozzle and a retractile electrode are placed in the chamber.

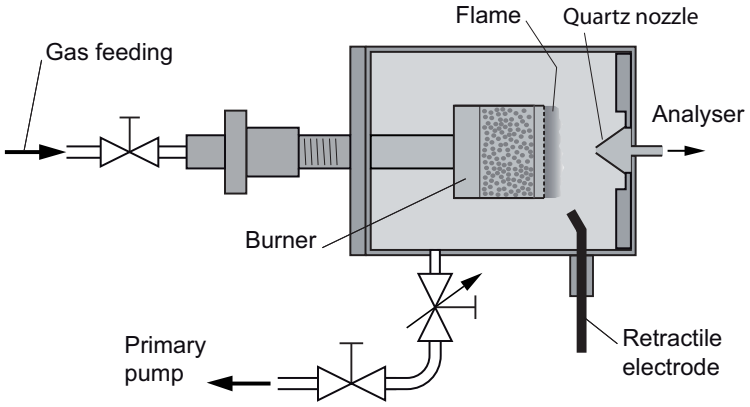

Combustion Chamber

This type of burner allows to obtain flat flame namely one–dimensional. It is constituted of a cylindrical body 8 cm in diameter closed at the extremity by a brass plate perforated with approximately 4400 holes 1 mm in diameter. The body of the burner is filled with 2 mm in diameter glass marbles to ensure a good homogenization of the gases. The burner is fixed with a screw thread to a stainless steel plate closing one side of the combustion chamber. The sampling position within the flame is varied successively from the fresh gases to the burned gases by moving the burner relative to the stationary quartz sampling cone. The spatial resolution during this sampling is around 0.1 mm.

The sampling cone has an angle of 45 degree, a hole of 0.15 mm in diameter and is 3 cm high. The quartz sampling cone has been treated by immersion in an aqueous solution of 5% hydrofluoric acid to deactivate the surface and reduce radical recombination reactions on the surface. The presence of significant radical recombination reactions on the sampling cone surface can result in a clearly visible displacement of the reaction zone in the center of the flame toward the cone or even flame attachment to the cone so that the flame is no longer one dimensional. The base of the cone is covered with a layer of wool ceramic. The overall arrangement reduces flow perturbations and heat losses induced by the quartz sampling cone being inserted into the flame. The sensitivity of the concentration measurements is greatly enhanced by reducing the distance from the top of the sampling cone to the ionization region of the mass spectrometer and by a very accurate alignment. The formation of the molecular beam allows to keep the composition of the flame unaltered, i.e. frozen, and permits to detect stable species as well as radicals.

The chamber behind the sampling cone

The chamber behind the sampling cone is evacuated to approximately 3.10^{-3} mbar thanks to a primary pump coupled to a oil diffusion pump. This extraction system can be represented by the figure below.

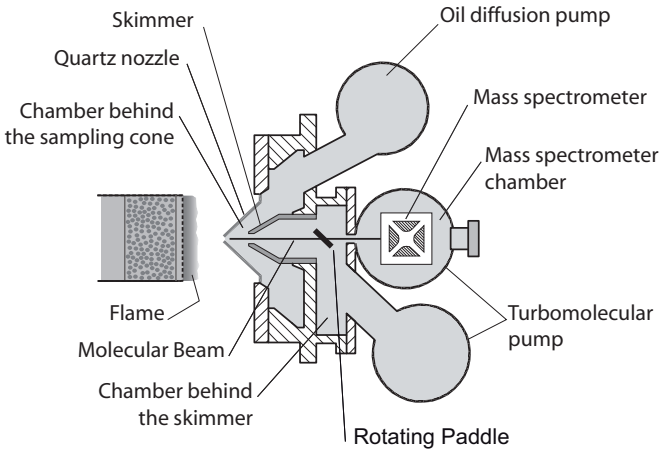

Formation of a molecular beam

The molecular beam is formed by the isentropic expansion of the sample coming from the high pressure gradient between the combustion chamber and this compartment. However, a recompression can occur when the molecular beam meets the residuals molecules in the chamber at a definite distance from the sampling cone tip. The molecular beam can thus be destroyed and a shock wave, named Mach disk [188], can be formed at a distance, x_m, of 13 mm from the nozzle, calculated by the following equation:

$$x_m = 0.67(\frac{P_{combustionchamber}}{P_{chamberbehindthenozzle)}})^{1/2}d$$

The pressure in the combustion chamber is around 50 mbar, the one behind the nozzle 3.10^{-3} mbar and the diameter of the quartz nozzle hole (d) 0.15 mm. Therefore to minimize this perturbation a conical skimmer is placed in the same axis than the sampling cone at a distance greatly smaller than x_m. The skimmer is a brass cone with a hole of 1 mm in diameter at the top. The molecular beam can thus penetrate in the next chamber, the chamber behind the skimmer. This arrangement allows to extract the central part of the molecular beam. Furthermore, a shock wave can not be formed in passing through the skimmer since the pressure difference between the two successive chambers is not high enough.

The chamber behind the skimmer

The chamber behind the skimmer is schematized in the extraction system figure. The pressure of around 10^{-5} mbar is smaller than the one in the chamber behind the sampling cone. Thanks to this pressure gradient, the molecular beam is accelerated again. To maintain such a low pressure a turbo-molecular pump coupled to the primary pumping system has been installed. The portion of the molecular beam sampled by the skimmer is modulated by a rotating paddle chopper at a frequency of 40Hz. This modulation is necessary to improve the signal to noise ratio by using an in–phase detection system which allows to discriminate easily the signal intensity of a species present in the molecular beam from that of residual species remaining in the ionization chamber of the mass spectrometer. Finally, the molecular beam reaches the mass spectrometer chamber by passing through a rectangular channel with a cross section of 1 cm by 1 mm and 2 cm long.

The mass spectrometer chamber

In this last chamber, the composition of the molecular beam is analyzed thanks to an Extrel C50 quadrupole mass spectrometer. The main steps of this mass spectrometer analysis are first the ionization by electronic impact of the chemical species present in the molecular beam, then the separation of the ions according to their mass on charge ratio and finally the signal treatment. The pressure in a mass spectrometer must be very low. Indeed, the definition of the mean free path [189], λ, shows that a high vacuum is necessary to decrease the number of collisions and therefore loosing as less ions as possible.

$$\lambda = \frac{RT}{\sqrt{2}PN_0\sigma_{AA}}$$

If this analysis is performed at atmospheric pressure, the mean free path would be around $6.5.10^{-8}$ m. In the mass spectrometer chamber, the pressure being around 10^{-7} mbar, the mean free path is about 660 m, high enough to ensure few interferences during the analyzes. This low pressure is obtained thanks to a turbo-molecular pump coupled with the rotary pump.

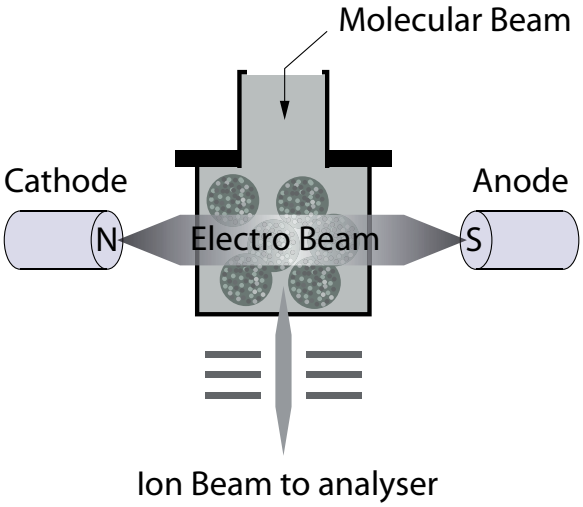

Ionization and extraction system

For the ionization process, schematized in the figure here above, a beam of electrons is created by applying an adjustable potential difference between a cathode, a heated Rhenium filament, and an anode. The molecular beam

meets this electronic beam perpendicularly. The electron energy depends on the applied potential difference. If the electron energy is higher or equals to the ionization potential (IP) of the gaseous molecules, a positive radical molecular ion is formed:

$$ABC + e^- \rightarrow ABC^{\bullet +} + 2e^-.$$

However, if the electron energy is sufficiently high to reach the fragmentation potential (FP) of the chemical species, there will be a fragmentation of the molecule:

$$\begin{array}{ccc} & [ABC]^{\bullet +} & \\ & \swarrow \quad \searrow & \\ [AB]^{\bullet +} + C & & [AB]^{+} + C^{\bullet} \end{array}$$

The use of the fragmentation process to identify chemical species is a routine technique and large reference tables exist. But for this quantitative study, it is essential to minimize fragmentation processes and to apply a work potential (WP) above the ionization potential but below the fragmentation potential :

$$IP < WP < FP.$$

The quadrupole is constituted of four electrodes with hyperbolic internal section. On these electrodes is applied a potential equals for two face–to–face electrodes and opposite for two side–by–side. This quadrupole is depicted in the figure below.

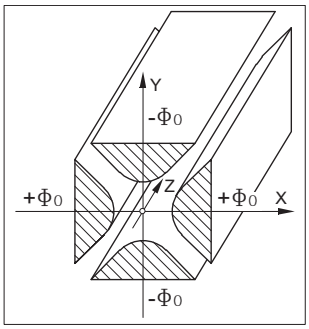

Quadrupole

For a given species, conditions are applied on these bars in the way that only specified m/z ratio ions will have a stable helicoidal trajectory to leave the quadrupole and to hit the detector. This means that all the ions with the same mass on charge ratio will be detected together, isomers can thus not be separated and the choice of the working potential to limit the formation of fragments coming from other molecules is of a great importance to obtain accurate results. Finally, the quadrupole signal is transformed in a voltage that can be measured. This is performed in the detector system. The ions meet the first dynode of an electron multiplier constituted of 17 dynodes. When an ion touches the first dynode, one or several electrons are ejected and directed towards the second dynode and so on until the last one. Since each dynode produces more electrons that it gets, the electron flow is amplified when it moves through the electron multiplier. Finally, an electrometer transforms the electronic current into a voltage. The signal–to–noise ratio is increased by a lock in amplifier at the frequency of the rotating paddle chopper.

Appendix B

Bian mechanism

Elements

O H N Ar

Species

N_2	H	O	O_2	OH	H_2O	HO_2
NH_3	NO	N_2O	NH_2	NH	N	NO_2
HNO	NNH	N_2H_2	H_2O_2	H_2	AR	

Reactions

			A	n	Ea (cal/mole)
H_2+O_2	=	2 OH	1.70E+13	0	47780
$OH+H_2$	=	H_2O+H	1.17E+09	1.3	3626
OH+O	=	$H+O_2$	4.00E+14	-0.5	0
$O+H_2$	=	OH+H	5.06E+04	2.67	6290
$H+O_2+M$	=	HO_2+M	3.61E+17	-0.72	0
$H_2O/18.6/$		$H_2/2.9/$	$N_2/1.3/$		
$OH+HO_2$	=	H_2O+O_2	7.50E+12	0	0
$H+HO_2$	=	2 OH	1.40E+14	0	1073
$O+HO_2$	=	O_2+OH	1.40E+13	0	1073
2 OH	=	$O+H_2O$	6.00E+08	1.3	0
2 H+M	=	H_2+M	1.00E+18	-1	0
$2 H+H_2$	=	2 H_2	9.20E+16	-0.6	0
$2 H+H_2O$	=	H_2+H_2O	6.00E+19	-1.25	0

H+OH+M	=	H_2O+M	1.60E+22	-2	0
H_2O/5/					
H+O+M	=	OH+M	6.20E+16	-0.6	0
H_2O/5/					
2 O+M	=	O_2+M	1.89E+13	0	-1788
H+HO_2	=	H_2+O_2	1.25E+13	0	0
HO_2+HO_2	=	H_2O_2+O_2	2.00E+12	0	0
H_2O_2+M	=	OH+OH+M	1.30E+17	0	45500
H_2O_2+H	=	HO_2+H_2	1.60E+12	0	3800
H_2O_2+OH	=	H_2O+HO_2	1.00E+13	0	1800
NH+O_2	=	HNO+O	1.00E+13	0	12000
NH+O_2	=	NO+OH	7.60E+10	0	1530
NH+NO	=	N_2O+H	2.40E+15	-0.8	0
N_2O+H	=	N_2+OH	7.60E+13	0	15200
N_2O+M	=	N_2+O+M	1.62E+14	0	51600
N_2O+O	=	N_2+O_2	1.00E+14	0	28200
N_2O+O	=	2 NO	1.00E+14	0	28200
N_2O+OH	=	N_2+HO_2	2.00E+12	0	10000
NH+OH	=	H+HNO	2.00E+13	0	0
NH+OH	=	N+H_2O	5.00E+11	0.5	2000
NH+N	=	N_2+H	3.00E+13	0	0
NH+H	=	N+H_2	1.00E+14	0	0
NH+O	=	NO+H	2.00E+13	0	0
NH_2+O	=	HNO+H	6.63E+14	-0.5	0
NH_2+O	=	NH+OH	6.75E+12	0	0
NH_2+OH	=	NH+H_2O	4.00E+06	2	1000
NH_2+H	=	NH+H_2	6.92E+13	0	3650
NH_2+NO	=	NNH+OH	6.40E+15	-125	0
NH_2+NO	=	N_2+H_2O	6.20E+15	-1.25	0
NH_3+OH	=	NH_2+H_2O	2.04E+06	2.04	566
NH_3+H	=	NH_2+H_2	6.36E+05	2.39	10171
NH_3+O	=	NH_2+OH	2.10E+13	0	9000
NNH	=	H+N_2	1.00E+04	0	0
NNH+NO	=	N_2+HNO	5.00E+13	0	0
NNH+H	=	N_2+H_2	1.00E+14	0	0
NNH+OH	=	N_2+H_2O	5.00E+13	0	0
NNH+NH_2	=	N_2+NH_3	5.00E+13	0	0

NNH+NH	=	N_2+NH_2	5.00E+13	0	0
NNH+O	=	N_2O+H	1.00E+14	0	0
HNO+M	=	H+NO+M	1.50E+16	0	48680
H_2O/10/		O_2/2/	N_2/2/	H_2/2/	
HNO+OH	=	NO+H_2O	3.60E+13	0	0
HNO+H	=	H_2+NO	5.00E+12	0	0
HNO+NH_2	=	NH_3+NO	2.00E+13	0	1000
HNO+HNO	=	N_2O+H_2O	3.95E+12	0	5000
HNO+NO	=	N_2O+OH	2.00E+12	0	26000
N+NO	=	N_2+O	3.27E+12	0.3	0
N+O_2	=	NO+O	6.40E+09	1	6280
N+OH	=	NO+H	3.80E+13	0	0
NO+HO_2	=	HNO+O_2	2.11E+12	0	-479
NO_2+H	=	NO+OH	3.50E+14	0	1500
NH_2+NH	=	N_2H_2+H	5.00E+13	0	0
2 NH	=	N_2+$_2$H	2.54E+13	0	0
NH_2+N	=	N_2+$_2$H	7.20E+13	0	0
N_2H_2+M	=	NNH+H+M	5.00E+16	0	50000
H_2O/15/		O_2/2/	N_2/2/	H_2/2/	
N_2H_2+H+M	=	NNH+H_2+M	5.00E+13	0	1000
N_2H_2+O	=	NH_2+NO	1.00E+13	0	0
N_2H_2+O	=	NNH+OH	2.00E+13	0	1000
N_2H_2+OH	=	NNH+H_2O	1.00E+13	0	1000
N_2H_2+NO	=	N_2O+NH_2	3.00E+12	0	0
N_2H_2+NH	=	NNH+NH_2	1.00E+13	0	1000
N_2H_2+NH_2	=	NH_3+NNH	1.00E+13	0	1000
2 NH_2	=	N_2H_2+H_2	5.00E+11	0	0
NH_2+O_2	=	HNO+OH	4.50E+12	0	25000

Lindstedt mechanism

Elements

O H N Ar

Species

N_2	H	O	O_2	OH	H_2O	HO_2
NH_3	NO	N_2O	NH_2	NH	N	NO_2
HNO	NNH	N_2H_2	H_2O_2	H_2	AR	NO_3
HNO_2						

Reactions

			A	n	Ea (cal/mole)
$H+O_2$	=	$OH+O$	2.00E+14	0	16802
$O+H_2$	=	$OH+H$	5.12E+04	2.67	6286
$OH+H_2$	=	H_2O+H	1.00E+08	1.6	3298)
$OH+OH$	=	H_2O+O	1.50E+09	1.14	100
O_2+H+M	=	HO_2+M	2.30E+15	-0.8	0
HO_2+H	=	$OH+OH$	1.68E+14	0	875
HO_2+H	=	H_2+O_2	4.27E+13	0	1410
HO_2+OH	=	H_2O+O_2	2.89E+13	0	-497
HO_2+H	=	H_2O+O	3.00E+13	0	1721
HO_2+O	=	$OH+O_2$	3.19E+13	0	0
HO_2+HO_2	=	$H_2O_2+O_2$	1.86E+12	0	1539
H_2O_2+H	=	H_2O+OH	1.00E+13	0	3585
H_2O_2+H	=	HO_2+H_2	1.70E+12	0	3752
H_2O_2+O	=	HO_2+OH	6.60E+11	0	3967
H_2O_2+OH	=	H_2O+HO_2	7.83E+12	0	1331
H_2O_2+M	=	$OH+OH+M$	1.20E+17	0	45411
$H+H+M$	=	H_2+M	6.50E+14	-1	0
$H+OH+M$	=	H_2O+M	2.20E+19	-2	0
$O+O+M$	=	O_2+M	1.88E+10	0	1788
NH_3+M	=	NH_2+H+M	1.40E+16	0.06	90600
NH_3+H	=	NH_2+H_2	6.36E+05	2.39	10171
NH_3+OH	=	NH_2+H_2O	2.04E+06	2.04	566
NH_3+O	=	NH_2+OH	2.10E+13	0	9000

NH_2+H	=	NH+H_2	5.67E+11	0.59	3648
NH_2+OH	=	NH+H_2O	9.00E+07	1.5	-457
NH_2+O	=	NH+OH	7.00E+12	0	0
NH_2+O	=	HNO+H	9.90E+14	-0.5	0
NH_2+N	=	N_2+H+H	7.20E+13	0	0
NH_2+NO	=	N_2+H_2O	3.00E+20	-2.6	924
NH+H	=	N+H_2	1.00E+13	0	0
NH+O	=	NO+H	7.00E+13	0	0
NH+OH	=	N+H_2O	2.00E+09	1.2	6
NH+OH	=	HNO+H	4.00E+13	0	0
NH+O_2	=	NO+OH	1.00E+13	-0.2	4799
NH+N	=	N_2+H	3.00E+13	0	0
NH+NO	=	N_2O+H	2.94E+14	-0.4	0
DUPLICATE					
NH+NO	=	N_2O+H	-2.16E+13	-0.23	0
DUPLICATE					
NH+NH	=	N_2+H+H	2.54E+13	0	0
N+O_2	=	NO+O	6.40E+09	1	6280
N+OH	=	NO+H	3.80E+13	0	0
N+NO	=	N_2+O	3.30E+12	0.3	0
NO+HO_2	=	NO_2+OH	2.11E+12	0	-479
NO_2	=	NO+O	7.60E+21	-1.27	73290
NO_2+H	=	NO+OH	3.50E+14	0	1500
NO_2+O	=	NO+O_2	3.90E+12	0	-238
NO_2+NO_2	=	NO+NO+O_2	1.62E+12	0	26124
N_2H_2+M	=	NNH+H+M	1.17E+17	0	50000
N_2H_2+H	=	NNH+H_2	5.00E+13	0	1000
N_2H_2+O	=	NH_2+NO	1.00E+13	0	0
N_2H_2+O	=	NNH+OH	2.00E+13	0	1000
N_2H_2+OH	=	NNH+H_2O	1.00E+13	0	1000
N_2H_2+NO	=	NH_2+N_2O	3.00E+12	0	0
N_2H_2+NH	=	NNH+NH_2	1.00E+13	0	1000
N_2H_2+NH_2	=	NNH+NH_3	1.00E+13	0	1000
NNH+M	=	N_2+H+M	1.70E+12	0	14307
NNH+OH	=	N_2+H_2O	5.00E+13	0	0
NNH+NH_2	=	N_2+NH_3	5.00E+13	0	0
NO+NNH	=	N_2+HNO	2.00E+12	0	0

NH_2+NH	=	N_2H_2+H	1.00E+15	-0.5	0
NH_2+NH_2	=	N_2H_2+H_2	4.00E+13	0	11843
NH_2+NO	=	NNH+OH	1.39E+12	0	0
N_2O+H	=	N_2+OH	2.53E+10	0	4550
DUPLICATE					
N_2O+H	=	N_2+OH	2.23E+14	0	16750
DUPLICATE					
N_2O+O	=	NO+NO	5.60E+14	0	27999
N_2O+O	=	N_2+O_2	7.00E+14	0	27999
N_2O+M	=	N_2+O+M	5.00E+13	0	60467
N_2O+OH	=	N_2+HO_2	2.00E+12	0	10000
HNO+M	=	H+NO+M	2.35E+16	0	48680
HNO+H	=	H_2+NO	5.00E+12	0	0
HNO+OH	=	H_2O+NO	7.20E+13	0	0
HNO+O	=	OH+NO	3.60E+13	0	0
HNO+HNO	=	H_2O+N_2O	3.90E+12	0	50000
HNO+NH_2	=	NH_3+NO	2.00E+13	0	1000
HNO+NO	=	N_2O+OH	2.00E+12	0	26000
NH_2+O_2	=	HNO+OH	1.51E+12	-3.9	36099
NH+O_2	=	HNO+O	4.61E+05	2	6500
HNO+NO_2	=	HNO_2+NO	6.02E+11	0	1987
HNO_2	=	OH+NO	1.20E+22	-1.23	49697
HNO_2+H	=	H_2+NO_2	1.20E+13	0	5961
HNO_2+OH	=	H_2O+NO_2	1.26E+10	1	135
HNO_2+O	=	OH+NO_2	1.20E+13	0	7352
NO_2+O	=	NO_3	1.32E+13	0	0
NO_3+O	=	NO_2+O_2	6.03E+12	0	0
NO_3+OH	=	NO_2+HO_2	1.39E+13	0	0
NO_3+H	=	NO_2+OH	6.62E+13	0	0
NO_3+NO	=	NO_2+NO_2	9.64E+12	0	-298
HNO+O_2	=	NO+HO_2	3.16E+12	0	3000
NH_2+O_2	=	NH+HO_2	1.00E+14	0	49997
NH_2+HO_2	=	NH_3+O_2	4.52E+13	0	0
NNH+NH	=	N_2+NH_2	5.00E+13	0	0
NH+NO	=	N_2+OH	2.16E+13	-0.23	0
NNH+O	=	NO+NH	1.00E+13	0	0
NNH+O	=	N_2+OH	1.00E+13	0	5000

NH_2+NH_2	=	$NH+NH_3$	5.00E+13	0	9935
NH_2+NO	=	N_2O+H_2	5.00E+13	0	24481
NH+O	=	N+OH	7.00E+12	0	0
NH_2+O	=	$NO+H_2$	5.00E+12	0	0

Konnov mechanism

Elements

O H N Ar

Species

N_2	H	O	O_2	OH	H_2O	HO_2
NH_3	NO	N_2O	NH_2	NH	N	NO_2
HNO	NNH	N_2H_2	H_2O_2	H_2	AR	NO_3
N_2O_3	HONO	HNO_3	N_2H_3	N_2H_4	N_2O_4	NH_2OH
HNOH	H_2NO	HNNO				

Reactions

			A	n	Ea (cal/mole)
H+H+M	=	H_2+M	7.00E+17	-1	0
H_2/0.0/		N_2/0.0/	H/0.0/	H_2O/14.3/	
H+H+H_2	=	H_2+H_2	1.00E+17	-0.6	0
H+H+N_2	=	H_2+N_2	5.40E+18	-1.3	0
H+H+H	=	H_2+H	3.20E+15	0	0
O+O+M	=	O_2+M	1.00E+17	-1	0
O/71.0/		O_2/20.0/	NO/5.0/	N_2/5.0/	N/5.0/
H_2O/5.0/					
O+H+M	=	OH+M	6.20E+16	-0.6	0
H_2O/5.0/					
H_2+O_2	=	OH+OH	2.50E+12	0	39000
O+H_2	=	OH+H	5.06E+04	2.67	6290
H+O_2	=	OH+O	9.75E+13	0	14850
H+O_2(+M)	=	HO_2(+M)	1.48E+12	0.6	0
LOW			3.50E+16	-0.41	-1116.0
TROE			0.5	100000	10
AR/0.0/		H_2O/10.6/	H_2/1.5/		
H+O_2(+AR)	=	HO_2(+AR)	1.48E+12	0.6	0
LOW			7.00E+17	-0.8	0.0
TROE			0.45	10	100000
H+OH+M	=	H_2O+M	2.20E+22	-2	0
H_2O/6.4/		AR/0.38/			
H_2+OH	=	H_2O+H	1.00E+08	1.6	3300

OH+OH	=	H_2O+O	1.50E+09	1.14	100
HO_2+OH	=	H_2O+O_2	2.89E+13	0	-500
HO_2+O	=	OH+O_2	1.63E+13	0	-445
H+HO_2	=	H_2+O_2	4.28E+13	0	1411
H+HO_2	=	OH+OH	1.70E+14	0	875
H+HO_2	=	H_2O+O	3.00E+13	0	1720
HO_2+HO_2	=	H_2O_2+O_2	4.20E+14	0	12000
DUPLICATE					
HO_2+HO_2	=	H_2O_2+O_2	1.30E+11	0	-1640
DUPLICATE					
OH+OH(+M)	=	H_2O_2(+M)	7.20E+13	-0.37	0
LOW			2.2E+19	-0.76	0.0
TROE			0.5	100000	10
H_2O/0.0/					
OH+OH(+H_2O)	=	H_2O_2(+H_2O)	7.20E+13	-0.37	0
LOW			1.45E+18	0	0.0
H_2O_2+OH	=	HO_2+H_2O	1.00E+12	0	0
DUPLICATE					
H_2O_2+OH	=	HO_2+H_2O	5.80E+14	0	9560
DUPLICATE					
H_2O_2+H	=	HO_2+H_2	1.70E+12	0	3755
H_2O_2+H	=	H_2O+OH	1.00E+13	0	3575
H_2O_2+O	=	HO_2+OH	2.80E+13	0	64000
N_2+O	=	NO+N	1.80E+14	0	76100
N+O_2	=	NO+O	9.00E+09	1	6500
NO+M	=	N+O+M	9.64E+14	0	148300
N_2/1.5/		NO /3.0/			
NO+NO	=	N_2+O_2	3.00E+11	0	65000
N_2O(+M)	=	N_2+O(+M)	1.26E+12	0	62620
LOW			4.00E+14	0	56640.0
O_2/1.4/		N_2/1.7/	H_2O/12.0/	NO/3.0/	N_2O/3.5/
N_2O+O	=	N_2+O_2	1.00E+14	0	28200
N_2O+O	=	NO+NO	6.92E+13	0	26630
N_2O+N	=	N_2+NO	1.00E+13	0	20000
N_2O+NO	=	N_2+NO_2	2.75E+14	0	50000

NO+O(+M)	=	NO_2(+M)	1.30E+15	-0.75	0
LOW			4.72E+24	-2.87	1551.0
TROE			0.962	10	7962
AR/0.6/		NO_2 /6.2/	NO /1.8/	O_2 /0.8/	N_2O/4.4/
H_2O/10.0/					
NO+O	=	NO_2	1.30E+15	-0.75	0
NO_2+O	=	NO+O_2	3.91E+12	0	-238
NO_2+N	=	N_2O+O	8.40E+11	0	0
NO_2+N	=	NO+NO	1.00E+12	0	0
NO_2+NO	=	N_2O+O_2	1.00E+12	0	60000
NO_2+NO_2	=	NO+NO+O_2	3.95E+12	0	27590
NO_2+NO_2	=	NO_3+NO	1.13E+04	2.58	22720
NO_2+O(+M)	=	NO_3(+M)	1.33E+13	0	0
LOW			1.49E+28	-4.08	2467
TROE			0.86	10	2800
H_2O/10.0/		O_2/0.8/	H_2/2.0/		
NO_2+O	=	NO_3	1.33E+13	0	0
NO_3	=	NO+O_2	2.50E+06	0	12120
NO_3+NO_2	=	NO+NO_2+O_2	1.20E+11	0	3200
NO_3+O	=	NO_2+O_2	1.02E+13	0	0
NO_3+NO_3	=	NO_2+NO_2+O_2	5.12E+11	0	4870
N_2O4(+M)	=	NO_2+NO_2(+M)	4.05E+18	-1.1	12840
LOW			1.96E+28	-3.8	12840
AR/0.8/		N_2O4/2.0/	NO_2/2.0/		
N_2O4+O	=	N_2O_3+O_2	1.21E+12	0	0
NO_2+NO(+M)	=	N_2O_3(+M)	1.60E+09	1.4	0
LOW			/1.0E+33	-7.7	0.0/
N_2/1.36/					
N_2O_3+O	=	NO_2+NO_2	2.71E+11	0	0
N_2+M	=	N+N+M	1.00E+28	-3.33	225000
N/5/		O/2.2/			
NH+M	=	N+H+M	2.65E+14	0	75500
NH+H	=	N+H_2	3.20E+13	0	325
NH+N	=	N_2+H	9.00E+11	0.5	0
NH+NH	=	NNH+H	5.10E+13	0	0
NH+NH	=	NH_2+N	5.95E+02	2.89	-2030
NH+NH	=	N_2+H_2	1.00E+08	1	0

NH_2+M	=	NH+H+M	3.16E+23	-2	91400
NH+H_2	=	NH_2+H	1.00E+14	0	20070
NH_2+N	=	N_2+H+H	6.90E+13	0	0
NH_2+NH	=	N_2H_2+H	1.50E+15	-0.5	0
NH_2+NH	=	NH_3+N	1.00E+13	0	2000
NH_3+NH	=	NH_2+NH_2	3.16E+14	0	26770
NH_2+NH_2	=	N_2H_2+H_2	1.00E+13	0	1500
N_2H_3+H	=	NH_2+NH_2	5.00E+13	0	2000
NH_3+M	=	NH_2+H+M	2.20E+16	0	93470
NH_3+M	=	NH+H_2+M	6.30E+14	0	93390
NH_3+H	=	NH_2+H_2	5.42E+05	2.4	9920
NH_3+NH_2	=	N_2H_3+H_2	1.00E+11	0.5	21600
NNH	=	N_2+H	3.00E+08	0	0
DUPLICATE					
NNH+M	=	N_2+H+M	1.00E+13	0.5	3060
DUPLICATE					
NNH+H	=	N_2+H_2	1.00E+14	0	0
NNH+N	=	NH+N_2	3.00E+13	0	2000
NNH+NH	=	N_2+NH_2	2.00E+11	0.5	2000
NNH+NH_2	=	N_2+NH_3	1.00E+13	0	0
NNH+NNH	=	N_2H_2+N_2	1.00E+13	0	4000
N_2H_2+M	=	NNH+H+M	5.00E+16	0	50000
H_2O/15.0/		O_2/2.0/	N_2/2.0/	H_2/2.0/	
N_2H_2+M	=	NH+NH+M	3.16E+16	0	99400
H_2O/15.0/		O_2/2.0/	N_2/2.0/	H_2/2.0/	
N_2H_2+H	=	NNH+H_2	8.50E+04	2.63	-230
N_2H_2+N	=	NNH+NH	1.00E+06	2	0
N_2H_2+NH	=	NNH+NH_2	1.00E+13	0	6000
N_2H_2+NH_2	=	NH_3+NNH	8.80E-02	4.05	-1610
N_2H_3+NH	=	N_2H_2+NH_2	2.00E+13	0	0
N_2H_3+NNH	=	N_2H_2+N_2H_2	1.00E+13	0	4000
N_2H_3+M	=	NH_2+NH+M	5.00E+16	0	60000
N_2H_3+M	=	N_2H_2+H+M	1.00E+16	0	37000
N_2H_3+H	=	N_2H_2+H_2	1.00E+13	0	0
N_2H_3+H	=	NH+NH_3	1.00E+11	0	0
N_2H_3+N	=	N_2H_2+NH	1.00E+06	2	0
N_2H_3+NH_2	=	NH_3+N_2H_2	1.00E+11	0.5	0
N_2H_3+N_2H_2	=	N_2H4+NNH	1.00E+13	0	6000

$N_2H_3+N_2H_3$	=	$NH_3+NH_3+N_2$	3.00E+12	0	0
$N_2H_3+N_2H_3$	=	$N_2H4+N_2H_2$	1.20E+13	0	0
$N_2H4(+M)$	=	$NH_2+NH_2(+M)$	5.00E+14	0	60000
LOW			1.50E+15	0	39000
N_2/2.4/		NH_3/3.0/	N_2H4/4.0/		
N_2H4+M	=	N_2H_3+H+M	1.00E+15	0	63600
N_2/2.4/		NH_3/3.0/	N_2H4/4.0/		
N_2H4+H	=	$N_2H_3+H_2$	7.00E+12	0	2500
N_2H4+H	=	NH_2+NH_3	2.40E+09	0	3100
N_2H4+N	=	N_2H_3+NH	1.00E+10	1	2000
N_2H4+NH	=	$NH_2+N_2H_3$	1.00E+09	1.5	2000
N_2H4+NH_2	=	$N_2H_3+NH_3$	1.80E+06	1.71	-1380
N+OH	=	NO+H	2.80E+13	0	0
N_2O+H	=	N_2+OH	2.20E+14	0	16750
N_2O+H	=	NH+NO	6.70E+22	-2.16	37155
N_2O+H	=	NNH+O	5.50E+18	-1.06	47290
N_2O+H	=	HNNO	8.00E+24	-4.39	10530
N_2O+OH	=	N_2+HO_2	1.00E+14	0	30000
HNO+NO	=	N_2O+OH	8.50E+12	0	29580
HNO+NO+NO	=	$HNNO+NO_2$	1.60E+11	0	2090
NH+NO+M	=	HNNO+M	1.63E+23	-2.6	1820
HNNO+H	=	N_2O+H_2	2.00E+13	0	0
HNNO+H	=	NH_2+NO	1.00E+12	0	0
HNNO+O	=	N_2O+OH	2.00E+13	0	0
HNNO+OH	=	H_2O+N_2O	2.00E+13	0	0
HNNO+OH	=	HNOH+NO	1.00E+12	0	0
HNNO+NO	=	N_2+HONO	2.60E+11	0	1610
HNNO+NO	=	$NNH+NO_2$	3.20E+12	0	540
HNNO+NO	=	N_2O+HNO	1.00E+12	0	0
$HNNO+NO_2$	=	N_2O+HONO	1.00E+12	0	0
$HNNO+NO_2$	=	$NNH+NO_3$	1.00E+13	0	17000
NO_2+H	=	NO+OH	1.32E+14	0	362
NO_2+OH	=	HO_2+NO	1.81E+13	0	6676
NO_2+HO_2	=	$HONO+O_2$	4.64E+11	0	-479
NO_2+H_2	=	HONO+H	7.33E+11	0	28800
NO_2+NH	=	N_2O+OH	8.65E+10	0	-2270
NO_2+NH	=	NO+HNO	1.25E+11	0	-2270

NO_3+H	=	NO_2+OH	6.62E+13	0	0
NO_3+OH	=	NO_2+HO_2	1.21E+13	0	0
NO_3+HO_2	=	HNO_3+O_2	5.55E+11	0	0
NO_3+HO_2	=	NO_2+OH+O_2	1.51E+12	0	0
N_2O4+H_2O	=	HONO+HNO_3	2.52E+14	0	11590
N_2O_3+H_2O	=	HONO+HONO	3.79E+13	0	8880
H+NO(+M)	=	HNO(+M)	1.52E+15	-0.41	0
LOW			4.00E+20	-1.75	0
H_2O/10.0/		O_2/1.5/	AR/0.75/	H_2/2.0/	
HNO+H	=	NO+H_2	4.46E+11	0.72	655
HNO+OH	=	NO+H_2O	1.30E+07	1.88	-956
HNO+O	=	OH+NO	5.00E+11	0.5	2000
HNO+O	=	NO_2+H	5.00E+10	0	2000
HNO+O_2	=	NO+HO_2	2.20E+10	0	9140
HNO+N	=	NO+NH	1.00E+11	0.5	2000
HNO+N	=	H+N_2O	5.00E+10	0.5	3000
HNO+NH	=	NH_2+NO	5.00E+11	0.5	0
HNO+NH_2	=	NH_3+NO	2.00E+13	0	1000
HNO+HNO	=	N_2O+H_2O	3.63E-03	3.98	1190
HNO+HNO	=	HNOH+NO	2.00E+08	0	4170
HNO+NO_2	=	HONO+NO	6.02E+11	0	2000
NO+OH(+M)	=	HONO(+M)	2.00E+12	-0.05	-721
LOW			5.08E+23	-2.51	-67.6
TROE			0.62	10	100000
H_2O/10.0/		O_2/2.0/	AR/0.75/	H_2/2.0/	
NO+OH	=	HONO	2.00E+12	-0.05	-721
NO_2+H+M	=	HONO+M	1.40E+18	-1.5	900
HONO+H	=	HNO+OH	5.64E+10	0.86	4970
HONO+H	=	NO+H_2O	8.12E+06	1.89	3840
HONO+O	=	OH+NO_2	1.20E+13	0	5960
HONO+OH	=	H_2O+NO_2	1.69E+12	0	-517
HONO+NH	=	NH_2+NO_2	1.00E+13	0	0
HONO+HONO	=	H_2O+NO_2+NO	1.00E+13	0	8540
HONO+NH_2	=	NO_2+NH_3	5.00E+12	0	0
NO_2+OH(+M)	=	HNO_3(+M)	2.41E+13	0	0
LOW			6.42E+32	-5.49	2350
TROE			1.0	10	1168
H_2O/10.0/		O_2/2.0/	AR/0.75/	H_2/2.0/	

NO_2+OH	=	HNO_3	2.41E+13	0	0
NO+HO_2+M	=	HNO_3+M	1.50E+24	-3.5	2200
HNO_3+H	=	H_2+NO_3	5.56E+08	1.53	16400
HNO_3+H	=	H_2O+NO_2	6.08E+01	3.29	6290
HNO_3+H	=	OH+HONO	3.82E+05	2.3	6980
HNO_3+OH	=	NO_3+H_2O	1.03E+10	0	-1240
NH_3+O	=	NH_2+OH	1.10E+06	2.1	5210
NH_3+OH	=	NH_2+H_2O	5.00E+07	1.6	950
NH_3+HO_2	=	NH_2+H_2O_2	3.00E+11	0	22000
NH_2+HO_2	=	NH_3+O_2	1.65E+04	1.55	2027
NH_2+O	=	H_2+NO	5.00E+12	0	0
NH_2+O	=	HNO+H	4.50E+13	0	0
NH_2+O	=	NH+OH	7.00E+12	0	0
NH_2+OH	=	NH+H_2O	9.00E+07	1.5	-460
NH_2+OH	=	NH_2OH	1.79E+13	0.2	0
NH_2+HO_2	=	HNO+H_2O	5.68E+15	-1.12	707
NH_2+HO_2	=	H_2NO+OH	2.91E+17	-1.32	1248
NH_2+O_2	=	HNO+OH	1.00E+13	0	26290
NH_2+O_2	=	H_2NO+O	6.00E+13	0	29880
NH_2+NO	=	NNH+OH	2.29E+10	0.425	-814
NH_2+NO	=	N_2+H_2O	2.77E+20	-2.65	1258
NH_2+NO	=	H_2+N_2O	1.00E+13	0	33700
NH_2+NO_2	=	N_2O+H_2O	1.62E+16	-1.44	270
NH_2+NO_2	=	H_2NO+NO	6.48E+16	-1.44	270
NH+O	=	NO+H	7.00E+13	0	0
NH+O	=	N+OH	7.00E+12	0	0
NH+OH	=	HNO+H	2.00E+13	0	0
NH+OH	=	N+H_2O	2.00E+09	1.2	0
NH+OH	=	NO+H_2	2.00E+13	0	0
NH+HO_2	=	HNO+OH	1.00E+13	0	2000
NH+O_2	=	HNO+O	4.00E+13	0	17880
NH+O_2	=	NO+OH	4.50E+08	0.79	1190
NH+H_2O	=	HNO+H_2	2.00E+13	0	13850
NH+N_2O	=	N_2+HNO	2.00E+12	0	6000
NNH+O	=	NH+NO	2.00E+14	0	4000
NH+NO	=	N_2+OH	6.10E+13	-0.5	120

N_2H4+O	=	$N_2H_2+H_2O$	8.50E+13	0	1200
N_2H4+O	=	N_2H_3+OH	2.50E+12	0	1200
N_2H4+OH	=	$N_2H_3+H_2O$	3.00E+10	0.68	1290
N_2H4+OH	=	NH_3+H_2NO	3.67E+13	0	0
N_2H4+HO_2	=	$N_2H_3+H_2O_2$	4.00E+13	0	2000
N_2H_3+O	=	N_2H_2+OH	2.00E+13	0	1000
N_2H_3+O	=	$NNH+H_2O$	3.16E+11	0.5	0
N_2H_3+O	=	NH_2+HNO	1.00E+13	0	0
N_2H_3+OH	=	$N_2H_2+H_2O$	3.00E+10	0.68	1290
N_2H_3+OH	=	NH_3+HNO	1.00E+12	0	15000
$N_2H_3+O_2$	=	$N_2H_2+HO_2$	3.00E+12	0	0
$N_2H_3+HO_2$	=	$N_2H_2+H_2O_2$	1.00E+13	0	2000
$N_2H_3+HO_2$	=	N_2H4+O_2	8.00E+12	0	0
N_2H_3+NO	=	$HNO+N_2H_2$	1.00E+12	0	0
N_2H_2+O	=	NH_2+NO	1.00E+13	0	0
N_2H_2+O	=	$NNH+OH$	2.00E+13	0	1000
N_2H_2+OH	=	$NNH+H_2O$	5.92E+01	3.4	-1360
$N_2H_2+HO_2$	=	$NNH+H_2O_2$	1.00E+13	0	2000
N_2H_2+NO	=	N_2O+NH_2	3.00E+10	0	0
$NNH+O$	=	N_2+OH	1.70E+16	-1.23	500
$NNH+OH$	=	N_2+H_2O	2.40E+22	-2.88	2444
$NNH+O_2$	=	N_2+HO_2	1.20E+12	-0.34	150
$NNH+O_2$	=	N_2O+OH	2.90E+11	-0.34	150
$NNH+HO_2$	=	$N_2+H_2O_2$	1.00E+13	0	2000
$NNH+NO$	=	N_2+HNO	5.00E+13	0	0
NH_2OH+OH	=	$HNOH+H_2O$	2.50E+13	0	4250
H_2NO+M	=	H_2+NO+M	7.83E+27	-4.29	60300
$H_2O/10.0/$					
H_2NO+M	=	$HNO+H+M$	2.80E+24	-2.83	64915
$H_2O/10.0/$					
H_2NO+M	=	$HNOH+M$	1.10E+29	-3.99	43980
$H_2O/10.0/$					
H_2NO+H	=	$HNO+H_2$	3.00E+07	2	2000
H_2NO+H	=	NH_2+OH	5.00E+13	0	0
H_2NO+O	=	$HNO+OH$	3.00E+07	2	2000
H_2NO+OH	=	$HNO+H_2O$	2.00E+07	2	1000
H_2NO+HO_2	=	$HNO+H_2O_2$	2.90E+04	2.69	-1600

H_2NO+NH_2	=	$HNO+NH_3$	3.00E+12	0	1000
H_2NO+O_2	=	$HNO+HO_2$	3.00E+12	0	25000
H_2NO+NO	=	HNO+HNO	2.00E+07	2	13000
H_2NO+NO_2	=	HONO+HNO	6.00E+11	0	2000
HNOH+M	=	HNO+H+M	2.00E+24	-2.84	58935
H_2O/10.0/					
HNOH+H	=	$HNO+H_2$	4.80E+08	1.5	380
HNOH+H	=	NH_2+OH	4.00E+13	0	0
HNOH+O	=	HNO+OH	7.00E+13	0	0
DUPLICATE					
HNOH+O	=	HNO+OH	3.30E+08	1.5	-360
DUPLICATE					
HNOH+OH	=	$HNO+H_2O$	2.40E+06	2	-1190
$HNOH+HO_2$	=	$HNO+H_2O_2$	2.90E+04	2.69	-1600
$HNOH+NH_2$	=	$HNO+NH_3$	1.80E+06	1.94	-1150
$HNOH+NO_2$	=	HONO+HNO	6.00E+11	0	2000
$HNOH+O_2$	=	$HNO+HO_2$	3.00E+12	0	25000
HNOH+HNO	=	NH_2OH+NO	1.00E+12	0	3000

GRI mechanism

Elements

O H C N Ar

Species

N_2	H	O	O_2	OH	H_2O	HO_2
NH_3	NO	N_2O	NH_2	NH	N	NO_2
HNO	NNH	H_2O_2	H_2	AR	C	CH
CH_2	$CH_2(S)$	CH_3	CH_4	CO	CO_2	HCO
CH_2O	CH_2OH	CH_3O	CH_3OH	C_2H	C_2H_2	C_2H_3
C_2H_4	C_2H_5	C_2H_6	HCCO	CH_2CO	HCCOH	CN
HCN	H_2CN	HCNN	HCNO	HOCN	HNCO	NCO
C_3H_7	C_3H_8	CH_2CHO	CH_3CHO			

Reactions

			A	n	Ea (cal/mole)
2O+M	=	O_2+M	1.20E+17	-1	0
H_2/2.40/		H_2O/15.40/	CH_4/2.00/	CO/1.75/	CO_2/3.60/
C_2H_6/3.00/		AR/0.83/			
O+H+M	=	OH+M	5.00E+17	-1	0
H_2/2.00/		H_2O/6.00/	CH_4/2.00/	CO/1.50/	CO_2/2.00/
C_2H_6/3.00/		AR/0.70/			
O+H_2	=	H+OH	3.87E+04	2.7	6260
O+HO_2	=	OH+O_2	2.00E+13	0	0
O+H_2O_2	=	OH+HO_2	9.63E+06	2	4000
O+CH	=	H+CO	5.70E+13	0	0
O+CH_2	=	H+HCO	8.00E+13	0	0
O+$CH_2(S)$	=	H_2+CO	1.50E+13	0	0
O+$CH_2(S)$	=	H+HCO	1.50E+13	0	0
O+CH_3	=	H+CH_2O	5.06E+13	0	0
O+CH_4	=	OH+CH_3	1.02E+09	1.5	8600
O+CO(+M)	=	CO_2(+M)	1.80E+10	0	2385
LOW/			6.02E+14	0	3000
H_2/2.00/		O_2/6.00/	H_2O/6.00/	CH_4/2.00/	CO/1.50/
CO_2/3.50/		C_2H_6/3.00/	AR/0.50/		

O+HCO	=	OH+CO	3.00E+13	0	0
O+HCO	=	H+CO_2	3.00E+13	0	0
O+CH_2O	=	OH+HCO	3.90E+13	0	3540
O+CH_2OH	=	OH+CH_2O	1.00E+13	0	0
O+CH_3O	=	OH+CH_2O	1.00E+13	0	0
O+CH_3OH	=	OH+CH_2OH	3.88E+05	2.5	3100
O+CH_3OH	=	OH+CH_3O	1.30E+05	2.5	5000
O+C_2H	=	CH+CO	5.00E+13	0	0
O+C_2H_2	=	H+HCCO	1.35E+07	2	1900
O+C_2H_2	=	OH+C_2H	4.60E+19	-1.41	28950
O+C_2H_2	=	CO+CH_2	6.94E+06	2	1900
O+C_2H_3	=	H+CH_2CO	3.00E+13	0	0
O+C_2H_4	=	CH_3+HCO	1.25E+07	1.83	220
O+C_2H_5	=	CH_3+CH_2O	2.24E+13	0	0
O+C_2H_6	=	OH+C_2H_5	8.98E+07	1.92	5690
O+HCCO	=	H+2CO	1.00E+14	0	0
O+CH_2CO	=	OH+HCCO	1.00E+13	0	8000
O+CH_2CO	=	CH_2+CO_2	1.75E+12	0	1350
O_2+CO	=	O+CO_2	2.50E+12	0	47800
O_2+CH_2O	=	HO_2+HCO	1.00E+14	0	40000
H+O_2+M	=	HO_2+M	2.80E+18	-0.86	0
O_2/0.00/		H_2O/0.00/	CO/0.75/	CO_2/1.50/	C_2H_6/1.50/
N_2/0.00/		AR/0.00/			
H+$2O_2$	=	HO_2+O_2	2.08E+19	-1.24	0
H+O_2+H_2O	=	HO_2+H_2O	1.13E+19	-0.76	0
H+O_2+N_2	=	HO_2+N_2	2.60E+19	-1.24	0
H+O_2+AR	=	HO_2+AR	7.00E+17	-0.8	0
H+O_2	=	O+OH	2.65E+16	-0.6707	17041
2H+M	=	H_2+M	1.00E+18	-1	0
H_2/0.00/		H_2O/0.00/	CH_4/2.00/	CO_2/0.00/	C_2H_6/3.00/
AR/0.63/					
2H+H_2	=	$2H_2$	9.00E+16	-0.6	0
2H+H_2O	=	H_2+H_2O	6.00E+19	-1.25	0
2H+CO_2	=	H_2+CO_2	5.50E+20	-2	0
H+OH+M	=	H_2O+M	2.20E+22	-2	0
H_2/0.73/	=	H_2O/3.65/	CH_4/2.00/	C_2H_6/3.00/	AR/0.38
H+HO_2	=	O+H_2O	3.97E+12	0	671
H+HO_2	=	O_2+H_2	4.48E+13	0	1068

$H+HO_2$	=	2OH	8.40E+13	0	635
$H+H_2O_2$	=	HO_2+H_2	1.21E+07	2	5200
$H+H_2O_2$	=	$OH+H_2O$	1.00E+13	0	3600
H+CH	=	$C+H_2$	1.65E+14	0	0
$H+CH_2(+M)$	=	$CH_3(+M)$	6.00E+14	0	0
LOW			1.04E+26	-2.76	1600
TROE		0.562	91	5836	8552
H_2/2.00/		H_2O/6.00/	CH_4/2.00/	CO/1.50/	CO_2/2.00/
C_2H_6/3.00/		AR/0.70/			
$H+CH_2(S)$	=	$CH+H_2$	3.00E+13	0	0
$H+CH_3(+M)$	=	$CH_4(+M)$	1.39E+16	-0.534	536
LOW			2.62E+33	-4.76	2440
TROE		0.783	74	2941	6964
H_2/2.00/		H_2O/6.00/	CH_4/3.00/	CO/1.50/	CO_2/2.00/
C_2H_6/3.00/		AR/0.70/			
$H+CH_4$	=	CH_3+H_2	6.60E+08	1.62	10840
$H+HCO(+M)$	=	$CH_2O(+M)$	1.09E+12	0.48	-260
LOW			2.47E+24	-2.57	425
TROE		0.7824	271	2755	6570
H_2/2.00/		H_2O/6.00/	CH_4/2.00/	CO/1.50/	CO_2/2.00/
C_2H_6/3.00/		AR/0.70/			
H+HCO	=	H_2+CO	7.34E+13	0	0
$H+CH_2O(+M)$	=	$CH_2OH(+M)$	5.40E+11	0.454	3600
LOW			1.27E+32	-4.82	6530
TROE		0.7187	103	1291	4160
H_2/2.00/		H_2O/6.00/	CH_4/2.00/	CO/1.50/	CO_2/2.00/
C_2H_6/3.00/					
$H+CH_2O(+M)$	=	$CH_3O(+M)$	5.40E+11	0.454	2600
LOW			2.20E+30	-4.8	5560
TROE		0.758	94	1555	4200
H_2/2.00/		H_2O/6.00/	CH_4/2.00/	CO/1.50/	CO_2/2.00/
C_2H_6/3.00/					
$H+CH_2O$	=	$HCO+H_2$	5.74E+07	1.9	2742
$H+CH_2OH(+M)$	=	$CH_3OH(+M)$	1.06E+12	0.5	86
LOW			4.36E+31	-4.65	5080
TROE		0.6	100	90000	10000
H_2/2.00/		H_2O/6.00/	CH_4/2.00/	CO/1.50/	CO_2/2.00/
C_2H_6/3.00/					

$H+CH_2OH$	=	H_2+CH_2O	2.00E+13	0	0
$H+CH_2OH$	=	$OH+CH_3$	1.65E+11	0.65	-284
$H+CH_2OH$	=	$CH_2(S)+H_2O$	3.28E+13	-0.09	610
$H+CH_3O(+M)$	=	$CH_3OH(+M)$	2.43E+12	0.515	50
LOW			4.66E+41	-7.44	14080
TROE		0.7	100	90000	10000
H_2/2.00/		H_2O/6.00/	CH_4/2.00/	CO/1.50/	CO_2/2.00/
C_2H_6/3.00/					
$H+CH_3O$	=	$H+CH_2OH$	4.15E+07	1.63	1924
$H+CH_3O$	=	H_2+CH_2O	2.00E+13	0	0
$H+CH_3O$	=	$OH+CH_3$	1.50E+12	0.5	-110
$H+CH_3O$	=	$CH_2(S)+H_2O$	2.62E+14	-0.23	1070
$H+CH_3OH$	=	CH_2OH+H_2	1.70E+07	2.1	4870
$H+CH_3OH$	=	CH_3O+H_2	4.20E+06	2.1	4870
$H+C_2H(+M)$	=	$C_2H_2(+M)$	1.00E+17	-1	0
LOW			3.75E+33	-4.8	1900
TROE		0.6464	132	1315	5566
H_2/2.00/		H_2O/6.00/	CH_4/2.00/	CO/1.50/	CO_2/2.00/
C_2H_6/3.00/		AR/0.70/			
$H+C_2H_2(+M)$	=	$C_2H_3(+M)$	5.60E+12	0	2400
LOW			3.80E+40	-7.27	7220
TROE		0.7507	98.5	1302	4167
H_2/2.00/		H_2O/6.00/	CH_4/2.00/	CO/1.50/	CO_2/2.00/
C_2H_6/3.00/		AR/0.70/			
$H+C_2H_3(+M)$	=	$C_2H_4(+M)$	6.08E+12	0.27	280
LOW			1.40E+30	-3.86	3320
TROE		0.782	207.5	2663	6095
H_2/2.00/		H_2O/6.00/	CH_4/2.00/	CO/1.50/	CO_2/2.00/
C_2H_6/3.00/		AR/0.70/			
$H+C_2H_3$	=	$H_2+C_2H_2$	3.00E+13	0	0
$H+C_2H_4(+M)$	=	$C_2H_5(+M)$	5.40E+11	0.454	1820
LOW			6.00E+41	-7.62	6970
TROE		0.9753	210	984	4374
H_2/2.00/		H_2O/6.00/	CH_4/2.00/	CO/1.50/	CO_2/2.00/
C_2H_6/3.00/		AR/0.70/			
$H+C_2H_4$	=	$C_2H_3+H_2$	1.33E+06	2.53	12240

$H+C_2H_5(+M)$	=	$C_2H_6(+M)$	5.21E+17	-0.99	1580
LOW			1.99E+41	-7.08	6685
TROE		0.8422	125	2219	6882
H_2/2.00/		H_2O/6.00/	CH_4/2.00/	CO/1.50/	CO_2/2.00/
C_2H_6/3.00/		AR/0.70/			
$H+C_2H_5$	=	$H_2+C_2H_4$	2.00E+12	0	0
$H+C_2H_6$	=	$C_2H_5+H_2$	1.15E+08	1.9	7530
H+HCCO	=	$CH_2(S)+CO$	1.00E+14	0	0
$H+CH_2CO$	=	$HCCO+H_2$	5.00E+13	0	8000
$H+CH_2CO$	=	CH_3+CO	1.13E+13	0	3428
H+HCCOH	=	$H+CH_2CO$	1.00E+13	0	0
$H_2+CO(+M)$	=	$CH_2O(+M)$	4.30E+07	1.5	79600
LOW			5.07E+27	-3.42	84350
TROE		0.932	197	1540	10300
H_2/2.00/		H_2O/6.00/	CH_4/2.00/	CO/1.50/	CO_2/2.00/
C_2H_6/3.00/		AR/0.70/			
$OH+H_2$	=	$H+H_2O$	2.16E+08	1.51	3430
$2OH(+M)$	=	$H_2O_2(+M)$	7.40E+13	-0.37	0
LOW			2.30E+18	-0.9	-1700
TROE		0.7346	94	1756	5182
H_2/2.00/		H_2O/6.00/	CH_4/2.00/	CO/1.50/	CO_2/2.00/
C_2H_6/3.00/		AR/0.70/			
2OH	=	$O+H_2O$	3.57E+04	2.4	-2110
$OH+HO_2$	=	O_2+H_2O	1.45E+13	0	-500
DUPLICATE					
$OH+H_2O_2$	=	HO_2+H_2O	2.00E+12	0	427
DUPLICATE					
$OH+H_2O_2$	=	HO_2+H_2O	1.70E+18	0	29410
DUPLICATE					
OH+C	=	H+CO	5.00E+13	0	0
OH+CH	=	H+HCO	3.00E+13	0	0
$OH+CH_2$	=	$H+CH_2O$	2.00E+13	0	0
$OH+CH_2$	=	$CH+H_2O$	1.13E+07	2	3000
$OH+CH_2(S)$	=	$H+CH_2O$	3.00E+13	0	0
$OH+CH_3(+M)$	=	$CH_3OH(+M)$	2.79E+18	-1.43	1330
LOW			4.00E+36	-5.92	3140
TROE		0.412	195	5900	6394
H_2/2.00/		H_2O/6.00/	CH_4/2.00/	CO/1.50/	CO_2/2.00/
C_2H_6/3.00/					

$OH+CH_3$	=	CH_2+H_2O	5.60E+07	1.6	5420
$OH+CH_3$	=	$CH_2(S)+H_2O$	6.44E+17	-1.34	1417
$OH+CH_4$	=	CH_3+H_2O	1.00E+08	1.6	3120
OH+CO	=	$H+CO_2$	4.76E+07	1.228	70
OH+HCO	=	H_2O+CO	5.00E+13	0	0
$OH+CH_2O$	=	$HCO+H_2O$	3.43E+09	1.18	-447
$OH+CH_2OH$	=	H_2O+CH_2O	5.00E+12	0	0
$OH+CH_3O$	=	H_2O+CH_2O	5.00E+12	0	0
$OH+CH_3OH$	=	CH_2OH+H_2O	1.44E+06	2	-840
$OH+CH_3OH$	=	CH_3O+H_2O	6.30E+06	2	1500
$OH+C_2H$	=	H+HCCO	2.00E+13	0	0
$OH+C_2H_2$	=	$H+CH_2CO$	2.18E-04	4.5	-1000
$OH+C_2H_2$	=	H+HCCOH	5.04E+05	2.3	13500
$OH+C_2H_2$	=	C_2H+H_2O	3.37E+07	2	14000
$OH+C_2H_2$	=	CH_3+CO	4.83E-04	4	-2000
$OH+C_2H_3$	=	$H_2O+C_2H_2$	5.00E+12	0	0
$OH+C_2H_4$	=	$C_2H_3+H_2O$	3.60E+06	2	2500
$OH+C_2H_6$	=	$C_2H_5+H_2O$	3.54E+06	2.12	870
$OH+CH_2CO$	=	$HCCO+H_2O$	7.50E+12	0	2000
$2HO_2$	=	$O_2+H_2O_2$	1.30E+11	0	-1630
DUPLICATE					
$2HO_2$	=	$O_2+H_2O_2$	4.20E+14	0	12000
DUPLICATE					
HO_2+CH_2	=	$OH+CH_2O$	2.00E+13	0	0
HO_2+CH_3	=	O_2+CH_4	1.00E+12	0	0
HO_2+CH_3	=	$OH+CH_3O$	3.78E+13	0	0
HO_2+CO	=	$OH+CO_2$	1.50E+14	0	23600
HO_2+CH_2O	=	$HCO+H_2O_2$	5.60E+06	2	12000
$C+O_2$	=	O+CO	5.80E+13	0	576
$C+CH_2$	=	$H+C_2H$	5.00E+13	0	0
$C+CH_3$	=	$H+C_2H_2$	5.00E+13	0	0
$CH+O_2$	=	O+HCO	6.71E+13	0	0
$CH+H_2$	=	$H+CH_2$	1.08E+14	0	3110
$CH+H_2O$	=	$H+CH_2O$	5.71E+12	0	-755
$CH+CH_2$	=	$H+C_2H_2$	4.00E+13	0	0
$CH+CH_3$	=	$H+C_2H_3$	3.00E+13	0	0
$CH+CH_4$	=	$H+C_2H_4$	6.00E+13	0	0

CH+CO(+M)	=	HCCO(+M)	5.00E+13	0	0
LOW			2.69E+28	-3.74	1936
TROE		0.5757	237	1652	5069
H_2/2.00/		H_2O/6.00/	CH_4/2.00/	CO/1.50/	CO_2/2.00/
C_2H_6/3.00/		AR/0.70/			
CH+CO_2	=	HCO+CO	1.90E+14	0	15792
CH+CH_2O	=	H+CH_2CO	9.46E+13	0	-515
CH+HCCO	=	CO+C_2H_2	5.00E+13	0	0
CH_2+O_2	=	OH+H+CO	5.00E+12	0	1500
CH_2+H_2	=	H+CH_3	5.00E+05	2	7230
2CH_2	=	H_2+C_2H_2	1.60E+15	0	11944
CH_2+CH_3	=	H+C_2H_4	4.00E+13	0	0
CH_2+CH_4	=	2CH_3	2.46E+06	2	8270
CH_2+CO(+M)	=	CH_2CO(+M)	8.10E+11	0.5	4510
LOW			2.69E+33	-5.11	7095
TROE		0.5907	275	1226	5185
H_2/2.00/		H_2O/6.00/	CH_4/2.00/	CO/1.50/	CO_2/2.00/
C_2H_6/3.00/		AR/0.70/			
CH_2+HCCO	=	C_2H_3+CO	3.00E+13	0	0
CH_2(S)+N_2	=	CH_2+N_2	1.50E+13	0	600
CH_2(S)+AR	=	CH_2+AR	9.00E+12	0	600
CH_2(S)+O_2	=	H+OH+CO	2.80E+13	0	0
CH_2(S)+O_2	=	CO+H_2O	1.20E+13	0	0
CH_2(S)+H_2	=	CH_3+H	7.00E+13	0	0
CH_2(S)+H_2O(+M)	=	CH_3OH(+M)	4.82E+17	-1.16	1145
LOW			1.88E+38	-6.36	5040
TROE		0.6027	208	3922	10180
H_2/2.00/		H_2O/6.00/	CH_4/2.00/	CO/1.50/	CO_2/2.00/
C_2H_6/3.00/					
CH_2(S)+H_2O	=	CH_2+H_2O	3.00E+13	0	0
CH_2(S)+CH_3	=	H+C_2H_4	1.20E+13	0	-570
CH_2(S)+CH_4	=	2CH_3	1.60E+13	0	-570
CH_2(S)+CO	=	CH_2+CO	9.00E+12	0	0
CH_2(S)+CO_2	=	CH_2+CO_2	7.00E+12	0	0
CH_2(S)+CO_2	=	CO+CH_2O	1.40E+13	0	0
CH_2(S)+C_2H_6	=	CH_3+C_2H_5	4.00E+13	0	-550
CH_3+O_2	=	O+CH_3O	3.56E+13	0	30480
CH_3+O_2	=	OH+CH_2O	2.31E+12	0	20315

$CH_3+H_2O_2$	=	HO_2+CH_4	2.45E+04	2.47	5180
$2CH_3(+M)$	=	$C_2H_6(+M)$	6.77E+16	-1.18	654
LOW			3.40E+41	-7.03	2762
TROE		0.619	73.2	1180	9999
H_2/2.00/		H_2O/6.00/	CH_4/2.00/	CO/1.50/	CO_2/2.00/
C_2H_6/3.00/		AR/0.70/			
$2CH_3$	=	$H+C_2H_5$	6.84E+12	0.1	10600
CH_3+HCO	=	CH_4+CO	2.65E+13	0	0
CH_3+CH_2O	=	$HCO+CH_4$	3.32E+03	2.81	5860
CH_3+CH_3OH	=	CH_2OH+CH_4	3.00E+07	1.5	9940
CH_3+CH_3OH	=	CH_3O+CH_4	1.00E+07	1.5	9940
$CH_3+C_2H_4$	=	$C_2H_3+CH_4$	2.27E+05	2	9200
$CH_3+C_2H_6$	=	$C_2H_5+CH_4$	6.14E+06	1.74	10450
$HCO+H_2O$	=	$H+CO+H_2O$	1.50E+18	-1	17000
HCO+M	=	H+CO+M	1.87E+17	-1	17000
H_2/2.00/		H_2O/0.00/	CH_4/2.00/	CO/1.50/	CO_2/2.00/
C_2H_6/3.00/					
$HCO+O_2$	=	HO_2+CO	1.35E+13	0	400
CH_2OH+O_2	=	HO_2+CH_2O	1.80E+13	0	900
CH_3O+O_2	=	HO_2+CH_2O	4.28E-13	7.6	-3530
C_2H+O_2	=	HCO+CO	1.00E+13	0	-755
C_2H+H_2	=	$H+C_2H_2$	5.68E+10	0.9	1993
$C_2H_3+O_2$	=	$HCO+CH_2O$	4.58E+16	-1.39	1015
$C_2H_4(+M)$	=	$H_2+C_2H_2(+M)$	8.00E+12	0.44	86770
LOW			1.58E+51	-9.3	97800
TROE		0.7345	180	1035	5417
H_2/2.00/		H_2O/6.00/	CH_4/2.00/	CO/1.50/	CO_2/2.00/
C_2H_6/3.00/		AR/0.70/			
$C_2H_5+O_2$	=	$HO_2+C_2H_4$	8.40E+11	0	3875
$HCCO+O_2$	=	OH+2CO	3.20E+12	0	854
2HCCO	=	$2CO+C_2H_2$	1.00E+13	0	0
N+NO	=	N_2+O	2.70E+13	0	355
$N+O_2$	=	NO+O	9.00E+09	1	6500
N+OH	=	NO+H	3.36E+13	0	385
N_2O+O	=	N_2+O_2	1.40E+12	0	10810
N_2O+O	=	2NO	2.90E+13	0	23150
N_2O+H	=	N_2+OH	3.87E+14	0	18880
N_2O+OH	=	N_2+HO_2	2.00E+12	0	21060

$N_2O(+M)$	=	$N_2+O(+M)$	7.91E+10	0	56020
LOW			6.37E+14	0	56640
H_2/2.00/		H_2O/6.00/	CH_4/2.00/	CO/1.50/	CO_2/2.00/
C_2H_6/3.00/		AR/0.625/			
HO_2+NO	=	NO_2+OH	2.11E+12	0	-480
$NO+O+M$	=	NO_2+M	1.06E+20	-1.41	0
H_2/2.00/		H_2O/6.00/	CH_4/2.00/	CO/1.50/	CO_2/2.00/
C_2H_6/3.00/		AR/0.70/			
NO_2+O	=	$NO+O_2$	3.90E+12	0	-240
NO_2+H	=	NO+OH	1.32E+14	0	360
NH+O	=	NO+H	4.00E+13	0	0
NH+H	=	$N+H_2$	3.20E+13	0	330
NH+OH	=	HNO+H	2.00E+13	0	0
NH+OH	=	$N+H_2O$	2.00E+09	1.2	0
$NH+O_2$	=	HNO+O	4.61E+05	2	6500
$NH+O_2$	=	NO+OH	1.28E+06	1.5	100
NH+N	=	N_2+H	1.50E+13	0	0
$NH+H_2O$	=	$HNO+H_2$	2.00E+13	0	13850
NH+NO	=	N_2+OH	2.16E+13	-0.23	0
NH+NO	=	N_2O+H	3.65E+14	-0.45	0
NH_2+O	=	OH+NH	3.00E+12	0	0
NH_2+O	=	H+HNO	3.90E+13	0	0
NH_2+H	=	$NH+H_2$	4.00E+13	0	3650
NH_2+OH	=	$NH+H_2O$	9.00E+07	1.5	-460
NNH	=	N_2+H	3.30E+08	0	0
NNH+M	=	N_2+H+M	1.30E+14	-0.11	4980
H_2/2.00/		H_2O/6.00/	CH_4/2.00/	CO/1.50/	CO_2/2.00/
C_2H_6/3.00/		AR/0.70/			
$NNH+O_2$	=	HO_2+N_2	5.00E+12	0	0
NNH+O	=	$OH+N_2$	2.50E+13	0	0
NNH+O	=	NH+NO	7.00E+13	0	0
NNH+H	=	H_2+N_2	5.00E+13	0	0
NNH+OH	=	H_2O+N_2	2.00E+13	0	0
$NNH+CH_3$	=	CH_4+N_2	2.50E+13	0	0
H+NO+M	=	HNO+M	4.48E+19	-1.32	740
H_2/2.00/		H_2O/6.00/	CH_4/2.00/	CO/1.50/	CO_2/2.00/
C_2H_6/3.00/		AR/0.70/			
HNO+O	=	NO+OH	2.50E+13	0	0

HNO+H	=	H_2+NO	9.00E+11	0.72	660
HNO+OH	=	NO+H_2O	1.30E+07	1.9	-950
HNO+O_2	=	HO_2+NO	1.00E+13	0	13000
CN+O	=	CO+N	7.70E+13	0	0
CN+OH	=	NCO+H	4.00E+13	0	0
CN+H_2O	=	HCN+OH	8.00E+12	0	7460
CN+O_2	=	NCO+O	6.14E+12	0	-440
CN+H_2	=	HCN+H	2.95E+05	2.45	2240
NCO+O	=	NO+CO	2.35E+13	0	0
NCO+H	=	NH+CO	5.40E+13	0	0
NCO+OH	=	NO+H+CO	2.50E+12	0	0
NCO+N	=	N_2+CO	2.00E+13	0	0
NCO+O_2	=	NO+CO_2	2.00E+12	0	20000
NCO+M	=	N+CO+M	3.10E+14	0	54050
H_2/2.00/		H_2O/6.00/	CH_4/2.00/	CO/1.50/	CO_2/2.00/
C_2H_6/3.00/		AR/0.70/			
NCO+NO	=	N_2O+CO	1.90E+17	-1.52	740
NCO+NO	=	N_2+CO_2	3.80E+18	-2	800
HCN+M	=	H+CN+M	1.04E+29	-3.3	126600
H_2/2.00/		H_2O/6.00/	CH_4/2.00/	CO/1.50/	CO_2/2.00/
C_2H_6/3.00/		AR/0.70/			
HCN+O	=	NCO+H	2.03E+04	2.64	4980
HCN+O	=	NH+CO	5.07E+03	2.64	4980
HCN+O	=	CN+OH	3.91E+09	1.58	26600
HCN+OH	=	HOCN+H	1.10E+06	2.03	13370
HCN+OH	=	HNCO+H	4.40E+03	2.26	6400
HCN+OH	=	NH_2+CO	1.60E+02	2.56	9000
H+HCN(+M)	=	H_2CN(+M)	3.30E+13	0	0
LOW			1.40E+26	-3.4	1900
H_2/2.00/		H_2O/6.00/	CH_4/2.00/	CO/1.50/	CO_2/2.00/
C_2H_6/3.00/		AR/0.70/			
H_2CN+N	=	N_2+CH_2	6.00E+13	0	400
C+N_2	=	CN+N	6.30E+13	0	46020
CH+N_2	=	HCN+N	3.12E+09	0.88	20130
CH+N_2(+M)	=	HCNN(+M)	3.10E+12	0.15	0
LOW			1.30E+25	-3.16	740
TROE		0.667	235	2117	4536
H_2/2.00/		H_2O/6.00/	CH_4/2.00/	CO/1.50/	CO_2/2.00/
C_2H_6/3.00/		AR/1.0/			

CH_2+N_2	=	HCN+NH	1.00E+13	0	74000
$CH_2(S)+N_2$	=	NH+HCN	1.00E+11	0	65000
C+NO	=	CN+O	1.90E+13	0	0
C+NO	=	CO+N	2.90E+13	0	0
CH+NO	=	HCN+O	4.10E+13	0	0
CH+NO	=	H+NCO	1.62E+13	0	0
CH+NO	=	N+HCO	2.46E+13	0	0
CH_2+NO	=	H+HNCO	3.10E+17	-1.38	1270
CH_2+NO	=	OH+HCN	2.90E+14	-0.69	760
CH_2+NO	=	H+HCNO	3.80E+13	-0.36	580
$CH_2(S)$+NO	=	H+HNCO	3.10E+17	-1.38	1270
$CH_2(S)$+NO	=	OH+HCN	2.90E+14	-0.69	760
$CH_2(S)$+NO	=	H+HCNO	3.80E+13	-0.36	580
CH_3+NO	=	$HCN+H_2O$	9.60E+13	0	28800
CH_3+NO	=	H_2CN+OH	1.00E+12	0	21750
HCNN+O	=	$CO+H+N_2$	2.20E+13	0	0
HCNN+O	=	HCN+NO	2.00E+12	0	0
$HCNN+O_2$	=	$O+HCO+N_2$	1.20E+13	0	0
HCNN+OH	=	$H+HCO+N_2$	1.20E+13	0	0
HCNN+H	=	CH_2+N_2	1.00E+14	0	0
HNCO+O	=	$NH+CO_2$	9.80E+07	1.41	8500
HNCO+O	=	HNO+CO	1.50E+08	1.57	44000
HNCO+O	=	NCO+OH	2.20E+06	2.11	11400
HNCO+H	=	NH_2+CO	2.25E+07	1.7	3800
HNCO+H	=	H_2+NCO	1.05E+05	2.5	13300
HNCO+OH	=	$NCO+H_2O$	3.30E+07	1.5	3600
HNCO+OH	=	NH_2+CO_2	3.30E+06	1.5	3600
HNCO+M	=	NH+CO+M	1.18E+16	0	84720
H_2/2.00/		H_2O/6.00/	CH_4/2.00/	CO/1.50/	CO_2/2.00/
C_2H_6/3.00/		AR/0.70/			
HCNO+H	=	H+HNCO	2.10E+15	-0.69	2850
HCNO+H	=	OH+HCN	2.70E+11	0.18	2120
HCNO+H	=	NH_2+CO	1.70E+14	-0.75	2890
HOCN+H	=	H+HNCO	2.00E+07	2	2000
HCCO+NO	=	HCNO+CO	9.00E+12	0	0
CH_3+N	=	H_2CN+H	6.10E+14	-0.31	290
CH_3+N	=	$HCN+H_2$	3.70E+12	0.15	-90

NH_3+H	=	NH_2+H_2	5.40E+05	2.4	9915
NH_3+OH	=	NH_2+H_2O	5.00E+07	1.6	955
NH_3+O	=	NH_2+OH	9.40E+06	1.94	6460
NH+CO_2	=	HNO+CO	1.00E+13	0	14350
CN+NO_2	=	NCO+NO	6.16E+15	-0.752	345
NCO+NO_2	=	N_2O+CO_2	3.25E+12	0	-705
N+CO_2	=	NO+CO	3.00E+12	0	11300
O+CH_3	=	H+H_2+CO	3.37E+13	0	0
O+C_2H_4	=	H+CH_2CHO	6.70E+06	1.83	220
O+C_2H_5	=	H+CH_3CHO	1.10E+14	0	0
OH+HO_2	=	O_2+H_2O	5.00E+15	0	17330
DUPLICATE					
OH+CH_3	=	H_2+CH_2O	8.00E+09	0.5	-1755
CH+H_2(+M)	=	CH_3(+M)	1.97E+12	0.43	-370
LOW			4.82E+25	-2.8	590
TROE		0.578	122	2535	9365
H_2/2.00/		H_2O/6.00/	CH_4/2.00/	CO/1.50/	CO_2/2.00/
C_2H_6/3.00/		AR/0.70/			
CH_2+O_2	=	2H+CO_2	5.80E+12	0	1500
CH_2+O_2	=	O+CH_2O	2.40E+12	0	1500
CH_2+CH_2	=	2H+C_2H_2	2.00E+14	0	10989
CH_2(S)+H_2O	=	H_2+CH_2O	6.82E+10	0.25	-935
C_2H_3+O_2	=	O+CH_2CHO	3.03E+11	0.29	11
C_2H_3+O_2	=	HO_2+C_2H_2	1.34E+06	1.61	-384
O+CH_3CHO	=	OH+CH_2CHO	2.92E+12	0	1808
O+CH_3CHO	=	OH+CH_3+CO	2.92E+12	0	1808
O_2+CH_3CHO	=	HO_2+CH_3+CO	3.01E+13	0	39150
H+CH_3CHO	=	CH_2CHO+H_2	2.05E+09	1.16	2405
H+CH_3CHO	=	CH_3+H_2+CO	2.05E+09	1.16	2405
OH+CH_3CHO	=	CH_3+H_2O+CO	2.34E+10	0.73	-1113
HO_2+CH_3CHO	=	CH_3+H_2O_2+CO	3.01E+12	0	11923
CH_3+CH_3CHO	=	CH_3+CH_4+CO	2.72E+06	1.77	5920
H+CH_2CO(+M)	=	CH_2CHO(+M)	4.87E+11	0.422	-1755
LOW			1.01E+42	-7.63	3854
TROE		0.465	201	1773	5333
H_2/2.00/		H_2O/6.00/	CH_4/2.00/	CO/1.50/	CO_2/2.00/
C_2H_6/3.00/		AR/0.70/			
O+CH_2CHO	=	H+CH_2+CO_2	1.50E+14	0	0

O_2+CH_2CHO	=	OH+CO+CH_2O	1.81E+10	0	0
O_2+CH_2CHO	=	OH+2HCO	2.35E+10	0	0
H+CH_2CHO	=	CH_3+HCO	2.20E+13	0	0
H+CH_2CHO	=	CH_2CO+H_2	1.10E+13	0	0
OH+CH_2CHO	=	H_2O+CH_2CO	1.20E+13	0	0
OH+CH_2CHO	=	HCO+CH_2OH	3.01E+13	0	0
CH_3+C_2H_5(+M)	=	C_3H_8(+M)	9.43E+12	0	0
LOW			2.71E+74	-16.82	13065
TROE		0.1527	291	2742	7748
H_2/2.00/		H_2O/6.00/	CH_4/2.00/	CO/1.50/	CO_2/2.00/
C_2H_6/3.00/		AR/0.70/			
O+C_3H_8	=	OH+C_3H_7	1.93E+05	2.68	3716
H+C_3H_8	=	C_3H_7+H_2	1.32E+06	2.54	6756
OH+C_3H_8	=	C_3H_7+H_2O	3.16E+07	1.8	934
C_3H_7+H_2O_2	=	HO_2+C_3H_8	3.78E+02	2.72	1500
CH_3+C_3H_8	=	C_3H_7+CH_4	9.03E-01	3.65	7154
CH_3+C_2H_4(+M)	=	C_3H_7(+M)	2.55E+06	1.6	5700
LOW			3.00E+63	-14.6	18170
TROE		0.1894	277	8748	7891
H_2/2.00/		H_2O/6.00/	CH_4/2.00/	CO/1.50/	CO_2/2.00/
C_2H_6/3.00/		AR/0.70/			
O+C_3H_7	=	C_2H_5+CH_2O	9.64E+13	0	0
H+C_3H_7(+M)	=	C_3H_8(+M)	3.61E+13	0	0
LOW			4.42E+61	-13.545	11357
TROE		0.315	369	3285	6667
H_2/2.00/		H_2O/6.00/	CH_4/2.00/	CO/1.50/	CO_2/2.00/
C_2H_6/3.00/		AR/0.70/			
H+C_3H_7	=	CH_3+C_2H_5	4.06E+06	2.19	890
OH+C_3H_7	=	C_2H_5+CH_2OH	2.41E+13	0	0
HO_2+C_3H_7	=	O_2+C_3H_8	2.55E+10	0.255	-943
HO_2+C_3H_7	=	OH+C_2H_5+CH_2O	2.41E+13	0	0
CH_3+C_3H_7	=	2C_2H_5	1.93E+13	-0.32	0

San Diego mechanism

Elements

O H C N Ar

Species

N_2	AR	O	NO	N	O_2	OH
H	CH	HCN	NCO	CO	NH	H_2
HNCO	HCCO	NH_2	CO_2	H_2O	CN	HNO
N_2O	N_2H	NH_3	CH_3	T-CH_2	HO_2	NO_2
H_2O_2						

Reactions

			A	n	Ea (cal/mole)
H+O_2	=	OH+O	3.52E+16	-0.7	17069.79
H_2+O	=	OH+H	5.06E+04	2.67	6290.63
H_2+OH	=	H_2O+H	1.17E+09	1.3	3635.28
H_2O+O	=	2 OH	7.60E+00	3.84	12779.64
H+O+M	=	OH+M	4.71E+18	-1	0
AR/0.75/	=	H_2/2.50/	H_2O/12.00/	CO/1.90/	CO_2/3.80/
2H+M	=	H_2+M	1.30E+18	-1	0
AR/0.50/	=	H_2/2.50/	H_2O/12.00/	CO/1.90/	CO_2/3.80/
H+OH+M	=	H_2O+M	4.00E+22	-2	0
AR/0.38/	=	H_2/2.50/	H_2O/12.00/	CO/1.90/	CO_2/3.80/
2O+M	=	O_2+M	6.17E+15	-0.5	0
AR/0.20/	=	H_2/2.50/	H_2O/12.00/	CO/1.90/	CO_2/3.80/
H+O_2(+M)	=	HO_2(+M)	4.65E+12	0.44	0
AR/0.70/	=	H_2/2.50/	H_2O/16.00/	CO/1.20/	CO_2/2.40/
LOW	=		5.75E+19	-1.4	0
TROE	=		0.5	1.00E-30	1.00E+30
O+OH+M	=	HO_2+M	1.00E+16	0	0
HO_2+H	=	2 OH	7.08E+13	0	294.93
HO_2+H	=	H_2+O_2	1.66E+13	0	822.9
HO_2+H	=	H_2O+O	3.10E+13	0	1720.84
HO_2+O	=	OH+O_2	2.00E+13	0	0
HO_2+OH	=	H_2O+O_2	2.89E+13	0	-497.13

2OH (+M)	=	H_2O_2(+M)	7.40E+13	-0.37	0
AR/0.70/	=	H_2/2.00/	H_2O/6.00/	CO/1.50/	CO_2/2.00/
LOW	=		2.30E+18	-0.9	-1701.72
TROE	=		0.735	1756	5182
2 HO_2	=	H_2O_2+O_2	3.02E+12	0	1386.23
H_2O_2+H	=	HO_2+H_2	4.79E+13	0	7958.89
H_2O_2+H	=	H_2O+OH	1.00E+13	0	3585.09
H_2O_2+OH	=	H_2O+HO_2	7.08E+12	0	1434.03
H_2O_2+O	=	HO_2+OH	9.55E+06	2	3970.12
O+N_2	=	NO+N	1.47E+13	0.3	75286.81
N+O_2	=	NO+O	6.40E+09	1	6285.85
N+OH	=	NO+H	3.80E+13	0	0
N_2+CH	=	HCN+N	4.40E+12	0	21988.53
HCN+O	=	NCO+H	1.40E+06	2.1	6118.55
NCO+M	=	N+CO+M	3.10E+16	-0.5	48040.15
N_2/1.50/	=	O_2/1.50/	H_2O/18.60/		
NCO+H	=	CO+NH	5.00E+13	0	0
NCO+O	=	NO+CO	4.70E+13	0	0
NCO+H_2	=	HNCO+H	7.60E+02	3	3991.4
HCCO+NO	=	HNCO+CO	2.00E+13	0	0
HNCO+M	=	NH+CO+M	1.10E+16	0	86042.07
N_2/1.50/	=	O_2/1.50/	H_2O/18.60/		
HNCO+H	=	NH_2+CO	2.20E+07	1.7	3800.19
HNCO+O	=	NCO+OH	2.20E+06	2.11	11448.37
HNCO+O	=	NH+CO_2	9.60E+07	1.41	8532.5
HNCO+OH	=	NCO+H_2O	6.40E+05	2	2557.36
CN+H_2	=	HCN+H	3.60E+08	1.55	3011.47
CN+H_2O	=	HCN+OH	7.80E+12	0	7456.98
CN+OH	=	NCO+H	4.20E+13	0	0
CN+O_2	=	NCO+O	7.20E+12	0	-418.26
NH+H	=	N+H_2	1.00E+13	0	0
NH+O	=	NO+H	9.20E+13	0	0
NH+OH	=	HNO+H	4.00E+13	0	0
NH+OH	=	N+H_2O	5.00E+11	0.5	2000.48
NH+O_2	=	HNO+O	4.60E+05	2	6500.96
NH+NO	=	N_2O+H	3.20E+14	-0.45	0
NH+NO	=	N_2+OH	2.20E+13	-0.23	0

NH_2+H	=	NH+H_2	4.00E+13	0	3652.01
NH_2+O	=	HNO+H	9.90E+14	-0.5	0
NH_2+OH	=	NH+H_2O	4.00E+06	2	1001.43
NH_2+NO	=	N_2+H_2O	2.00E+20	-2.6	924.95
NH_2+NO	=	N_2H+OH	9.30E+11	0	0
NH_3+M	=	NH_2+H+M	2.20E+16	0	93451.24
NH_3+H	=	NH_2+H_2	6.40E+05	2.39	10181.64
NH_3+O	=	NH_2+OH	9.40E+06	1.94	6465.11
NH_3+OH	=	NH_2+H_2O	2.04E+06	2.04	566.44
N_2H	=	N_2+H	1.00E+08	0	0
N_2H+H	=	N_2+H_2	1.00E+14	0	0
N_2H+O	=	N_2O+H	1.00E+14	0	0
N_2H+OH	=	N_2+H_2O	5.00E+13	0	0
HNO+M	=	H+NO+M	1.50E+16	0	48757.17
N_2/2.00/	=	O_2/2.00/	H_2/2.00/	H_2O/10.00/	
HNO+H	=	NO+H_2	4.40E+11	0.72	650.1
HNO+OH	=	NO+H_2O	3.60E+13	0	0
NO+CH_3	=	HCN+H_2O	8.30E+11	0	16085.09
NO+T-CH_2	=	HNCO+H	2.90E+12	0	-597.51
NO+CH	=	HCN+O	1.10E+14	0	0
N_2O(+M)	=	N_2+O(+M)	8.00E+11	0	62619.5
LOW	=		2.00E+14	0	56644.36
N_2O+H	=	N_2+OH	2.23E+14	0	16754.3
N_2O+O	=	2NO	2.90E+13	0	23159.66
N_2O+OH	=	N_2+HO_2	2.00E+12	0	10000
NO_2+M	=	NO+O+M	1.00E+16	0	65965.58
NO+HO_2	=	NO_2+OH	2.10E+12	0	-480.4
NO_2+H	=	NO+OH	3.50E+14	0	1500.96
NO_2+O	=	NO+O_2	1.00E+13	0	599.9